

# NOTE TO USERS

This reproduction is the best copy available.

**UMI<sup>®</sup>**



61500T-001

**VOLUMETRIC DEFORMATIONS AND CRACK CONTROL  
IN REINFORCED CONCRETE STRUCTURES**

**By**

**Mahmut Acarcan**

**B.Sc., University of Dicle, Turkey, 1994**

A thesis

Presented to Ryerson University

in Partial Fulfillment of the

Requirements for the Degree of

Master of Applied Science

In the Program of

Civil Engineering

Toronto, Ontario, Canada, 2004

©Copyright by Mahmut Acarcan 2004

PROPERTY OF  
RYERSON UNIVERSITY LIBRARY

UMI Number: EC52911

## INFORMATION TO USERS

The quality of this reproduction is dependent upon the quality of the copy submitted. Broken or indistinct print, colored or poor quality illustrations and photographs, print bleed-through, substandard margins, and improper alignment can adversely affect reproduction.

In the unlikely event that the author did not send a complete manuscript and there are missing pages, these will be noted. Also, if unauthorized copyright material had to be removed, a note will indicate the deletion.

**UMI**<sup>®</sup>

---

UMI Microform EC52911

Copyright 2008 by ProQuest LLC.

All rights reserved. This microform edition is protected against unauthorized copying under Title 17, United States Code.

ProQuest LLC  
789 E. Eisenhower Parkway  
PO Box 1346  
Ann Arbor, MI 48106-1346



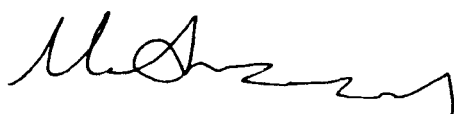
## **AUTHOR'S DECLARATION**

I hereby declare that I am the sole author of this thesis.

I authorize Ryerson University to lend this thesis to other institution or individuals for the purpose of scholarly research.

A handwritten signature in black ink, appearing to be 'M. Shuman', written in a cursive style.

I further authorize Ryerson University to reproduce this thesis by photocopying or by other means, in total or in part, at the request of other institution or individuals for the purpose of scholarly research.

A handwritten signature in black ink, appearing to be 'M. Shuman', written in a cursive style, identical to the one above.

**BORROWERS PAGE**[illegible]

# **VOLUMETRIC DEFORMATIONS AND CRACK CONTROL IN REINFORCED CONCRETE STRUCTURES**

Mahmut Acarcan, Master of Applied Science, 2004

Department of Civil Engineering  
Ryerson University

## **ABSTRACT**

Restraint temperature and shrinkage strains are one of the major reasons for cracking of reinforced concrete. Cracking of concrete reduces structural integrity, initiates or accelerates deterioration mechanisms, causes serviceability problems and may raise esthetical concerns. Particularly for liquid retaining structures, cracks are vital for structural functionality. Measures must be taken to prevent or control crack. In most cases, it may not be feasible to prevent crack formation, but crack width can be controlled by providing sufficient amount of reinforcement. Design guides provide limited information on adequate reinforcement ratio for temperature and shrinkage cracks. Optimized reinforcement design for temperature and shrinkage cracks requires additional guidelines. This study deals with temperature and shrinkage cracks in reinforced concrete structures. The Finite Element Method (FEM) was used in order to investigate the crack risk, magnitude of crack width, and adequate reinforcement ratio for controlling cracks within the design specifications. In order to find the thermal and shrinkage strains effect during early ages, computer simulations was performed for hardening concrete. Using the computer program ABAQUS/6.4, incremental numerical analysis technique was implemented that provided realistic simulation of stress/strain history. Considering an appropriate value for thermal and shrinkage strains, a parametric study was carried out to estimate the reinforcement ratio for fixed base walls. The crack width was estimated based on the calculated steel stress and the ACI 318-02 crack prediction equation. With consideration of ACI 350-01 specification for allowable crack width, the required amount of reinforcement ratio for various wall dimensions was recommended.



## **ACKNOWLEDGEMENTS**

I would like to thank to my research supervisor Professor R. Kianoush. Without his support, my journey in Ryerson University would not have been possible. His guidance, encouragement, valuable advise, and constructive suggestions played a major role throughout my studies at graduate level. His patience and understanding made this study to be completed.

## **TABLE OF CONTENTS**

AUTHOR'S DECLARATION	iii
BORROWERS PAGE	iv
ABSTRACT	v
ACKNOWLEDGEMENTS	vi
TABLE OF CONTENTS	vii
LIST OF TABLES	x
LIST OF FIGURES	xii
<b>CHAPTER 1 - Introduction</b>	<b>1</b>
1.1 Introduction	1
1.2 Background	7
1.3 Objective	16
1.4 Organization	17
 <b>CHAPTER 2 - Hydration Temperature</b>	 <b>19</b>
2.1 Introduction	19
2.2 Time Dependent Temperature Distribution Analysis	20
2.3 Thermal Properties	21
2.3.1 Specific Heat of Concrete	21
2.3.2 Thermal Conductivity of Concrete	22
2.4 Boundaries for Heat Transfer Analysis	23
2.5 Heat of Hydration	26
2.6 Case Study	30
2.7 Summary	38
 <b>CHAPTER 3 - Material Modeling</b>	 <b>39</b>
3.1 Introduction	39
3.2 Equivalent Age	39
3.3 Compressive Strength	42
3.4 Modulus of Elasticity	43

3.5 Tensile Strength	43
3.6 Case Study-Concrete Strength in Culvert Wall	46
3.7 Creep and Relaxation	50
3.7.1 Case Study-Creep Coefficient of Concrete in Culvert Wall	55
3.8 Shrinkage	56
3.8.1 Case Study-Shrinkage of Culvert Wall	60
3.9 Effect of Section Thickness on Material Properties	61
3.9 Summary	65
<b>CHAPTER 4 – Stress/Displacement Analysis</b>	<b>67</b>
4.1 Introduction	67
4.2 Finite Element Formulation for Mechanical Problem	67
4.3 Reinforced Concrete in FEM	70
4.4 Defining Material in ABAQUS/6.4	71
4.4.1 Modeling Creep Effect	77
4.4.2 Modeling Shrinkage Effects	78
4.5 Coefficient of Thermal Expansion	78
4.6 Analysis-Case Study	79
4.7 Summary	87
<b>CHAPTER 5 - Restraint Factor</b>	<b>89</b>
5.1 Introduction	89
5.2 Degree of Restraint	91
5.3 Calculation of Degree of Restraint using ABAQUS/6.4	93
5.4 Degree of Restraint in Reinforced Concrete Walls	94
5.5 Application of Restraint Factor in Design	107
5.6 Summary	111
<b>CHAPTER 6 - Crack Control</b>	<b>112</b>
6.1 Introduction	112
6.2 Crack Control	113

6.3 Estimating the Crack Width	117
6.4 Cracking Model for Concrete	127
6.5 Case Study	129
6.6 Minimum Reinforcement for Liquid Retaining Structures	133
6.6.1 Total Thermal and Shrinkage Strain	135
6.6.2 Calculated Crack Width	139
6.7 Summary	155
 <b>CHAPTER 7 – Conclusion</b>	 158
7.1 Summary	158
7.2 Conclusion	159
7.3 Suggestions for Future Research	160
 REFERENCES	 162
 APPENDIX A	 A-1

## LIST OF TABLES

Table 2.1 Thermal conductivity of three concrete mixes for various temperatures	23
Table.2.2 Concrete Mix Design used in culvert wall	31
Table 2.3 Approximated total heat energy capacity of cement hydration	32
Table 2.4 Approximated adiabatic temperature rise data	33
Table 2.5 Number of steps during analysis with corresponding time period for 168 hr	34
Table 3.1 Calculated equivalent age of concrete in culvert wall	47
Table 3.2 Strength development history of concrete in culvert wall	48
Table 3.3 Creep coefficient variation over the time, and calculated required parameters for determination of creep coefficient	56
Table 3.4 Estimated shrinkage and equivalent temperature changes over the time and required calculated parameters for shrinkage prediction	62
Table 4.1 Compressive strains and corresponding stresses for concrete at different ages	74
Table 4.2 Tensile strains and corresponding stresses for concrete at different ages	75
Table 4.3 Variation of thermal expansion coefficient of different concrete types in hardening process	79
Table 5.1 Comparison of calculated degree of restraint with CIRIA report (L/H=4)	94
Table 5.2 Degree of restraint at wall centerline (ACI 207.2R-95)	95
Table 5.3 Degree of restraint at centerline of wall (ABAQUS/6.4 Linear analysis)	98
Table.5.4: Degree of restraint at centreline of wall (ABAQUS/6.4 Non-linear analysis)	99
Table 5.5 Theoretical Degree of Restraint at center section (Harrison, 1981)	106
Table 6.1 Minimum shrinkage and temperature reinforcement, (ACI 318-02)	115
Table 6.2 Minimum shrinkage and temperature reinforcement, (ACI 350-01)	115
Table 6.3 Nominal limit value of crack width specified for cases with expected functional consequences of cracking (ACI 224R-01)	116
Table 6.4 Design walls that are in the range of code guide (Table6.2), and ACI 350-01 recommendation for temperature and shrinkage	

reinforcement ratios	134
Table 6.5 Variables for parametric study (Dimensions for selected walls)	135
Table 6.6 Average monthly temperature of Toronto	136
Table 6.7 CEB-FIP recommendations for ultimate shrinkage strain	137
Table 6.8 Recommended shrinkage and temperature reinforcement ratio	155

## LIST OF FIGURES

Figure 1.1 Types of volumetric deformation of concrete and primary reasons	2
Figure 1.2 Typical temperature history of concrete after placing	2
Figure 1.3 Typical internal restraint condition in a thick concrete element	4
Figure 1.4 Typical external restraint conditions, (new concrete wall is cast on previously cast base)	5
Figure 2.1 Variation of specific heat of oven-dried concretes with temperature	22
Figure 2.2 Temperature rises of 30, 70, and 100 MPa concretes during temperature matched curing	28
Figure 2.3 Wall cast on previously cast foundation in culvert construction	30
Figure 2.4 Locations of the temperature sensors and strain gauges	31
Figure 2.5 Approximated adiabatic temperature rise	34
Figure 2.6 Contour plot of temperature distribution in studied culvert section	35
Figure 2.7 Calculated and measured temperature history at Point 1	36
Figure 2.8 Calculated and measured temperature history at Point 2	36
Figure 2.9 Calculated and measured temperature history at Point 3	37
Figure 2.10 Calculated and measured temperature history at Point 4	37
Figure 3.1 Compressive strength development of concrete in culvert wall	49
Figure 3.2 Modulus of elasticity development of concrete in culvert wall	50
Figure 3.3 Tensile strength development of concrete in culvert wall	50
Figure 3.4 Idealized graphical representation of creep and relaxation	51
Figure 3.5 Creep classification (basic and drying creep)	53
Figure 3.6 Shrinkage classification	57
Figure 3.7 FE mesh of a square slab with thickness of 300 mm divided in to 8 layers	63
Figure 3.8 Different temperature history of different layers in example slab	64
Figure 3.9 Variation of compressive strength through the thickness of the example slab	65
Figure 3.10 Variation of tensile strength through the thickness of example slab	65
Figure 3.11 Variation of modulus of elasticity through the thickness of example slab	66

Figure 4.1 Typical tension stiffening curve	71
Figure 4.2 Stress-strain diagram for uniaxial compression	73
Figure 4.3 Stress-strain curve of concrete in compression at different ages	74
Figure 4.4 Stress-strain curve of concrete in tension at different ages	76
Figure 4.5 Compression tests results for 70 MPa concrete at different ages	76
Figure 4.6 Example of modified stress-strain curve due to creep effect	77
Figure 4.7 Modified temperature history curve to include shrinkage effect	78
Figure 4.8 Finite element mesh-density of Culvert wall	80
Figure 4.9 Contour plot of longitudinal stresses in Culvert part	82
Figure 4.10 Comparison of measured and calculated strain history at Point 1	83
Figure 4.11 Comparison of measured and calculated strain history at Point 2	83
Figure 4.12 Comparison of measured and calculated strain history at Point 3	84
Figure 4.13 Comparison of measured and calculated strain history at Point 4	84
Figure 4.14 Calculated stress history at different points and tensile strength development	86
Figure 4.15 Summary of simulation of hardening concrete	88
Figure 5.1 Continuous edge restraint of wall cast on a base	91
Figure 5.2 Potential crack formation for different rigidity of foundation	92
Figure 5.3 Restraint factors for an uncracked wall on a rigid base (length/height ratio=4)	93
Figure 5.4 Degree of Restraint variation at the centre of wall	95
Figure 5.5 Standard model for calculation of degree of restraint variation at the centre of wall	96
Figure 5.6 Degree of Restraint variation at the centreline of wall, ABAQUS/6.4 Linear analysis	98
Figure 5.7 Degree of Restraint variation at centreline of wall, ABAQUS/6.4 Non-Linear analysis	99
Figure 5.8 Comparison of Degree of Restraint variation at the centreline of wall for $L/H=1$	100
Figure 5.9 Comparison of Degree of Restraint variation at the centreline of wall for $L/H=2$	100



Figure 5.10 Comparison of Degree of Restraint variation at the centreline of wall for $L/H=3$	101
Figure 5.11 Comparison of Degree of Restraint variation at the centreline of wall for $L/H=4$	101
Figure 5.12 Comparison of Degree of Restraint variation at the centreline of wall for $L/H=5$	102
Figure 5.13 Comparison of Degree of Restraint variation at the centreline of wall for $L/H=6$	102
Figure 5.14 Comparison of Degree of Restraint variation at the centreline of wall for $L/H=7$	103
Figure 5.15 Comparison of Degree of Restraint variation at the centreline of wall for $L/H=8$	103
Figure 5.16 Comparison of Degree of Restraint variation at the centreline of wall for $L/H=9$	104
Figure 5.17 Comparison of Degree of Restraint variation at the centreline of wall for $L/H=10$	104
Figure 5.18 Comparison of Degree of Restraint variation at the centreline of wall for $L/H=20$	105
Figure 6.1 Crack formation due to volumetric deformation in a fully restrained beam	114
Figure 6.2 Strain Gradient, and determination of $\beta$ and $A$	118
Figure 6.3 Physical model of flexural crack	122
Figure 6.4 Determination of control cover distance, $d^*$ , for a beam cross section	123
Figure 6.5 State of stress in reinforced concrete after cracking	124
Figure 6.6 Steel stress just after first cracking and numerical approximation	126
Figure 6.7 Crack formation and recorded crack widths in a base fixed wall	130
Figure 6.8 Mesh density of the simulated wall, and contour plot of longitudinal steel strains (Standard spectrum)	132
Figure 6.9 Contour plot of longitudinal steel strains,	

reduced spectrum	132
Figure 6.10 Calculated maximum crack widths for different crack spacing factors that are based on ACI 350 minimum reinforcement ratio	141
Figure 6.11 Calculated maximum crack widths for walls that are designed based on ACI 350 minimum reinforcement ratio	142
Figure 6.12 Calculated maximum crack widths in walls with different heights	144
Figure 6.13 Calculated maximum crack widths in walls with different heights, non-linearity of the steel is included	144
Figure 6.14 Effect of wall length to height ratio on crack width	145
Figure 6.15 Effect of wall length to height ratio on crack width, non-linearity of the steel is included	145
Figure 6.16 Effect of variation of wall thickness on crack width	146
Figure 6.17 Effect of variation of wall thickness on crack width, non-linearity of the steel is included	147
Figure 6.18 Variation of crack width with different reinforcement ratios	149
Figure 6.19 Variation of crack width with different reinforcement ratios	150
Figure 6.20 Variation of crack width with different reinforcement ratios	151
Figure 6.21 Effect of increasing temperature and shrinkage strains on maximum crack width	152
Figure 6.22 Effect of increasing temperature and shrinkage strains on maximum crack width	152
Figure 6.23 Effect of increasing temperature and shrinkage strains on maximum crack width	153
Figure 6.24 Effect of increasing temperature and shrinkage strains on maximum crack width	153
Figure 6.25 Effect of increasing temperature and shrinkage strains on maximum crack width	154
Figure 6.26 Effect of increasing temperature and shrinkage strains on maximum crack width	154
Figure 6.27 Idealized design chart for temperature and shrinkage reinforcement	156
Figure A.2.1 Contour plot of longitudinal steel strains	

( $L = 7m, H = 4m, t = 300mm, \rho = 0.3\%, \varepsilon = 600 \times 10^{-6}$ )	A-1
Figure A.2.2 Contour plot of longitudinal steel strains	
( $L = 8m, H = 4m, t = 300mm, \rho = 0.3\%, \varepsilon = 600 \times 10^{-6}$ )	A-1
Figure A.2.3 Contour plot of longitudinal steel strains	
( $L = 6m, H = 4m, t = 300mm, \rho = 0.5\%, \varepsilon = 600 \times 10^{-6}$ ),	
formation of cracks with increasing wall length	A-2
Figure A.2.4 Contour plot of longitudinal steel strains	
( $L = 9m, H = 4m, t = 300mm, \rho = 0.5\%, \varepsilon = 600 \times 10^{-6}$ ),	
formation of cracks with increasing wall length	A-2
Figure A.2.5 Contour plot of longitudinal steel strains	
( $L = 12m, H = 4m, t = 300mm, \rho = 0.5\%, \varepsilon = 600 \times 10^{-6}$ ),	
formation of cracks with increasing wall length	A-3
Figure A.2.6 Contour plot of longitudinal steel strains	
( $L = 18m, H = 4m, t = 300mm, \rho = 0.5\%, \varepsilon = 600 \times 10^{-6}$ ),	
formation of cracks with increasing wall length	A-3
Figure A.2.7 Contour plot of longitudinal steel strains	
( $L = 24m, H = 4m, t = 300mm, \rho = 0.5\%, \varepsilon = 600 \times 10^{-6}$ ),	
formation of cracks with increasing wall length	A-3
Figure A.2.8 Contour plot of longitudinal steel strains	
( $L = 30m, H = 4m, t = 300mm, \rho = 0.5\%, \varepsilon = 600 \times 10^{-6}$ ),	
formation of cracks with increasing wall length	A-4
Figure A.2.9 Contour plot of longitudinal steel strains	
( $L = 60m, H = 4m, t = 300mm, \rho = 0.5\%, \varepsilon = 600 \times 10^{-6}$ ),	
formation of cracks with increasing wall length	A-4
Figure A.2.10 Contour plot of longitudinal steel strains	
( $L = 30m, H = 4m, t = 300mm, \rho = 0.5\%, \varepsilon = 0.00$ ),	
development of cracks with increasing volumetric deformation	A-5
Figure A.2.11 Contour plot of longitudinal steel strains	
( $L = 30m, H = 4m, t = 300mm, \rho = 0.5\%, \varepsilon = 75 \times 10^{-6}$ ),	

development of cracks with increasing volumetric deformation	A-5
Figure A.2.12 Contour plot of longitudinal steel strains ( $L = 30m$ , $H = 4m$ , $t = 300mm$ , $\rho = 0.5\%$ , $\varepsilon = 150 \times 10^{-6}$ ),	
development of cracks with increasing volumetric deformation	A-5
Figure A.2.13 Contour plot of longitudinal steel strains ( $L = 30m$ , $H = 4m$ , $t = 300mm$ , $\rho = 0.5\%$ , $\varepsilon = 225 \times 10^{-6}$ ),	
development of cracks with increasing volumetric deformation	A-6
Figure A.2.14 Contour plot of longitudinal steel strains ( $L = 30m$ , $H = 4m$ , $t = 300mm$ , $\rho = 0.5\%$ , $\varepsilon = 300 \times 10^{-6}$ ),	
development of cracks with increasing volumetric deformation	A-6
Figure A.2.15 Contour plot of longitudinal steel strains ( $L = 30m$ , $H = 4m$ , $t = 300mm$ , $\rho = 0.5\%$ , $\varepsilon = 375 \times 10^{-6}$ ),	
development of cracks with increasing volumetric deformation	A-6
Figure A.2.16 Contour plot of longitudinal steel strains ( $L = 30m$ , $H = 4m$ , $t = 300mm$ , $\rho = 0.5\%$ , $\varepsilon = 450 \times 10^{-6}$ ),	
development of cracks with increasing volumetric deformation	A-7
Figure A.2.17 Contour plot of longitudinal steel strains ( $L = 30m$ , $H = 4m$ , $t = 300mm$ , $\rho = 0.5\%$ , $\varepsilon = 525 \times 10^{-6}$ ),	
development of cracks with increasing volumetric deformation	A-7
Figure A.2.18 Contour plot of longitudinal steel strains ( $L = 30m$ , $H = 4m$ , $t = 300mm$ , $\rho = 0.5\%$ , $\varepsilon = 600 \times 10^{-6}$ ),	
development of cracks with increasing volumetric deformation	A-7
Figure A.2.19 Contour plot of longitudinal steel strains ( $L = 24m$ , $H = 4m$ , $t = 300mm$ , $\rho = 0.8\%$ , $\varepsilon = 600 \times 10^{-6}$ ),	
affect of high reinforcement ratio on crack formation	A-8
Figure A.1.20: Contour plot of longitudinal steel strains ( $L = 24m$ , $H = 4m$ , $t = 300mm$ , $\rho = 0.7\%$ , $\varepsilon = 600 \times 10^{-6}$ ),	
affect of high reinforcement ratio on crack formation	A-8

## **CHAPTER 1**

### **INTRODUCTION**

#### **1.1 Introduction**

Concrete is used as a structural material because it is economical and it is easy to fabricate in different forms. But, use of concrete is limited due to its brittle properties. Concrete cracks easily and that may have significant effects on structure in both short and long term. In concrete design and application, measures must be taken either to prevent or control crack formations. Deterioration mechanisms are initiated or accelerated by crack formation. Cracked concrete is susceptible to water penetration and any aggressive substances with water such as chloride and sulphate that either initiate or accelerate deterioration mechanisms in concrete. Crack formations influence durability, functionality and performance of the concrete structures. Reduced life span, reduced strength at later ages, increased porosity, and damaged aesthetic appearances are some consequences due to cracking. For these reasons, prevention or limitation of crack width in concrete is vital.

One of the reasons for crack formation is restrained volumetric change that starts after placing concrete. Just after placing, concrete materials exhibit volumetric changes due to temperature and moisture content variation. Volumetric changes continue as long as concrete is exposed to temperature and moisture content variation. Generally, the highest rate of volumetric deformation occurs during hardening period and this rate steadily decreases until the end of first year (ACI 207.1R-96). The primary reasons for volumetric deformations are temperature variation and change in moisture content. Both temperature and moisture content variations may cause expansion (swelling) as well as contraction (shrinkage) in concrete. Volumetric deformation of concrete is a particular concern when it is in the form of restrained contraction (shrinkage), (Figure 1.1). Even though change of volume may be invisibly small, its magnitude may be sufficient to cause crack in concrete.

Generally, the terms expansion and contraction are used to describe thermal deformation, while the terms swelling and shrinkage are used to describe volumetric deformation that results from moisture loss. Practically, expansion/swelling and contraction/shrinkage are

the same phenomenon, and single term could be used to refer either reduction of volume or increase in volume.

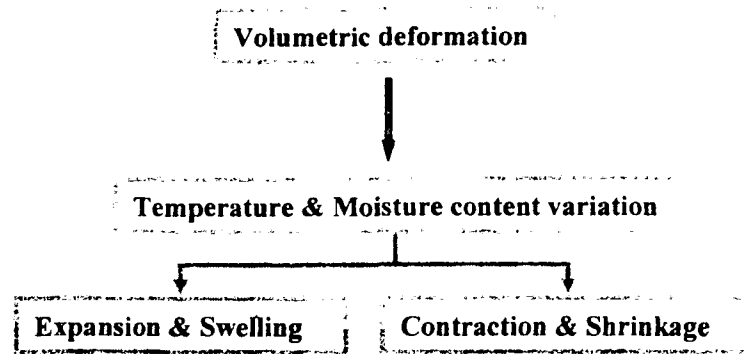


Figure 1.1: Types of volumetric deformation of concrete and primary reasons

Thermal deformation starts with hydration temperature. Exothermic nature of hydration reaction generates heat that causes increase of body temperature in concrete. Like most other natural materials, concrete expands due to increased body temperature in this first phase, (Figure 1.2). When rate of hydration starts to decrease, concrete temperature also decreases. Decrease in temperature continues until the structural body temperature reaches to ambient temperature level (Figure 1.2). At this second phase, concrete naturally contracts. When these two phases, expansion and contraction, are not restrained, deformation would be free and no stresses would develop. However, in reality all structural elements are restrained to certain degree and restrained volumetric deformations create stresses.

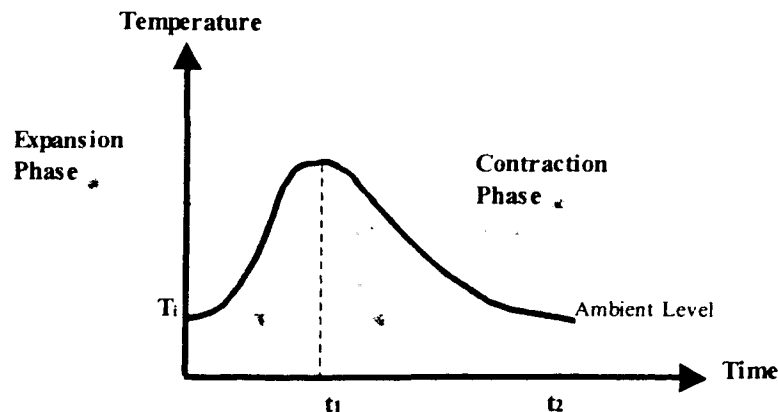


Figure 1.2: Typical temperature history of concrete after placing

Volumetric deformation that is caused by moisture content variation is more complex. Swelling is a rare phenomenon and it may occur when concrete is exposed to moisture. Shrinkage on the other hand can develop in various forms. Plastic, drying, chemical, and autogenous shrinkage mechanisms are primary shrinkage types. Plastic, chemical, and autogenous shrinkage are generally observed in early ages, while drying shrinkage occurs in relatively long term.

Full strength gain of concrete may take a long time. Shortly after placement, strength gain increases rapidly starting from almost zero stiffness. Approximately in a week, concrete reaches 60 to 70% of its full strength. While young concrete is at the first strength gain stage, restraint induced stresses may cause cracking. Generally, restraint induced stresses are well below the stresses that is caused by structural loads, but they may exceed the tensile strength of concrete. When restraint induced tensile stresses exceed tensile strength of concrete, cracks are inevitable. Depending on structural geometry, there are two types of restraint conditions. One of the restraint conditions occurs from the element itself, which is called internal restraint. Internal restraint is a common problem in thick sections, while external restraint exists in most structures. Internal restraint is caused by out-of-phase deformation of inner and outer parts of thick sections (Figure 1.3). During hydration period, temperature distribution in the section is not uniform. External faces are exposed to surroundings and heat generation rate is low, while inner section is insulated with outer concrete and has higher heat generation rate. Deviation of heat generation rate through the section and non-uniform heat conduction creates non-uniform temperature field and a thermal gradient occurs. Thermal gradient may be negligible when the section thickness is small, but increased thickness may increase thermal gradient significantly. Large thermal gradient can be observed particularly in massive concrete sections. During hydration, inner part of concrete that has higher temperature would try to expand more than the outer part. But expansion of inner part is restrained by outer concrete. This out-of-phase deformation (differential deflection) mechanism creates compressive stresses in inner part while creating tensile stresses in outer concrete. Surface cracks would develop when tensile stresses exceed tensile strength of surface concrete (Figure 1.3). This deformation mechanism is called internal restraint. After concrete reaches peak

temperature, second phase of deformation starts. In contraction phase, inner part of section contracts more than the outer part, which reverses the stress distribution through the entire section. In second phase, contracted inner part is under tension while compression stresses would develop in outer part. For this reason, the surface cracks that are formed during hydration are generally temporary and they tend to close when concrete reaches ambient temperature level.

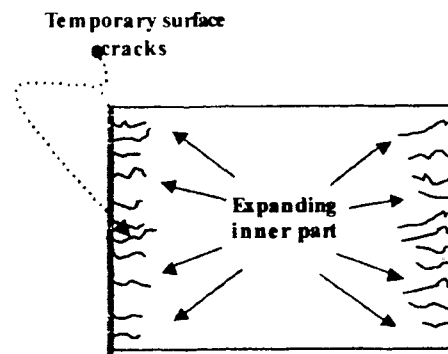


Figure 1.3: Typical internal restraint condition in a thick concrete element

More important and common form of restraint is external restraint condition. Unlike internal restraint case, cracks in external restraint condition are permanent and full depth cracks. External restraint occurs when there is differential deflection between newly cast elements and previously cast adjoining structure. Similar to internal restraint conditions, there are two phases of deformation in external restraint condition. In the first phase, new concrete would expand while this expansion is restrained by the interaction in contact face between new concrete and adjoining structural part. A typical case for external restraint condition is shown in Figure 1.4 that is a new wall cast on previously cast base slab. When the wall is expanding due to hydration temperature, compressive stresses would develop in most part of the wall while tensile stresses being generated in the base. In second phase, when the wall starts to contract, interaction between wall and the base would restraint contraction. Again, stress distribution is reversed and tensile stresses would develop in most part of the wall this time. At this stage, when generated tensile stresses exceed the tensile strength of concrete, full depth cracks would form. Typical full depth cracks (through cracks) formation in a restrained wall is shown in Figure 1.4.



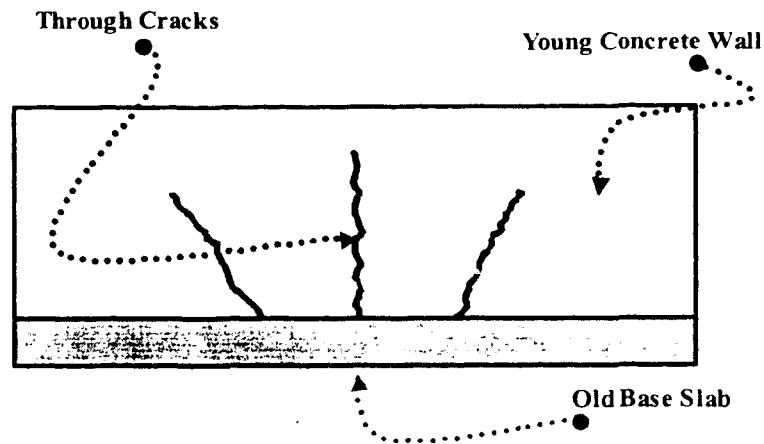


Figure 1.4: Typical external restraint condition, (new concrete wall is cast on previously cast base)

Obviously crack in concrete structures is always undesirable for many reasons. For many years, engineers have recognized effects of restrained volumetric deformation and resulting cracks; but the importance of the problem has been increased with development of concrete technology. Previously, early-age cracks that are caused by restraint deformation were referred as thermal cracks. But today, this term has become out of date. While durability aspect of concrete has become more of interest in recent years, designers started to use high performance concrete (HPC), which is proved to be more durable. In terms of performance and durability, advantages of HPC compared to traditional quality concrete may be undisputable, but there are some unfavorable properties of HPC. Chemical and autogenous deformations at early ages make HPC more sensitive to early-age cracks. Awareness of contribution of shrinkage in to early age crack risks is increased with new concrete technology. Therefore, to describe restraint deformation related cracks the term thermal cracking is not sufficient. In this thesis, the term volumetric changes are used to include all reasons for volumetric deformation during hardening and for hardened concrete.

Until recent years, crack controlling at early ages have been focused mainly on control of temperature of poured concrete. In the past, cracks were predicted from the calculated maximum temperature difference in structural elements. Prevention of cracking was

based on limitation of temperature difference between new and old element as well as within the element. Limits for temperature difference to be applied were developed based on practical and laboratory experiments. The main disadvantage of temperature based crack risk estimation is that only temperature change considered and other important parameters ignored. In reality, volumetric changes induced cracks are result of combination of temperature, shrinkage, material properties and restraint conditions. Regardless of temperature history, a structural element may crack when it is restrained while the other may not if it is free to deform. Therefore, restraint is a precondition for stress generation that may change for different structures according to their geometric properties. Another important parameter that influences crack formation is the material properties and its development in hardening concrete. In general case, compressive stresses are generated in the first phase of volumetric changes, which is the expansion phase. In contraction phase, tensile stresses are developed. Assuming that the material properties were constant, compressive stresses would compensate the tensile stresses and crack risks would be reduced significantly. However, in normal strength concrete, fresh concrete has very low modulus of elasticity and high relaxation. Accordingly, as it expands, creates very low compressive stresses. When concrete temperature cools down and contracts, it has high elastic modulus and that creates relatively high tensile stresses and increase crack risk. Compare to normal strength concrete, strength gain of HPC is very rapid during hardening. Higher elastic modulus during expansion phase may create relatively high compressive stresses and that may compensate part of tensile stresses during contraction. In practice, zero stress condition is assumed when concrete is at the peak temperature, which may overestimate tensile stresses particularly for HPC.

It is evident that material properties and restraint condition are important parameters on volumetric changes induced stress. Until recent years, due to practical reasons and lack of proper tools, design engineers considered only temperature in crack risk estimation. Today, development of computer technology and laboratory testing methods has improved understanding of concrete structures. Problems associated with volume changes of concrete can be minimized or solved more accurately by realistic analysis techniques. In this research, effect of volumetric changes on reinforced concrete is studied analytically by using the finite element method (FEM). The risks of crack formation are

investigated. Crack development and effects of reinforcement on crack width is analyzed with FEM.

## **1.2 Background**

Normally, concrete may crack either under structural loads or under restrained volumetric deformation. Because of the important role of volumetric deformation in crack formation, it has attracted significant interest for researchers. During the last decades, there has been extensive studies and publications within this field. Research institutes such as ACI, and RILEM have produced substantial publications and guidance for engineers to deal with temperature and shrinkage deformation and associated crack problems.

The problems associated with temperature and shrinkage has been addressed by ACI committees 207 and 209. ACI 209R (1992), ACI 207.1R (1996) and ACI 207.2R (1995) are three different reports that provide guidance for engineers to deal with problems associated temperature and shrinkage. Previously, it was thought that cracks due to temperature are a risk for only mass concrete (Andersen, 1998). But today, it is well known that, with new type concrete (HPC), temperature and shrinkage induced cracks can occur even in slender structures. ACI's reports were produced based on normal quality concrete. Crack risk prediction in construction process is mainly based on experiments. Although, in terms of design, ACI may provide practical approaches on prediction of crack risks, the simplicity and assumptions made cause poor correlation between the predictive analysis and actual measurement. ACI 207.2R (1995) discusses restraint volumetric deformation mainly for mass concrete. Some slender structures, such as walls, are also discussed in ACI 207.2R-95. ACI 224R (2001) is a design guideline for control of cracking in concrete structures. Although ACI 224R-01 discusses temperature and shrinkage cracks, it does not provide particular guide for reinforcement design. Temperature and shrinkage induced stresses are excessive particularly at early ages of concrete. Because of complexity of understanding early age concrete behavior, there were not sufficient publications until recent years. In Europe however, especially by RILEM contributions, substantial amount of studies have been dedicated to understand early-age concrete behavior and volumetric changes. In the following, studies on restraint

volumetric deformation, early-age concrete properties, and cracking of concrete are discussed.

In early 1980's, concrete mix designs evolved and applications of HPC became more popular. With this development, temperature and shrinkage problems became increasingly an interesting issue. In a case study, Liou (1999) showed that under certain conditions thermal stresses alone could be much larger than those caused by actual structural loads. A record size wall is constructed as part of Kawasaki Island in Japan. In the middle of Tokyo Bay, construction of 103 m diameter, 119 m deep and 2.8 m thick wall illustrates importance of hydration temperature and resulting stresses. Recorded data indicate that thermal stresses could be more important than soil and water pressure exerted from outside the wall. Considering the fact that such wall may crack not because of huge external loads but just because of internal hydration temperature, it is not surprising that in recent years design codes pays more attention to temperature load.

The report published by CIRIA (Harrison, 1981) responded to demand for general guide to deal with temperature problem. Harrison described restraint strain as product of the coefficient of thermal expansion, total temperature change during the hydration, and restraint factor. It is stated that if restrained strain exceeds the tensile strain capacity of concrete, cracks would occur. Harrison described young concrete properties and discussed parameters involved in restraint-induced stresses. It was shown that by taking appropriate measures during the design and construction process, early-age thermal strains could be reduced. Harrison presented values for coefficient of thermal expansion for different concrete mixes with different type of aggregate content. Based on experimental observations, maximum change in temperature and parameters involved in temperature development presented in a classical way. Harrison described types of restraint conditions, degrees of restraint for a simple case, and the resulting cracks. Mix proportion to optimize temperature development, concrete placing temperature, influence of formwork, influence of construction sequence, provision of movement joints, and crack control with reinforcement was discussed in this report. CIRIA report did not include effect of strength development of concrete, and shrinkage phenomenon.

Incremental numerical analysis technique may be used for realistic simulation of early-age concrete behaviour. Truman, et al. (1991) implemented incremental numerical

analysis technique on a mass-concrete structure. It was shown that realistic simulation method could be used to optimize construction procedure, which may result remarkable saving in cost. In massive concrete structures significant amount of temperature may develop within the section. Excessive thermal gradient may create excessive tensile stress and eventually form cracks. For this reason, these types of structures are constructed in sequences that would allow dissipation of hydration temperature. Minimizing the number of lifts for construction may result significant amount of savings in the cost. Determination of number of lifts requires heat transfer and stress analysis. Truman, et al. performed Finite Element (FE) heat transfer analysis for a dam construction to determine temperature history of concrete. Using an experimental material model and calculated temperature history, stress analysis was performed. The material model used in the stress analysis was developed based on experiments. However, instead of experimental material model, an analytical method could be used for complete simulation of hardening concrete. Material model can be prepared from temperature history of structure since concrete properties can be described as function of time and temperature.

Branco et al. (1992) published a similar study that uses incremental analysis technique. Based on test results, concrete heat of hydration characteristics were determined. The produced data implemented in numerical temperature analysis that considered both environmental interaction and concreting phases. Calculated temperature values used in a three-dimensional finite element formulation to compute the stress distribution. For material modeling, linear elastic behaviour was assumed for concrete. Branco et al. ignored shrinkage and creep effects during computer simulation. Although researchers have used an advance analysis technique, material modeling that implemented can be improved to be more realistic. Consideration of non-linear behaviour of reinforced concrete is essential particularly under tensile loads. Also, it is known that shrinkage due to moisture loss may cause higher volumetric deformation and should not be neglected. Another shortcoming of this study as in Truman et al. (1991) paper is that test results were used for determination of strength development instead of equivalent age approach. However, it is worth to mention that Branco et al. (1992) used an analytical method to determine temperature history of concrete. A detailed model is given for surface environmental interaction in heat transfer analysis that will be explained in Chapter 2.

It is a common approach to estimate crack risks based on the magnitude of temperature differences either within the cast section or between sections cast in different stages. Emborg and Bernander (1994) criticized current design codes that estimates crack risks based on temperature differences. It was suggested that restraint condition and material properties are as important as temperature in stress generation. Most important parameters involved in early age stress development are temperature in the element, temperature of adjoining structure, material mechanical properties, and the restraint condition. Emborg and Bernander showed that temperature differences provide only general information about the risk of early-age cracking. A material model developed by Emborg and Bernander to represent early-age concrete that consist of three elements (viscoelastic, fracture behaviour and thermal displacement). Researchers used one-dimensional FEM in stress analysis that allowed assigning different temperature and mechanical properties to each element. Results of an example problem showed the difference between temperature based and proposed material model may vary significantly. In proposed material model by Emborg and Bernander, incremental total strain was described as sum of thermal, fracturing, elastic and creep strain. This model does not include shrinkage strains. This is because authors have considered only thermal strains and not total early-age strains. Presently, concrete mix designs require additional shrinkage parameter in total strain calculation. Unlike previous studies, all the mechanical properties were modeled on the basis of maturity (equivalent age) development. Modeling concrete properties based on its equivalent age provides analytical technique that will be discussed in Chapter 3.

With progress of numerical analysis technique, cracking of concrete is modeled by smeared crack approach that is originated in decomposition of the strain tensor into concrete strain and cracking strain. Smeared crack model includes cracking strain in deformability. Borst and Boogaard (1994) paper included effect of cracking strain in numerical analysis of early-age concrete by FE software DIANA. Numerical strategies for deformational and fracture behaviour of early-age concrete was presented. Total deformation model is modified via replacement of fracture strain by smeared crack strain. Tensile strength development is one of the key parameters in material modeling. But in Borst and Boogaard's paper it was assumed to be constant.

Saetta et al. (1995) summarized the FE formulations for heat transfer and stress displacement analysis of concrete structures exposed to variable thermal loads. However, as in classical way, the study did not include mechanical properties and restraint effect on thermal stresses.

Ayotte et al. (1997) used the FE software ADINA to simulate thermal deformation of a mass concrete element. Measurements were taken from a mass-scale structure and computer simulation was compared with this data. Comparison of calculated and measured data showed good agreement. However, the number of assumption made during the simulation may be regarded as unrealistic. Material strength development was determined by experiments rather than equivalent age concept. Non-linear behaviour of concrete and shrinkage properties was neglected. It is common technique to model creep behaviour of concrete in numerical analysis by effective elastic modulus concept. They used modified elastic modulus to include creep effect in FE analysis.

Baetens et al. (2002) emphasised the importance of computer tool in analysis of early-age concrete. In recent years, special computer programs such as DIANA, HEAT, and FEMMASSE are developed particularly to deal with early age concrete problems. Huang (1999) simulated early age concrete with FE software TEC-PLOT to study the internal restraint and crack formation. It was suggested that internal restraint condition might cause cracks not only for thick sections but in slender structures as well. Bosnjak and Kanstad (2001) performed simulation of a structure to compare with experimental measures. During construction of a culvert structure in Oslo, temperature and strain development in different part of the structure were measured. Using FE software DIANA, stress history of concrete was analyzed. It is very noticeable that improvement of studies in early-age concrete simulation is parallel to the advancement on numerical analysis tool. Bosnjak and Kanstad (2001) used DIANA in simulation that is particularly powerful in simulation of hardening concrete. But surprisingly, effect of reinforcement is ignored in this study.

In this thesis, the computer program ABAQUS/6.4 will be used as FE tool. Although ABAQUS/6.4 does not provide options to simulate hardening concrete, it is possible to analyse reinforced concrete. Providing detailed input data, and implementing incremental

analysis technique, ABAQUS/6.4 can also simulate hardening concrete that will be discussed in Chapter 4.

Andersen (1998) presented a complete review of the methods that can be taken to prevent early-age cracks. Requirements to prevent cracking based on temperature differences, allowable strain, and allowable stresses were explained. It was suggested that temperature based requirements is most practical and applicable during construction. Limiting thermal gradient in concrete element is a classical technique that has been part of codes and standards for a long time.

Elbadry and Ghali (1995), addresses thermal load effect on prestressed concrete elements. It is suggested that thermal loads to be considered in design process can be as high as live loads. Including thermal loads in design of prestressed elements may require high level of prestressing since the design criteria is zero tensile stress. However, high prestressing is not preferable because it increases cost in addition to losses that result from high creep and can produce excessive camber. Elbadry and Ghali suggest that partial prestressing may be more beneficial that allows cracking. In partial prestressed elements reinforcement can be used to control crack width. Obviously hydration temperature is not the concern in prestressed structures since the prestresses are applied after most of the hydration process is completed. Also, prestressed elements generally have well designed expansion joints, which eliminates external restraint and consequent cracks. However, thermal gradient may develop due to surrounding temperature variation in thick sections that are under service conditions. Therefore, internal restraint may be a concern in designing of prestressed concrete. Elbadry and Ghali suggested that the designer has to decide whether partial prestressing is beneficial or not when the internal restraint creates crack risk. Vitharana et al. (1998, 1999) discussed similar problem for reservoir walls. After crack formation, significant reduction of thermal stresses was observed. The reason for stress reduction is similar to the bridge girders. Relaxation of structure should be anticipated since cracking of concrete eliminates or reduces restraint effect.

Vitharana et al. (1998, 1999) reported that concrete tensile strength that is subjected to thermal and service loads, is much lower than those recommended in design codes. This may be explained by effect of rate of loading on specimens. Chantelois et al. (1999)



observations on several experiments have shown that thermal load rate has significant effect on crack formation. Tensile strength can be reached easily and create cracks when the loading rate is high. It was observed that during fast loading a thermal difference of 18 °C was sufficient to form cracks while 30 °C thermal difference was required to form cracks in slow rate loading. Concrete wall specimens subjected to severe thermal loads were tested. It was observed that strength increases in low temperature while expansion coefficient decreases. Creep coefficient of 0.35 is suggested for mature concrete subjected to thermal loads.

Mitchell et al. (1998) reported results of experimental study on hardened concrete properties. Concrete specimens with strength of 30, 70, and 100 MPa were tested. Development of temperature rise in adiabatic conditions, specific heat, thermal conductivity, coefficient of thermal expansion, compressive strength, modulus of elasticity, and tensile strength was observed. Strength development under different curing conditions was compared. Creep and shrinkage behaviours were examined and experimental study was compared with code predictions. It was shown that CEB-FIP model had good agreement with experiments.

Restraint factor for base fixed walls that are recommended by ACI 207.2R-95 are developed based on Carlson and Reading's (1988) experimental study. They determined the degree of restraint in walls by using rubber models in experiments to simulate shrinkage of concrete walls. Rubber has good and well-known elastic properties, which provides simplicity, but it can only represent elastic range of concrete material. Several mortar model experiments were also conducted to confirm the finding from the rubber models. In experiments, it was shown that the calculated restraint factor could be used in actual concrete design.

Kheder et al. (1994) and Kheder (1997) studied the base restraint walls that are exposed to volumetric changes. They showed that geometric properties of wall are important parameters on restraint factor that generates stresses. Full-scale reinforced concrete walls were monitored during experiments. Authors mention that there is a relation between geometric properties and crack formation, which indicates effect of degree of restraint. Numerical analysis was performed to determine approximate variation of degree of restraint. It was suggested that reinforcement could be used effectively based on

calculated degree of restraint. Effective reinforcement concept is the distribution of reinforcement based on the magnitude of stresses.

In determination of temperature rise in concrete and consequent stresses, the rate and total quantity of heat evolved play an essential role. Lu et al. (2000) conducted experiments to determine characteristics of temperature rise in concrete during hydration reaction. It is very common in literature to see use of Arrhenius Law in determination of hydration heat rate. Lu et al. proposed a more practical way for determination of heat rate that is not less realistic than conventional methods. Arrhenius Law contains a number of parameters that are selected based on adiabatic temperature rise of concrete. Profile of adiabatic curve directly related to the concrete mix and reflects its characteristics. Lu et al. suggest that the rate and total quantity of heat evolved during the hydration could be estimated directly from adiabatic curve. Numerical analysis was performed for determination of degree of internal restraint that is the ratio of restrained strain to free strain. Previously, Harrison (1981) and Andersen (1998) had discussed limiting thermal gradient to prevent internal restraint cracks. Anderson mentions that it is common to limit maximum temperature difference between internal and external part of the concrete to 20 °C. Lu et al. used 20°C difference to calculate internal degree of restraint, which is found to be 0.36. This value is similar to Harrison's recommendations, which is based on European codes. The difference in Lu et al. study is that degree of restraint was determined as function of creep, shrinkage and thermal strains.

Cusson and Repette (2000) investigated reasons for early age cracks on a bridge barrier wall that is constructed by HPC. Assuming linear material behaviour, numerical analysis was performed that included effects of reinforcement on degree of restraint. It was shown that degree of external restraint does not change through the depth of section and reinforcement slightly increases degree of restraint. Calculated variation of degree of restraint in a base fixed wall showed that ACI 207.2R-95 formulation might underestimate restraint for reinforced concrete. It was suggested that using HPC for secondary structural members such as barrier wall is not necessary and may have disadvantages in terms of durability. Excessive autogenous shrinkage and high hydration heat capacity of HPC increases crack risks significantly.

Generally, in design codes minimum reinforcement requirements for crack control are based on one-dimensional conceptual approach. Pettersson and Thelandersson (2001) suggested that this might cause over estimation of reinforcement. Results of linear elastic numerical analysis of a reinforced concrete walls have shown that crack spacing is also controlled by external restraint. In fact, Kheder (1997) had observed this in experimental study. External restraint acts as reinforcement and limits crack spacing. Even if reinforcement is not used, crack width is limited due to certain crack spacing. Reduced crack spacing would require less reinforcement to limit crack width. Pettersson and Thelandersson performed two-dimensional FE analysis for mature reinforced concrete wall that is externally restrained. Critical total volume change that may cause cracks was calculated. It was seen that effect of reinforcement in stress development might be disregarded as it is acting after crack formation. Relation between reinforcement ratio, crack width and critical volume change was searched. A formulation to determine crack width that is developed based on one-dimensional spring element was proposed. Pettersson and Thelandersson suggest that design code requirements might be conservative in estimation of required reinforcement. However, Pettersson and Thelandersson's critic on design codes may not be correct for ACI 318 (2002) and ACI 350 (2001). ACI 318-02 and ACI 350-01 requirements for minimum temperature and shrinkage reinforcement are shown in Tables 6.1 and 6.2. Maximum reinforcement ratio in ACI 350-01 specification is 0.6%. To keep the crack width in allowable range, Kheder (1997) and Gilbert (1992) mentions that required reinforcement ratio may exceed 1%. It is also mentioned in ACI 224R-01 that 0.18 to 0.20% reinforcement ratio may not keep crack width in acceptable level. Interestingly, ACI 318-02 recommendation for minimum reinforcement ratio ranges between 0.18 to 0.20%. This comparison may raise a question whether ACI codes underestimate required temperature and shrinkage reinforcement ratio rather than being conservative. In fact, according to Gilbert, compared to ACI, Australian code AS 3600-1988 requirement is much more conservative. In any case, it is difficult to say whether codes are conservative or underestimate the required reinforcement. The required reinforcement ratio to control crack totally depends on restraint induced stresses, which is almost totally random for each structure.

Temperature and shrinkage reinforcement design is based on the estimated crack width. Considering the allowable crack width, the amount of reinforcement may be determined. To predict crack width, the design codes such as ACI and CEB-FIP offers formulations. ACI crack prediction equation is developed from Gergely-Lutz model. In addition to Gergely-Lutz model, 1999 version of ACI 318 included a new crack prediction equation that is proposed by Frosch (1999). Gilbert (1992) also proposed a model to estimate crack width for fully restrained concrete members subjected to shrinkage strains. Although it was shown that estimated crack widths based on the proposed model showed good agreement with Australian code, Gilbert's model is not practical to use in design. Major crack prediction equations involve the steel stress/strain in calculations. In practice, it is difficult to estimate the exact stress/strain in reinforcing steel. For this reason, both ACI and CEB-FIP codes allows approximation when predicting the crack width. However, the FEM may be used to calculate steel stress/strain, which will be discussed in Chapter 6.

In recent years, with the development of HPC, conventional techniques to calculate concrete properties have become more questionable. Therefore, recent studies are trying to develop new mathematical models to calculate concrete properties such as creep, shrinkage, and activation energy of concrete hydration. Huo et al. (2001) proposed a modified version of ACI 209R (1992) formulations for creep and shrinkage and suggested that it is more reliable for HPC. Oh and Cha (2003) developed a different approach for calculation of degree of hydration that includes moisture effect in hydration reaction. Presently, degree of hydration is calculated based on the temperature history, but Oh and Cha's mathematical model includes temperature history as well as moisture distribution. Finally, Schindler (2004) questioned the value of activation energy that is a parameter in equivalent age calculation. Currently, an approximation is recommended in literature and in design codes (CEB-FIP). However activation energy may vary for different concrete mixes that affects temperature development.

### **1.3 Objective**

This research focuses on understanding of reinforced concrete structures behaviour that is subjected to volumetric deformations. The goal is to contribute to the improvement of concrete technology and suggest practical design guide for engineers. The main objective

is to determine the required amount of reinforcement to control shrinkage and temperature cracks.

Particular aims of this study are as follows:

- To study the restrained volumetric deformations, material properties, restraint factor.
- To carry out a realistic simulation of reinforced concrete structure that is subjected to volumetric deformation and predict stress/strain history.
- To study hydration temperature, shrinkage and time dependent material properties.
- To study temperature and shrinkage cracks, and estimate the minimum amount of reinforcement for crack control.
- To expand the recommendations given by design guides for required amount of reinforcement.

#### **1.4 Organization**

The entire work in this thesis is presented in seven chapters. Introduction, literature review, and objectives are presented in Chapter 1. Volumetric deformations and restraint conditions are described in introduction. Effects of temperature and shrinkage strains on cracks development is also explained in Introduction. Literature review is given under the Background section.

Chapters 2, 3 and 4 present the methods on estimating temperature and shrinkage induced stresses. In Chapter 2, determination of temperature history using the FEM is described. Time dependent material properties are discussed in Chapter 3. Based on code formulations, estimation of shrinkage strains is shown in the same chapter. Chapter 4 describes the stress-displacement analysis of maturing reinforced concrete using ABAQUS/6.4. Concrete modeling using the FEM, and an example simulation to predict stress/strain history is presented in Chapter 4.

The restraint factor for base fixed reinforced concrete walls is studied. This is discussed in Chapter 5. The restraint factor is calculated for various walls and the results are compared with those design guidelines.

In Chapter 6, the code requirements for temperature and shrinkage reinforcement is discussed. Conceptual models and equations to predict crack width are discussed. Estimating crack width using the FE analysis is shown in same Chapter. Parametric study is conducted on various dimensional walls in order to determine the required amount of reinforcement ratio. Based on allowable crack width and results of parametric study, the required amount of temperature and shrinkage reinforcement ratios are presented in Chapter 6.

Chapter 7 concludes the work presented. Suggestions for further studies in this field are provided. Examples of input files for computer simulations are listed in Appendix A.

## CHAPTER 2

### HYDRATION TEMPERATURE

#### 2.1 Introduction

The main factor that leads to deformation and consequent stress development at early ages is the hydration temperature. Because of the exothermic behavior of the hydration, reaction there would be heat generation and thermal gradient within the concrete. Within few days after casting, concrete body temperature would decrease to ambient temperature. During this process, just like most of any other natural materials, concrete would undergo bulk volume change.

For hardened concrete, amount of temperature induced volume changes is simply product of temperature and thermal expansion coefficient. However, neither of parameters involved are constant during early ages of concrete. Especially significant variation of concrete temperature increases complexity of the problem.

Even though the key parameter that converts temperature into strain is the coefficient of thermal expansion, it is relatively constant at early ages. Before setting of concrete, in the first 8 to 16 hours, concrete may have high expansion coefficient due to dominant water phase of fresh concrete. But after setting, concrete expansion coefficient drops to about  $10 \times 10^{-6} / ^\circ\text{C}$  and becomes more stable. On the other hand, exact temperature of concrete and its variation at any given time depends on many variables. It is a necessity to know the exact deformation due to temperature for stress analysis. But to calculate the exact deformation, it is essential to know the temperature at any given time. Hydration temperature depends on the quantity of heat energy during hydration. Amount of heat energy that is gained or lost depends on size of the member, its geometry and exposure conditions. On the other hand, heat generation rate and its magnitude depend on amount of cement, supplementary cementing materials, fineness of cementing material and temperature during hydration. Number of parameters that involved in temperature history makes it very difficult to predict the exact temperature over the time.

Determination of temperature history is not only required to calculate thermally induced volumetric changes, but it is also an essential base to estimate concrete strength development that is necessary to assess induced stress at early ages. There are several

reasons that may cause stress in concrete at early ages. Primary concern at this stage is restrained induced stresses. But there might be additional early age stresses because of form removal or prestressing as well. To find the effect of forces at early age of concrete, the strength at that age need to be determined.

Strength development and concrete mechanical properties are directly related to its temperature history. Firstly, temperature history needs to be determined in order to estimate strength development that is required for early age stress analysis. Calculated temperature history can be used to estimate time dependent material properties as well as temperature induced stresses.

## 2.2 Time Dependent Temperature Distribution Analysis

Temperature development of hardening concrete is generally described by Fourier's law. According to Fourier's law, temperature distribution of a body is a dynamic heat balance between internal and external energy sources. From this basic principle of energy balance, it is evident that sum of heat generated inside the body of concrete structure plus heat gain or losses from the boundaries must be equal to temperature distribution. Widely known Fourier's law of temperature distribution of a cross section for a homogeneous and isotropic material is expressed as follows (Mitchell et al. 1998):

$$k \left( \frac{\partial^2 T}{\partial x^2} + \frac{\partial^2 T}{\partial y^2} + \frac{\partial^2 T}{\partial z^2} \right) + Q = \rho c \frac{\partial T}{\partial t} \quad (2.1)$$

where,

$k$  = thermal conductivity,  $W / m^{\circ}C$

$Q$  = rate of heat generated inside the body,  $W / m^3$

$\rho$  = density of material,  $kg / m^3$

$c$  = specific heat of material,  $J / (kg^{\circ}C)$

$T$  = temperature,  $^{\circ}C$

$t$  = time, sec



The terms that are on the left side of Eq.2.1 represents the boundary conditions, and the right side of this differential equation is the primary unknown with its coefficient parameters. For a simple structural geometry, the solution of Eq.2.1 can be found by one of variational methods, providing that thermal conductivity, specific heat and density of material are known. However, the smallest complexity of the geometric shape may require FEM in order to find temperature distribution. Obviously the scale of problems always requires massive computation and an advanced computer program is required to find the solution of Eq.2.1.

### **2.3 Thermal Properties**

Thermal properties of concrete that need to be specified to solve Eq.2.1 are thermal conductivity and specific heat. Thermal expansion coefficient is another thermal properties of material, which is considered in stress displacement analysis. In following brief description of specific heat and thermal conductivity will be given. Thermal expansion coefficient will be described in Chapter 4.

#### **2.3.1 Specific Heat of Concrete**

Specific heat is defined as the amount of heat energy required to increase temperature of a unit mass of material by one degree. Since concrete is a composition of several components, its specific heat depends on these components. For example, specific heat of water is 4.18 J/g.°C, whereas the specific heat of aggregate and cement is about 0.9 and 0.75 J/g.°C respectively. Therefore, value of concrete specific heat depends on water's, aggregate and cement's specific heat.

During early ages, similar to other properties of concrete, specific heat of concrete also changes during hydration process. The primary reason for variation of specific heat of young concrete is the significant variation of moisture content present in the body. Reduction of moisture content during the hydration process reduces its specific heat.

Although amount of specific heat of saturated concrete may change significantly with changing temperature, for dry concrete it is relatively stable when temperature changes. Because of technical difficulties of measuring specific heat of hardening concrete, it is generally measured on mature concrete at different temperature. Figure 2.1 shows

variation of specific heat at different temperature that is taken from test of mature concrete.

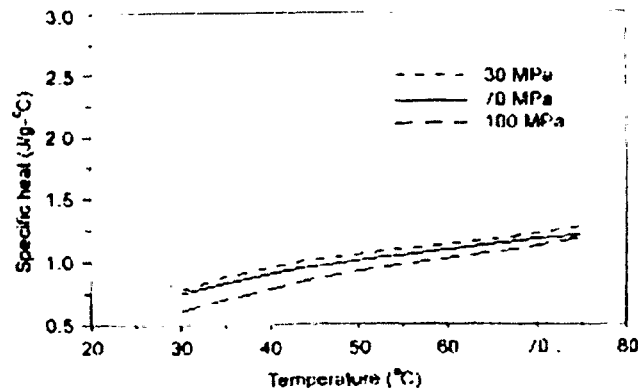


Figure 2.1: Variation of specific heat of oven-dried concretes with temperature (Mitchell et al. 1998)

The value of specific heat of concrete in heat transfer analysis is generally assumed to be about 1.0 J/g-°C. But this value may change slightly according to its content and its temperature.

### 2.3.2 Thermal Conductivity of Concrete

Thermal conductivity can be defined as the rate of heat flow through a unit area of a material under a unit temperature gradient. Thermal conductivity is measured in joules per second per square meter of area of a body, when the temperature difference is 1°C per meter of thickness of the body. Conductivity of concrete depends on moisture conditions, type and amount of aggregate, porosity, and density of material.

Thermal conductivity of hardened concrete ranges generally between 1.4 and 3.6 W/m°C (Neville, 1995). Mitchell et al. (1998) reported that thermal conductivity is relatively constant at different temperature level. Table 2.1 shows change of thermal conductivity at variable temperature. Observation of this table indicates that in hardening process, thermal conductivity is stable particularly for high strength concrete and does not change significantly even for normal strength concrete.

Table 2.1: Thermal conductivity of three concrete mixes for various temperatures (Mitchell et al., 1998)

Concrete Strength (MPa)	Density (kg/m <sup>3</sup> )	Hardened Concrete		Maturing Concrete	
		Temperature (°C)	Conductivity (W/m°C)	Temperature (°C)	Conductivity (W/m°C)
30	2130	25	1.17	28	1.72
		37	1.14	31	1.74
70	2419	27.5	1.59	—	—
100	2505	26	1.77	—	—
		73	1.77	22	1.8
		82	1.65	—	—

## 2.4 Boundaries for Heat Transfer Analysis

For the solution of Eq.2.1, heat boundary conditions must be defined, which also may change at different time intervals and for variable temperature. Generally speaking, for concrete structures, the heat exchange between the concrete body and its surroundings may be in the form of solar radiation, thermal radiation, and convection. Heat gain is primarily due to exothermic hydration reaction that defines part of the boundary condition for Eq.2.1. Heat exchange or losses may be result of numerous factors: Geographical location, orientation, altitude, atmospheric conditions, time of the day, day of the year, solar radiation absorptivity of the surface, color and texture of the surface material, surrounding air movement, wind speed, temperature difference between the concrete and air, heat radiation emission by the concrete body, form characteristics, contact surface to adjoining structures would determine amount of convection heat transfer, solar and thermal radiation. Energy transfer or environmental interaction that determines boundary conditions of Fourier's law may be expressed as follows (Branco et al., 1992):

$$q = q_c + q_r + q_s \quad (2.2)$$

where,

$q$  = rate of energy transferred between the boundary and the environment per unit area, W/m<sup>2</sup>

$q_c$  = energy transfer due to convection

$q_r$  = energy transfer due to thermal radiation

$q_s$  = energy transfer due to solar radiation

Heat transfer due to convection,  $q_c$ , is a parameter of movement of air particles, and the difference between air and surface temperature. Branco et al. showed this relation by Newton's law that is shown in following:

$$q_c = h_c (T_s - T_{air}) \quad (2.3)$$

where,

$h_c$  = convection heat transfer coefficient,  $W/(m^2 \cdot ^\circ C)$

$T_s$  = surface temperature of the structure,  $^\circ C$

$T_{air}$  = air temperature,  $^\circ C$

The value of convection heat transfer coefficient,  $h_c$ , depends on many factors and it is usually determined experimentally. Branco et al. used an empirical equation to determine convection coefficient as follows:

$$h_c = h_n + h_f \quad (2.4)$$

where,

$h_n$  = coefficient that is a function of surface roughness (average value is  $6 \text{ W/m}^2 \text{ }^\circ C$  for concrete)

$h_f$  = coefficient that is a function of wind speed (average value is  $h_f = 3.7v \text{ W/m}^2 \text{ }^\circ C$ , where " $v$ ", m/sec, is the wind speed)

Heat transfer due to thermal irradiation,  $q_r$ , is expressed similar to convection and it is shown in following, which is simplified form of Stefan-Boltzmann law (Branco et al., 1992).

$$q_r = h_r (T_s - T_{air}) \quad (2.5)$$

where,

$h_r$  = Coefficient of irradiation ( $\text{W/m}^2 \text{ } ^\circ\text{C}$ ). It depends on surface temperature, concrete emissivity, and the Stefan-Boltzmann constant, ( $5.68 \times 10^{-8} \text{ W/m}^2 \text{K}^4$ )

Approximate estimation of coefficient of thermal irradiation is expressed as follows (Branco et al., 1992):

$$h_r = \varepsilon \left[ 4.8 + 0.075(T_{air} - 5) \right] \quad (2.6)$$

where,

$\varepsilon$  = concrete emissivity, ( $0 \leq \varepsilon \leq 1$ )

Heat absorption due to solar radiation,  $q_s$ , is affected by time of day and year, latitude and altitude of the structure, and cloudiness of the sky. An approximate expression for solar radiation is given in following (Branco et al., 1992):

$$q_s = a \left( I_d \sin \theta + I_i \frac{1 + \cos \gamma}{2} \right) \quad (2.7)$$

where,

$a$  = absorptivity coefficient of the surface material, ( $0 \leq a \leq 1$ )

$I_d$  and  $I_i$  are direct and indirect solar radiation.

$\theta$  is the incidence angle of the radiation in the structure surface elements, and  $\gamma$  is their inclination.

Equations 2.2 to 2.7 are approximated and empirical expressions. But, they can be used to define heat transfer boundary conditions in an analytical way. Generally, it is difficult to determine values for involved parameters. Detailed information about field conditions is necessary to model boundary conditions in analytical method. In most cases, field data is not available. For this reason, it is common to perform heat transfer analysis in a simplified way and then calibrate the resulting temperature field. Based on field temperature data, calibration of computer model is necessary for different structures to reach a reasonably accurate solution.

## 2.5 Heat of Hydration

In Eq.2.1, “ $Q$ ” represents the body heat flux or the rate of heat generated during hydration inside the structure. For determination of hydration heat flux in a concrete element, the generated heat per volume unit is of interest. Hydration of Portland cement is an exothermal process that may release up to 500 Joules of heat per gram of cement (Neville, 1995). Total heat of hydration of a particular mix depends on cement type and content. Accurate amount of heat release for particular cement can be determined in lab tests. Based on lab data, the generated heat per mass unit of cement can be multiplied by the cement content to find total heat energy to be released.

Increase in temperature of an object is proportional to energy put in to it. This basic law is expressed as in following equation, which is the fundamental form of Eq.2.1.

$$\Delta T = \frac{q}{c \cdot \rho} \quad (2.8)$$

where,

$\Delta T$  = Increase in temperature of an object, °C

$q$  = amount of heat put in to object, *joule*

$c$  = specific heat, *joule/(m.°C)*

$\rho$  = density, *kg / m<sup>3</sup>*

To find temperature variation history of an object by Eq.2.8, time derivative of heat energy must be known and that is the heat generation rate. In adiabatic conditions; concrete element temperature due to hydration reaction at a particular time depends on the hydration reaction rate. And the reaction rate depends on total heat already released, fineness of cement and temperature of concrete during hydration reaction. Determination of hydration rate requires a temperature function that can be used to model temperature development. Aloia (2002) explained Arrhenious Law (Eq.2.9), which is a common temperature function. Arrhenious law is basically allows to describe basic kinetics of chemical reactions. Providing that reaction activation energy, proportionality constant

and initial temperature are known, the rate of heat in concrete hydration process can be determined as follows (Aloia, 2002):

$$K(T) = A \exp\left(-\frac{E_a}{RT}\right) \quad (2.9)$$

$K(T)$  = Rate of a particular temperature

$A$  = Proportionality constant, 1/s

$E_a$  = Apparent activation energy of concrete, J/mol

$R$  = Gas constant, 8.314 J/(molK)

$T$  = Temperature, °C

Parameters involved in Eq.2.9 may change for each different concrete mix. Providing that the test results on adiabatic temperature rise are available, proportionality constant and apparent activation energy for each mix can be determined. Determination of concrete temperature due to cement hydration reaction by using a temperature function as in Eq.2.9 is essentially an approximation because hydration involves several simultaneous and interdependent chemical reactions. Application of Arrhenious law to estimate hydration rate requires temperature history of concrete during hydration and accurate value of activation energy. Apparent activation energy and proportionality constant can be derived from the field temperature history and adiabatic temperature raise data. This would provide estimation of hydration rate. However, in incremental numerical analysis, a temperature function is not necessary to determine the heat rate. Figure 2.2 shows temperature development of different mix concretes in adiabatic conditions. Rate of temperature-increase varies because the rate of heat release changes during hydration.

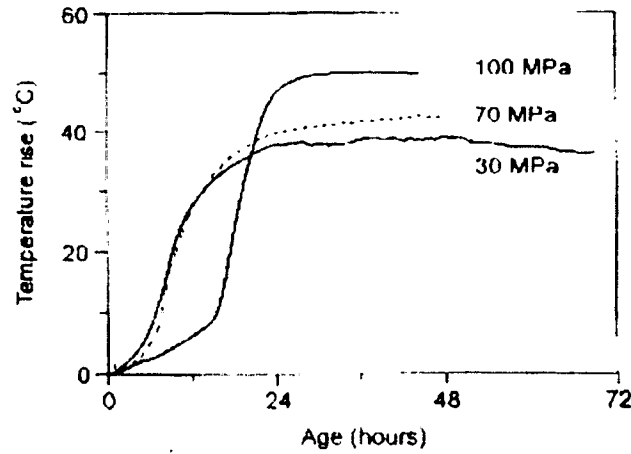


Figure 2.2: Temperature rises of 30, 70, and 100 MPa concrete during temperature matched curing (Mitchell et al., 1998)

FE program ABAQUS/6.4 (Hibbitt et al., 2004) provides option of incremental analysis, which is very convenient to model hydration heat rate when the adiabatic curve is known. Truman et al. (1991) used a simple equation to model the heat rate in incremental numerical analysis. Following equation and an adiabatic temperature rise data of a particular concrete (Figure 2.2) can be implemented in any incremental analysis to calculate the heat of hydration (Truman et al., 1991).

$$Q = \frac{c \rho \Delta T}{\Delta t} \quad (2.10)$$

where,

$Q$  = heat of hydration, J

$c$  = specific heat, joule/(m.°C)

$\rho$  = density, kg / m<sup>3</sup>

$\Delta T$  = the change in temperature, °C

$\Delta t$  = the change in time, sec



Eq.2.10 is a modification of Eq.2.8 that accounts for differentiation of temperature over the time. From adiabatic temperature rise,  $\Delta T$  and  $\Delta t$  can be easily determined and then hydration heat can be calculated for each time increment.

Amount of total generated heat in concrete element is a product of amount of cement content in the element and generated heat per mass unit of cement. Providing that specific heat, density and generated heat per mass unit of cement are known, adiabatic temperature rise can be estimated from Eq.2.8.

For example; consider 1 m<sup>3</sup> of concrete with specific heat of 1000 J/kg°C and density of 2400 kg/m<sup>3</sup>. If concrete has 300 kg of cement, which generates 400 J/gr energy, increase in temperature can be calculated from Eq.2.9 as follows:

$$\Delta T = \frac{q}{c \cdot \rho} = \frac{300 \times 400 \times 1000}{1000 \times 2400} = 50 \text{ } ^\circ\text{C}$$

Normally, most of heat is generated within first 24 hours of hydration that can be observed in Figure 2.2. Generally about 70% of heat is released in first 24 hours after placement (ACI 207.1R-96). After first 24 hr, heat release may continue up to three years or longer with almost a constant rate. Considering these facts, it may be assumed that, in adiabatic conditions, concrete element in this example will reach to 35 °C within first 24 hours.

Approximate determination of development history of 35 °C in concrete body would require a temperature function. However, use of temperature function not only requires adiabatic curve data but also detailed temperature field data. However, implementing Eq's.2.8 and 2.9 in incremental numerical analysis that is performed step by step, the total heat energy released during hydration can be estimated. This would complete the required input data for the solution of Eq.2.1. In this thesis, the computer program ABAQUS/6.4 was used that is suitable for incremental analysis. The following case study describes temperature history analysis of concrete structure.

## 2.6 Case Study

Bosnjak and Kanstad (2001) have reported an experimental study on a culvert structure in Oslo. In total 340 m culvert has been cast as alternative bays in sections of 15 m length. During the construction, three of these sections were instrumented by temperature sensors and strain gauges. From the casting, temperature and strain development was monitored and recorded. A section of this culvert construction with the locations of temperature sensors and strain gauges are shown in Figures 2.3 and 2.4 (Bosnjak and Kanstad, 2001).

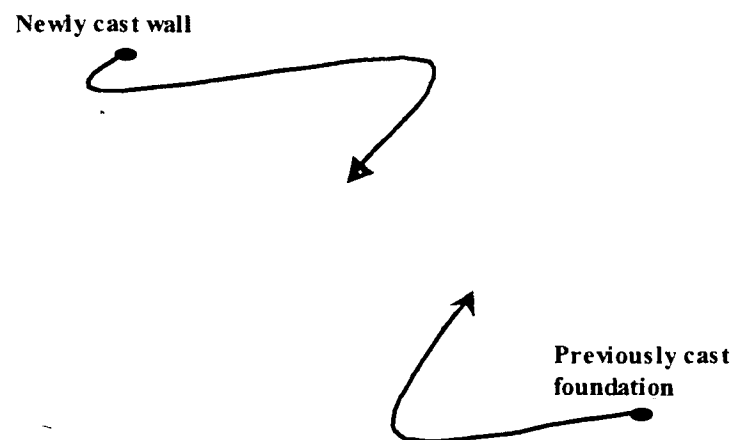


Figure 2.3: Wall cast on previously cast foundation in culvert construction

Mix design of concrete that is used in culvert construction is shown in Table 2.2. The amount of cement used is 350 kg for 1 m<sup>3</sup> of concrete, which is the heat source during hydration. In addition to cement, there is also 18 kg of silica fume in this mix that is actually more reactive than cement and generates more heat.

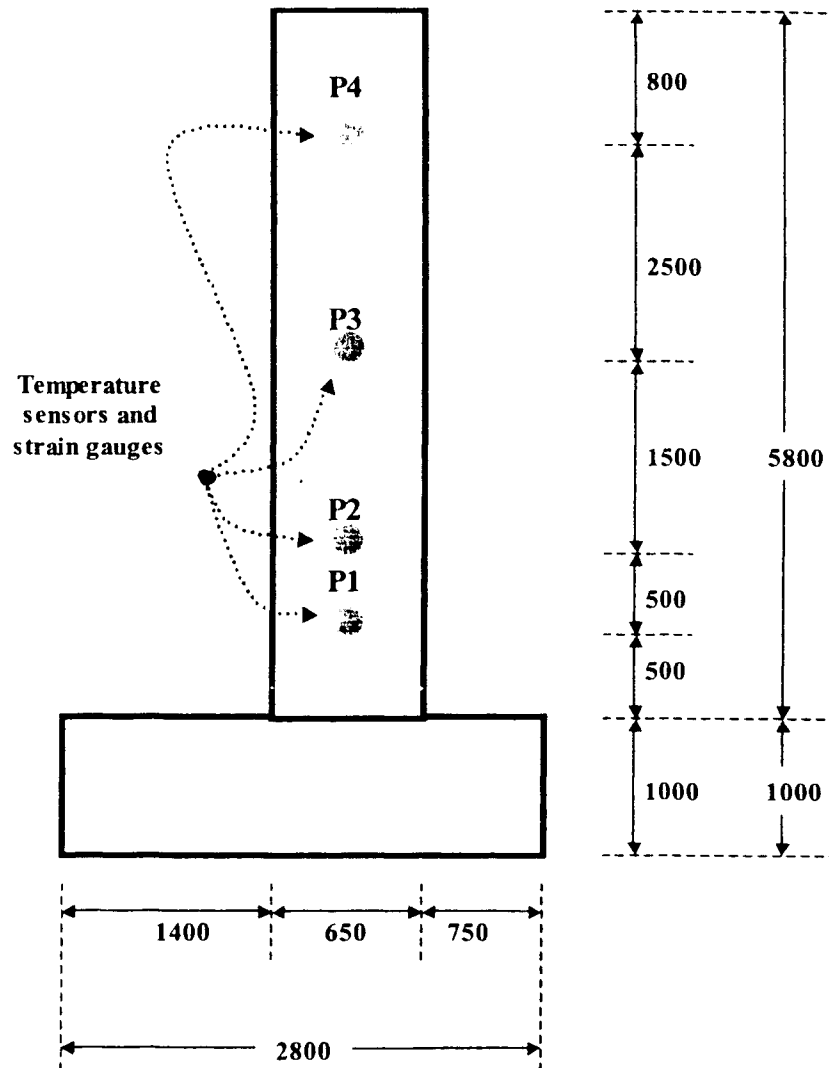


Figure 2.4: Locations of the temperature sensors and strain gauges

Table.2.2: Concrete Mix Design used in culvert wall

Material	Content(kg/m <sup>3</sup> )
Cement, OPC Type CEMI52.5	350
Silica Fume	18
Plasticizer, Sika AER	4
Superplastiziser, Sikament 92	3
Air, Sika AER	0.7
Svelvik Sand 0-8 mm	953
Svelvik Gravel 8-14 mm.	206
Svelvik Gravel 14-24 mm	658
Total water content	154.4
Water/binder-ratio	0.4

Lab tests have been conducted to determine material properties. Thermal conductivity and specific heat of this particular concrete are determined as follows:

Thermal Conductivity: 2.2 J/ms°C

Specific Heat: 1100 J/kg°C

Cement content in this mix is given as 350 kg/m<sup>3</sup>. The mix contained silica fume, which has higher hydration rate. For practical reasons, it can be assumed that cement and silica fume have same reaction rate and would generate 400 J of heat per gram. By multiplying the amount of cement content to the heat energy per gram, the total heat energy to be released can be calculated. 70% of calculated energy would be released in first 24 hours. The remaining energy would be released with exponentially decreasing rate over the time. Also, before concrete placing, a small amount of energy would have been already released. A certain percentage of heat energy need to be considered as losses that would account for very early and late ages of hydration. For this analysis, 10% losses assumed that is shown in Table 2.3.

Table 2.3: Approximated total heat energy capacity of cement hydration

Cement Content (gr/m3)	Heat Energy (J/gr)	Total Heat Energy per m3	Losses (%)	Residual heat to be released (J)
368000	400	147200000	10	132480000

For this case study, temperature history of one week will be determined. Length of the heat transfer analysis is 168 hours, which is equivalent to one week. 90% of 400 J/gr energy would be released in this time period. First, adiabatic temperature rise need to be determined. Using Figure 2.2, Eq's.2.8, and 2.10, and given concrete mix design, Table 2.4 is prepared for approximate adiabatic curve. Corresponding adiabatic curve is shown in Figure 2.5.

Table 2.4: Approximated adiabatic temperature rise data

Time (hr)	Heat Release (%)	Incremental Heat (J)	Incremental Tmpr.	Adiabatic Rise (°C)
0	0.0	0.00E+00	0.0	0.0
6	8.0	1.06E+07	3.9	3.9
12	12.0	1.59E+07	5.8	9.6
18	28.0	3.71E+07	13.5	23.1
24	22.0	2.91E+07	10.6	33.7
30	6.0	7.95E+06	2.9	36.6
36	2.0	2.65E+06	1.0	37.6
42	1.0	1.32E+06	0.5	38.1
48	1.0	1.32E+06	0.5	38.5
54	1.0	1.32E+06	0.5	39.0
60	1.0	1.32E+06	0.5	39.5
66	1.0	1.32E+06	0.5	40.0
72	1.0	1.32E+06	0.5	40.5
78	1.0	1.32E+06	0.5	40.9
84	1.0	1.32E+06	0.5	41.4
90	1.0	1.32E+06	0.5	41.9
96	1.0	1.32E+06	0.5	42.4
102	1.0	1.32E+06	0.5	42.9
108	1.0	1.32E+06	0.5	43.4
114	1.0	1.32E+06	0.5	43.8
120	1.0	1.32E+06	0.5	44.3
126	1.0	1.32E+06	0.5	44.8
132	1.0	1.32E+06	0.5	45.3
138	1.0	1.32E+06	0.5	45.8
144	1.0	1.32E+06	0.5	46.2
150	1.0	1.32E+06	0.5	46.7
156	1.0	1.32E+06	0.5	47.2
162	1.0	1.32E+06	0.5	47.7
168	1.0	1.32E+06	0.5	48.2

100.0

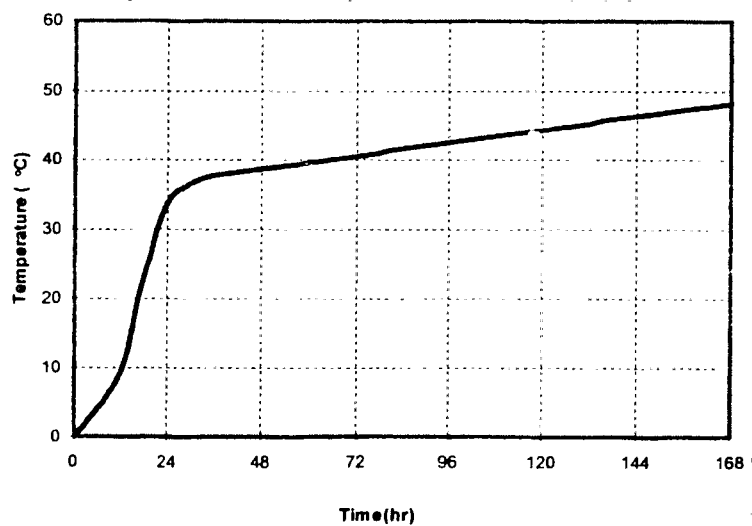


Figure 2.5: Approximated adiabatic temperature rise

It is assumed that 70% of total heat would be released in first 24 hours, and remaining hydration reaction would be approximately constant for rest of the analysis. Proportionality of first four increments is being calibrated based on field temperature data. Using the computer program ABAQUS/6.4, analysis can be performed in multiple steps, which is known as incremental analysis. For this case study, length of the analysis is divided into 10 steps. During the first 24 hours of analysis, variation in heat release rate is high. Therefore, smaller increments for first 24 hours are necessary, which would allow modification of heat rate. After first 24 hours, heat release rate is relatively constant, and longer period could be used. Selected length of each time increment is shown in Table 2.5.

Table 2.5: Number of steps during analysis with corresponding time period for 168 hr (7 days)

Step#	Step Length (day)
Initial	Initial
1	0.25
2	0.25
3	0.25
4	0.25
5	0.25
6	0.25
7	0.50
8	1.00
9	2.00
10	2.00

Total Length 7

Ambient temperature is assumed to be constant at  $-12^{\circ}\text{C}$ . Thermal conductivity between wall and foundation is selected as  $0.8 \text{ W/m}^{\circ}\text{C}$ . Unlike some other commercial FEM softwares, ABAQUS/6.4 does not offer exact tools to model surrounding conditions of concrete during hydration period and heat dissipation. But there are several options in this program that can be successfully implemented to simulate heat dissipation of concrete body. In addition to that, incremental analysis provides an option to modify these tools over time. In this case study, ambient thermal radiation option was used to model heat

dissipation from concrete. Formwork characteristics were modeled by modifying emissivity of radiation to ambient. During the construction, forms were removed approximately after 36 hr. Removal of forms was simulated by changing emissivity from 0.4 to 1 after 36 hr. Reduced emissivity in first 36 hr was used to simulate the insulation effects of forms. Transient heat transfer analysis performed and history output of each recorded point compared with the field data. Comparison of measured and calculated temperature histories are shown in Figures 2.7 to 2.10. A contour plot of temperature distribution through the wall section is also shown in Figure 2.6 that represents temperature stage of each node at the end of the analysis.

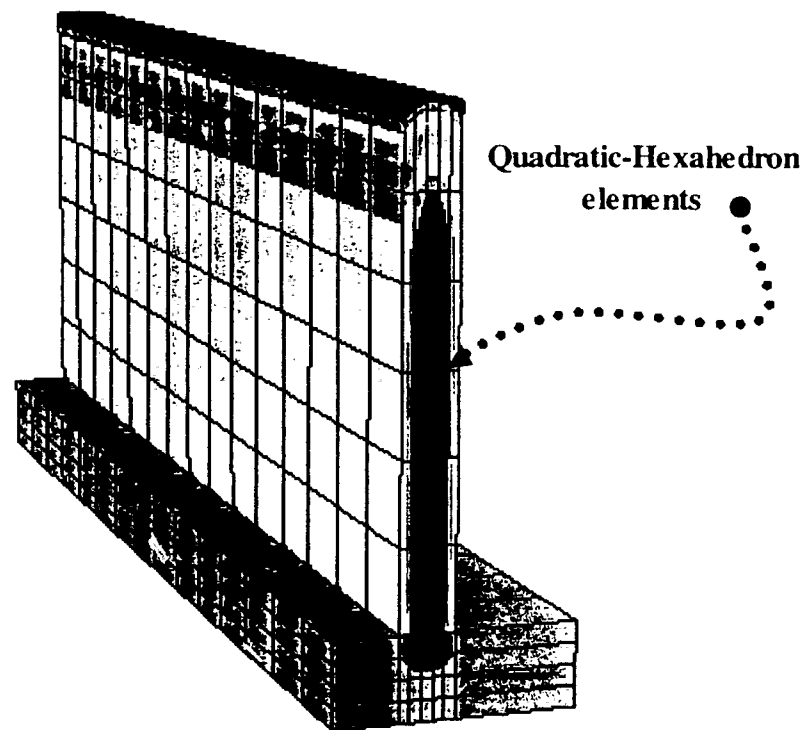


Figure 2.6: Contour plot of temperature distribution in studied culvert section

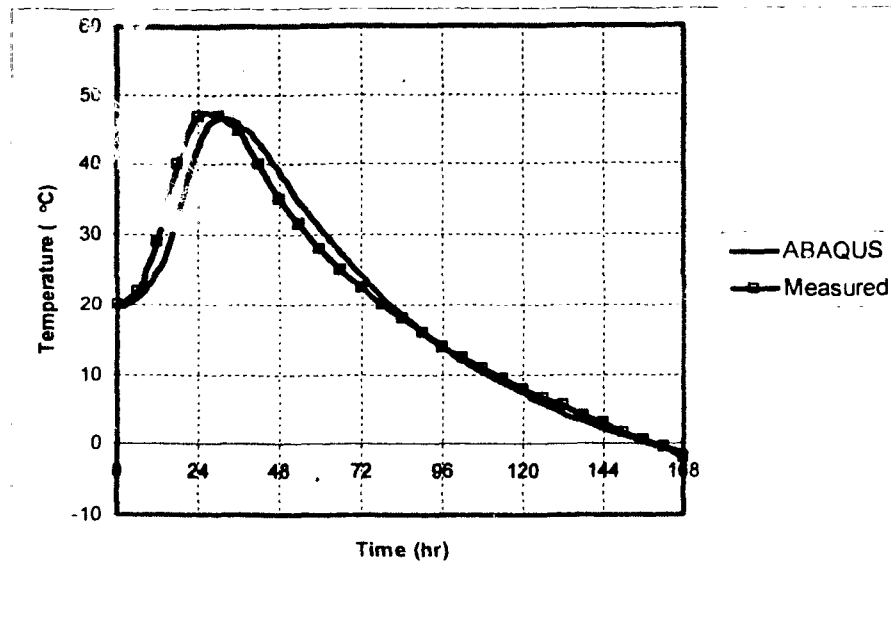


Figure 2.7: Calculated and measured temperature history at Point 1

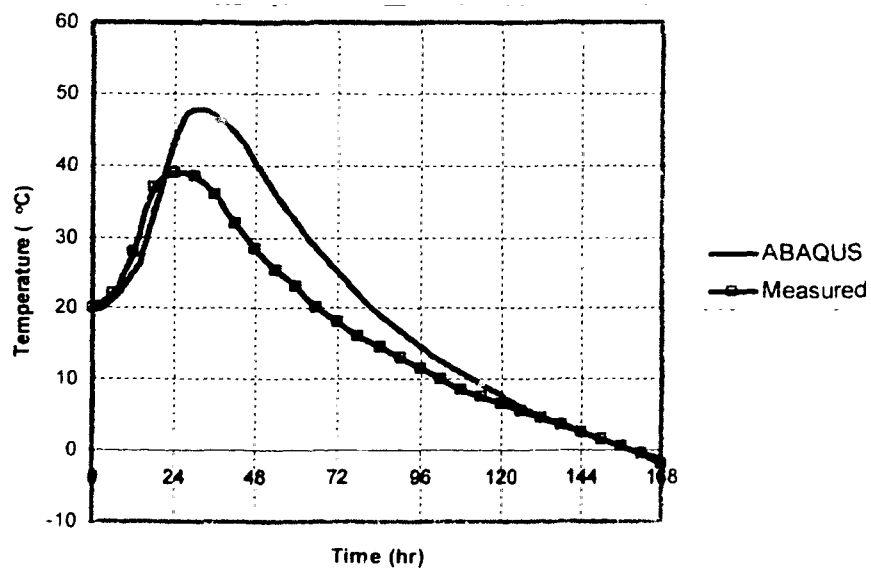


Figure 2.8: Calculated and measured temperature history at Point 2



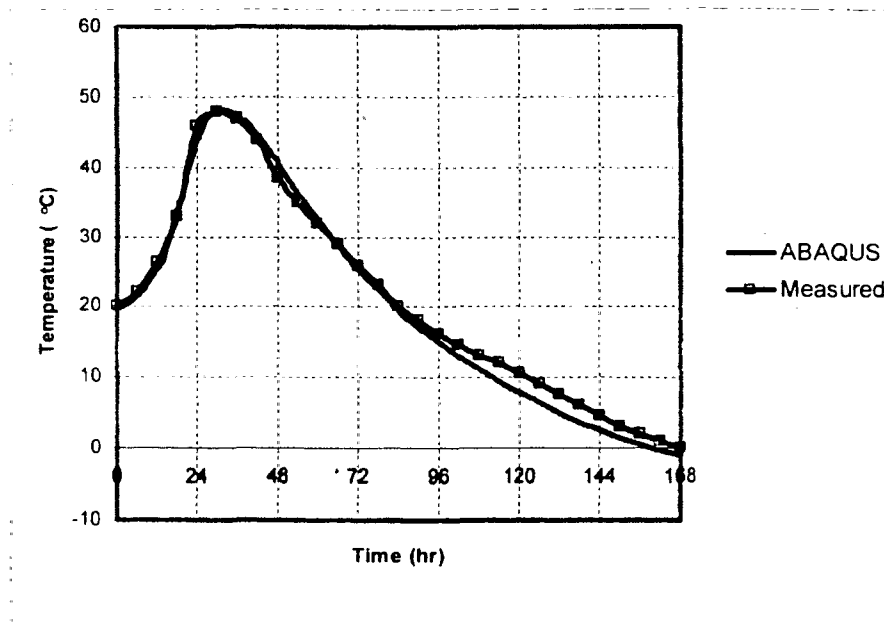


Figure 2.9: Calculated and measured temperature history at Point 3

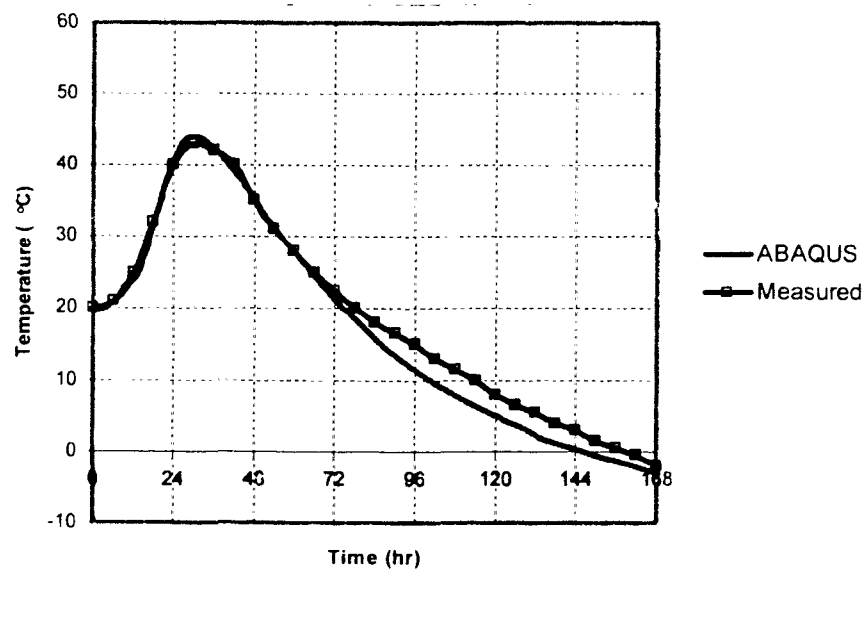


Figure 2.10: Calculated and measured temperature history at Point 4

It is clear that except Point 2, calculated and measured data has good agreement in three other locations. But even considering only the field temperature data, it is apparent that

Point 2 temperature data has some errors. Point 2 is located between Point 1 and Point 3. Temperature of Point 2 should be between temperatures of neighboring locations at certain time. Also, Point 1 is closer to the foundation contact surface and heat dissipation rate would be faster. This would cause lower maximum temperature at Point 1, as compared to Point 2. These facts suggest that there might be some variation of the form and insulation behavior of the forms or an error in temperature sensors.

## **2.7 Summary**

There are two major factors for volumetric changes of concrete that are shrinkage due to moisture loss and expansion or contraction due to temperature. To estimate thermal expansion or contraction, it is necessary to know temperature history of the concrete during early ages. Calculated temperature history during hydration and climatological conditions in further stages can help to determine total thermal deformation of concrete that is required for stress analysis. Also, in this chapter it was shown that incremental analysis option using the ABAQUS computer program provides practical solution for simulation of concrete hydration process. In each step of heat transfer analysis, heat energy gain and losses can be modified to simulate field conditions of concrete. In addition to that, it is shown that Truman et al. (1991) method to simulate hydration process works well with incremental analysis. Instead of a temperature function that requires detailed lab and field data, Eq.2.10 and adiabatic curve could be used to find temperature history of concrete. This method is applicable in incremental analysis and it is practical to use. Application of this method requires only limited information about temperature in the field, and a calibration of very initial hours to determine proportionality of heat release. On the other hand, use of a temperature function requires detailed lab tests and calibration process based on field temperature data.

## CHAPTER 3

### MATERIAL MODELING

#### 3.1 Introduction

Thermally induced strains, chemical and drying shrinkage are the main forces for the stress development and crack formation at early ages. Magnitude of this early age stresses and crack risks depends on restraint conditions as well as young concrete mechanical properties. Just after setting, concrete mechanical properties start to develop. Realistic simulation of young concrete stress development requires consideration of developing mechanical properties. Compressive strength, tensile strength, and modulus of elasticity increase as a function of hydration time and degree of hydration. Characteristics of strength development are being studied for years by many researchers. Development of compressive strength is generally modeled as dependent on age or on the degree of hydration. A concept called Maturity (Equivalent age) is used to model strength development, which accounts for combined influence of temperature and age. In this Chapter, based on the calculated temperature history, time dependent material input data will be developed, which will be used in stress-displacement analysis.

#### 3.2 Equivalent Age

Important mechanical properties in the simulation of hardening concrete are the modulus of elasticity, strength and creep properties. Determination of development of these properties as function of time and temperature is of major concern and can be calculated using the equivalent age approach. Equivalent age is a parameter that combines time and temperature effects in calculation of concrete strength. Maturity is the concrete age at which the hydration at the reference temperature has reached the same stage. There are several methods to calculate maturity and corresponding strength characteristics. Neville (1995) expresses the relation between temperature and strength of concrete as following:

$$\text{Strength of concrete} = f(\Sigma \text{ time interval} \times \text{temperature}) \quad (3.1)$$

ACI 306R-97 adapted this description for estimating maturity of concrete but does not suggest any analytical method for a function that can be used to calculate strength. Equivalent age calculation using ACI 306R method as follows:

$$M = \sum (T - T_o) \Delta t \quad (3.2)$$

where,

M = maturity factor, deg-hr

T = temperature of concrete, °C

T<sub>o</sub> = datum temperature, °C

Δt = duration of curing period at temperature T, hr

ACI 306R presents some charts to find the strength of concrete cured in certain conditions according to calculated maturity using Eq.3.2. Using charts requires some calibration to find the strength of concrete with different characteristics and this method is not that feasible compared to CEB-FIP method. On the other hand, CEB-FIP method to calculate maturity seems to be more realistic. CEB-FIP formulation to estimate equivalent is developed based on Arrhenius law, which was discussed earlier in Chapter 2. According to CEB-FIP model code (1990), the effect of elevated or reduced temperatures on the maturity of concrete may be taken in to account by adjusting the concrete age as follows:

$$t_T = \sum_{i=1}^n \Delta t_i \exp \left[ 13.65 - \frac{4000}{273 + T(\Delta t_i) / T_o} \right] \quad (3.3)$$

where,

t<sub>T</sub> = temperature adjusted concrete age which replaces t in the corresponding equations

Δt<sub>i</sub> = number of days where a temperature T prevails

T(Δt<sub>i</sub>) = temperature during the time period Δt<sub>i</sub>

T<sub>o</sub> = 1, °C

Cusson et al. (2000), discusses Eq.3.3 as it is only valid for Portland-cement concrete. The constant parameters 13.65 and 4000 in Eq.3.3 are factors related to activation energy of concrete, which depends on cement type and additives used in the concrete mix. However, CEB-FIP method is used widely in literature with slight modifications. More general shape of maturity function based on Arrhenius equation that is capable of accounting for the influence of temperature from -10° to 80 °C, is defined by Mitchell et al. (1998) as shown in following:

$$H(t) = \exp \left[ \frac{E}{R} \left( \frac{1}{293} - \frac{1}{T_c + 273} \right) \right] \quad (3.4)$$

where,

E = activation energy, kJ/(mol.°C)

$T_c$  = temperature of concrete, °C

R = gas constant, 8.314 kJ/mol.°C

The energy activation parameter, E, depends on chemical composition of the cement and it has following form:

$$E(T_c) = 33.5 \text{ kJ/mol for } T_c > 20 \text{ °C}$$

$$E(T_c) = 33.5 + 1.47(20 - T_c) \text{ for } T_c < 20 \text{ °C}$$

Using the maturity function given in Eq.3.4, equivalent age of a particular concrete can be calculated over the time as follows (Bosnjak and Kanstad, 2001):

$$t_{eq} = \int_0^t H(t) dt$$

$$t_{eq} = \int_0^t \exp \left[ \frac{E}{R} \left( \frac{1}{293} - \frac{1}{T_c + 273} \right) \right] dt \quad (3.5)$$

Observation of Eq.3.5 clearly indicates that it is equal to Eq.3.3, which CEB-FIP recommends for the calculation of maturity. To simplify the problems, CEB-FIP code recommends a value of activation energy,  $E$ , as 33 kJ/mol for temperature ranges from 0° to 80 °C.

### 3.3 Compressive Strength

Since concrete strength development is a function of temperature, it can be calculated based on given equivalent age. Analytical technique that is used to calculate compressive strength from the equivalent age is recommended by the CEB-FIP model code. CEB-FIP model code 1990 recommendation for calculation of compressive strength based on calculated maturity as follows:

$$f_{cm}(t) = \beta_{cc}(t) f_{cm} \quad (3.6)$$

where,

$f_{cm}(t)$  = mean concrete compressive strength at an age of  $t$  days

$f_{cm}$  = mean compressive strength after 28 days

$\beta_{cc}$  = coefficient which depends on the age of concrete  $t$  (calculated as in following equation)

$$\beta_{cc}(t) = \exp \left\{ s \left[ 1 - \sqrt{\frac{28}{t/t_1}} \right] \right\} \quad (3.7)$$

where,

$t$  = equivalent age of concrete calculated from Eq.3.3

$t_1 = 1$ , day

$s$  = coefficient which depends on the type of cement.  $s = 0.20$  for rapid hardening high strength cement,  $s = 0.25$  for normal and rapid hardening cement,  $s = 0.38$  for slowly hardening cement.

### 3.4 Modulus of Elasticity

One of the primary parameters in stress analysis is the elastic modulus of concrete. In addition to ACI and CEB methods, there are several equations used commonly to calculate modulus of elasticity. Well known ACI equation to calculate elastic modulus as parameter of compressive strength is shown in the following (ACI 207.2R-95):

$$E = 4700\sqrt{f'_c} \text{ (in MPa)} \quad (3.8)$$

ACI 207.2R does not specify whether Eq.3.8 can be used for calculation of time dependent elastic modulus. But, since elastic modulus is defined as a function of compressive strength, this equation may be used to calculate time dependent elastic modulus. Compressive strength can be calculated as time dependent, then for each time increment elastic modulus also can be calculated as time dependent with Eq.3.8. However, one can question that constant coefficient may need modification over the time. CEB-FIP model code 1990 suggests use of coefficient given in Eq.3.7 that accounts time variation with 28 days elastic modulus to calculate time dependent modulus of elasticity, which is shown in following:

$$E_{ci}(t) = E_{ci} \sqrt{\beta_{cc}(t)} \quad (3.9)$$

where,

$E_{ci}(t)$  = modulus of elasticity at an age of  $t$  days

$E_{ci}$  = modulus of elasticity at an age of 28 days

$\beta_{cc}(t)$  = coefficient which depends on the age of concrete  $t$ , (Eq.3.7)

### 3.5 Tensile Strength

Since induced compressive stresses are negligible compare to compressive strength of concrete, the main concern for early age stresses and consequent crack formation is the tensile strength. Restraint induced early age stresses are generally tensile and concrete is weak in tension. For this reason tensile strength development of concrete should be carefully assessed at early age stress analysis.

Generally tensile strength of mature concrete is defined by simple equation relating it to compressive strength of concrete. But development of tensile strength is not as clear as compressive strength. The ratio of compressive and tensile strength development is generally not constant and changes for different concrete mixes. Effect of curing and drying conditions as well as dimension of structure are significant for tensile strength development. Despite the known effect of curing and drying conditions on tensile strength, except the approximate equations of ACI 207.2R-95 given in Eq.3.10, most known and used equations do not include these effects on tensile strength estimation. For calculation of tensile strength, ACI 207.2R-95 recommends the following equations that considers effects of drying shrinkage:

$$f_t = 6\sqrt{f_c} \text{ (negligible drying shrinkage)} \quad (3.10)$$

$$f_t = 4\sqrt{f_c} \text{ (influenced by drying shrinkage)} \quad (3.11)$$

From Equations 3.10 and 3.11 it can be seen that concrete that is influenced by drying would have lower tensile strength. Common equations to estimate tensile strength are developed based on relation between compressive and tensile strength of concrete. CEB and ACI's formulations are examples that allow calculation of tensile strength as parameter of compressive strength. CEB-FIP model code 1990 formulation for tensile strength is given in following:

$$f_{ctm} = f_{ctko,m} \left( \frac{f_{ck}}{f_{cko}} \right)^{\frac{2}{3}} \quad (3.12)$$

where,

$f_{ctm}$  = mean tensile strength

$f_{ctko,m}$  = 1.4 MPa

$f_{cko}$  = 10 MPa

$f_{ck}$  = characteristic compressive strength



$$f_{ck} = f_{cm} + \Delta f$$

$f_{cm}$  = mean concrete compressive strength

$$\Delta f = 8 \text{ MPa}$$

Both CEB and ACI methods to estimate tensile strength are basically approximation and both can be used. CEB model code suggests that for concrete older than 28 days, development of tensile strength is similar to compressive strength. Therefore, Eq.3.12 can be used for determination of tensile strength of concrete older than 28 days. For concrete younger than 28 days experimental determination is recommended. Bosnjak et al. (2001) and Cusson et al. (2000) both have used Eq.3.7 to determine tensile strength over the time. Based on the assumption that tensile strength development is similar to the compressive strength development, following equation can be written for calculation of tensile strength development that is used by Cusson et al.(2000):

$$f_{ct} = \beta_{cc} f_{ct28} \quad (3.13)$$

where,

$f_{ct}$  = concrete tensile strength

$\beta_{cc}$  = coefficient which depends on the age of concrete t, (calculated from Eq.3.7)

$f_{ct28}$  = 28 days tensile strength

Bosnjak et al. (2001) have also used Eq.3.7 and Eq.3.13 with additional modifications based on lab tests.

ACI 207.1R-96 suggests another approximation that relates compressive strength to tensile strength, which is shown in following:

$$\begin{aligned} f_t &= 1.7 f_c^{2/3}, \text{ (psi).} \\ f_t &= 0.32 f_c^{2/3}, \text{ (MPa).} \end{aligned} \quad (3.14)$$

Although all of equations for tensile strength estimations listed from 3.10 to 3.14, are more or less the same, Eq.3.14 seems to be more practical and represent an average of

approximate equations. Therefore, for modeling of tensile strength development Eq.3.14 is used in this thesis.

### 3.6 Case Study-Concrete Strength in Culvert Wall

Before starting stress-displacement analysis of young concrete, input file have to be prepared and as part of this task material properties chart has to be developed. As an example, the concrete that is used in culvert as discussed in section 2.6 will be considered. In Chapter 2, temperature history of culvert section was determined by performing heat transfer analysis. Output file of performed heat transfer analysis could be used to estimate concrete mechanical properties over the time. From the temperature history of four different points of culvert wall, average temperature for every six hours is calculated. Based on this data, Table 3.1 is prepared that shows equivalent age of concrete at different ages calculated using Eq.3.3.

Table 3.1: Calculated equivalent age of concrete in culvert wall

Time (hour)	Average Temperature (°C)	Incremental Maturity (day)	Total Maturity (day)
0	20.0	0.0	0.0
6	21.8	0.3	0.3
12	27.1	0.3	0.6
18	35.5	0.5	1.1
24	43.0	0.7	1.8
30	44.1	0.7	2.5
36	42.5	0.7	3.2
42	39.0	0.6	3.7
48	34.3	0.5	4.2
54	30.8	0.4	4.6
60	27.8	0.4	5.0
66	24.8	0.3	5.3
72	22.2	0.3	5.5
78	19.8	0.2	5.8
84	17.6	0.2	6.0
90	15.9	0.2	6.2
96	14.1	0.2	6.4
102	12.5	0.2	6.6
108	11.0	0.2	6.7
114	9.8	0.2	6.9
120	8.3	0.1	7.0
126	6.9	0.1	7.2
132	5.8	0.1	7.3
138	4.4	0.1	7.4
144	3.3	0.1	7.5
150	1.9	0.1	7.6
156	0.9	0.1	7.7
162	-0.1	0.1	7.8
168	-1.5	0.1	7.9

The 28 days strength and elastic modulus is determined in lab tests and values are given as follows:

$$f_{c(28)} = 75.8, (MPa)$$

$$E_{c(28)} = 40005, (MPa)$$

Using data calculated in Table 3.1 and tests results for 28 days strength, development of strength can be estimated. With combination of Table 3.1, Equations 3.6, 3.7, 3.9 and 3.14 can be used to determine strength development history table that is shown in Table 3.2.

Table 3.2: Strength development history of concrete in culvert wall

Time (hr)	$t_e$	$\beta_{cc}(t)$	$f_{cm}(t)$	$E_{ci}(t)$	$f_t(t)$
(hr)	(day)		(MPa)	(MPa)	(MPa)
0	0.00	0.000	0.0	0	0.0
6	0.27	0.101	7.7	12711	1.2
12	0.62	0.238	18.0	19512	2.2
18	1.11	0.366	27.7	24204	2.9
24	1.79	0.477	36.2	27631	3.5
30	2.49	0.555	42.1	29810	3.9
36	3.15	0.609	46.2	31230	4.1
42	3.72	0.647	49.0	32176	4.3
48	4.19	0.673	51.0	32819	4.4
54	4.60	0.693	52.5	33300	4.5
60	4.95	0.709	53.7	33677	4.6
66	5.26	0.721	54.7	33977	4.6
72	5.54	0.732	55.5	34226	4.7
78	5.79	0.741	56.2	34434	4.7
84	6.01	0.749	56.7	34612	4.7
90	6.21	0.755	57.3	34768	4.8
96	6.40	0.761	57.7	34905	4.8
102	6.58	0.767	58.1	35027	4.8
108	6.74	0.771	58.5	35136	4.8
114	6.89	0.776	58.8	35236	4.8
120	7.03	0.780	59.1	35325	4.9
126	7.16	0.783	59.4	35406	4.9
132	7.29	0.787	59.6	35481	4.9
138	7.40	0.790	59.9	35550	4.9
144	7.51	0.792	60.1	35613	4.9
150	7.61	0.795	60.3	35670	4.9
156	7.71	0.797	60.4	35724	4.9
162	7.80	0.800	60.6	35773	4.9
168	7.89	0.802	60.8	35819	4.9

$t_e$  = equivalent age, day

$\beta_{cc}(t)$  = coefficient which depends on the age of concrete

$f_{cm}(t)$  = mean compressive strength, MPa

$E_{ci}(t)$  = modulus of elasticity at age of  $t$  days, MPa

$f_t(t)$  = tensile strength at an age of  $t$  days, MPa

Graphical representation of Table 3.2 is shown in Figures 3.1 to 3.3.

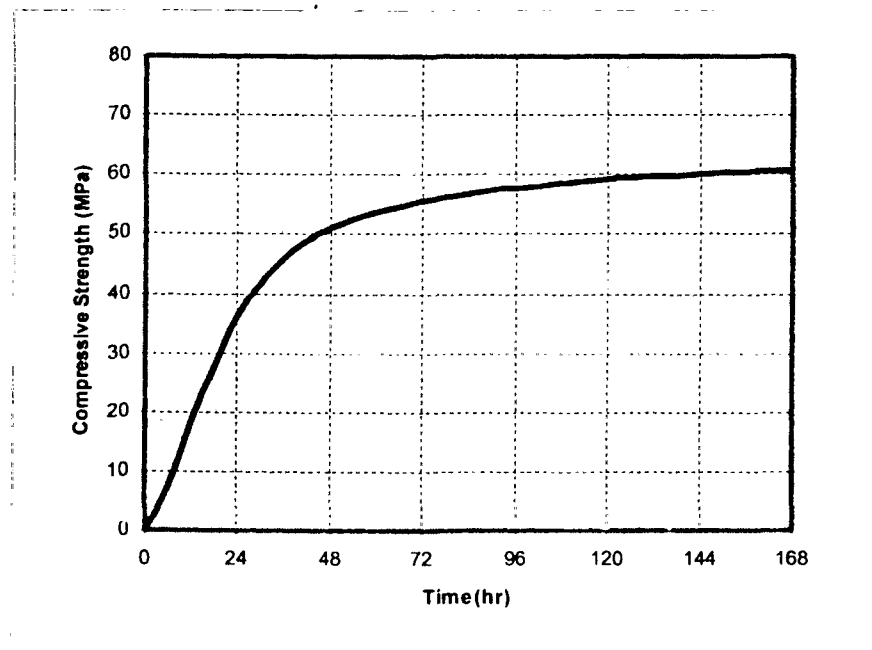


Figure 3.1: Compressive strength development of concrete in culvert wall

Concrete strength development history for one week can be observed in Figures 3.1 to 3.3. For stress-displacement analysis of maturing concrete a table like Table 3.2 is necessary. ABAQUS/6.4 input file requires stress-strain curve of given material and this can be prepared by Table 3.2.

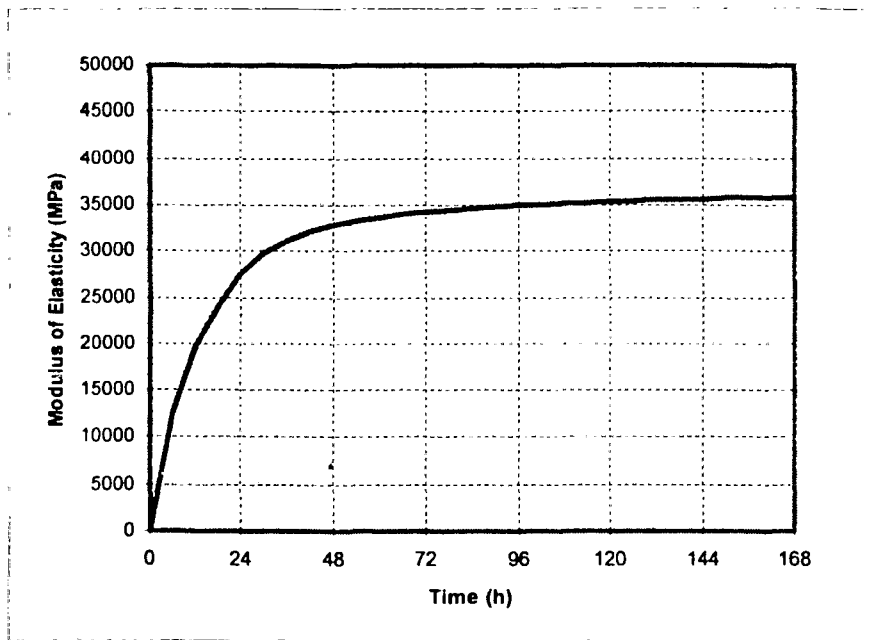


Figure 3.2: Modulus of elasticity development of concrete in culvert wall

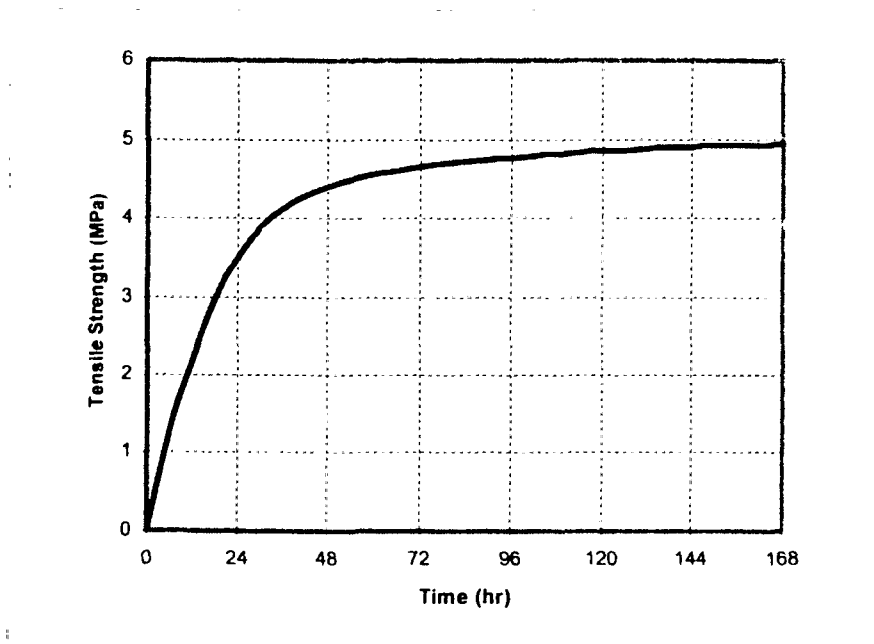


Figure 3.3: Tensile strength development of concrete in culvert wall

### 3.7 Creep and Relaxation

Time dependent deformation of concrete under sustained load is called creep. Relaxation on the other hand is a decrease in stress with time in concrete subjected to constant deformation. An idealized graphical representation of creep and relaxation is shown in Figure 3.4. From these definitions it is obvious that both creep and relaxation are due to the same phenomenon. For this reason only term creep is generally used to describe combination of creep and relaxation.

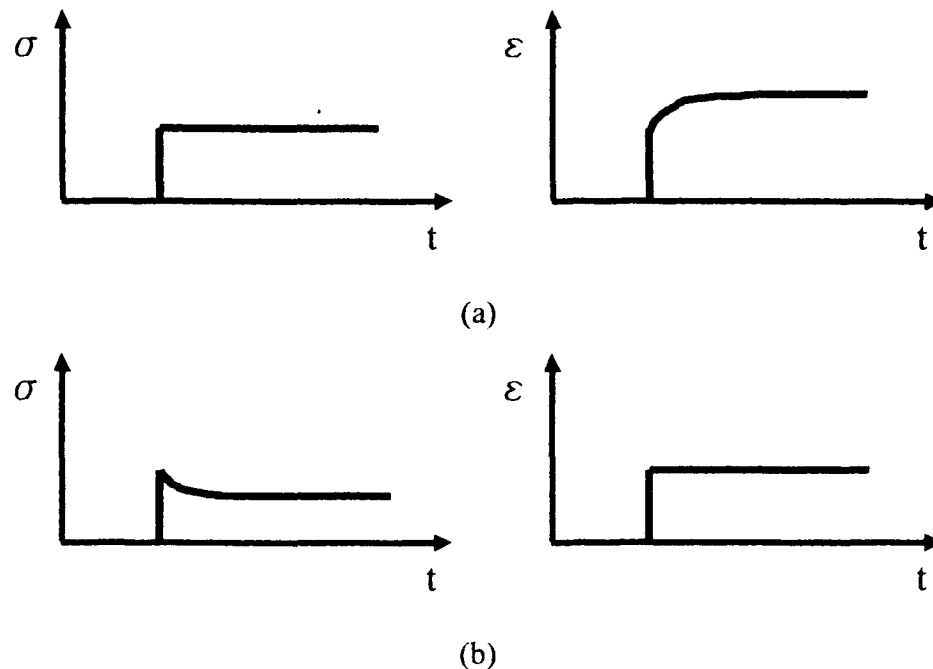


Figure 3.4: Idealized graphical representation of creep and relaxation, (a) Creep strain (Increased deformation under constant sustained stress), (b) Relaxation of stress (reduction on stress under constant sustained strain)

Creep magnitude depends on the magnitude of stress, the strength of concrete when stress is applied, age of concrete when it is stressed, length of time period for applied stress, type of cement used in concrete, amount of cement in the mix, properties of aggregate used in the mix, geometric properties of concrete element, reinforcement ratio, and curing conditions.

Creep may have negative or positive effects to the structure such as redistribution of the stress due to loads and reduction of strength due to large deformation. It is one of very

important mechanical properties of concrete, but it is at the same time the least understood even for mature concrete. For young concrete, complexity of creep phenomenon increases for various reasons. When restrained induced stresses are high enough, creep may have a significant effect by relaxing the stresses and increasing the amount of total strain.

ACI 207.2R states that when maximum temperature changes occur over a relatively short time period, creep can only slightly modify temperature stresses. However, this may not be the case for all structures. Effect of creep on early age deformation is discussed by ACI 207.1R-96, Mitchell et al. (1998), Cusson et al. (2000), and Bosnjak et al. (2001). It is suggested that since concrete has low elastic modulus at early ages, concrete have high creep that reduces crack risks at early ages. Generally, during hydration period maximum temperature changes occur when concrete is gaining strength. Thermal and shrinkage induced stresses may exceed tensile strength capacity of concrete but creep reduces these stresses and crack risks. Effect of creep on reducing stresses depends on the magnitude of stresses. Creep effect may be significant on reducing stresses when the stresses are high. But in low stress condition, there would not be significant effect by creep.

For normal stress concrete, creep is proportional to stress. In order to complete the modeling of material properties, sufficient model data for early age concrete tensile creep behaviour is needed. But, it is believed that most creep prediction models are based on mature concrete compressive creep behavior. This is probably because of tensile creep tests are difficult to perform. Also, creep is known to be a non-linear phenomenon. But common creep prediction models are based on assumption that concrete is a linear visco-elastic material. In reality part of creep is unrecoverable and causes permanent deformation. This non-linear behavior of creep is one of the reasons that in general creep is divided into two parts as basic creep and drying creep. Creep classification is shown in Figure 3.5.

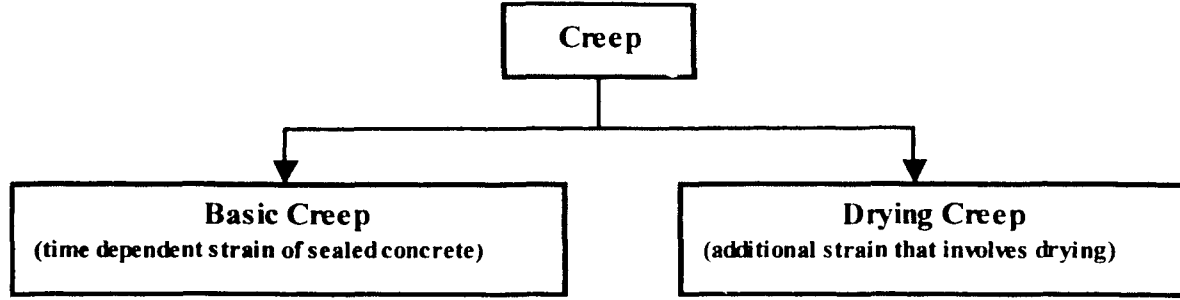


Figure 3.5: Creep classification (basic and drying creep)

Basic creep is the creep under sealed conditions, and drying creep is the additional creep due to moisture loss under constant stress. Creep estimation models are generally developed based on Maxwell and Kelvin Chain, which is a system consist of a spring and a dashpot. Concrete research institutes such as ACI and CEB offers different models to estimate creep. Mitchell et al. (1998) showed that CEB-FIP formulation has good performance for early age concrete creep prediction. Considering the fact that both ACI and CEB creep models are developed based on compressive creep tests, and they involve certain assumptions, estimating young concrete tensile creep behavior is quite approximate. According to Mitchell et al. CEB-FIP formulation produce good results. In this thesis CEB-FIP model was used in estimation of creep coefficient.

The first assumption made to estimate creep is that creep and stress are linearly related. For a constant stress applied at time  $t$ , creep strain may be calculated using the following equation (CEB-FIP, 1990):

$$\varepsilon_{cc}(t, t_o) = \frac{\sigma_c(t_o)}{E_{ci}} \phi(t, t_o) \quad (3.15)$$

where,

$\varepsilon_{cc}(t, t_o)$  = creep strain at time  $t$  that is loaded at  $t_o$

$\sigma_c(t_o)$  = stress in a uniaxially loaded concrete element

$E_{ci}$  = 28 days modulus of elasticity

$\phi(t, t_o)$  = creep coefficient that is given in following



$$\phi(t, t_0) = \phi_0 \beta_c (t - t_0) \quad (3.16)$$

where,

$\phi_0$  = notional creep coefficient

$\beta_c$  = coefficient to describe the development of creep with time after loading

$t$  = age of concrete (days) at the moment considered

$t_0$  = age of concrete at loading calculated as follows

$$t_0 = t_{0,T} \left[ \frac{9}{2 + (t_{0,T} / t_{1,T})^{1.2}} + 1 \right]^\alpha \geq 0.5 \text{ days} \quad (3.17)$$

where,

$t_{0,T}$  = age of concrete at loading give in Eq.3.3

$t_{1,T} = 1$ , (day)

$\alpha$  = a coefficient that depends on the type of cement (-1 for slowly hardening cement, 0 for normal and rapid hardening cement, and 1 for rapid hardening high strength cement)

Notional creep coefficient,  $\phi_0$ , is expressed as follows:

$$\phi_0 = \phi_{RH} \beta(f_{cm}) \beta(t_0) \quad (3.18)$$

$$\phi_{RH} = 1 + \frac{1 - RH / RH_0}{0.46(h / h_0)^{1/3}} \quad (3.19)$$

where,

$RH$  = relative humidity of the ambient environment, %

$RH_0 = 100$  %

$h_0 = 100$  mm

$h$  = notational size of member, mm

Notational size of member can be calculated as follows:

$$h = \frac{2A_c}{u} \quad (3.20)$$

where,

$A_c$  = cross section of the member

$u$  = perimeter of the member in contact with the atmosphere

$$\beta(f_{cm}) = \frac{5.3}{(f_{cm} / f_{cm0})^{0.5}} \quad (3.21)$$

where,

$f_{cm}$  = mean compressive strength of concrete at the age of 28 days, MPa

$f_{cm0} = 10$  MPa

$$\beta(t_0) = \frac{1}{0.1 + (t_0 / t_1)^{0.2}} \quad (3.22)$$

where,

$t_0$  is given in Eq.3.17.

$t_1$  is 1 day

Development of creep with time is given in following:

$$\beta_c(t-t_0) = \left[ \frac{(t-t_0)/t_1}{\beta_H + (t-t_0)/t_1} \right]^{0.3} \quad (3.23)$$

where,

$$\beta_H = 150 \left\{ 1 + \left( 1.2 \frac{RH}{RH_0} \right)^{18} \right\} \frac{h}{h_0} + 250 \leq 1500 \quad (3.24)$$

### 3.7.1 Case Study-Creep Coefficient of Concrete in Culvert Wall

CEB-FIP formulations for creep model were summarized in Equations 3.15 to 3.24. Using this model to estimate creep coefficient at different time intervals is a tedious task if a spreadsheet is not used. Eq.3.3 and Eq's.3.15 to 3.24 were used in Excel to calculate creep coefficient for different time intervals that is shown in Table 3.3. This table can be used for creep effect in stress-displacement analysis that will be discussed in Chapter 4.

Table 3.3: Creep coefficient variation over the time, and calculated required parameters for determination of creep coefficient

$f_{cm} = 75$		$U = 10650$		$RH = 60$		$\beta_H = 1168$	
$f_{cmo} = 10$		$A_c = 3250000$		$RH_0 = 100$		$\phi_{RH} = 1.48$	
$\alpha = 0$		$h = 610$		$h_0 = 100$		$\beta(f_{cm}) = 1.94$	
Time (hr)	Equivalent Age	$t_0 \geq 0.5$	Time (day)	$\beta_c(t-t_0)$	$\beta(t_0)$	$\phi_0$	$\psi(t, t_0)$
0	0.00	0.00	0.00	0.00	1.03	2.94	0.00
6	0.27	0.27	0.25	0.08	1.03	2.94	0.23
12	0.62	0.62	0.50	0.10	0.99	2.83	0.28
18	1.11	1.11	0.75	0.11	0.89	2.55	0.28
24	1.79	1.79	1.00	0.12	0.82	2.34	0.28
30	2.49	2.49	1.25	0.13	0.77	2.20	0.28
36	3.15	3.15	1.50	0.14	0.74	2.10	0.29
42	3.72	3.72	1.75	0.14	0.71	2.04	0.29
48	4.19	4.19	2.00	0.15	0.70	1.99	0.29
54	4.60	4.60	2.25	0.15	0.69	1.96	0.30
60	4.95	4.95	2.50	0.16	0.68	1.93	0.31
66	5.26	5.26	2.75	0.16	0.67	1.91	0.31
72	5.54	5.54	3.00	0.17	0.66	1.89	0.32
78	5.79	5.79	3.25	0.17	0.66	1.88	0.32
84	6.01	6.01	3.50	0.17	0.65	1.87	0.33
90	6.21	6.21	3.75	0.18	0.65	1.85	0.33
96	6.40	6.40	4.00	0.18	0.65	1.84	0.34
102	6.58	6.58	4.25	0.19	0.64	1.83	0.34
108	6.74	6.74	4.50	0.19	0.64	1.83	0.34
114	6.89	6.89	4.75	0.19	0.64	1.82	0.35
120	7.03	7.03	5.00	0.19	0.63	1.81	0.35
126	7.16	7.16	5.25	0.20	0.63	1.80	0.36
132	7.29	7.29	5.50	0.20	0.63	1.80	0.36
138	7.40	7.40	5.75	0.20	0.63	1.79	0.36
144	7.51	7.51	6.00	0.21	0.63	1.79	0.37
150	7.61	7.61	6.25	0.21	0.62	1.78	0.37
156	7.71	7.71	6.50	0.21	0.62	1.78	0.37
162	7.80	7.80	6.75	0.21	0.62	1.78	0.38
168	7.89	7.89	7.00	0.22	0.62	1.77	0.38

### 3.8 Shrinkage

Shrinkage can be defined as volume reduction of concrete due to moisture loss during and after the hardening. Primary driving forces for shrinkage are moisture exchange with surroundings and cement hydration or carbonation. Although concrete volume change sometimes cause swelling due to moisture exchange with environment, generally reduction of volume is a concern. Total shrinkage is sum of volume reduction of concrete due to several different shrinkage phenomenon. Total shrinkage is generally categorized as chemical shrinkage, autogenous shrinkage, carbonation shrinkage, plastic shrinkage, and drying shrinkage. Primary shrinkage types are shown in Figure 3.6.

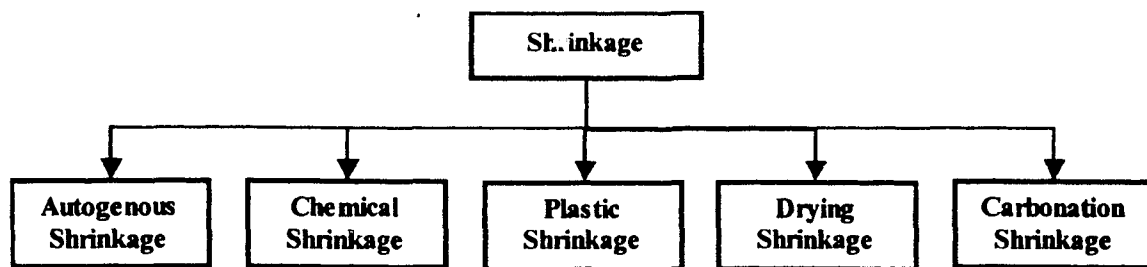


Figure 3.6: Shrinkage classification

Hydration of cement causes reduction of absolute volume of the paste, which is chemical shrinkage. Part of chemical shrinkage is called autogenous shrinkage that is visible. Autogenous shrinkage is the macroscopic volume reduction of cement paste, mortar, or concrete caused by cement hydration (Kosmatka et al., 2002). Drying shrinkage is the reduction of volume due to moisture exchange between concrete element and its surrounding. When drying shrinkage takes place close to the surface before final setting, it is called plastic shrinkage.

Previously drying shrinkage was considered dominant in total shrinkage, and therefore chemical shrinkage was generally neglected. With development of high performance concrete, proportionality of total shrinkage has changed. Due to high water cement ratio, total shrinkage of normal concrete may be primarily the result of drying. In high performance concrete, chemical shrinkage may dominate total shrinkage amount, due to special mix design. High performance concrete mix characteristics such as low w/c ratio and additional supplementary cementing materials are primary reasons for chemical shrinkage.

Similar to other associated properties, estimation of total shrinkage at early ages is a complicated difficult task. Volume change due to plastic shrinkage may be considerably large but this type of shrinkage does not impose significant stresses. Before final setting, concrete has negligible elastic modulus and plastic shrinkage, which mainly affects the surface region of concrete and can be neglected in stress calculations.

Drying shrinkage may be dominant for normal quality concrete when it is exposed to drying for very long time at mature ages. But the length of stress analysis considered for the simulation of case study is relatively short time as compared to development of drying shrinkage. Even though there might be certain amount of drying shrinkage, because of relatively short simulation length it might be neglected. Also present concrete mix design trend is toward low water cement ratio, which also reduces drying shrinkage. Remaining shrinkage class need to be considered is chemical shrinkage. This type of shrinkage is particularly high for high performance concrete. Main problem with the estimation of chemical shrinkage is that design codes do not specify whether they account for chemical shrinkage in their estimation methods.

ACI 207.2R introduces a method to estimate drying shrinkage. Since thermal and shrinkage volume changes are similar (stress independent strains), they can be superposed. ACI 207.2R uses equivalent temperature change concept to convert shrinkage to thermal strain. In design of concrete structures, to consider volumetric changes it is very convenient to consider only temperature, rather than temperature and drying. For this reason, it is desirable to express drying shrinkage in terms of equivalent change in concrete temperature. According to ACI 207.2R-95, equivalent temperature change with the consideration of long-term affect of creep can be expressed as follows:

$$T_{DS} = \left( 30 - \frac{2V}{S} \right) \left( \frac{W_u - 125}{100} \right) \quad (3.25)$$

where,

$T_{DS}$  = equivalent temperature change due to drying shrinkage, in deg F

$W_u$  = water content of fresh concrete, (not less than 225 lb / yd<sup>3</sup>)

$V$  = total volume, in<sup>3</sup>

$S$  = area of the exposed surface,  $in^2$

At first, ACI 207.2R method for calculation of shrinkage that also accounts for creep effect may be very attractive to use, but obviously it is too simplistic for prediction of complicated creep and shrinkage characteristics.

ACI 209R-92 that is a detailed report on shrinkage and creep of concrete, also suggest a method to estimate shrinkage. But it is not mentioned for what kind of shrinkage this method is applicable. Following equation is recommended by ACI 209R-92 to estimate shrinkage strains.

$$\left(\varepsilon_{sh}\right)_t = \frac{t^\alpha}{f + t^\alpha} \left(\varepsilon_{sh}\right)_u \quad (3.26)$$

where,

$\left(\varepsilon_{sh}\right)_t$  = shrinkage strain ( $415 \times 10^{-6}$  to  $1070 \times 10^{-6}$  m/m)

$\left(\varepsilon_{sh}\right)_u$  = ultimate shrinkage strain

$t$  = time after the loading

$f$  (days) and  $\alpha$  are coefficients depending shape and size

$f$  = 20 to 130 days

$\alpha$  = 0.9 to 1.1

CEB-FIP model code has a method to calculate total shrinkage as well. But again there is no clear statement whether this method includes autogenous shrinkage. Cusson et al. (2000) reported that CEB-FIP formulation may not be reliable for estimation of autogenous shrinkage. In a case study, it was seen that CEB-FIP prediction for shrinkage was largely exceeded by the corresponding autogenous shrinkage strain predicted by an empirical model. According to CEB-FIP model code, the total shrinkage or swelling strains may be calculated as follows:

$$\varepsilon_{cs}(t, t_s) = \varepsilon_{cs0} \beta_s(t - t_s) \quad (3.27)$$

where,

$\epsilon_{cs}(t, t_s)$  = total shrinkage strains

$\epsilon_{cso}$  = notional shrinkage coefficient

$\beta_s(t - t_s)$  = coefficient to describe development of shrinkage with time

$t$  = age of the concrete

$t_s$  = age of concrete at the beginning of shrinkage

Notional shrinkage coefficient is given in following:

$$\epsilon_{cso} = \epsilon_s(f_{cm}) \beta_{RH} \quad (3.28)$$

with

$$\epsilon_s(f_{cm}) = 10^{-6} \cdot \left[ 160 + 10 \beta_{sc} \left( 9 - \frac{f_{cm}}{f_{cmo}} \right) \right] \quad (3.29)$$

where,

$f_{cm}$  = mean compressive strength of concrete at the age of 28 days, MPa

$f_{cmo} = 10$  MPa

$\beta_{sc}$  = coefficient which depends on the type of cement, (4 for slowly hardening cement, 5 for normal and rapid hardening cement, 8 for rapid hardening high strength cement)

$\beta_{RH} = -1.55 \beta_{sRH}$  for  $40\% \leq RH \leq 99\%$

$\beta_{RH} = +0.25$  for  $RH \geq 99\%$

$$\beta_{sRH} = 1 - \left( \frac{RH}{RH_0} \right)^3 \quad (3.30)$$

where,

$RH$  = relative humidity of the ambient atmosphere, %

$RH_0 = 100$ , %

Development of shrinkage with time is given by:

$$\beta_s(t-t_s) = \left[ \frac{(t-t_s)/t_1}{350(h/h_0)^2 + (t-t_s)/t_1} \right]^{0.5} \quad (3.31)$$

where,

$h$  = to be calculated by Eq.3.20

$h_0$  = 100 mm

$t_1$  = 1 day

### 3.8.1 Case Study-Shrinkage of Culvert Wall

Although throughout this chapter it would have been more preferable to use ACI formulations for modeling properties of material, in many cases it was not possible. For example, using the ACI formulations, equivalent age cannot be calculated in analytical way. For most of the properties CEB-FIP code was used so far. In this section, shrinkage will be estimated based on this code. For practical reasons, calculated shrinkage strains will be converted to the equivalent temperature change. This is required to include shrinkage effect in stress-displacement analysis using ABAQUS/6.4.

Part of the culvert structure, which was discussed in Chapter 2 and in this chapter, is exposed to atmospheric conditions. According to CEB-FIP model Code, relative humidity of 80% can be assumed for this structure. Bosnjak et al. (2001) reported the value of thermal expansion coefficient as  $8.5 \times 10^{-6}$ . Same value is chosen in this case study since it was determined with lab tests. Shrinkage strains were calculated using equations 3.27 to 3.31, and then strains were converted to the equivalent temperature change. Table 3.4 shows predicted equivalent temperature change due to shrinkage.

For this case study, the length of the analysis considered is the first week of concrete. The time at which concrete starts to be exposed (form removal) is after 36 hours of placement. Total time that concrete is allowed to shrink is very short for this case study. For this reason expected shrinkage should not cause significant volume changes, and calculated equivalent temperature would not cause significant thermal contraction. However, to complete the model, calculated shrinkage strains will be included in stress-displacement analysis.



Table 3.4: Estimated shrinkage and equivalent temperature changes over the time and required calculated parameters for shrinkage prediction

$u = 10650$		$h_0 = 100$		$RH = 60$	
$A_c = 3250000$		$\beta_{sc} = 5$		$RH_0 = 100$	
$h = 610$		$\beta_{RH} = -1.22$		$\beta_{sRH} = 0.78$	
$f_{cm} = 75$		$\varepsilon_{cso} = -2.9E-04$		$f_{cmo} = 10$	
$\varepsilon_s(f_{cm}) = 2.4E-04$		Thermal Expansion Coefficient 8.50E-06			
Time (hr)	Time (days)	$\beta_s(t-t_s)$	$\varepsilon_{cs}$	$\Delta T_{sh}$	$\sum \Delta T_{sh}$
0	0.00	0.0000	0.0E+00	0.0	0.0
6	0.25	0.0000	0.0E+00	0.0	0.0
12	0.50	0.0000	0.0E+00	0.0	0.0
18	0.75	0.0000	0.0E+00	0.0	0.0
24	1.00	0.0000	0.0E+00	0.0	0.0
30	1.25	0.0000	0.0E+00	0.0	0.0
36	1.50	0.0000	0.0E+00	0.0	0.0
42	1.75	0.0044	-1.3E-06	-0.1	-0.1
48	2.00	0.0044	-1.3E-06	-0.1	-0.3
54	2.25	0.0044	-1.3E-06	-0.1	-0.4
60	2.50	0.0044	-1.3E-06	-0.1	-0.6
66	2.75	0.0044	-1.3E-06	-0.1	-0.7
72	3.00	0.0044	-1.3E-06	-0.1	-0.9
78	3.25	0.0044	-1.3E-06	-0.1	-1.0
84	3.50	0.0044	-1.3E-06	-0.1	-1.2
90	3.75	0.0044	-1.3E-06	-0.1	-1.3
96	4.00	0.0044	-1.3E-06	-0.1	-1.5
102	4.25	0.0044	-1.3E-06	-0.1	-1.6
108	4.50	0.0044	-1.3E-06	-0.1	-1.8
114	4.75	0.0044	-1.3E-06	-0.1	-1.9
120	5.00	0.0044	-1.3E-06	-0.1	-2.1
126	5.25	0.0044	-1.3E-06	-0.1	-2.2
132	5.50	0.0044	-1.3E-06	-0.1	-2.4
138	5.75	0.0044	-1.3E-06	-0.1	-2.5
144	6.00	0.0044	-1.3E-06	-0.1	-2.6
150	6.25	0.0044	-1.3E-06	-0.1	-2.8
156	6.50	0.0044	-1.3E-06	-0.1	-2.9
162	6.75	0.0044	-1.3E-06	-0.1	-3.1
168	7.00	0.0044	-1.3E-06	-0.1	-3.2

### 3.9 Effect of Section Thickness on Material Properties

In this chapter, it was assumed that section thickness has negligible effect on strength variation through the section. This is true if the temperature history is relatively similar through the thickness. But, when the section is thick enough and there is significant variation of temperature history, the problem would be much more complex. This would occur in mass concrete structures if proper construction procedure were not followed.

Mass concrete is described as the structures with minimum dimension of 2 m in any direction. Since the section in mass concrete is thick, the total mature age of inner concrete may be much higher than exposed surface region. This would create a section with different material properties and may cause significant problems. Generally, in slender structures this effect is negligible. The following example illustrates effect of section thickness on material properties.

Consider a slab with thickness of 300 mm that is exposed to ambient temperature from the casting, and supported by soil with relatively higher temperature. To investigate the effect of section thickness, slab thickness should be as many layers as possible during heat transfer analysis. FE mesh of the example slab is shown in Figure 3.7.

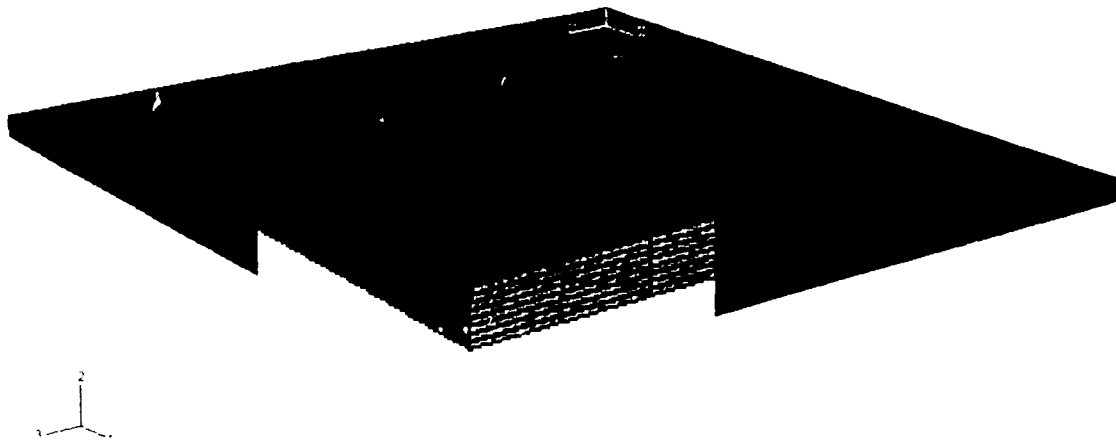


Figure 3.7: FE mesh of a square slab with thickness of 300 mm divided in to 8 layers (layers are named from the top starting from Ly1 to Ly8)

Inner layers of the slab are insulated by other layers and would have higher temperature at any time through the hydration period. Higher temperature of inner layers would create faster rate of strength gain. On the other hand, the exposed layers that are closer to the top of the slab would gain strength in a slower rate. Heat transfer analysis was performed as in culvert structure and temperature history of different layers is presented in Figure 3.8.

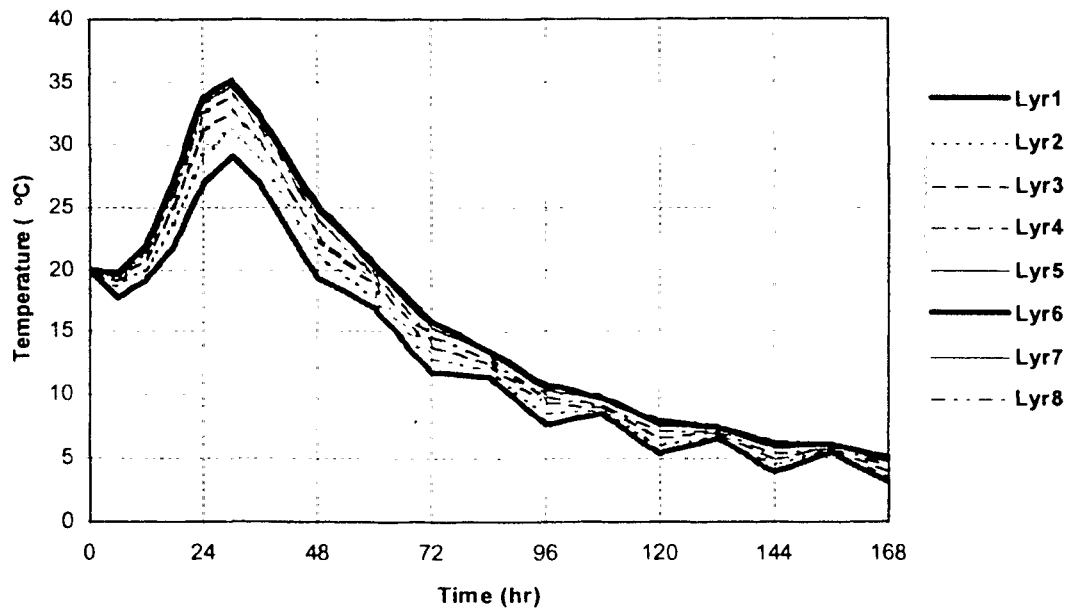


Figure 3.8: Different temperature history of different layers in example slab

The figure clearly shows that the exposed layers have lower temperature at any time resulting in lower equivalent age for the concrete at these layers. Particularly Lyr1, which is at the top of the slab, has the lowest temperature history. Effect of variation of ambient temperature during the day, can be observed in broken parts of Lyr1.

Using the methodology described previously in this chapter, properties of each layer can be calculated. Figures 3.9, 3.10, and 3.11 show variation of compressive strength, tensile strength and elastic modulus respectively through the thickness of the slab.

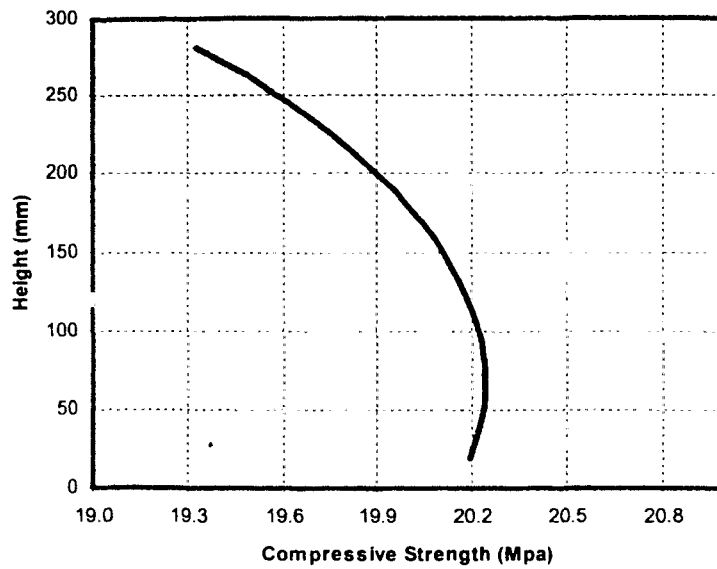


Figure 3.9: Variation of calculated compressive strength through the thickness of the example slab

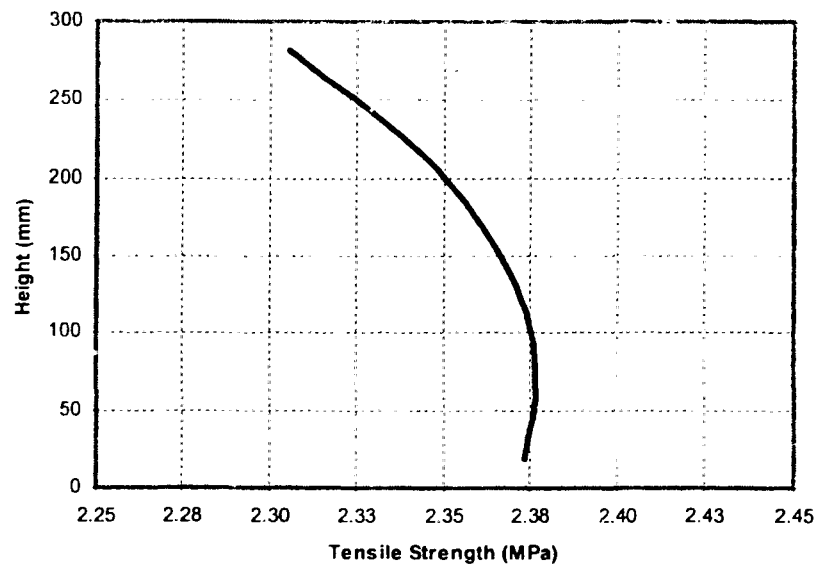


Figure 3.10: Variation of calculated tensile strength through the thickness of example slab

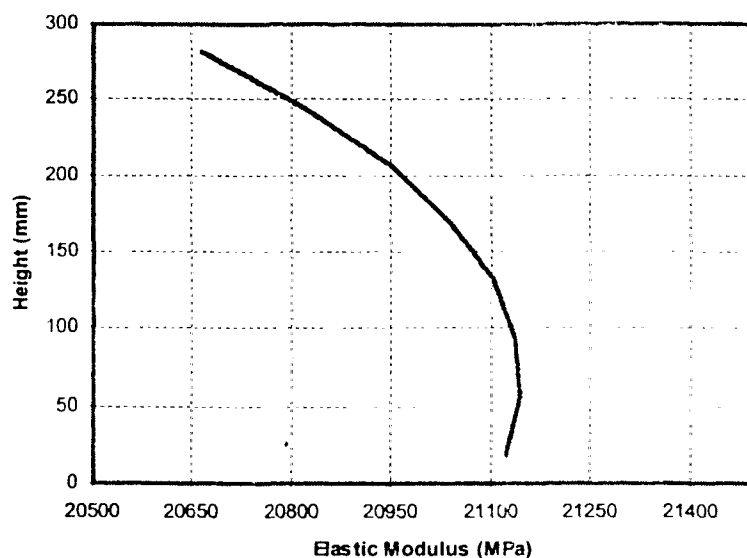


Figure 3.11: Variation of calculated modulus of elasticity through the thickness of example slab

Observation of Figures 3.9, 3.10 and 3.11 indicates that variation of strength through the thickness is very small and may be neglected. Particularly tensile strength, which is the most important parameter, is almost constant. This is because total range of tensile strength is much smaller than the total range for compressive strength and elastic modulus. However, in case of thick sections, variation of strength might be considerably large and could not be neglected. Different material properties of structural element would require definition of material for each layer in stress-displacement analysis. This is a problem generally with mass concrete sections and that is out of the scope of this thesis.

### 3.10 Summary

In Chapter 2, determination of temperature history of concrete during the hydration period was shown. Throughout this chapter, output of the heat transfer analysis was used to model concrete and analyze material properties with time. Calculated data will be used in the next chapter to perform stress-displacement analysis. Strength parameters were calculated for a case study, which is part of a culvert construction. The section thickness

of culvert wall is 600 mm, and strength development is estimated based on the temperature history of middle of the section.

## CHAPTER 4

### STRESS-DISPLACEMENT ANALYSIS

#### 4.1 Introduction

Simulation of early age concrete requires solution of thermal and mechanical problem. ABAQUS/6.4 offers an analysis technique called fully coupled-thermal-stress analysis (Hibbitt et al., 2004). This option is used when the solution of temperature and stress development histories influence each other strongly. But for volumetric changes induced stresses in concrete, effect of mechanical response to temperature development is negligible and heat transfer and stress-displacement analysis can be separated. Hibbitt et al. uses the term sequentially coupled thermal-stress for a particular type of analysis. This analysis technique is used when the stress/displacement solution is dependent on a temperature field but there is no inverse dependency. Sequentially coupled thermal-stress analysis method is performed by first solving the pure heat transfer problem, then reading the heat transfer analysis solution into the stress analysis as a predefined field. In Chapter 2, dynamic heat equilibrium equation that is used in FEM for thermal problems was discussed. In the following section, general non-linear FEM formulation will be discussed. Principles of virtual work statement that is used for the solution of any mechanical problem is briefly described.

#### 4.2 Finite Element Formulation for Mechanical Problem:

Most problems that are solved using the finite element formulation are developed based on basic equilibrium statement that is shown in following (Hibbitt et al., 2004):

$$\left( \frac{\partial}{\partial x} \right) \sigma + f = 0 \quad (4.1)$$

$\sigma$  = stress tensor

$f$  = vector representing body force per unit volume

$x$  represents cartesian coordinate system

Interpretation of the equilibrium statement is that the forces applied to a body must be equal to the stresses in the body. In stress-displacement analysis, approximate solution of equilibrium statement is sought in the subdivision of structural body by replacing it with a weaker form. The weaker form of equilibrium equation is presented in following equation, which is classical form of virtual work statement (Hibbitt et al., 2004).

$$\int_V \delta \varepsilon : \sigma dV = \int_S t^T \delta v dS + \int_V f^T \delta v dV \quad (4.2)$$

$V$  = volume of the structure

$S$  = surface of the structure

$f$  = volume load

$t$  = surface load (surface traction)

$\delta v$  = arbitrary test function that satisfies boundaries and continuity (weighting function/ admissible virtual displacement)

$\varepsilon$  and  $\sigma$  are any conjugate pairing of material stress and strain measures (operation “:” symbolises scalar product of two matrices).

Derivation of the principles of virtual work formulation (Eq.4.2) can be found in many FEM textbooks as well as in ABAQUS/6.4 theory manual. Physical interpretation of virtual work equation shows that “the rate of work done by the external forces subjected to any virtual velocity field is equal to the rate of work done by the equilibrating stresses on the rate of deformation of the same virtual velocity field” (Hibbitt et al., 2004). The solution of stress-displacement problems by application of Eq.4.2 is difficult and not feasible for complex geometries. For this reason, the entire body of the structure is divided in to smaller geometries (elements), and then the solution of Eq.4.2 is sought in each element. This solution technique is called FEM and provides solution of Eq.4.2 in a simple numerical way. In FEM, the field variable is calculated by interpolating it from the nodal variables. Naming the element nodal variable as  $u^n$ , interpolated field variable can be written as follows (Hibbitt et al., 2004):



$$u = N_N u^n \quad (4.3)$$

$N_N$  is a vector of interpolation (FEM interpolator) functions that satisfy the element boundary conditions.

Field variable of Eq.4.2 is simply the displacement and nodal variable would be the nodal displacement. Because of compatibility requirements virtual field,  $\delta v$ , in Eq.4.2 must satisfy all kinematic constraints. Introducing FEM interpolator as in Eq.4.3 constraints the displacement to certain variation, and virtual field must be compatible with this as shown in following:

$$\delta v = N_N \delta v^N \quad (4.4)$$

Virtual rate of material strain,  $\delta \varepsilon$ , is linearly related to the field variable  $\delta v$  and it can be written as follows (Hibbitt et al., 2004):

$$\delta \varepsilon = \beta_N \delta v^N \quad (4.5)$$

$\beta_N$  is a matrix that depends on the current position,  $x$ , of the material point being considered and has a form of  $\beta_N = \beta_N(x, N_N)$ .

Substituting Eq.4.4 and Eq.4.5 in to Eq.4.2 yields:

$$\delta v^N \int \beta_N : \sigma dV = \delta v^N \left[ \int_S N_N^T t dS + \int N_N^T f dV \right] \quad (4.6)$$

Eq.4.6 can be used for any admissible virtual displacement  $\delta v^N$ . Also, considering that nodal variables are independent, each one can be chosen to be nonzero and all others zero in turn, to arrive at a system of non-linear equilibrium equations (Hibbitt et al., 2004).

$$\int \beta_N : \sigma dV = \int_S N_N^T t dS + \int N_N^T f dV \quad (4.7)$$

Eq.4.7 is essential system for the solution of stress-displacement problems that FEM and ABAQUS/6.4 uses. However, for most of the material types (including concrete), Eq.4.7 is not complete. This formulation needs to be modified to include viscoelastic behaviour, creep and relaxation characteristics of the material.

#### **4.3 Reinforced Concrete in FEM**

In non-linear structural analysis using the FE softwares require well-defined material behaviour in linear and non-linear range. For most of the structural materials this is not an issue since the stress-strain behaviour of most materials is well known. But, for reinforced concrete this was not the case until recent years. As a composite material, non-linear behaviour of reinforced concrete is still a challenging research subject. Due to low strength of concrete under tension, it is used with reinforcing steel to overcome weakness problem in tension. After cracking of concrete, there is a degradation of concrete stiffness and stress transfer between concrete and reinforcement called tension stiffening. There are two basic approaches to model cracking and tension stiffening, which are discrete crack approach and smeared crack approach.

In discrete crack modeling for tension stiffening, individual cracks are modeled by using separate nodal points for concrete elements located at the cracks, which allows separation of elements at cracks. Then, separate linear or non-linear bond-slip linkage elements are used to model tension stiffening.

Smeared crack approach is more practical as compared to discrete crack approach and most commercial FE softwares, including ABAQUS/6.4 have adapted this approach. In smeared crack approach, two methods are available to model tension stiffening. In first method, concrete elastic modulus is decreased gradually after crack formation while the steel elastic modulus is unchanged. In the second method of modeling tension stiffening, concrete elastic modulus is set to zero as crack progresses and steel elastic modulus is first increased then gradually decreased. Although it is suggested that using modified stiffness for steel is numerically most efficient (ACI 224.2R-92), ABAQUS/6.4 uses first method that steel stiffness kept constant while concrete stiffness is degraded. A typical tension-stiffening curve with smeared crack approach is shown in Figure 4.1. It can be

observed that after cracking of concrete, stiffness of concrete gradually decreases while steel stiffness kept constant. Amount of strain that allow stress transfer between concrete and steel is about 10 times of concrete tensile strain capacity.

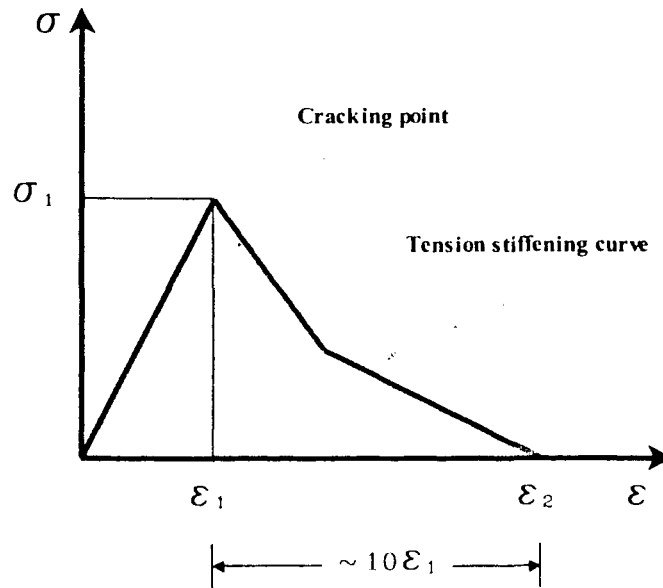


Figure 4.1: Typical tension stiffening curve (Hibbit et al., 2004)

#### 4.4 Defining Material in ABAQUS/6.4

ABAQUS/6.4 offers three different options for concrete material modeling; “the Smeared Crack Concrete Modeling” in ABAQUS/Standard; “the Brittle Crack Modeling” in ABAQUS/Explicit; and “the Concrete Damaged Plasticity” in both ABAQUS/Standard and in ABAQUS/Explicit. Although only first model is named as smeared crack modeling, all three types of concrete models are based on smeared crack approach for tension stiffening. From these three models, Smeared Crack Modeling is the most practical and simple method to model concrete. The main problem with “Smeared Crack” material option is that it is not possible to model tensile behaviour of concrete in details and it is not possible to model viscoelastic behaviour of concrete. Concrete Damaged Plasticity model is different than the other two options because it is possible to define tensile and compressive behaviours separately and it is also possible to introduce degradation of elastic stiffness. Although this model is developed for cyclic loading, it

can also be used for monotonic loading. The main advantage of Concrete Damaged Plasticity option is that concrete tensile and compressive behaviour can be defined separately. Concrete damaged plasticity model accepts viscoelastic regularization and elastic degradation option and it can be used to model creep and relaxation both in tension and compression. Brittle Crack Modeling option is used when primary stresses in concrete are tensile. Since different solution technique is used with this material option, it is very powerful to solve convergence problems. Brittle Crack Modeling will be discussed in details in Chapter 6.

The objective of non-linear FEM analysis is to capture material behaviour from initial loading up to failure. To increase accuracy of the solution, material stress-strain curve must be well defined in elastic and in inelastic range. Since hardening concrete properties changes over time, firstly stress-strain curve of concrete for each time interval need to be determined.

Concrete is assumed to behave linearly from initial loading to about 35-40% of maximum compressive strength. But early age volumetric changes induced stresses are well below the elastic limit in compression. Although concrete can be modeled to behave linearly in tension and up to 40% of the compression, complexity of hardening concrete properties requires detailed definition even in linear range. To define detailed definition of stress-strain curves, a function is required that would predict concrete behaviour in linear and non-linear range. CEB-FIP model code 1990 provides an equation that can be used to develop the stress-strain curve for concrete. Following equation is an approximate relation between stresses and strain that is valid when  $|\varepsilon_c| < |\varepsilon_{cl}|$  (CEB-FIP, 1990).

$$\sigma_c = - \frac{\frac{E_{cl}}{E_{cl}} \frac{\varepsilon_c}{\varepsilon_{cl}} - \left( \frac{\varepsilon_c}{\varepsilon_{cl}} \right)^2}{1 + \left( \frac{E_{cl}}{E_{cl}} - 2 \right) \frac{\varepsilon_c}{\varepsilon_{cl}}} f_{cm} \quad (4.8)$$

where,

$E_{cl}$  is the initial tangent modulus, (it is shown in Figure 4.2)

$\sigma_c$  is the compression stress, MPa

$\varepsilon_c$  is the compression strain

$\varepsilon_{cl}$  is strain at maximum stress, (it is shown in Figure 4.2)

$$\varepsilon_{cl} = 0.0022$$

$E_{cl}$  is the secant modulus from the origin to the peak compressive stress which is defined as in following (it is shown in Figure 4.2):

$$E_{cl} = f_{cm} / 0.0022 \quad (4.9)$$

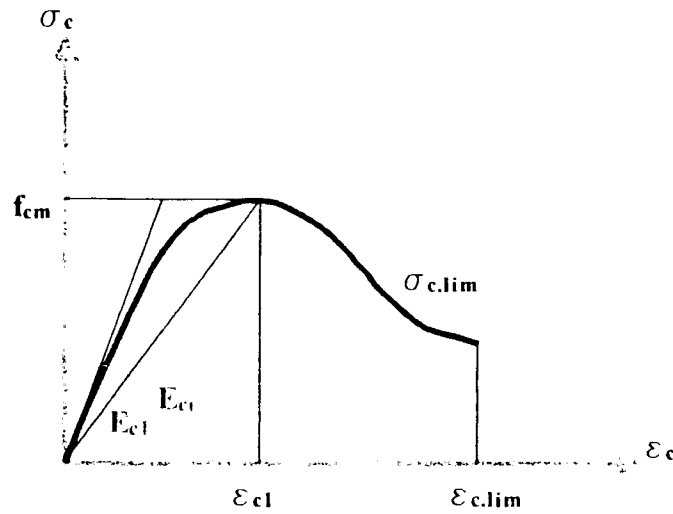


Figure 4.2: Stress-strain diagram for uniaxial compression (CEB-FIP model code 1990)

In a case study that is discussed in Chapters 2 and 3, based on temperature history and equivalent age, concrete strength development was estimated. Incremental analysis of young concrete requires separate definition of material behaviour for each time increment, and Eq.4.08 will be used to develop material input data.

In Chapter 2, to perform heat transfer analysis, the length of the analysis was divided into 10 steps. To be consistent, same time intervals would be used for stress-displacement analysis. Using the previous material development data that is explained in Chapter 3, and Eq.4.8, Table 4.1 is prepared. This table presents details of compressive behaviour of concrete at different ages. A graphical representation of Table 4.1 is shown in Figure 4.3.

Table 4.1: Compressive strains and corresponding stresses for concrete at different ages(units are in MPa)

Time (hr)	6	12	18	24	30	36	48	72	120	168
<b>f<sub>cm</sub></b>	7.7	18.0	27.7	36.2	42.1	46.2	51.0	55.5	59.1	60.8
<b>E<sub>i</sub></b>	12711	19512	24204	27631	29810	31230	32819	34226	35325	35819
<b>E<sub>s</sub></b>	3478	8196	12612	16437	19131	20997	23189	25219	26865	27621
<b>C. Strain</b>	<b>fc1</b>	<b>fc2</b>	<b>fc3</b>	<b>fc4</b>	<b>fc5</b>	<b>fc6</b>	<b>fc7</b>	<b>fc8</b>	<b>fc9</b>	<b>fc10</b>
1	0.00004	0.5	0.8	1.0	1.1	1.2	1.2	1.3	1.4	1.4
2	0.00008	0.9	1.5	1.9	2.2	2.4	2.5	2.6	2.7	2.9
3	0.00012	1.4	2.2	2.8	3.3	3.5	3.7	3.9	4.1	4.3
4	0.00016	1.8	2.9	3.7	4.3	4.7	4.9	5.2	5.4	5.7
5	0.00100	6.4	13.5	19.2	23.6	26.4	28.3	30.3	32.2	34.2
6	0.00200	7.6	17.9	27.5	35.7	41.5	45.5	50.1	54.4	59.4
7	0.00220	7.7	18.0	27.7	36.2	42.1	46.2	51.0	55.5	59.1
8	0.00250	7.6	17.8	27.2	35.1	40.5	44.1	48.2	51.7	55.1

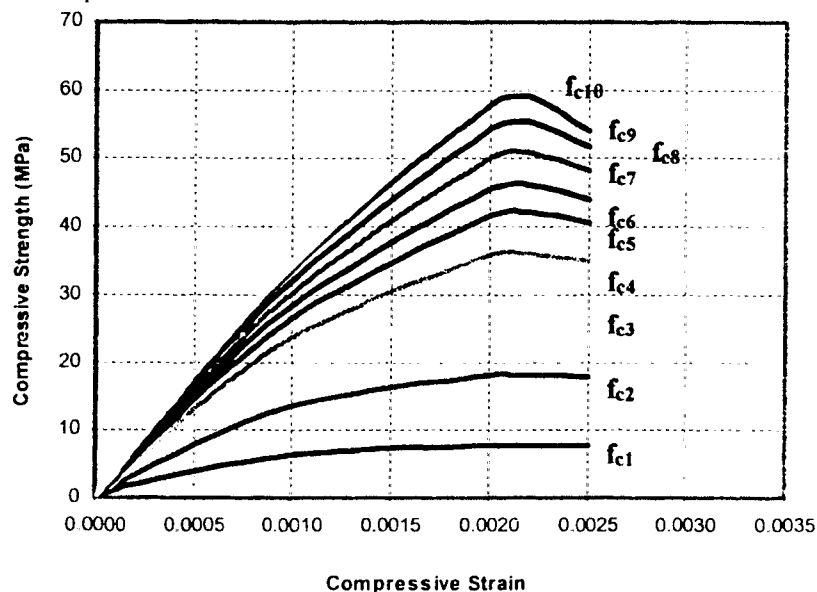


Figure 4.3: Stress-strain curve of concrete in compression at different ages

The key parameter in Eq.4.8 is the strain at the maximum stress, which is 0.0022 for compression. For determination of tensile behaviour, the value of tensile strain capacity at maximum tensile stress that can be used in Eq.4.8 and 4.9 is needed. Amount of strain at maximum stress, directly affects the magnitude of secant modulus. In Eq.4.8 all the parameters are interrelated and good approximation requires reasonably accurate

selection of strain capacity at maximum stress ( $\varepsilon_{cl}=0.0022$ ). If magnitude of  $\varepsilon_{cl}$  is changed in Eq.4.9, deviation between row#2 and row#7 (coloured row) in Table 4.1 increases. With this simple iterative approach and using previously calculated data for initial elastic modulus and tensile strength values, it is found that for the value of tensile strain capacity at maximum strength,  $\varepsilon_{t1} = 0.00016$  produces a good approximation. This value of  $\varepsilon_{t1}$  is reasonable (MacGregor, 2000) to use for this particular concrete and it is selected to produce input data for tensile properties. Since concrete is acting similarly in tension and in compression, Eq.4.8 should be able to model stress-strain relation in tension as well. Similar to compression behaviour, Eq.4.8 and 4.9 were used to develop Table 4.2 and Figure 4.4 that show tensile behaviour of concrete at different ages.

Table 4.2: Tensile strains and corresponding stresses for concrete at different ages (units are in MPa)

Time (hr)	6	12	18	24	30	36	48	72	120	168
<b>ftm</b>	1.24	2.20	2.93	3.50	3.87	4.12	4.40	4.65	4.86	4.95
<b>Ei</b>	12711	19512	24204	27631	29810	31230	32819	34226	35325	35819
<b>Es</b>	7767	13753	18330	21870	24199	25748	27510	29094	30346	30913
<b>T. Strain</b>	<b>ft1</b>	<b>ft2</b>	<b>ft3</b>	<b>ft4</b>	<b>ft5</b>	<b>ft6</b>	<b>ft7</b>	<b>ft8</b>	<b>ft9</b>	<b>ft10</b>
1	0.00004	0.47	0.75	0.95	1.09	1.18	1.23	1.30	1.36	1.42
2	0.00008	0.86	1.42	1.82	2.11	2.30	2.42	2.56	2.68	2.81
3	0.00012	1.14	1.96	2.56	3.01	3.30	3.49	3.70	3.89	4.04
4	0.00016	1.24	2.20	2.93	3.50	3.87	4.12	4.40	4.65	4.95

Mitchell et al. (1998) performed experimental study to determine stress-strain behaviour of concrete at different ages that is shown in Figure 4.5. Comparing the prepared input data shown in Figures 4.3 to Figure 4.5, which is experimental data for hardening concrete, shows good agreement. It is important to note that the ages of concrete in Figures 4.3 and 4.5 does not match, which would produce different stress-strain curve. Also, 28 days strength changes for concrete in both Figures, which would cause deviation. However, ignoring the post failure behaviours, similarity of Figure 4.3 and 4.5 is satisfactory.

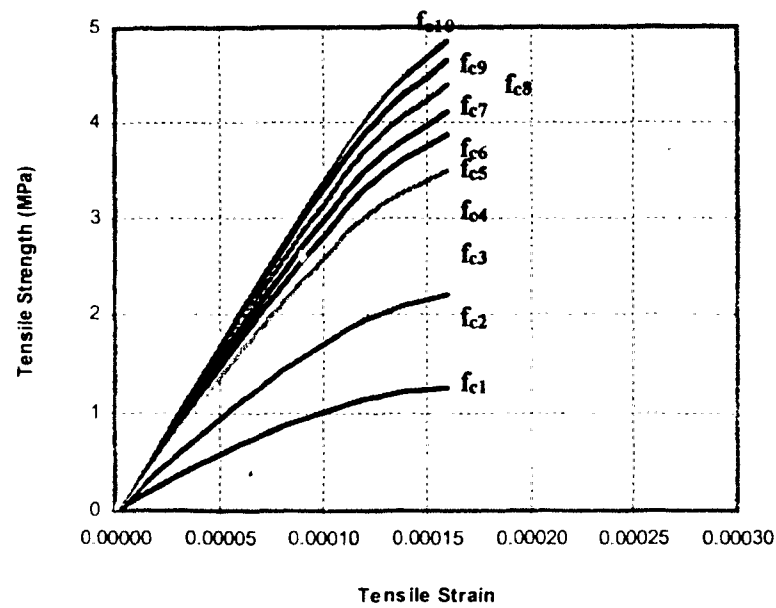


Figure 4.4: Stress-strain curve of concrete in tension at different ages (tension stiffening is not included)

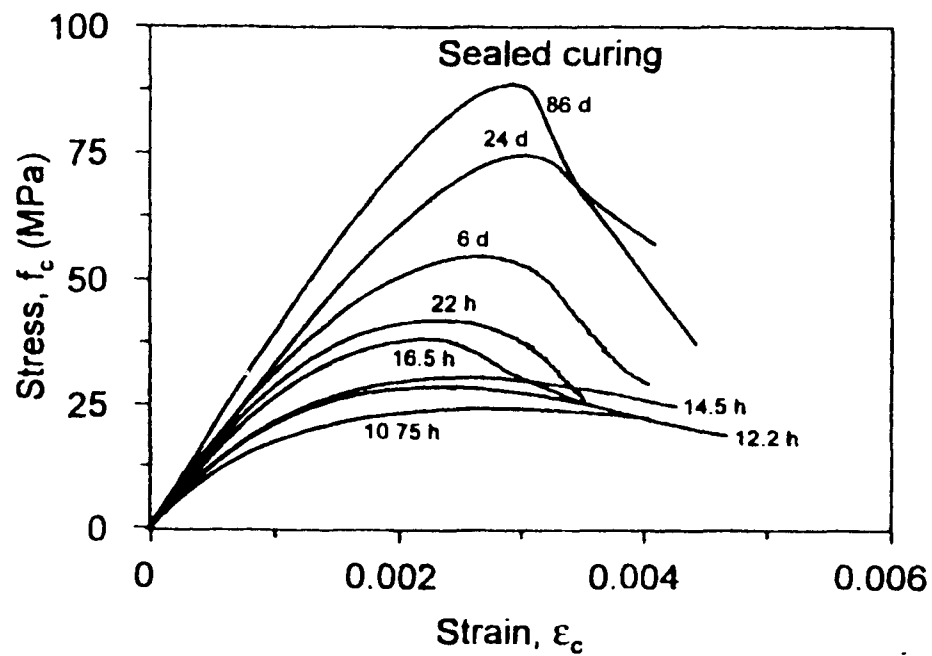


Figure 4.5: Compression tests results for 70 MPa concrete at different ages (Mitchell et al., 1998)



#### 4.4.1 Modeling Creep Effect

Generally, in FE analysis, creep effect on concrete stresses is modeled using a concept called effective elastic modulus (Ayotte et al. 1997, Cusson et al. 2000). Effective elastic modulus is basically reduced concrete stiffness that accounts for creep and relaxation of concrete under stresses. In this thesis, the effective elastic modulus concept was used to include creep effect in stress-displacement analysis. Since material stress-strain curves were defined from origin to non-linear range, instead of elastic modulus, stress-strain curve of each increment were modified. In Chapter 3, calculation of creep coefficient for hardening concrete was shown. Using calculated creep coefficients, creep strains can be calculated from the CEB-FIP creep equation that is given in Eq.3.15.

Using calculated creep coefficients, and predicted stress-strain curves shown in Tables 4.1 and 4.2, creep strains can be calculated. Estimated creep strains can be used to modify actual stress-strain curves of concrete. Example of creep modification is shown in Figure 4.6.

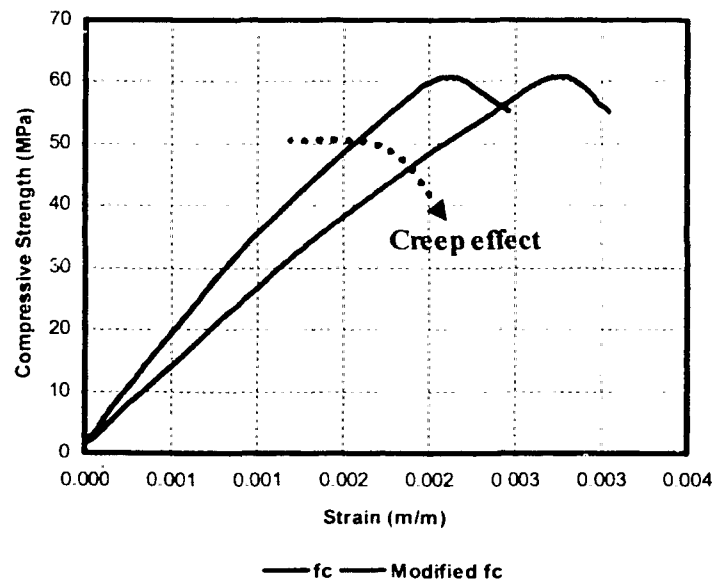


Figure 4.6: Example of modified stress-strain curve due to creep effect

#### 4.4.2 Modeling Shrinkage Effects

Creep effect was included in to stress-displacement analysis by modifying material properties. Shrinkage however, can be included in model by modifying applied thermal loads. In Chapter 3, shrinkage strains based on CEB-FIP model was calculated. Calculated shrinkage strains were converted to equivalent thermal change. Based on calculated equivalent thermal change, previously calculated temperature history can be modified. Thus, shrinkage effect could be included in stress-displacement analysis. Modified temperature history is shown in Figure 4.7.

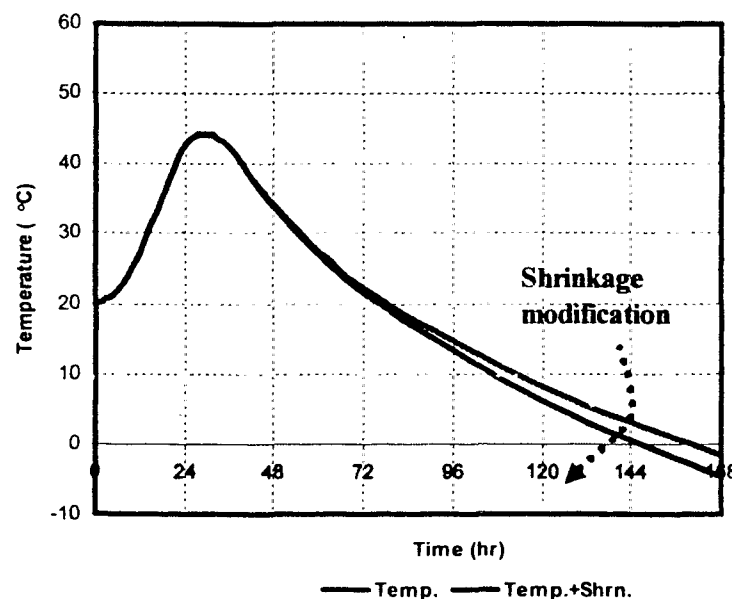


Figure 4.7: Modified temperature history curve to include shrinkage effect

#### 4.5 Coefficient of Thermal Expansion

The coefficient of thermal expansion, which is also called thermal dilation, is a primary parameter in calculation of thermal strains. Thermal expansion coefficient must be defined during stress-displacement analysis, which would create volumetric deformation according to given thermal difference. Most natural materials have certain expansion potential that determines expansion coefficient. Concrete expansion coefficient is

combination of its content properties and it is influenced by mix properties. Particularly, aggregate type has a dominant role on concrete thermal expansion potential. Thermal expansion coefficient of concrete can be found by determining the dimensional change in a specimen with temperature change as defined in following (Neville, 1995):

$$\alpha_c = \frac{\Delta \varepsilon_{th}}{\Delta T} \quad (4.10)$$

where,

$\alpha_c$  = coefficient of thermal expansion,  $1/^\circ\text{C}$

$\Delta \varepsilon_{th}$  = thermal strain, m/m

$\Delta T$  = change in temperature,  $^\circ\text{C}$

Traditionally, concrete expansion coefficient is assumed to be  $10 \times 10^{-6}/^\circ\text{C}$ . But depending on mix properties, its value may vary from  $5 \times 10^{-6}/^\circ\text{C}$  to  $15 \times 10^{-6}/^\circ\text{C}$ . Mitchell et al. (1998) tested mature and hardening concrete to compare expansion coefficient for different concrete mixes that are shown in Table 4.3. It was reported that thermal expansion coefficient is almost constant during hardening. It is also clear in Table 4.3 that, particularly for normal strength concrete, thermal expansion coefficient does not vary significantly.

Table 4.3: Variation of thermal expansion coefficient of different concrete types in hardening process

		Mature Concrete	Hardening Concrete	
Concrete Strength (Mpa)	Aggregate Type	$\alpha$ ( $1 \times 10^{-6}$ )/ $^\circ\text{C}$	Age (h)	$\alpha$ ( $1 \times 10^{-6}$ )/ $^\circ\text{C}$
30	Limestone	10.00	24	9.50
70	Limestone	10.91	24	10.20
100	Limestone	7.35	—	—

#### 4.6 Analysis - Case Study

Analysis is performed for previously considered case study. The FE mesh of stress-displacement analysis is shown in Figure 4.8. Structural model consist of four different

parts: culvert wall, culvert foundation and two layers of reinforcement. Selected mesh density is optimized to ensure accuracy of solution. Solid elements are linear eight nodes brick type. Reinforcement is modeled in the embedded surface region. Element types in surface region are four node-linear surface elements. All elements in the selected mesh are reduced integration type that has one integration point in the centre of the element. Linear reduced integration elements are recommended to predict strains in the structure (Hibbitt et al., 2004). However, using reduced integration elements requires relatively finer mesh, which is provided in this analysis. Alternatively, full-integration elements can also be used in the model. But using fully integrated elements would increase computational cost. Also, stiffer nature of full-integration elements causes poor results for strain prediction.

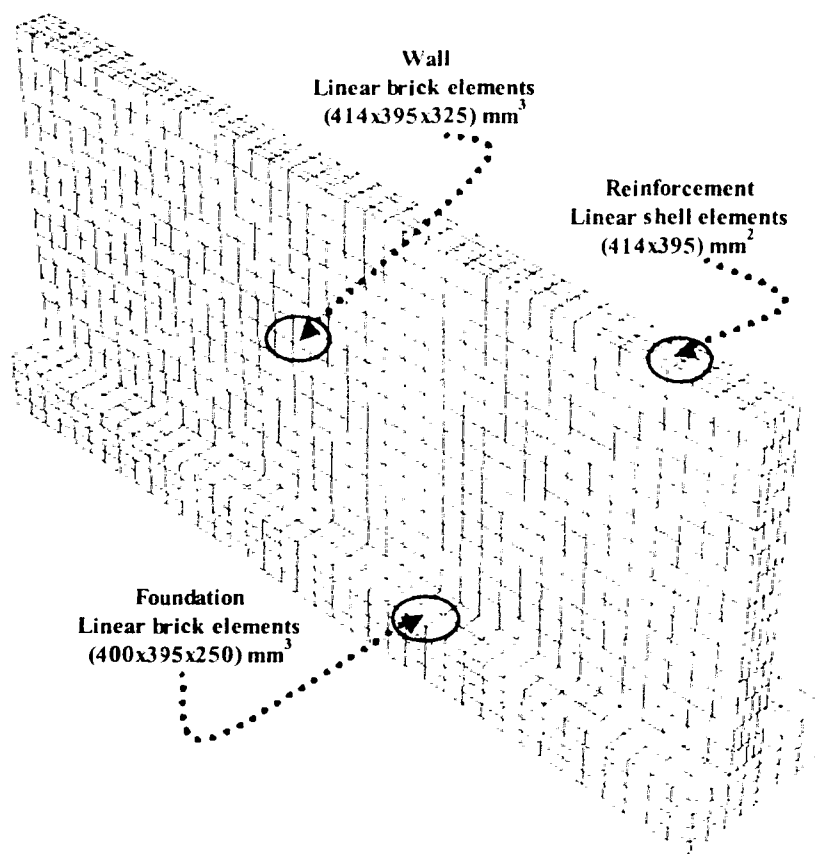


Figure 4.8: Finite element mesh-density of Culvert wall

Shrinkage and temperature reinforcement ratio is assumed to be about 0.3%, and it is distributed uniformly in two layers. Considering that provided reinforcement is placed continuously between the foundation and wall, which would provide very stiff connection, it was assumed that wall and foundation have perfect bond and multi-point-constraint was provided. Base of the foundation was modeled by elastic foundation interaction option in ABAQUS/6.4. Bosnjak suggested that 60 MN/m<sup>3</sup> is sufficient for the interaction between the structure and soil. The same value is used to define interaction forces on foundation. Foundation part of the structure is a one-week-old concrete. Since the stresses are too small, material non-linearity in foundation can be neglected. Material non-linearity for reinforcement can also be ignored since the stresses are well below the yield strength of the steel. Poisson's ratio of concrete ranges between 0.1 and 0.2 (CEB-FIP model code 1990). For this case study, it is assumed that poisson's ratio is equal to 0.18. Thermal expansion coefficient,  $\alpha$ , is determined in lab tests and it is given as  $8.5 \times 10^{-6}/^{\circ}\text{C}$ . List of assumed parameters are as follows:

$$\nu_{concr} = 0.18 \text{ (poissons ratio for concrete)}$$

$$\nu_{steel} = 0.0 \text{ (Poison's ratio for steel can be neglected in numerical analysis of reinforced concrete, Hibbitt, 2004)}$$

$$E_{foundation} = 25000 \text{ MPa (foundation elastic modulus)}$$

$$E_{steel} = 210000 \text{ MPa (reinforcement elastic modulus)}$$

General-static type analysis was performed in 10 steps and contour plot for resulting longitudinal stresses is shown in Figure 4.9. Total strains were recorded during the construction at four different points that are located in the centre of wall. The locations of four different strain gages were shown in Figure 2.4. Strain history output is requested from ABAQUS/6.4, and calculated strains were compared with measurements. Figures 4.10 to 4.13 show comparison of measured and calculated strains.

Observation of Figures 4.10 to 4.13 indicates that calculated strains are relatively in good agreement with measured values. At P4, which is shown in Figure 4.13, it is noticeable that there is a uniform shift between measurements and ABAQUS/6.4 results. The

uniform shift is an indication of possible errors in measured values. Considering the difficulties associated with strain measurement of hardening concrete starting from the initial pour, such an error is expected. If uniform deviation in P4 was ignored, calculated strains in Figures 4.12 and 4.13 have almost perfect match.

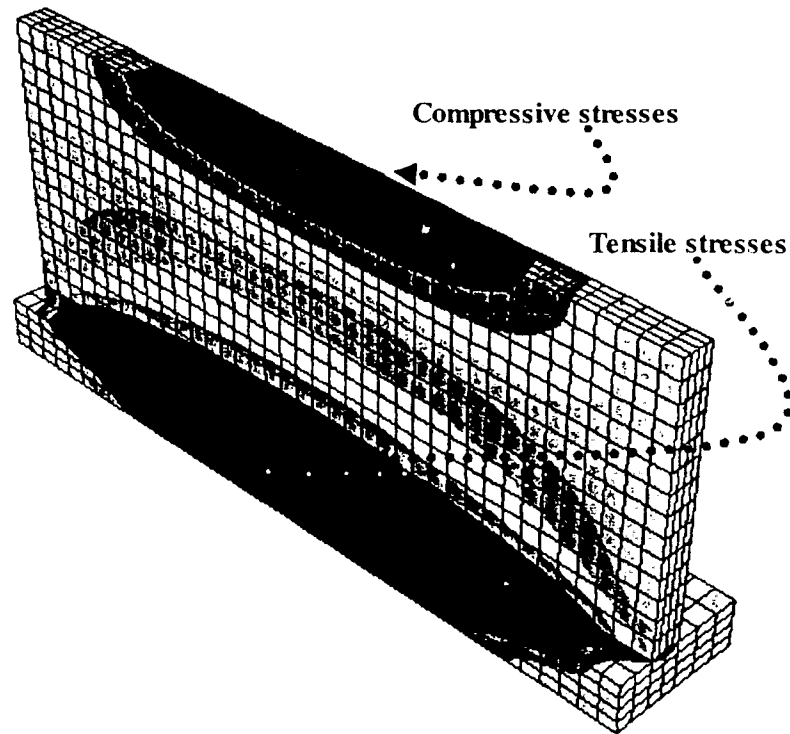


Figure 4.9: Contour plot of longitudinal stresses in Culvert part

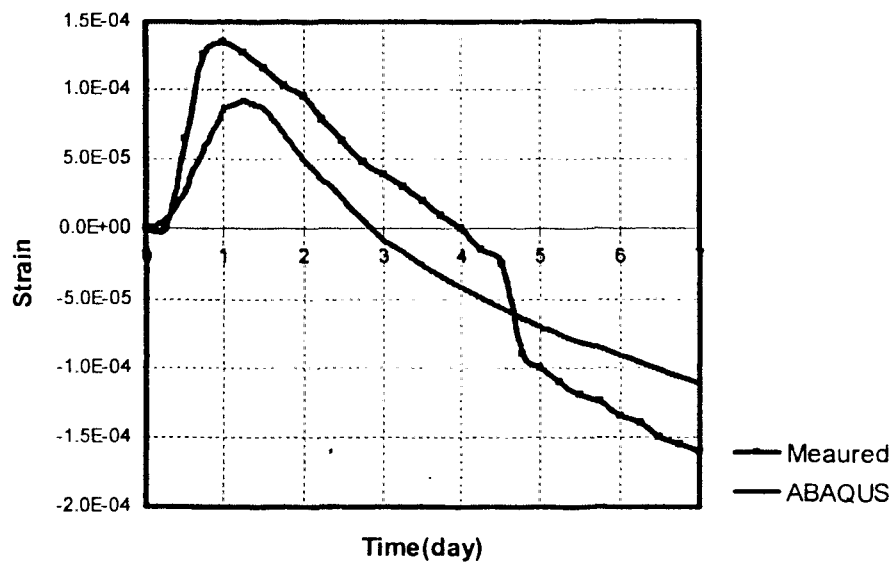


Figure 4.10: Comparison of measured and calculated strain history at Point 1

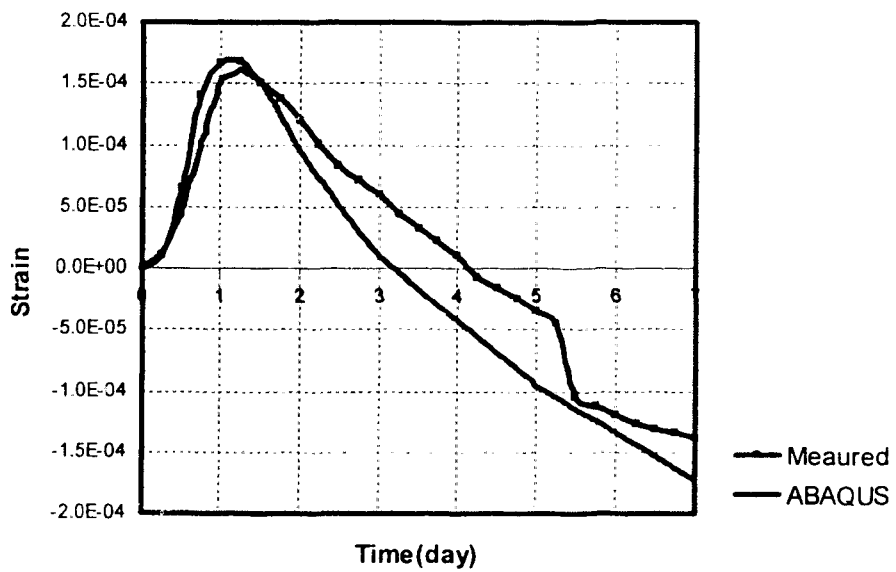


Figure 4.11: Comparison of measured and calculated strain history at Point 2

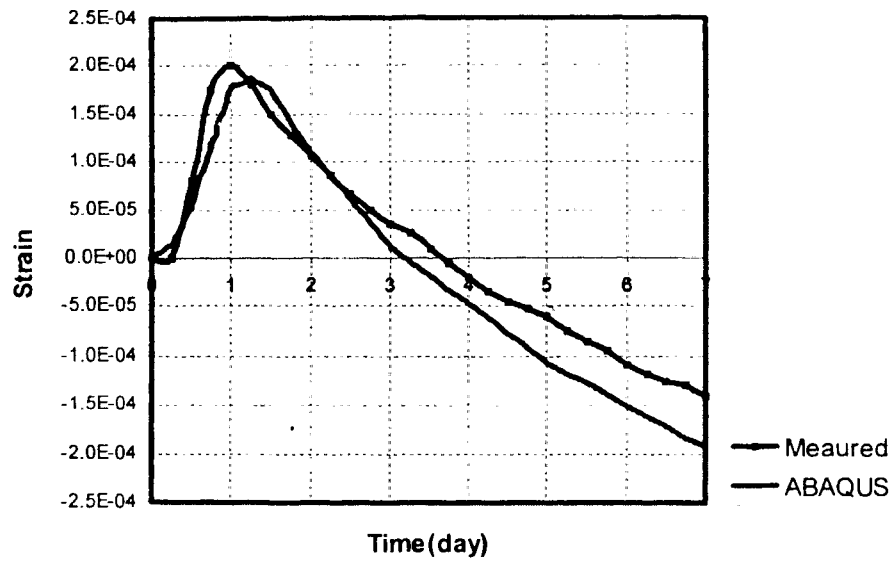


Figure 4.12: Comparison of measured and calculated strain history at Point 3

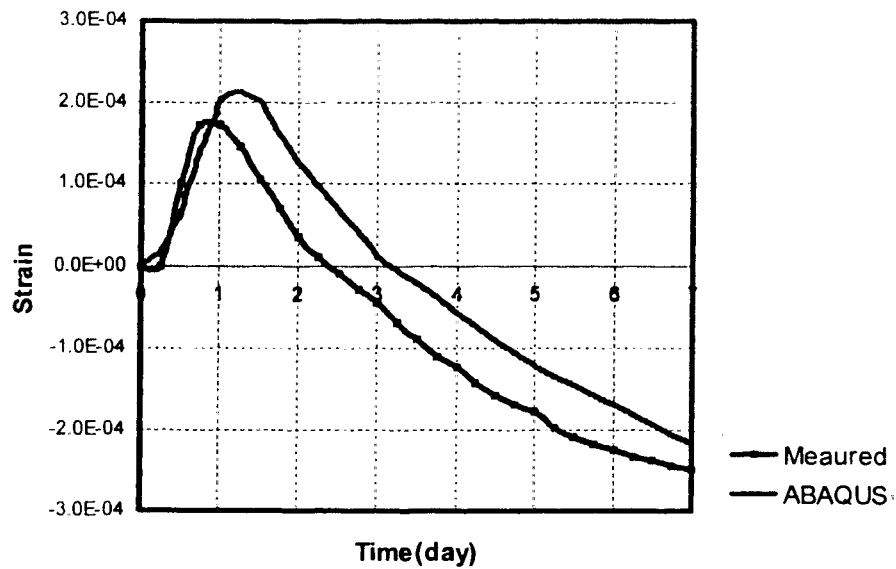


Figure 4.13: Comparison of measured and calculated strain history at Point 4

In Figures 4.10 and 4.11, the shape of deviation is different. These two figures represent the points that are closer to the foundation. There might be several reasons for deviation



of calculated and measured strains at P1 and P2. One speculation for the reason is that the calculated and measured temperatures are not the same, which would result different thermal strains in actual structure and simulated strains. However, in Chapter 2 it was shown that calculated temperature histories and field data are in very good agreement. Other speculations for deviation at P1 and P2 may be underestimated shrinkage, creep modeling that is adapted from CEB-FIP code, the slip between foundation and wall that is not considered in the numerical analysis, and the effect of volumetric deformation of foundation itself.

Each of the suggested reasons for deviation at P1 and P2 can be discussed. First speculation is that underestimated shrinkage of wall should not be the reason because the trends of the four different calculated strain curves are downward compare to measured strains. Shrinkage of wall is not underestimated since measured strain curves are not below the calculated strains.

Second speculation is that the effect of creep at P1 and P2. Effect of creep depends on the magnitude of stress and the duration of loading. In Figure 4.14 stress history of four points are shown. It is clear that generated stresses are very small, which implies that creep has negligible effect on strain history. Also duration of loading, which is one week, is relatively short for creep strains to develop. These facts eliminate the second speculation for the reason of deviation at P1 and P2.

Remaining possibilities for the difference in strain curves at P1 and P2, are the effect of volumetric deformation of foundation and the slip between the foundation and wall. An evidence of such slip is the sharp decrease in measured strain data that is visible in Figure 4.10 and 4.11. Using ABAQUS/6.4, it is possible to model even complex contact problems that may simulate the slip between foundation and wall. However, different analysis techniques are recommended to solve complex contact problems that are available in ABAQUS/Explicit (Hibbitt et al., 2004). For crack analysis of reinforced concrete, ABAQUS/Explicit was used in this thesis, which will be discussed in Chapter 6.

Calculated longitudinal stresses at four different points are shown in Figure 4.14. Developing tensile strength of concrete is also plotted in this figure. Maximum tensile stresses have developed in P1, which was expected. But, even in P1 generated stresses

are below the tensile strength, which would eliminate crack risk at this point. However, it is important to note that this simulation is performed for one week. A week after placement, most of tensile strength has developed and after this point concrete strength would not increase. On the other hand, drying shrinkage is just at the starting point of development. In longer time, particularly if the atmospheric conditions are dry, significant drying shrinkage may be expected. But, the concrete used in this structure is HPC and generally this type of concrete does not have significant long-term shrinkage. HPC shrinkage problems occur in short term and that is mainly due to chemical shrinkage. It was discussed in Chapter 3 that CEB-FIP shrinkage model is not reliable for estimating chemical shrinkage. CEB-FIP model may be questionable in prediction of chemical shrinkage. But in this particular simulation this model has produced good result, and the evidence for that is comparison of strain curves discussed above. Considering the time of construction, the location and the nature of the structure, which is placed below ground level, it can be concluded that relative humidity was very low during hardening period and chemical shrinkage did not affect this structure significantly.

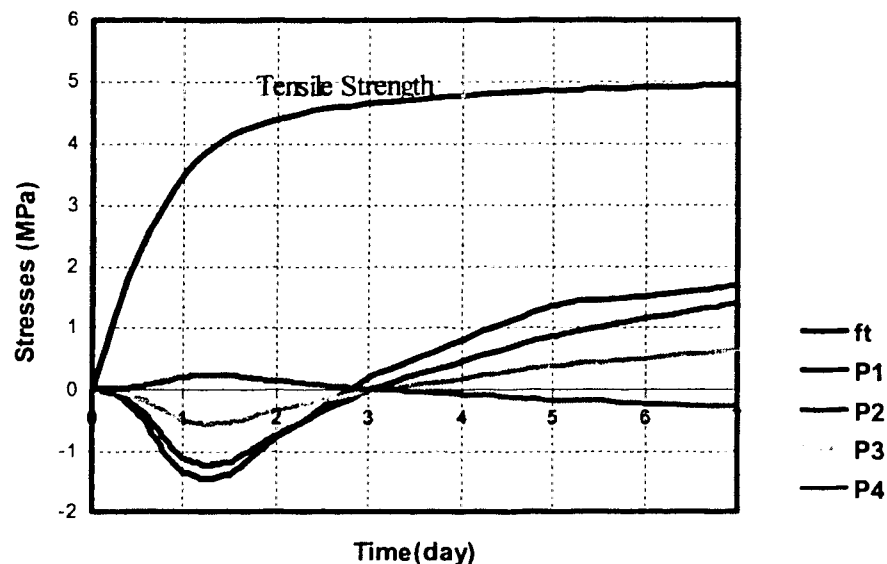


Figure 4.14: Calculated stress history at different points and tensile strength development

#### **4.7 Summary**

Based on the given data on concrete mix and environmental conditions, temperature history of hardening concrete was calculated in Chapter 2. Mechanical properties of concrete are related to its temperature history. In Chapter 3 calculated temperature history was used to determine concrete properties. Shrinkage of concrete was estimated based on code recommendations. Finally in this chapter, thermal and shrinkage strains were applied to an example structure that has developing properties. A summary of this procedure is given in Figure 4.15.

Methodology followed during this simulation is a realistic method for analysis that includes most parameters involved in the problem. Using the presented analysis technique, tensile stresses that are generated due to thermal and shrinkage strains can be simulated and assessed realistically. Thermal and shrinkage strains are one of the important problems in concrete technology. In practical engineering, there are many ways to deal with volumetric changes induced stresses such as selecting proper concrete mix, proper curing, proper geometry to reduce restraint, use of reinforcement etc. The main problem with these control measures that it is difficult to quantify the effect of each application. The analysis method presented here may be able to solve this problem and applied successfully to concrete materials in structures. For example, selected concrete mix may have low hydration heat, which would cause lower thermal strains. This effect can be observed throughout analysis. Another example can be the effect of shrinkage compensating concrete, which may be used in construction. Construction joints or reinforcement effects are some other parameters that can be assessed with presented analysis method. In fact, even the effect of curing temperature on stresses can be quantified in presented simulation technique. At last, a realistic simulation technique may contribute to reduce the cost and increase durability of structure that will improve concrete engineering.

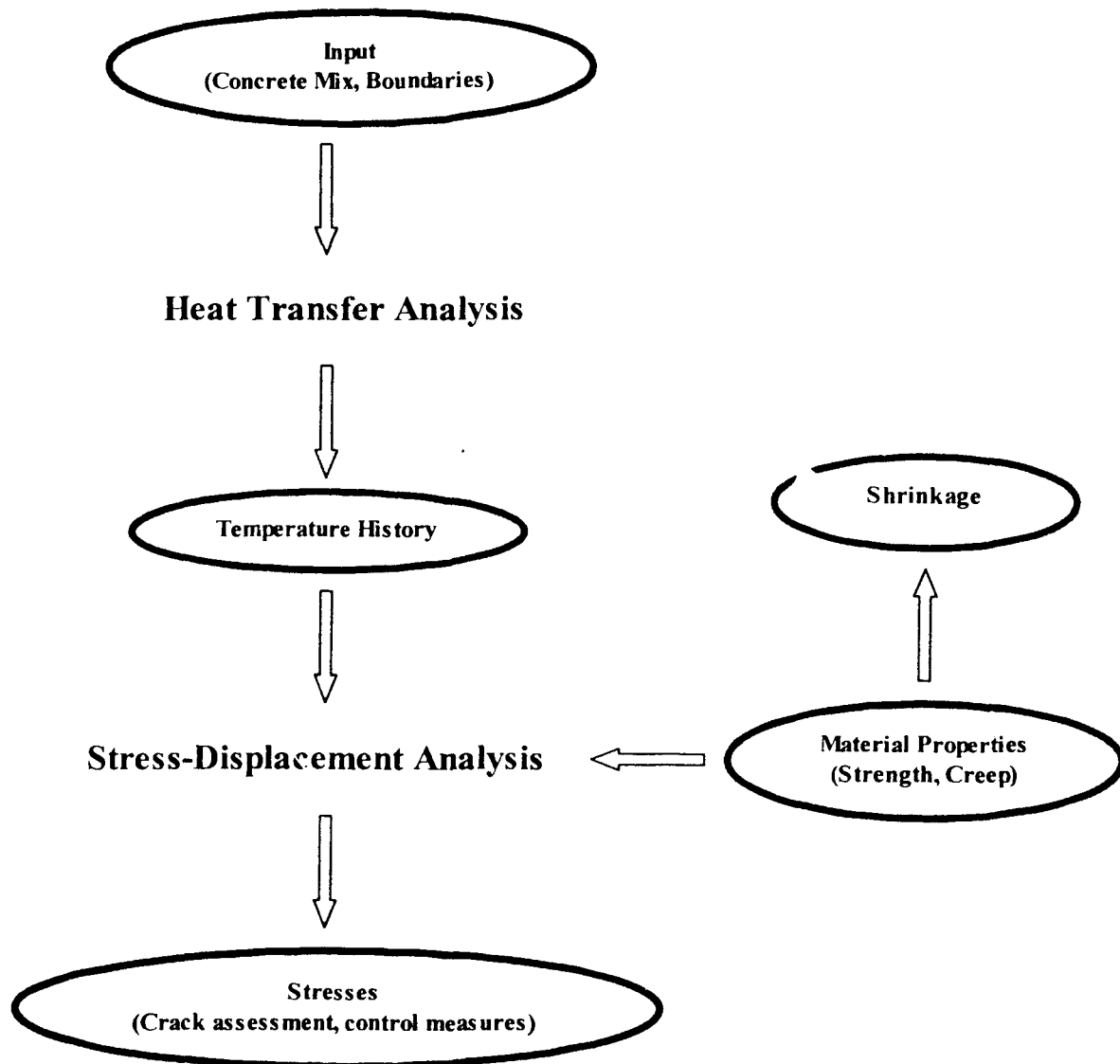


Figure 4.15: Summary of simulation of hardening concrete

## CHAPTER 5

### RESTRAINT FACTOR

#### 5.1 Introduction

In reality, almost all structures have some kind of restraining that prevents or limits the movement of the structure. Limiting or restraining the movement of the structure either by supporting structural part or by adjoining element would induce stresses in the structure. Determination of magnitude of restraining is required to analyze possible effects of induced stresses. ACI 207.2R-95 defines the degree of restraint as the ratio of actual stress resulting from volume change to the stress, which would result when completely restrained. Numerically, the strain is equal to the product of the degree of restraint existing at the point in question and the change in unit length, which would occur when the concrete were not restrained. Description of restraint factor given by ACI can be formulated as shown in following that is the same as Anderson (1998) formulation for degree of restraint.

$$R = \frac{\epsilon_{restrained}}{\epsilon_{free}} \quad (5.01)$$

where,

$R$  = restraint factor

$\epsilon_{restrained}$  = restrained strain

$\epsilon_{free}$  = free strain

Restrained strains can cause tensile, compressive or flexural stresses in concrete structural elements. Primary concern with concrete is tensile stresses that may cause cracks. Concrete ability to resist compression is considerably large, and restraint induced compressive stresses are negligible compared to other structural loads. Harrison (1981) describes restrained strain, by referring only to volumetric changes due to thermal strains. However, volumetric changes of concrete structural elements can be for various reasons such as temperature variation, chemical, drying and autogenous shrinkage. Both, thermal and shrinkage strains are stress independent strains, and they can be superposed for

design purposes. Whether shrinkage is the result of thermal contraction or moisture loss, degree of restraint does not change. It is the geometric properties of structure that governs the magnitude of degree of restraint. If total volume change is determined, structure can be designed to meet certain requirements such as maximum crack width. In Chapters 2 and 3, the methods to calculate total thermal and shrinkage strains were explained. For convenience, shrinkage strains were converted to equivalent temperature change and generated stresses were calculated based on total restraint thermal deformations. Problem arises when the product of restraint factor and thermal strain exceeds tensile strain capacity of concrete. In concrete structures, excessive restrained strain would cause crack development. Harrison (1981) expresses this relation in simple format as shown in following:

$$(\alpha.\Delta T.R) > \text{Tensile Strain Capacity} \quad (5.2)$$

where,

$\alpha$  = thermal expansion coefficient

$\Delta T$  = change in temperature

$R$  = restraint factor

The left side of Eq.5.2 include restraint factor,  $R$ , and total free strain that includes thermal and shrinkage strains ( $\alpha.\Delta T$ ). Right side of the equation is the tensile strain capacity of concrete, which is maximum restrained strain that concrete can resist. From Eq.5.2, it is clear that Harrison also describe restraint factor as the ratio of restrained strain to thermal strain. In most situations, the product of restraint factor and free strain exceeds tensile strain capacity and cracks develop. Concrete design as structural material requires limited crack width and that is achieved by reinforcement. Determination of sufficient amount of reinforcement requires correct estimation of degree of restraint. However, there is no particular design guide that provides analytical data for degree of restraint. Instead of analytical method, certain amount of temperature and shrinkage reinforcement is recommended in most design guides. One of the design guides produced by ACI committee 207 (ACI 207.2R-95), provides limited information to calculate degree of restraint. ACI 207.2R-95 recommendation for degree of restraint is developed

by experiments for plain concrete, and its validity for reinforced concrete is a matter of interest. In this chapter, numerical analysis of reinforced concrete is performed to determine degree of restraint in a simple structure and results are compared with ACI 207.2R-95 data.

## 5.2 Degree of Restraint

Degree of restraint changes according to geometric properties of concrete. Based on the geometry, each structure may have internal, external, continuous and discontinuous restraining condition. Generally speaking, internal restraint is the result of section thickness, while external restraint is the result of adjoining or supporting structure. An example of external continuous edge restraint is shown in Figure 5.1 that is explained in CIRIA report (Harrison, 1981). This common case may occur when a wall cast onto a rigid or on a flexible base. When concrete wall starts to cool down to ambient temperature level, it attempts to contract. But previously cast base restrains any movement by contact friction. When the wall is allowed to contract freely, a theoretical shape as shown in Figure 5.1(b) would appear. In reality, depending on base rigid or flexible condition, volumetric changes of wall would form a shape as shown in Figure 5.2 (a, b).

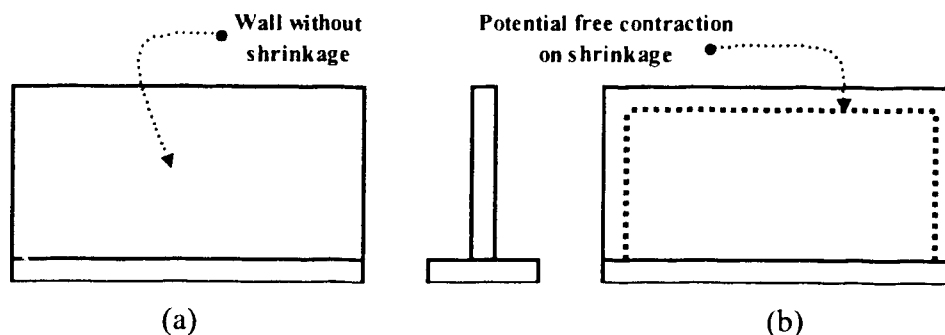


Figure 5.1: Continuous edge restraint of wall cast on a base, (a) wall without shrinkage, (b) potential free contraction

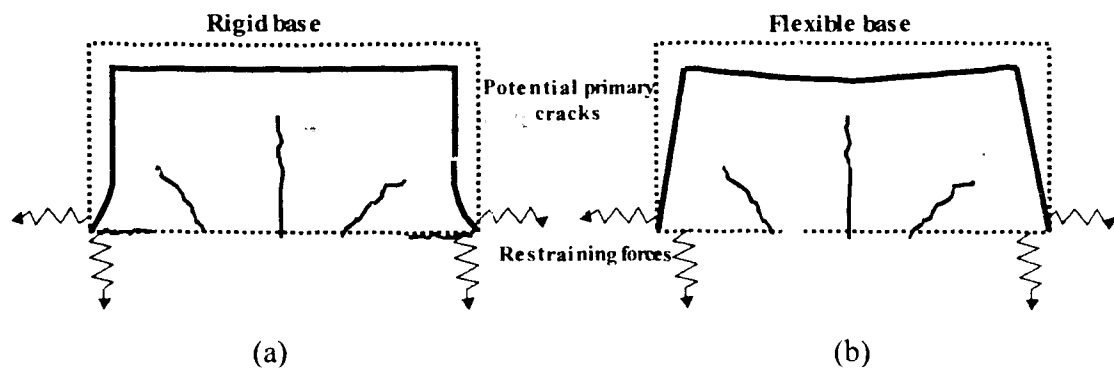
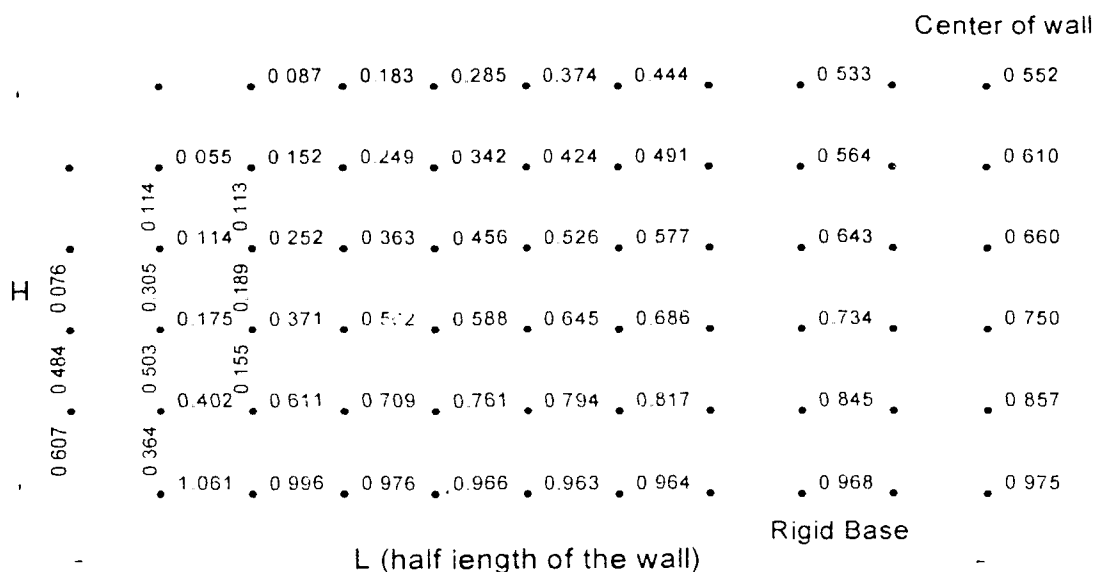


Figure 5.2: Potential crack formation for different rigidity of foundation (a) rigid base, (b) flexible base

Figure 5.2 shows primary crack formations due to restraining condition. Secondary cracks would form and crack width would be under control when sufficient amount of reinforcement is provided in the wall section. Restraining condition shown in Figures 5.1 and 5.2, called continuous edge restraining condition and it is a simple model to illustrate restraining. Similar restraining condition can occur in successive lifts of a wall or in adjoining strips of a slab. This condition can also occur when a wall cast on a fully or partially restrained slab. In reality, boundaries of the structure may have different configuration and accordingly different restraining condition may develop. This would modify critical sections in the wall and create different crack pattern. For example, the wall may have boundaries at both ends, which is defined as three-side fully restrained wall. Three-side fully restrained condition may occur when a wall is constructed in stages as different bays.

In order to reach an optimum or an economical structural design, determination of restraining factor is required. In CIRIA (Harrison, 1981) report, variation of restraint factor for an uncracked wall that is placed on a rigid base was calculated and shown in Figure 5.3. Harrison does not present the details of calculations, but it is mentioned that curvature formulas was used. Similar wall will be analyzed using ABAQUS/6.4 and degree of restraint will be compared in the following section.





observed. Degree of restraint is negligibly small at points of deviation and can be ignored. In CIRIA report (Harrison, 1981), determination of restraint factors by using formulas of curvature may have introduced small errors. Several researchers have named free corner of wall as no crack zone due to zero restraint factor (Kheder, 1997). The negative signs for calculated degree of restraint means compressive stresses on that region, and no crack would form. Overall results shows very good match between calculated degree of restraint and given numbers.

Table 5.1: Comparison of calculated degree of restraint with CIRIA report (L/H=4)

X/Y or L/H Coordinates in the wall		Length from center of the wall										
		0.0L	0.1L	0.2L	0.3L	0.4L	0.5L	0.6L	0.7L	0.8L	0.9L	1.0L
Height from base of the wall	1.0H	0.592	0.581	0.545	0.484	0.396	0.283	0.153	0.029	-0.049	-0.040	0.001
		0.552		0.533		0.444	0.374	0.285	0.183	0.087		
	0.8H	0.613	0.604	0.576	0.530	0.464	0.382	0.286	0.184	0.089	0.020	-0.002
		0.610		0.564		0.491	0.424	0.342	0.249	0.152	0.055	
	0.6H	0.671	0.665	0.646	0.613	0.567	0.506	0.425	0.317	0.183	0.055	-0.017
		0.660		0.643		0.577	0.526	0.456	0.363	0.252	0.114	
	0.4H	0.756	0.752	0.741	0.722	0.693	0.652	0.592	0.497	0.329	0.074	0.004
		0.750		0.734		0.686	0.645	0.588	0.502	0.371	0.175	
	0.2H	0.859	0.857	0.852	0.844	0.831	0.813	0.786	0.738	0.655	0.420	-0.253
		0.857		0.845		0.817	0.794	0.761	0.709	0.611	0.402	
	0.0H	0.972	0.971	0.971	0.970	0.970	0.971	0.975	0.983	1.017	0.948	1.237
		0.975		0.968		0.964	0.963	0.966	0.976	0.996	1.061	

\*Dark (blue) colored lines indicates calculated degree of restraint with ABAQUS/6.4

#### 5.4 Degree of Restraint in Reinforced Concrete Walls

ACI committee 207 has special report that covers degree of restraint. Although, ACI 207.2R-95 mainly deals with mass concrete, degree of restraint for walls is also discussed. Based on experimental studies, a chart is prepared that can be used to estimate the degree of restraint. Experiments were performed with rubber material and then several plain concrete walls were used to verify the values with the rubber model. Figure 5.4 provides estimation of degree of restraint in the centerline of wall that is recommended by ACI 207.2R-95. A tabulated format of this figure is prepared and shown in Table 5.2.

Degree of restraint variation along the mid section of wall, and its graphical representation (Figure 5.4) is a test data for plain concrete placed without time lapses. However, it is unknown whether Figure 5.4 can be used to estimate degree of restraint for

reinforced concrete model. Cusson et al. (2000) questions validity of Figure 5.4, and it is suggested that using this figure may underestimate degree of restraint for reinforced concrete walls. With ABAQUS/6.4, it is possible to analyze reinforced concrete, and from analysis output degree of restraint can be calculated.

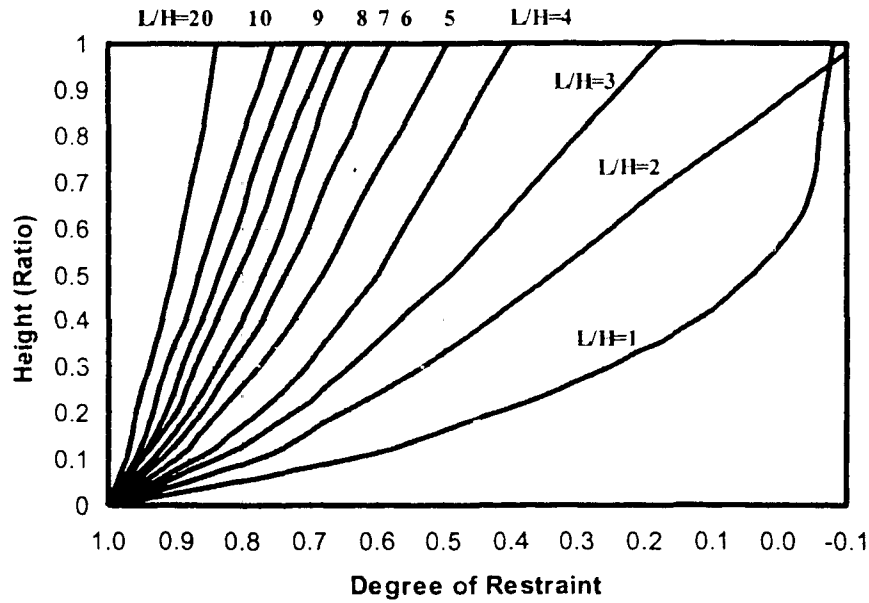


Figure 5.4: Degree of Restraint variation at the centre of wall (ACI 207.2R-95)

Table 5.2: Degree of restraint at wall centerline (ACI 207.2R-95)

Height Above Base	Restraint Factor Variation at the Middle of Wall (AC.207.2R-95)										
	L/H=1	L/H=2	L/H=3	L/H=4	L/H=5	L/H=6	L/H=7	L/H=8	L/H=9	L/H=10	L/H=20
0.0	1.000	1.000	1.000	1.000	1.000	1.000	1.000	1.000	1.000	1.000	1.000
0.1	0.640	0.780	0.840	0.870	0.900	0.920	0.935	0.950	0.950	0.960	0.972
0.2	0.420	0.650	0.725	0.775	0.835	0.860	0.880	0.900	0.915	0.935	0.960
0.3	0.250	0.530	0.640	0.706	0.775	0.816	0.840	0.872	0.890	0.915	0.940
0.4	0.120	0.430	0.565	0.650	0.725	0.772	0.800	0.840	0.862	0.885	0.920
0.5	0.040	0.340	0.490	0.600	0.680	0.738	0.770	0.810	0.836	0.865	0.905
0.6	-0.020	0.250	0.425	0.560	0.645	0.702	0.740	0.780	0.810	0.845	0.890
0.7	-0.050	0.165	0.365	0.520	0.610	0.675	0.720	0.755	0.790	0.823	0.878
0.8	-0.060	0.065	0.300	0.480	0.570	0.640	0.695	0.730	0.766	0.800	0.860
0.9	-0.070	-0.025	0.235	0.440	0.530	0.612	0.670	0.700	0.738	0.775	0.850
1.0	-0.080	-0.120	0.175	0.400	0.495	0.580	0.640	0.670	0.710	0.755	0.838

In this section, calculated degree of restraint in 11 different models that have different L/H ratios will be shown. Analyses of these walls were performed first in linear range and then in non-linear range. Height of the walls were kept constant while the lengths were increased to have L/H ratio ranging from 1 to 20. A standard model of a wall cast on a rigid base is shown in Figure 5.5.

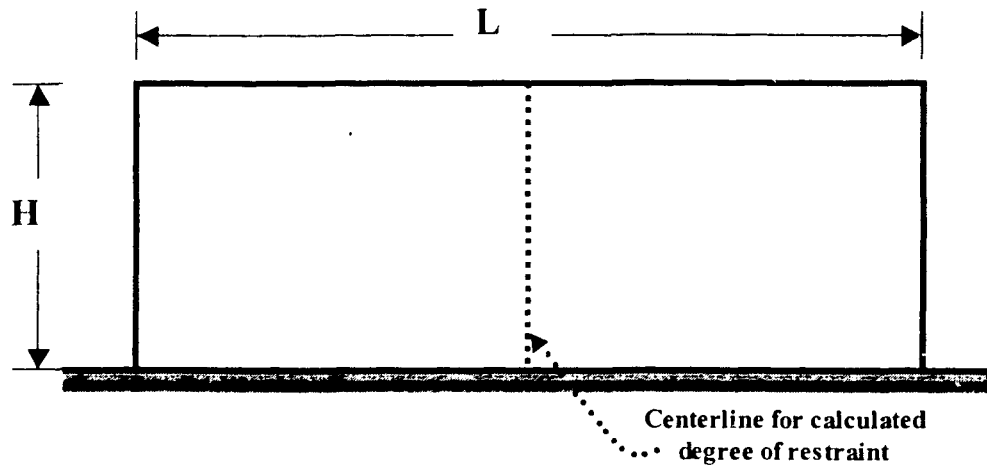


Figure 5.5: Standard model for calculation of degree of restraint variation at the centre of wall

From the definition of restraint factor that is given in Eq.5.1, it is clear that degree of restraint is a parameter of relative dimensions. Increasing total thermal and shrinkage strains does not affect degree of restraint. If the magnitude of free strain were increased, the magnitude of restrained strain would also increase. Since degree of restraint is the ratio of restraint strain to free strain, it does not change with variation of total thermal and shrinkage strain. As a result, degree of restraint is constant with increased free strain. For analysis, a certain amount of shrinkage can be assumed. Parameters that is used in numerical analysis are as follows:

$$f_c = 30 \text{ MPa (concrete compressive strength)}$$

$$E_c = 25000 \text{ MPa (concrete modulus of elasticity)}$$

$$\nu_c = 0.15 \text{ (Poisson's ratio for concrete)}$$

$\alpha_c = 10 \times 10^{-6} / ^\circ C$  (thermal expansion coefficient for concrete)

$f_y = 400$  MPa (steel yield stress)

$E_s = 210$  GPa (steel modulus of elasticity)

$\nu_s = 0.0$  (Poisson's ratio for steel)

$\alpha_s = 0.0 / ^\circ C$  (thermal expansion coefficient for steel)

$1 \text{ m} \leq \text{Length} \leq 20 \text{ m}$

Height = 1 m

Wall thickness = 200 mm

$\rho = 0.5\%$  (reinforcement ratio)

Concrete cover for reinforcement = 30 mm

$\Delta T = 60$   $^\circ C$  (equivalent temperature change)

Element type = Quadratic, reduced integration, 8 node shell element (S8R)

Figure 5.6 and Table 5.3 show calculated degree of restraint based on linear analysis, while results of non-linear analysis are presented in Figure 5.7 and Table 5.4. Although the results shows similarity with ACI's figure, when L/H ratio is more than 3, large deviation in degree of restraint can be observed. ACI's figure is produced for plain concrete and that does not represent reinforced concrete strain response for volumetric changes. Comparison of calculated degree of restraint and ACI's recommendation for each wall is plotted separately in Figures 5.8 to 5.18. Each figure contains ACI's data, ABAQUS/6.4-Linear and -Nonlinear analysis results.

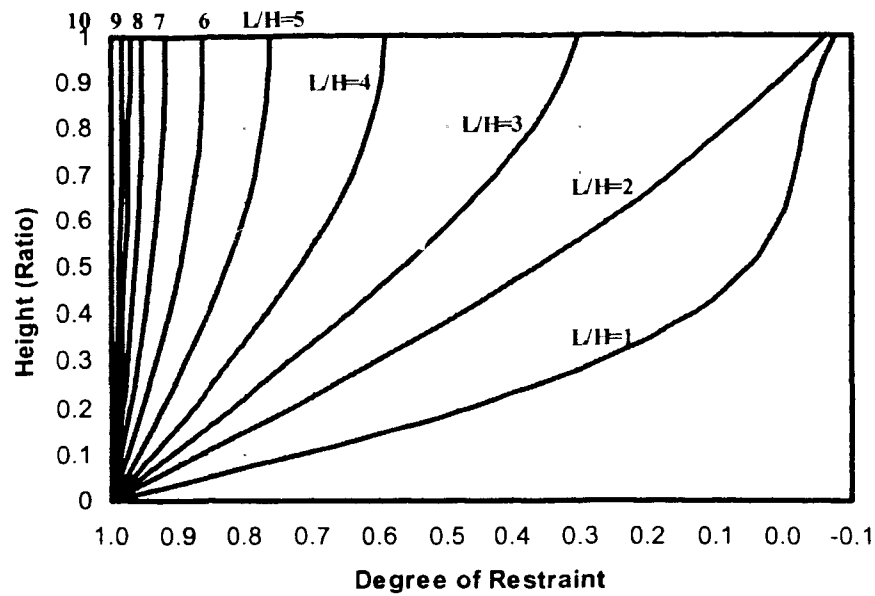


Figure 5.6: Degree of restraint variation at the centreline of wall (ABAQUS/6.4 Linear analysis)

Table 5.3: Degree of restraint at centerline of wall (ABAQUS/6.4 Linear analysis)

Height Above Base	Restraint Factor Variation at the Middle of Wall (ABAQUS Linear Analysis)										
	L/H=1	L/H=2	L/H=3	L/H=4	L/H=5	L/H=6	L/H=7	L/H=8	L/H=9	L/H=10	L/H=20
0.0	1.000	1.000	1.000	1.000	1.000	1.000	1.000	1.000	1.000	1.000	1.000
0.1	0.723	0.868	0.911	0.938	0.960	0.976	0.986	0.992	0.995	0.997	1.000
0.2	0.469	0.734	0.821	0.879	0.923	0.953	0.972	0.984	0.990	0.994	1.000
0.3	0.269	0.602	0.732	0.822	0.888	0.933	0.960	0.977	0.985	0.992	1.000
0.4	0.133	0.477	0.646	0.769	0.857	0.914	0.949	0.970	0.985	0.990	1.000
0.5	0.051	0.362	0.565	0.720	0.829	0.898	0.940	0.965	0.980	0.988	1.000
0.6	0.006	0.258	0.490	0.677	0.805	0.884	0.932	0.960	0.975	0.986	1.000
0.7	-0.016	0.165	0.424	0.642	0.786	0.874	0.926	0.956	0.975	0.985	1.000
0.8	-0.030	0.081	0.369	0.615	0.773	0.867	0.922	0.954	0.975	0.984	1.000
0.9	-0.045	0.006	0.327	0.598	0.765	0.863	0.920	0.953	0.970	0.984	1.000
1.0	-0.075	-0.061	0.302	0.592	0.764	0.863	0.919	0.953	0.970	0.984	1.000

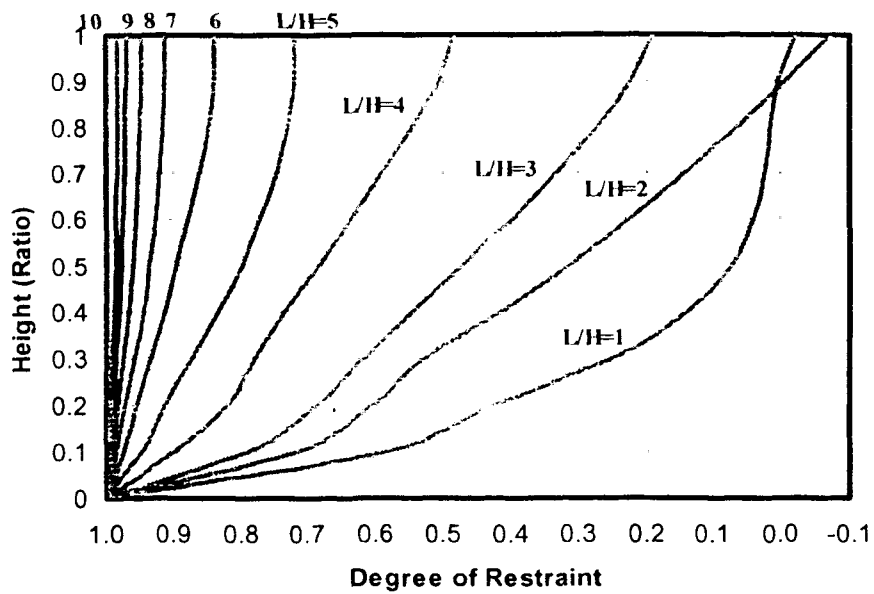


Figure 5.7: Degree of restraint variation at centreline of wall (ABAQUS/6.4 Non-Linear analysis)

Table.5.4: Degree of restraint at centerline of wall (ABAQUS/6.4 Non-linear analysis)

Height Above Base	Restraint Factor Variation at the Middle of Wall (ABAQUS Non-linear Analysis)										
	L/H=1	L/H=2	L/H=3	L/H=4	L/H=5	L/H=6	L/H=7	L/H=8	L/H=9	L/H=10	L/H=20
0.0	1.008	1.007	1.004	1.002	1.001	1.001	1.000	1.000	1.000	1.000	1.000
0.1	0.585	0.717	0.790	0.898	0.949	0.975	0.986	0.992	0.995	0.997	1.000
0.2	0.427	0.606	0.687	0.820	0.913	0.956	0.972	0.983	0.990	0.994	1.000
0.3	0.247	0.527	0.620	0.780	0.871	0.934	0.959	0.975	0.986	0.992	1.000
0.4	0.139	0.416	0.547	0.736	0.833	0.914	0.947	0.968	0.982	0.989	1.000
0.5	0.074	0.313	0.473	0.685	0.800	0.896	0.936	0.962	0.978	0.987	1.000
0.6	0.042	0.222	0.398	0.636	0.772	0.879	0.928	0.957	0.975	0.985	1.000
0.7	0.026	0.140	0.331	0.591	0.748	0.863	0.921	0.953	0.973	0.984	1.000
0.8	0.017	0.066	0.272	0.548	0.732	0.848	0.917	0.950	0.972	0.983	1.000
0.9	0.006	-0.004	0.224	0.506	0.722	0.841	0.914	0.949	0.971	0.983	1.000
1.0	-0.020	-0.072	0.189	0.484	0.719	0.840	0.914	0.949	0.971	0.982	1.000

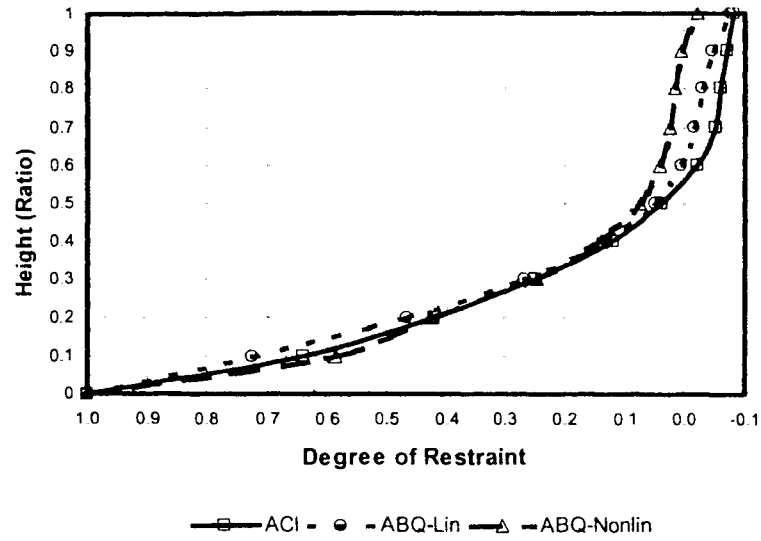


Figure 5.8: Comparison of degree of restraint variation at the centreline of wall for  $L/H=1$

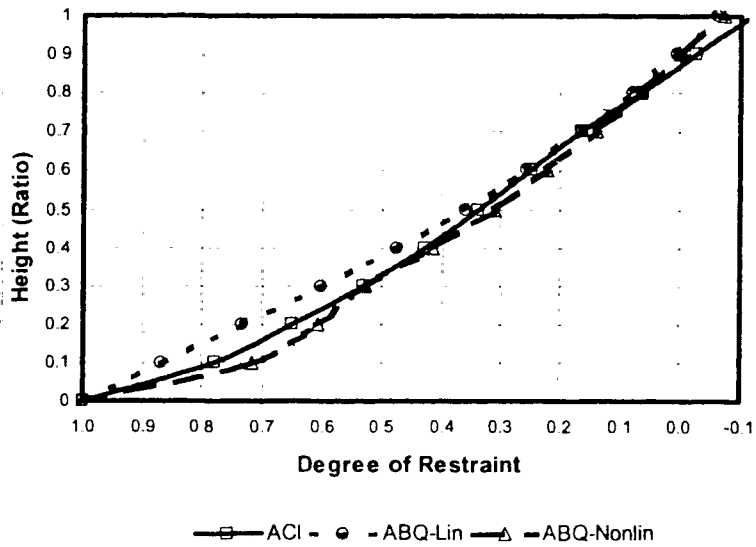


Figure 5.9: Comparison of degree of restraint variation at the centreline of wall for  $L/H=2$



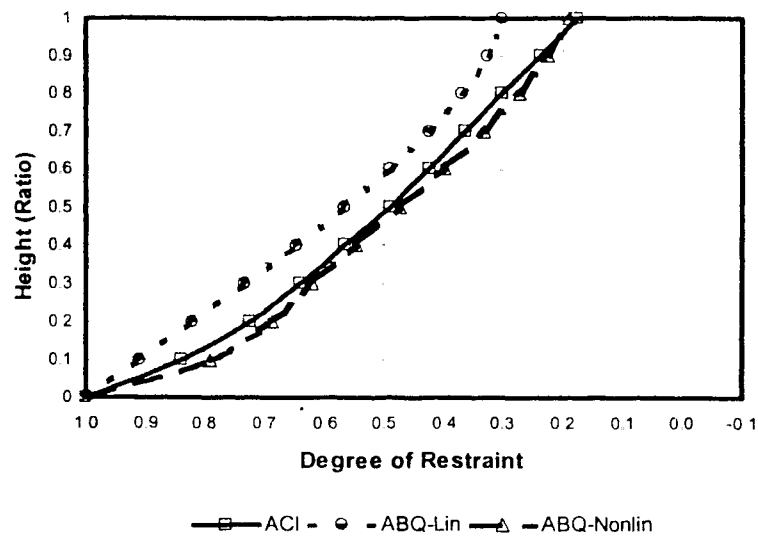


Figure 5.10: Comparison of degree of restraint variation at the centreline of wall for  $L/H=3$

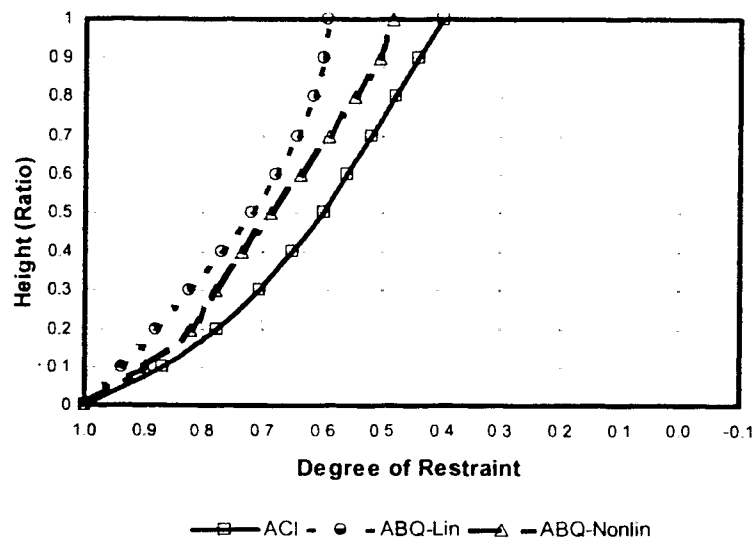


Figure 5.11: Comparison of degree of restraint variation at the centreline of wall for  $L/H=4$

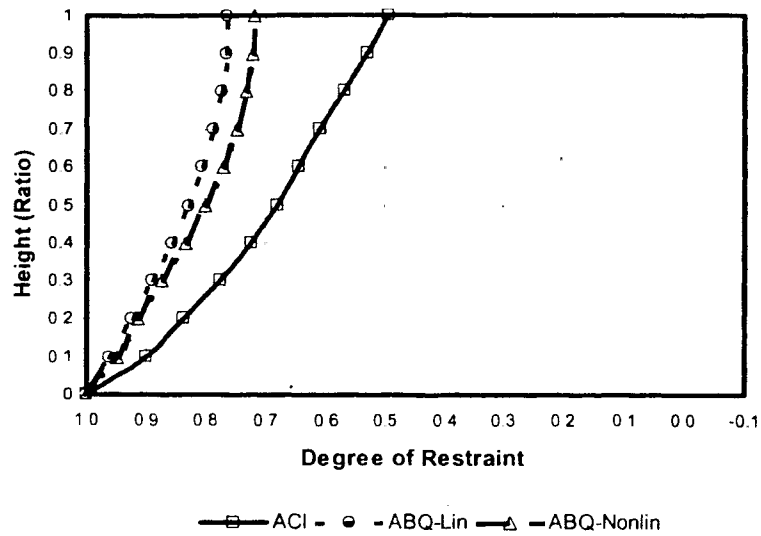


Figure 5.12: Comparison of degree of restraint variation at the centreline of wall for  $L/H=5$

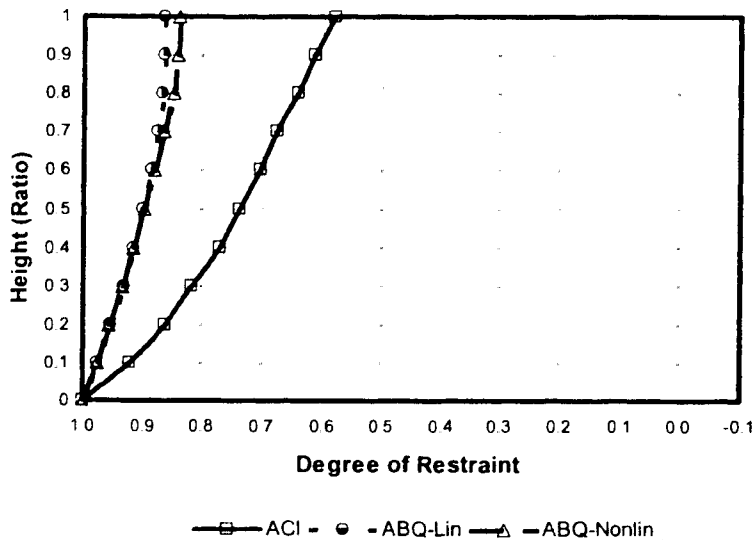


Figure 5.13: Comparison of degree of restraint variation at the centreline of wall for  $L/H=6$

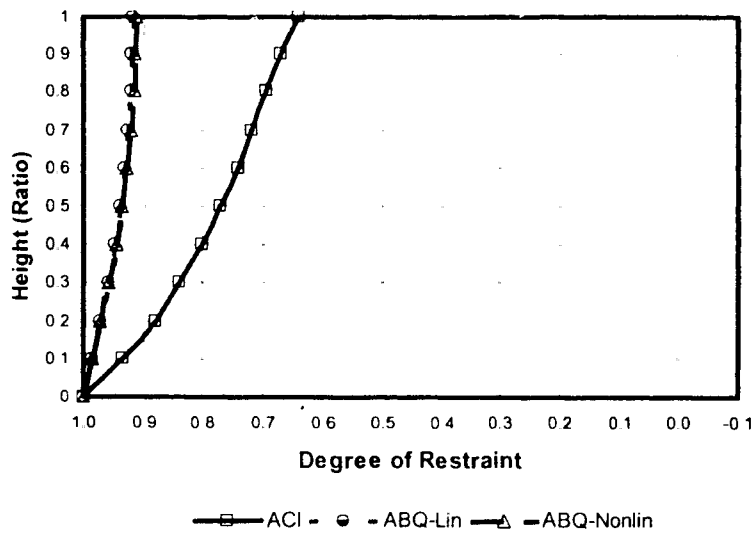


Figure 5.14: Comparison of degree of restraint variation at the centreline of wall for  $L/H=7$

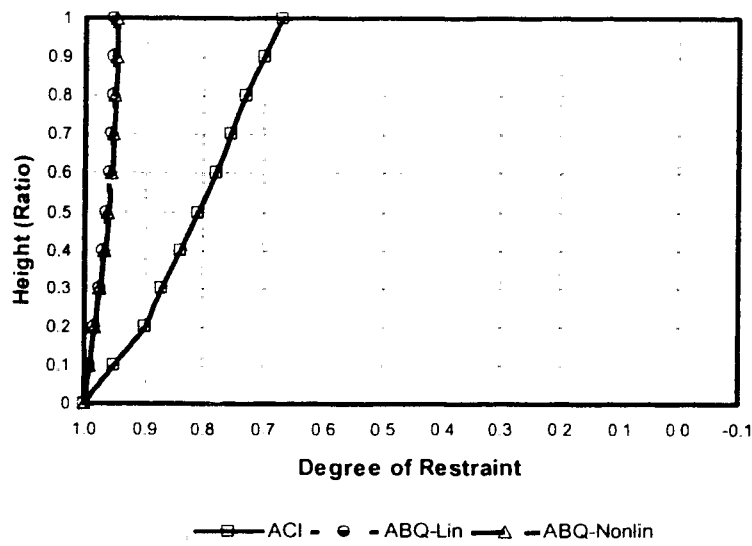


Figure 5.15: Comparison of degree of restraint variation at the centreline of wall for  $L/H=8$

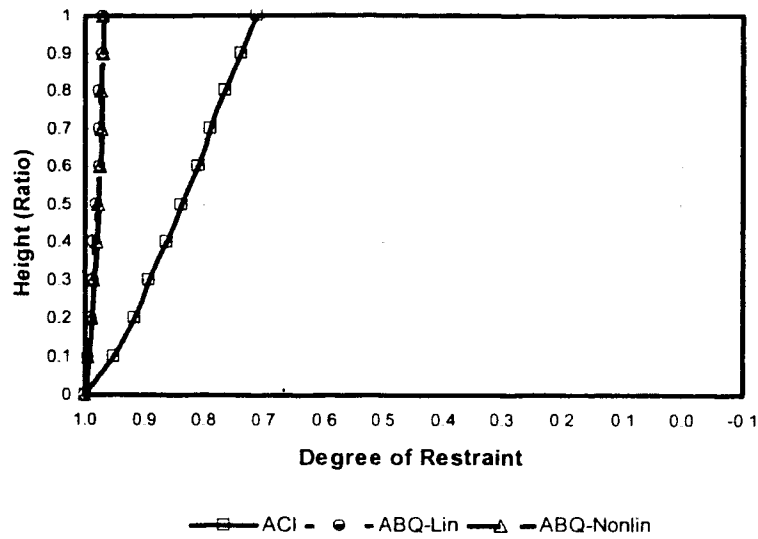


Figure 5.16: Comparison of degree of restraint variation at the centreline of wall for  $L/H=9$

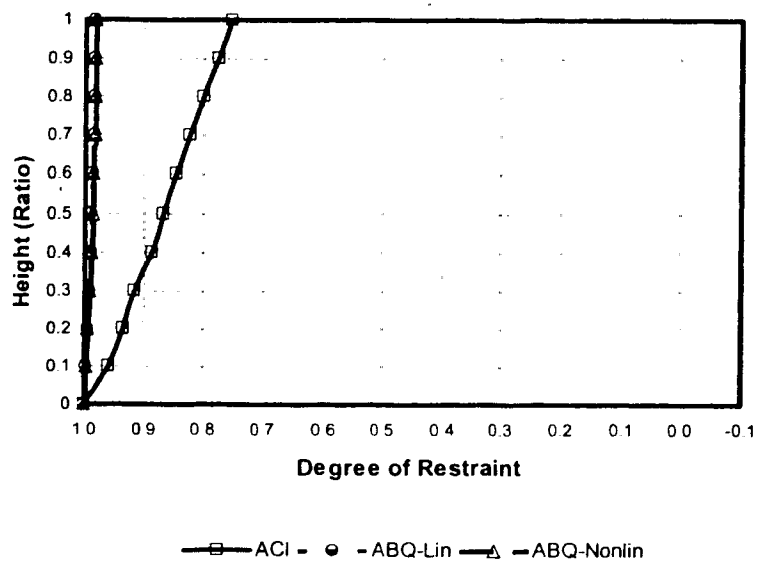


Figure 5.17: Comparison of degree of restraint variation at the centreline of wall for  $L/H=10$

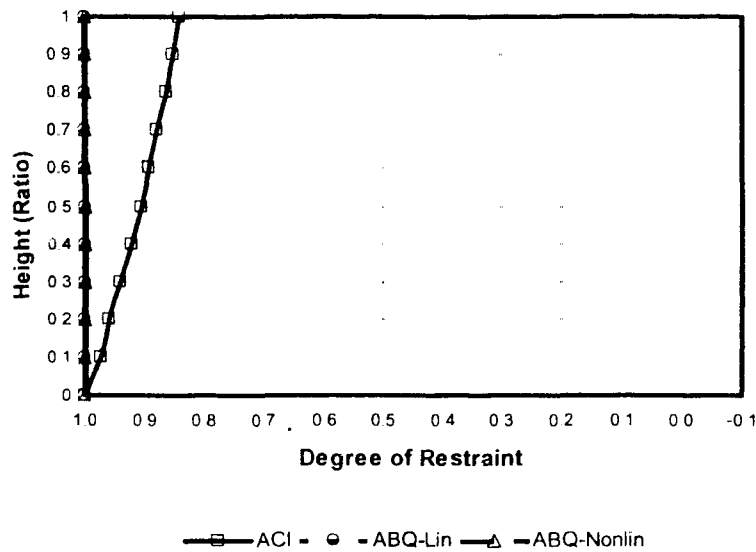


Figure 5.18: Comparison of degree of restraint variation at the centreline of wall for  $L/H=20$

In Figures 5.8, 5.9 and 5.10 it can be seen that for  $L/H$  ratio 1, 2 and 3, deviation between calculated values and ACI's data is negligible. In Figure 5.8, approximately above  $0.6H$ , degree of restraint changes its sign, which is an indication of compressive strains. Since the sign of degree of restraint is negative above  $0.6H$ , full-height crack is unlikely to occur. This is an evidence of no crack zone, which was observed in Table 5.1. In Figure 5.8, degree of restraint for ABAQUS/6.4-Nonlinear analysis starts to shift from other two lines above  $0.5H$ . This is anticipated because reinforced concrete is stiffer compare to plain concrete and the degree of restraint should be higher. Cusson et al. (2000) also discussed effect of reinforcement on degree of restraint. In a case study, increased restraint factor for reinforced concrete was verified. Cusson et al. (2000) analyzed only one wall with  $L/H=1$ , and result of their analysis perfectly matches with Figure 5.8.

Harrison (1981), Kheder et al. (1994), and Cusson et al. (2000) have suggested that full-height cracks are unlikely to occur when  $L/H$  ratio is equal to or less than 1. For this reason, external restraint for  $L/H=1$  is not as important as when  $L/H$  ratio is higher. Cusson et al. studied only one wall with  $L/H=1$  and stated that the effect of reinforcement is negligible on restraint factor for this value of  $L/H$ . Calculated restraint factors with

ABAQUS/6.4 also show that effect of reinforcement is negligible when  $L/H$  ratio is relatively small (Figure 5.8, 5.9, and 5.10). However, when the length of wall increases relative to height of the wall, large effect of reinforcement can be observed. From the results of linear and non-linear analysis and comparison to ACI 207.2R-95 data, it can be concluded that, the effect of reinforcement is negligible for  $L/H < 4$ . However, it is clear that when the length increases, degree of restraint approaches to its maximum value at a faster rate. Particularly when  $L/H$  ratio is higher than 5, degree of restraint in the center of wall can be assumed constant and equal to 1. Summary of calculated restraint factor would be that for  $L/H < 5$ , ACI's figure gives good result to predict degree of restraint not only for plain concrete but reinforced concrete as well. On the other hand, if  $L/H$  ratio is more than 5, ACI's prediction underestimates degree of restraint for reinforced concrete. In addition to ACI 207.2R-95 report, CIRIA report (Harrison, 1981) also suggests theoretical data for degree of restraint for various walls and slabs, which is shown in Table 5.5.

Table 5.5: Theoretical Degree of Restraint at center section (Harrison, 1981)

<b>L/H ratio</b>	<b>Centerline Horizontal Restraint Factor</b>	
	<b>Base of Section</b>	<b>Top of Section</b>
<b>1</b>	<b>1</b>	<b>0</b>
<b>2</b>	<b>1</b>	<b>0</b>
<b>3</b>	<b>1</b>	<b>0.1</b>
<b>4</b>	<b>1</b>	<b>0.6</b>
<b><math>\geq 8</math></b>	<b>1</b>	<b>1</b>

Comparison of Table 5.5 with calculated values using ABAQUS/6.4 analysis output shows very good match. It is clear that suggested theoretical data by CIRIA, is more reliable for reinforced concrete walls. In addition to Figure 5.4, ACI 207.2R-95 gives option to designer that is an approximate relation between  $L/H$  ratio and restraint factor. The following equations are alternative method suggested by ACI 207.2R-95 to estimate degree of restraint.

For  $L/H$  less than 2.5, approximate restraint factor is given in following:

$$R = \left[ \left( \frac{L}{H} - 1 \right) / \left( \frac{L}{H} + 10 \right) \right]^{\left( \frac{h}{H} \right)} \quad (5.3)$$

For L/H equal to or greater than 2.5, approximate restraint factor is given in following:

$$R = \left[ \left( \frac{L}{H} - 2 \right) / \left( \frac{L}{H} + 1 \right) \right]^{\left( \frac{h}{H} \right)} \quad (5.4)$$

where,

R is restraint factor

L is length of wall

H is height of wall

h is the height from base for the point being considered

Eq.5.3 and 5.4 are well approximation when L/H ratio is less than 5. But beyond that range, degree of restraint is higher than estimated values by Eq.5.3 and 5.4. Eq's.5.3 and 5.4 can provide approximate value of degree of restraint for up to L/H=6. But, for L/H > 6, degree of restraint should be selected as 1. General perception among engineers is that the design guidelines, such as ACI's, are in conservative side. However, in this case, comparison of numerical analysis and ACI's data shows that ACI approach underestimates the degree of restraint for reinforced concrete walls. On the other hand, calculated restraint factors using FEM are for fixed base walls and in reality such structures hardly exist. Considering that the real structures would have small amount of flexibility in their base, ACI values for degree of restraint may be valid for reinforced concrete walls as well.

### 5.5 Application of Restraint Factor in Design

In this part, a simple design example will be considered to illustrate application of restraint factor according to ACI 207.2R-95 design procedure. Based on calculated degree of restraint, stress distribution can be determined as a parameter of degree of

restraint, expansion coefficient and temperature change as shown in following (ACI 207.2R-95):

$$f_t = R.\alpha.\Delta T \quad (5.5)$$

$\alpha$  = thermal expansion coefficient

$\Delta T$  = change in temperature

$R$  = restraint factor

$f_t$  = stresses due to restrained strain

Design procedures limits the widths of anticipated cracks according to the functionality of the structure. Allowable crack width, maximum crack spacing and accordingly allowable steel stress equations, can be used to design reinforcement in the wall. Sum of total crack widths is equal to total number of cracks multiplied to mean crack width, and that would be equal to total free strain minus concrete tensile strain. According to ACI 207.2R-95, this relation can be described as follows:

$$N.w_{mean} = L(R.\alpha.\Delta T - \varepsilon_t) \quad (5.6)$$

where,

$$\varepsilon_t = \frac{f_t'}{E_c}$$

$R$  = restraint factor

$\alpha$  = thermal expansion coefficient

$\Delta T$  = temperature change

$N$  = total number of cracks

$w_{mean}$  = mean crack width

$\varepsilon_t$  = tensile strain capacity

$f_t'$  = tensile stress capacity

$E_c$  = elastic modulus

$L$  = total wall length



Maximum crack width and mean crack width are related to each other. For normal range of service load, this relation is described by ACI 207.2R-95 as in following:

$$w = 1.5w_{mean} \quad (5.7)$$

where,  $w$  is maximum crack width.

Also, if average crack spacing is equal to  $s$ , then  $N.s = L$ . Using the relation between average crack spacing and wall length and Eq.5.5, 5.6, and 5.7, following equation can be written (ACI 207.2R-95).

$$s = \frac{w}{1.5(R.\alpha.\Delta T - \frac{f_t'}{E_c})} \quad (5.8)$$

where,  $s$  is mean crack spacing

There are several methods to determine maximum crack width, which will be explained in Chapter 6. A common formulation in determination of maximum crack width is given in Gergely-Lutz equation. According to specified maximum allowable crack width, stresses in the reinforcing steel can be determined with this formulation. ACI 207.2R-95 rearranged this equation as shown in following:

$$f_s = \frac{w.10^3}{0.076\sqrt{d_c A}} \text{ (in ksi)} \quad (5.9)$$

$d_c$  = distance from extreme tension fiber to the center of the reinforcing bar located closest to it

$A$  = effective tension area of concrete surrounding the tension reinforcement, and having the same centroid as that reinforcement, divided by the number of bars

Based on the assumption that most of the cracks would not be full height, and there is concrete tensile strength before crack development, an approximate equation is provided by ACI 207.2R-95 that can be used to calculate reinforcement ratio. According to ACI 207.2R-95, reinforcement ratio can be calculated as follows:

$$A_b = 0.4 \frac{f_t' \cdot B \cdot h}{f_s \cdot N_H} \left( 1 - \frac{s}{2h} \right) \quad (5.10)$$

$A_b$  = area of bars required in each face of the wall

$N_H$  = total number of bars in the  $h$  distance above the base

$h$  = interval distance above the base being considered

$B$  = wall thickness

$s$  = mean crack spacing

The advantage of Eq.5.10 is that it can be used to design reinforcement effectively. In lower part of the wall, degree of restraint is higher and more reinforcement is required. On the other hand, some regions in the wall have very low stresses and only minimum amount of reinforcement is necessary. Eq.5.10 is useful to design reinforcement effectively at several wall intervals.

The following example illustrates use of degree of restraint, and ACI design procedure. Assume a retaining wall with  $L/H=8$  ( $L=16$  m and  $H=2$  m). Wall thickness is 400 mm, and tensile strength of concrete is 3 MPa. Modulus of elasticity is 25000 MPa ( $E_c$ ), and expansion coefficient is  $5 \times 10^{-6}$  ( $\alpha$ ). In this example designing reinforcement for maximum crack width of 0.22 mm is required. The total equivalent temperature change may be assumed as  $\Delta T = 36$  °C.

To find the required amount of reinforcement, firstly restraint factor need to determined. For this particular case, degree of restraint would be equal to 1 since  $L/H = 8$  ( $R=1$ ). Now Eq.5.8 can be used to find mean crack spacing, which would be  $s = 1830$  mm. Concrete cover is assumed to be 60 mm and reinforcement spacing is 250 mm ( $d_c = 60$  mm,  $A = 2 \times 60 \times 250$  mm); from Eq.5.9 steel stress is found to be 170 MPa. Finally, using

Eq.5.10, it is found that  $500 \text{ mm}^2$  reinforcement is required to resist restraint induced forces, and keep the crack width within the limit.

## **5.6 Summary**

In this chapter, the degree of restraint for reinforced concrete walls was investigated. ACI 207.2R-95 provision for degree of restraint is valid for plain concrete. Using the same approach for definition of degree of restraint and FEM, magnitude of restraint factor was calculated for reinforced concrete walls. It is shown that ACI 207.2R-95 underestimates degree of restraint for reinforced concrete walls when length to height ratio of wall is more than 6. However, analyzed walls had totally fixed base, which increases degree of restraint. In practice, totally rigid base structures hardly constructed. With this fact in mind, ACI 207.2R-95 recommendation for degree of restraint may be adequate to use in design.

## CHAPTER 6

### CRACK CONTROL

#### 6.1 Introduction

In concrete structures, crack formation is normally objectionable. However, cracks are almost inevitable in most situations, because of the low tensile strength of concrete. One of the main objectives of designers is to prevent or control cracking of concrete. In the short term, cracks cause reduction of strength and decay in appearance of the structure, which is an esthetical concern. In the long term, crack formation causes reduction in structural durability by increasing permeability and reducing structural integrity. Based on their negative effects, Harrison (1981) classifies significance of cracks under four categories:

1. Cracks which affect the structural integrity
2. Cracks which lead to durability problems and consequently a reduction in structural capacity
3. Cracks which lead to a loss of serviceability of the structure (e.g. the leakage of water or radiation, sound transfer or damage to finishes)
4. Cracks, which are esthetically unacceptable

Due to significant negative effects of crack on structural concrete, consideration must be given to reduce or control their formation. But, in most design cases, it is not essential to prevent cracks since such requirement would not be feasible for concrete design. In fact, basic principles of reinforced concrete design are developed based on the assumption that concrete cracks in tension zones. This is a clear indication that crack formation alone is not a sufficient criteria for structural failure. Due to associated difficulties and high costs, preventing cracks may not be essential, but control of crack width and their spacing is certainly a requirement. In this Chapter, methods for crack control will be reviewed. Using reinforcing steel in concrete is the main application method to control cracks. The effect of reinforcement on crack width will be shown using the FEM. Based on design requirements for crack width, the amount and percentage of reinforcement will be investigated.

## 6.2 Crack Control

There are different reasons for crack formation in concrete. Control of each crack type may have different methods and applications. The primary reasons for crack formation are either structural loads or restrained volumetric changes due to thermal and shrinkage strains. There are a number of methods available for control of cracking that is caused by restrained volumetric changes. These methods include selecting proper materials and construction procedure, reducing degree of restraint by suitable joints and most importantly using sufficient amount of reinforcing steel that will preserve continuity of the structure.

Reducing the degree of restraint by including proper joints that would allow movement of the structure is very effective in eliminating cracks but it is relatively expensive. Use of movement joints may have maintenance problems particularly in liquid retaining structures. Depending on restraint condition and type of the structure, movement joints may have different functions. Some movement joints allow fully or partially expansion and contraction, and some allow only contraction.

In some situations, reduction of degree of restraint may be achieved by planning of construction sequence. Timing of vertical lifts, casting of slabs in alternative bays are some of the techniques used for crack control. Proper and long enough curing are also important factors for crack control (Harrison, 1981).

Selection of proper mix design, that has minimum peak hydration temperature and minimum shrinkage, would minimize volume changes and consequently would reduce crack risks. One of the common techniques to minimize shrinkage strains is to use shrinkage-compensating concrete.

In most cases, in addition to crack control method discussed so far, the minimum amount of reinforcement is also necessary to control crack width. Sufficient amount of reinforcement would limit the crack width by distributing strains over the section, which leads to fine pattern of cracks rather than single and wide crack (Figure 6.1).

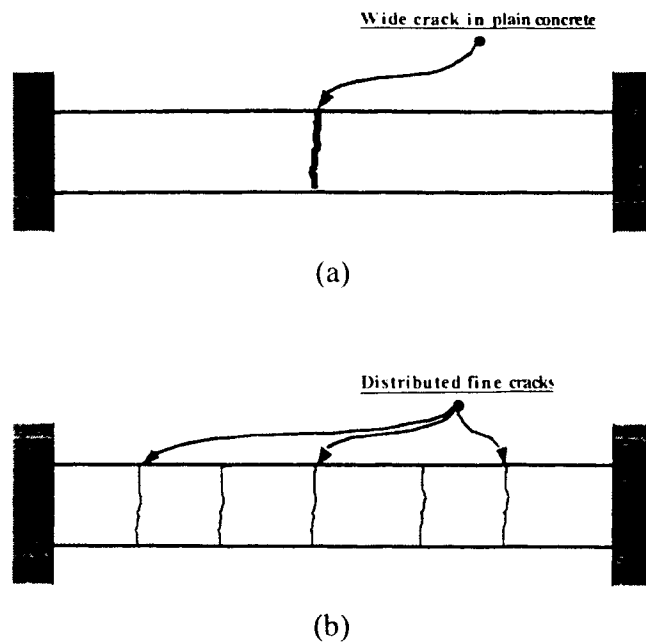


Figure 6.1: Crack formation due to volumetric deformation in a fully restrained beam, (a) crack formation in a plain concrete beam (single wide crack), (b) crack formation in a reinforced concrete beam (distributed fine cracks)

The amount of reinforcement ratio used in practice for controlling volume change induced cracks ranges from 0.1 to 0.2 percent to more than 1.0 percent of the concrete cross-sectional area (Kheder, 1997). Not only the amount, but also proper placement of reinforcement is important to control cracks. ACI 318 (2002) and ACI 350 (2001) recommend minimum amount of reinforcement and maximum spacing for control of temperature and shrinkage cracks in structural floors, roof slabs, and walls. The recommended minimum shrinkage and temperature reinforcement using ACI 318-02 and ACI 350-01 are shown in Tables 6.1 and 6.2 respectively.

Table 6.1: Minimum shrinkage and temperature reinforcement, (ACI 318-02)

Minimum shrinkage and temperature reinforcement ratio	0.0014
Slabs where Grade 300 or 350 deformed bars are used	0.0020
Slabs where Grade 60 deformed bars or welded wire fabric (plain or deformed) are used	0.0018
Slabs where reinforcement with yield stress exceeding 420 Mpa measured at a yield strain of 0.35 percent is used	$(0.0018 \times 420) / f_y$

Table 6.2: Minimum shrinkage and temperature reinforcement, (ACI 350-01)

Length Between Joints, m	Minimum shrinkage and temperature reinforcement ratio	
	Grade 300	Grade 420
Less than 4	0.0030	0.0030
4 to less than 6.6	0.0040	0.0030
6.6 to less than 8	0.0050	0.0040
8 and greater	0.006*	0.005*

\*Maximum shrinkage and temperature reinforcement where movement joints are not provided.

Spacing of reinforcing bars affects crack width and it is an important parameter for crack control. ACI 318-02 and ACI 350-01 requirements for maximum spacing of shrinkage and temperature reinforcement ( $s_{max}$ ) are as follows.

$$s_{max} = 500 \text{ mm or } 5 \times (\text{slab thickness}) \quad (\text{ACI 318-02})$$

$$s_{max} = 300 \text{ mm \& } d_{b(min)} = 13 \text{ mm} \quad (\text{ACI 350-01})$$

where,

$$s_{max} = \text{maximum bar spacing}$$

$$d_{b(min)} = \text{minimum bar diameter}$$

In both, ACI 350 and ACI 318, it is stated that the specified reinforcement ratio is for end restraint slabs. It is indicated that, when continuous base restraint exist, the required reinforcement might be reduced up to 50%.

The ACI 224R (2001) report provides guidelines to crack control for reinforced concrete structures. ACI 224R-01 refers to ACI 318 and ACI 350 for spacing of reinforcement but not for the amount of reinforcement that is adequate to control cracks. The report suggests that the minimum reinforcement ratio that ranges between 0.18% to 0.20%, does not normally control cracks within the design limits. Further, to control cracks to a more acceptable level, reinforcement ratio needs to exceed 0.60% (ACI 224R-01). This comment indicates that ACI 224R-01 is more conservative for minimum shrinkage and temperature reinforcement. Tables 6.1 and 6.2 that are ACI 318-02 and ACI 350-01 recommendations for reinforcement ratio, suggest a maximum of 0.6% reinforcement ratio. In both ACI 318-02 and ACI 350-01, it is stated that the recommended reinforcement ratios are the results of experimental studies and, design requirements would be satisfied when recommended reinforcement ratios were used. This implies that the minimum reinforcement ratios in Tables 6.1 and 6.2 are sufficient to limit the crack width within the allowable range. Based on the functionality of structure, acceptable crack width is discussed in ACI 224R-01 and recommended values are shown in Table 6.3.

Table 6.3: Nominal limit value of crack width specified for cases with expected functional consequences of cracking (ACI 224R-01)

Guide to reasonable* crack widths under service loads		
Exposure condition	Crack width	
	(in)	(mm)
Dry air or protective membrane	0.016	0.41
Humidity, moist air, soil	0.012	0.30
Deicing chemicals	0.007	0.18
Seawater and seawater spray, wetting and drying	0.006	0.15
Water-retaining structures**	0.004	0.10

\*It should be expected that a portion of the cracks in the structure would exceed these values. With time, a significant portion can exceed these values. These are general guidelines for design to be used in conjunction with sound engineering judgment.

\*\*Excluding non-pressure pipes.



The allowable crack width for liquid retaining structures (0.1 mm) that is shown in Table 6.3 is not the same as ACI 350-01 requirement. Commentary of ACI 350-01/10.6.4 suggests that for watertight structures, the maximum crack width in normal and severe environmental exposure should be 0.25 and 0.23 mm respectively. The difference between the limits of crack width by ACI 224R-01 and ACI 350-01 is probably the result of type of crack under consideration. When crack is the result of flexural stresses, larger crack width may be acceptable. But, when crack is the result of direct tensile stresses, stricter rules should apply and crack width should be reduced. In this perspective, it can be concluded that crack width in liquid retaining structures should be limited to 0.10 mm when it is formed by direct tensile stresses. However, the limit may be increased to 0.25 mm when cracks are the result of flexural stresses.

### 6.3 Estimating the Crack Width

There are different formulations in different design codes and guidelines to estimate the crack width. A detailed review of crack width estimation methods is covered in ACI 224R-01. Three popular formulations by American and European codes need to be discussed.

ACI 318-95 has a crack prediction formulation for beams and for thick one-way slabs that is based on statistical model developed by Gergely and Lutz (1968). According to Gergely-Lutz model, the reinforcing steel stress is the most important parameter. Two important geometric variables that effect crack width are the thickness of the concrete cover and the area of concrete surrounding each reinforcing bar. Originally, the equation was in two parts and it was used for predicting bottom and side cracks separately. ACI 318-95 simplified the Gergely-Lutz model as shown below:

$$w = 11 \times 10^{-6} \beta f_s \sqrt[3]{d_c A} \quad (6.1)$$

where,

$w$  = most probable maximum crack width, mm

$\beta$  = distance from the neutral axis to the bottom fibre, divided by the distance to the reinforcement (about 1.20 in beams)

$f_s$  = reinforcing steel stress, MPa

$d_c$  = distance from the extreme tension fibre to the centre of the reinforcing bar located closest to it, mm

$A$  = effective tension area of concrete surrounding the tension reinforcement, and having the same centroid as that reinforcement, divided by the number of bars or wires, mm<sup>2</sup>

$\beta$  is an amplification factor that accounts for increase in crack width at the surface level of member, and it is calculated based on strain gradient. Estimation of “ $\beta$ ” and effective tension area “ $A$ ” are shown in Figure 6.2. An average value for “ $\beta$ ” can be selected. For flexural cracks, value of  $\beta=1.2$  is used in ACI 318-95 and Eq.6.1 is rearranged as shown below.

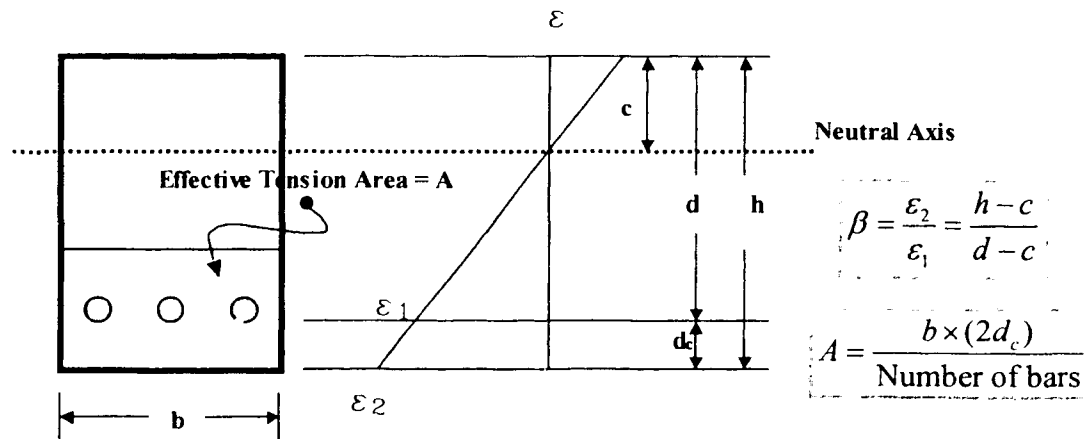


Figure 6.2: Strain Gradient, and determination of  $\beta$  and  $A$ , (Frosch, 1999)

$$z = f_s \sqrt[3]{d_c A} \quad (6.2)$$

The value of “ $z$ ” in the above equation is limited to a certain value to satisfy the crack width requirement. Also ACI 318-95 allows using 60% of the specified yield strength instead of actual steel stress. The limit for “ $z$ ” would change according to serviceability requirements and allowable crack width. Although Eq.6.1 is used to estimate flexural cracks, ACI 224R-01 states that this equation may be modified to estimate tensile crack

width, since crack development in concrete is similar for tension and flexure. ACI 318-95 uses  $\beta=1.2$  for flexural type of cracks. Expected crack widths are larger for tensile cracks and that would require a higher value for “ $\beta$ ”. ACI 224R-01 recommends  $\beta=1.31$  as an appropriate approximation to use in estimation of tensile cracks.

In recent years, more studies have focused on estimating crack width. Frosch (1999) suggested that Eq.6.1 is valid for relatively narrow range of cracks. Gergely-Lutz model and statistical cracking data was reevaluated. Based on Frosch’s recommendations, the 1999 version of ACI 318 have included another equation to limit the tension reinforcement spacing closest to the surface, which is shown in following:

$$s = \frac{95000}{540f_s} - 2.5c_c \quad (6.3)$$

where,

$s$  = center-to-center spacing of flexural tension reinforcement nearest to the surface of the extreme tension face, mm

$f_s$  = calculated stress in reinforcement at service load ( $0.6f_y$ ), MPa

$c_c$  = clear cover from the nearest surface in tension to the flexural tension reinforcement, mm

European codes such as CEB-FIP and EC2 provide different models for crack width estimation. CEB-FIP method to estimate characteristic crack width in beams is given below:

$$w_k = l_{s,\max} (\varepsilon_{sm} - \varepsilon_{cm} - \varepsilon_{cs}) \quad (6.4)$$

where,

$w_k$  = the characteristic crack width, mm

$l_{s,\max}$  = the length over which crack occurs between the steel reinforcement and the concrete, mm

$\varepsilon_{sm}$  = average reinforcement strain within segment length, m/m

$\epsilon_{cm}$  = average concrete strain within segment length, m/m

$\epsilon_{cs}$  = strain of concrete due to shrinkage, m/m

CEB-FIP code requires that characteristic crack width should be below the limiting crack width and that is approximately 0.3 mm for ordinary structures. But in special cases, such as liquid retaining structures, the limit is stricter as in Table 6.3. Segment length,  $l_{s,max}$ , or the crack spacing for stabilized cracks can be estimated using the following equation:

$$l_{s,max} = \frac{\phi_s}{3.6\rho_{s,ef}} \quad (6.5)$$

where,

$\phi_s$  = reinforcing bar diameter or equivalent diameter of bundled bars, mm

$\rho_{s,ef}$  = effective reinforcement ratio, ( $\rho_{s,ef} = A_s / A_{c,ef}$ )

$A_s$  = area of tension reinforcement, mm<sup>2</sup>

$A_{c,ef}$  = effective concrete area in tension, mm<sup>2</sup>

$$A_{c,ef} = b[2.5(h-d)]$$

b = beam width at the tension side, mm

h = total section depth, mm

d = effective depth to the centroid of the tensile reinforcement, mm

For stabilized cracking, the average width of crack can be estimated on the basis of the average crack spacing. Formulation of average crack spacing is given in following, (CEB-FIP Model Code 1990):

$$S_{rm} = \frac{2}{3} l_{s,max} \quad (6.6)$$

where,

$S_{rm}$  = the mean crack spacing value in beams, mm

Another European Code, EC2 has similar equation as in CEB-FIP. EC2 requires that crack width in structure should not cause any functional or esthetical problem. Maximum design crack width for sustained load under normal environmental conditions is 0.3 mm, which is similar to the CEB-FIP's requirement. EC2's formulation for crack width estimation as follows:

$$w_k = \beta s_{rm} \varepsilon_{sm} \quad (6.7)$$

where,

$w_k$  = design crack width, mm

$\beta$  = coefficient relating the average crack width to design value (1.7 for load induced cracking and for restraint cracking in sections with minimum dimensions in excess of 800 mm)

$s_{rm}$  = average stabilized crack spacing, mm

$\varepsilon_{sm}$  = mean strain under relevant combination of loads and allowing for the effect such as tension stiffening or shrinkage, m/m

The average crack spacing,  $s_{rm}$ , for stabilized cracks can be estimated as follows (ACI 224R-01):

$$s_{rm} = 50 + \frac{0.25 k_1 k_2 d_b}{\rho_t} \quad (6.8)$$

where,

$k_1$  = 0.8 for deformed bars and 1.6 for plain bars

$k_2$  = 0.5 for bending and 1.0 for pure tension

$d_b$  = bar diameter, mm

$\rho_t$  = effective reinforcement ratio, ( $\rho_t = A_s / A_{cr}$ )

Both CEB-FIP and EC2 equations are similar in principles. The principle of crack width estimation in European codes is that the product of mean steel strain and crack spacing

the crack width. In principles, new formulation of ACI 318-99 (Eq.6.3) is similar to European code's formulation for crack width. The only difference is in the estimation of crack spacing. To show the similarity of CEB-FIP, EC2, and ACI 318-99 equations, the development of the concept needs to be examined. Frosch (1999) used a theoretical model to develop new crack width equation. The physical model of cracking is shown in Figure 6.3. From the model, it is clear that the width of a crack can be estimated from the steel strain and spacing of cracks.

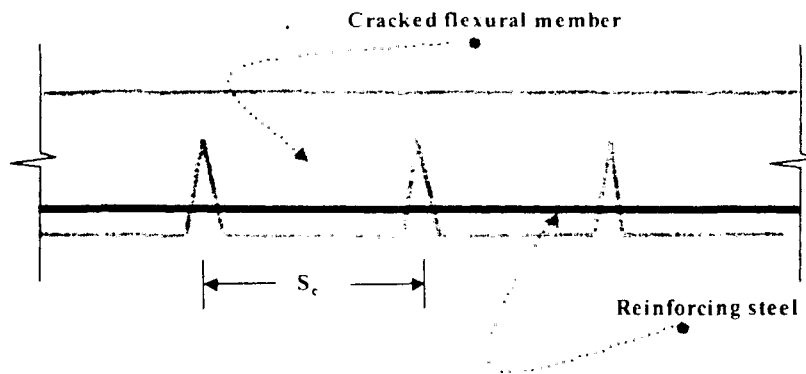


Figure 6.3: Physical model of flexural crack

The crack width at the level of reinforcement can be calculated as follows (Frosch, 1999):

$$w_c = \epsilon_s S_c \quad (6.9)$$

where,

$w_c$  = crack width

$\epsilon_s$  = reinforcing steel strain

$S_c$  = crack spacing

The equation above is the basic model for crack width estimation by CEB, EC2 and ACI 318-99. Frosch has used this model to develop a new equation for ACI. Although the principles of the three models are the same, estimation of the crack spacing changes in each formulation. ACI adapted Frosch's model for estimation of crack spacing that

relates crack spacing to distribution of reinforcement. Based on statistical data, Frosch studied crack spacing “ $S_c$ ”, and the following equation was proposed:

$$S_c = \Psi_s d^* \quad (6.10)$$

where,

$\Psi_s$  = crack spacing factor (1.0 for minimum crack spacing; 1.5 for average crack spacing; and 2.0 for maximum crack spacing)

$d^*$  = controlling cover distance

Description and estimation of controlling cover distance,  $d^*$ , is shown in Figure 6.4.

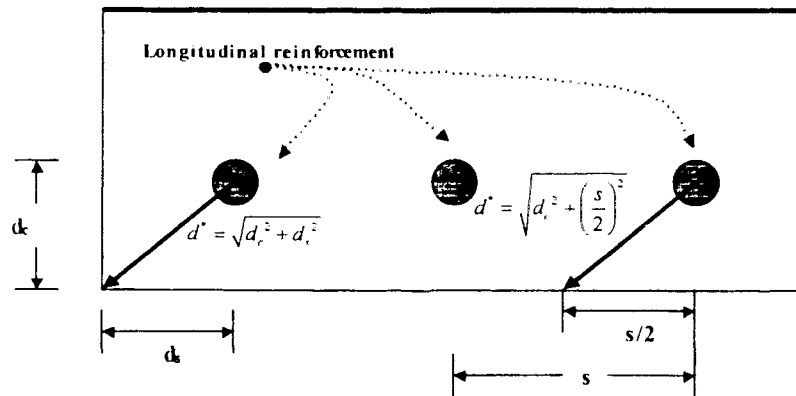


Figure 6.4: Determination of control cover distance,  $d^*$ , for a beam cross section (Frosch, 1999)

Substituting equations for control cover distance into Eq.6.9, and then substituting Eq.6.9 into Eq.6.10 and rearranging gives Eq.6.11, which is nothing more than ACI 318-99 crack control equation.

$$s = 2 \sqrt{\left( \frac{w_c E_s}{2 f_s \beta} \right)^2 - d_c^2} \quad (6.11)$$

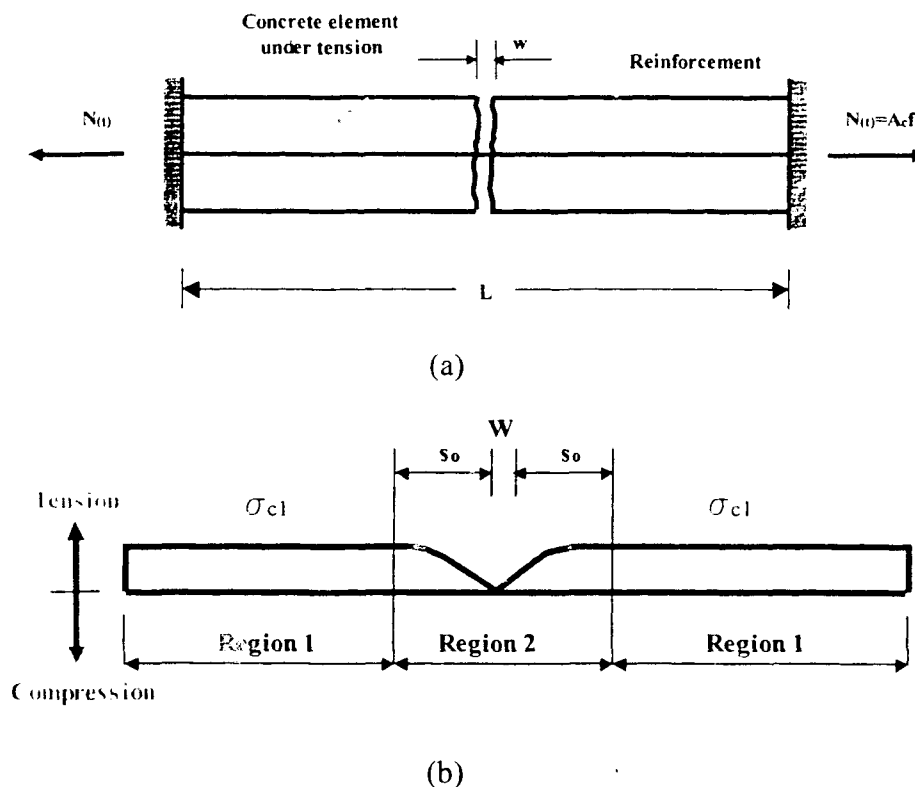
where,

$$\beta = 1.0 + 0.08 d_c$$

$d_c$  = bottom cover measured from centre of the lowest bar

It is important to note that in all three equations by ACI 318, CEB and EC2, the steel strain is taken as an average value over the cracked segment. Besides, in Eq.6.11, ACI 318-99 allows to use 60% of the yield stress instead of actual stress in the steel.

Gilbert (1992) provided a theoretical model that is helpful to understand the development of crack, and stress state of reinforced concrete members after the crack formation. Restrained thermal and shrinkage strains generate tensile stresses, which is considered in this theoretical model. Gilbert showed the stress state in a reinforced concrete member that is cracked under direct tension, which is shown in Figure 6.5.





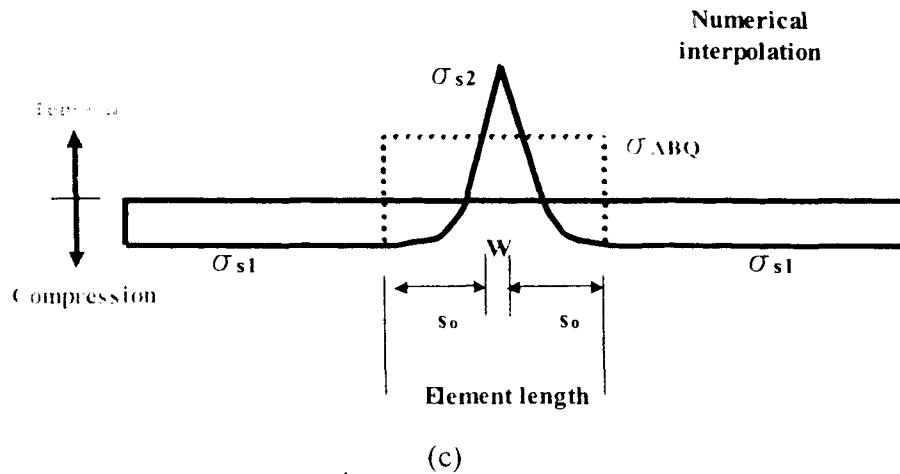


Figure 6.5: State of stress in reinforced concrete after cracking (a) Just after first cracking in a restrained direct tension member, (b) Average concrete stress just after first cracking, (c) Steel stress just after first cracking (Gilbert, 1992)

Concrete tensile stresses can be observed in Figure 6.5(b) that is uniform before cracks (Region 1). After cracking, concrete stresses drops to zero smoothly (Region 2). Steel stresses are different, which is shown in Figure 6.5(c). Before cracks, steel is in compression. Just after crack formation, tensile stresses in steel increase significantly. Crack width that is in region 2 can be easily determined provided that the average steel strain in this region is known. In Figure 6.5(c), an additional line (broken line) is drawn in order to discuss whether Gilbert's model and the FEM can be used directly to estimate crack width. The question is whether numerical interpolation would provide the profile of the steel stress in crack location. Obviously calculated stress and strain values using the FEM are average values over the element and not at the crack. Considering the principle crack model shown in Figure 6.3 and Gilbert's crack model that is used for restraint concrete members under direct tension, average values of element stress/strains may be used to estimate crack width as shown in the following equation:

$$w = (\epsilon_{steel} - \epsilon_{ct}) L_{element} \quad (6.12)$$

where,

$w$  = crack width in element

$\varepsilon_{steel}$  = steel strain in element

$\varepsilon_{ct}$  = concrete tensile strain capacity

$L_{element}$  = length of the element

Concrete tensile strain capacity is a known quantity. After calculating the steel strains for each element, crack width can be easily determined. However, as can be observed in Figure 6.5(c), using Eq.6.12 to estimate the crack width would require a sufficiently large element size and that increases error margin in numerical method. The basic idea of FEM is that the high mesh density provides more accurate results. Compromising from the accuracy of numerical solution to estimate crack width is not preferable. Using ABAQUS/6.4 with fine mesh does not provide a profile for steel stresses as shown in Figure 6.5(c). With high mesh density, steel stresses in neighbouring elements do not show tensile stresses as illustrated in Figure 6.6. Unless the estimated steel stresses are too high, neighbouring elements to the crack location show compressive stresses, which is probably due to smeared crack modeling. Therefore, Eq.6.12 cannot be used to estimate crack width.

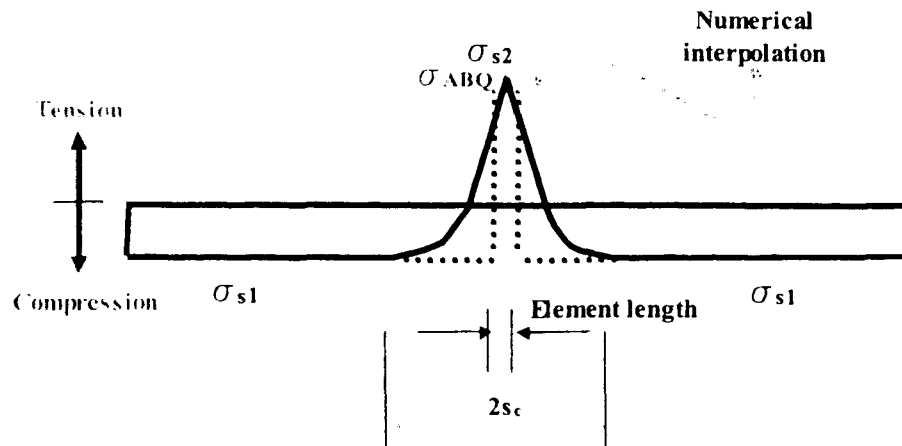


Figure 6.6: Steel stress just after first cracking and numerical approximation

However, for a particular analysis, Eq.6.12 may be used with an optimized mesh density to estimate crack width. But, in case of parametric study and when comparative analyses have to be performed, fine mesh size is essential. Calculated average steel stress/strain in

finely mesh model can be used with one of the code's formulations to estimate crack width.

In this research, to avoid errors of mesh sensitivity, the highest required mesh density was used to calculate stress/strain in reinforcement. In practice, it is difficult to estimate actual steel stress/strains to calculate crack width by one of the code's equations provided. However, numerical analysis may be used to estimate steel stress/strains and that can be used to predict the crack width. The computer program ABAQUS/6.4, which is used in this study, does not predict crack width directly. Instead, output of stress-displacement analysis can be used to estimate crack width in concrete. Eq.6.9 that is a strain based equation is used in this thesis to estimate the crack width.

Difficulties associated with calculating steel stress/strain in cracked concrete are convergence problems, which depends on computer software used in the simulation, and the solution technique used by that software. At start of cracking and after cracking, severe material and geometric non-linearity could occur. Most numerical analysis tools, including ABAQUS/Smeared Crack and ABAQUS/Damaged Plasticity options, are not able to solve non-linearity of this magnitude. However, the cracking model for concrete option with ABAQUS/Explicit can overcome convergence problems that will be discussed in the following section.

#### **6.4 Cracking Model for Concrete**

Crack width estimation by FE tool is a complex procedure. Cracks occur after the peak tensile stress of concrete material is reached, which obviously requires non-linear analysis. Most FE computer programs, including ABAQUS/6.4, are capable of performing non-linear analysis. Provided that the material non-linearity does not show abrupt changes and negative stiffness, stress analysis can be performed without a major problem. However, concrete stress-strain curve shows sharp changes after the crack and stiffness become negative during tension stiffening (Figure 4.1). Volumetric changes induced stress on concrete are mostly tensile, and even a very small amount of tensile strain would cause cracking. Tensile strain due to thermal and shrinkage strains may easily reach to 1000 micro strain, but concrete may resist only as low as 100 micro strains. After the first crack formation, stresses would be redistributed while the crack

opens. Concrete stresses would be reduced to zero at crack location and the steel tensile stresses start to develop. Increased tensile stresses will cause secondary cracks and that will again redistribute the already redistributed stresses; steel stress in the first crack location would be reduced and first crack would narrow down. These cycles will continue as long as the stresses are continuously increased. Considering these sharp changes in the stress-strain responses, it is quite difficult for the software to provide convergence using standard analysis technique. For this reason, analysis of highly cracked reinforced concrete members faces severe convergence problems.

As discussed in Chapter 4, in addition to “Concrete Smeared Crack”, and “Concrete Damaged Plasticity”, ABAQUS/6.4 offers an option to model concrete called “Cracking Model for Concrete” (CMC). Unlike other concrete models, CMC is available only in ABAQUS/Explicit. This is a special purpose analysis technique that uses explicit-dynamic FE formulation. Although ABAQUS/Explicit is developed for dynamic type of problems, it is also very effective in highly non-linear problems. The main difference between ABAQUS/Standard and ABAQUS/Explicit is in the solution technique used. ABAQUS/Standard uses stiffness based solution technique that is unconditionally stable. On the other hand, ABAQUS/Explicit uses explicit integration solution technique that is conditionally stable. ABAQUS/Standard may be used when non-linearity of material is smooth. In this kind of problems, ABAQUS/Standard would solve the non-linearity with iterative procedure. When severe non-linearity exists, iterative procedure can cause severe convergence problems. However, explicit solution technique can solve such a problem without iteration by explicitly advancing the kinematic state from the previous increment. Explicit solution technique generally requires more increments as compared to Standard solution, but this does not increase the computational cost.

In this chapter, ABAQUS/CMC was used to simulate non-linear behavior of concrete after cracking. After determination of stress-strain state of material, Eq.6.9 was used to estimate the crack width. The following case study is intended to verify ABAQUS/CMC performance in analysis of post failure behavior of concrete and search for possible calibration of the model.

### 6.5 Case Study

Kheder (1997) conducted an experimental study on several full-scale base restrained walls in search of variation of restraint factor and formation of the cracks on monitored walls. Crack width, their shapes and the spacing of cracks were measured. Instead of normal concrete mix, a mortar mix of 1:2 cement:sand with W/C ratio of 0.45 was used in order to speed up shrinkage of the wall. Mortar mixes have high and rapid drying shrinkage that would minimize the required time for experimental study. To measure the total free shrinkage, free to slide walls were cast in addition to base fixed walls. Both, free to slide and fixed walls had the same mix design and cured in the same conditions. After casting, cracking formation of the walls were monitored and crack width, spacing and height of cracks were recorded. Figure 6.7 presents cracking of full-scale experimental wall that is fixed at base.

Dimensions, reinforcement ratio, and the measured shrinkage in free to slide wall are as follows:

$$L / H = 2$$

$$\text{Length } ( L ) = 4 \text{ m}$$

$$\text{Height } ( H ) = 2 \text{ m}$$

$$\text{Wall Thickness } ( t ) = 150 \text{ mm}$$

$$\text{Reinforcement ratio } ( \rho ) = 0.2 \%$$

$$\text{Bar diameter } ( d_b ) = 10 \text{ mm}$$

$$\text{Recorded total free thermal and shrinkage strains } ( \varepsilon_{th+shr} ) = 1050 \times 10^{-6}$$

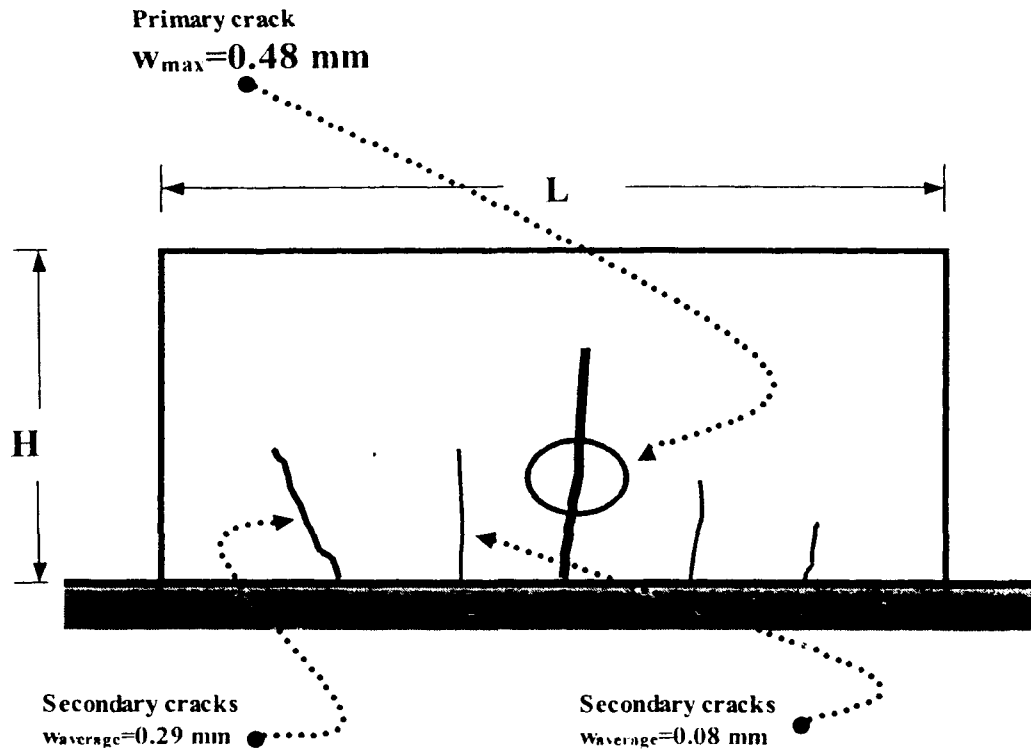


Figure 6.7: Crack formation and recorded crack widths in a base fixed wall (Kheder, 1997)

The shrinkage strains can be included in stress-displacement analysis by defining equivalent temperature change. Therefore, the measured total free strain should be converted to equivalent temperature change. The following calculation illustrates conversion of strains to equivalent temperature change.

$$\varepsilon_{free} = 1050 \times 10^{-6} \text{ (recorded total free strain)}$$

$$\varepsilon_{free} = \alpha \cdot \Delta T$$

$$\alpha = 10 \times 10^{-6} / ^\circ\text{C}, \text{ (thermal expansion coefficient)}$$

$$\Delta T = \text{change in temperature (} ^\circ\text{C)}$$

$$\Delta T = \frac{1050 \times 10^{-6}}{10 \times 10^{-6}} \Rightarrow \Delta T = 105 \text{ } ^\circ\text{C} \text{ (equivalent temperature change)}$$

The following properties were assumed:

Concrete elastic modulus ( $E_c$ ) = 25000 MPa

Concrete tensile strength ( $f_t$ ) = 3.0 MPa

Poisson's ratio for concrete ( $\nu_c$ ) = 0.18

Poisson's ratio for steel ( $\nu_s$ ) = 0.0

Reinforcement elastic modulus ( $E_s$ ) = 210 GPa

Reinforcement yield strength ( $f_y$ ) = 400 MPa

Cracking Model for Concrete in ABAQUS/6.4 is developed based on the assumption that the primary forces in the structure are tensile. For this reason, non-linearity of concrete in compression is ignored. Therefore, it is not necessary to define the compressive strength for concrete. Mesh density and type of the elements used in the simulation are shown in Figure 6.8. Analysis was performed, and the resulting longitudinal strain contour plots are also shown in Figure 6.8.

A reduced spectrum of contour plot can be viewed that is shown on Figure 6.9. Primary and secondary crack widths were calculated based on Frösch (1999) model (Eq.6.9) and the results are also shown in Figure 6.9. It can be observed that calculated crack widths are very close to the actual crack widths measured from the experiment. Maximum crack width that was measured from the experimental wall is 0.48 mm and it is somewhere in the middle of wall. Calculated maximum strains were also in the middle of wall. Crack width that is calculated using ABAQUS/6.4 output is found to be 0.43 mm. In Figure 6.9, it is also interesting to note that overall crack pattern from the experimental wall, matches very well with simulated positive strain concentrations. In fact not only major cracks, but also secondary and even smaller cracks are comparable with experimental results. Based on this case study, it is evident that “Cracking Model for Concrete” in ABAQUS/6.4 works very well in predicting crack width.

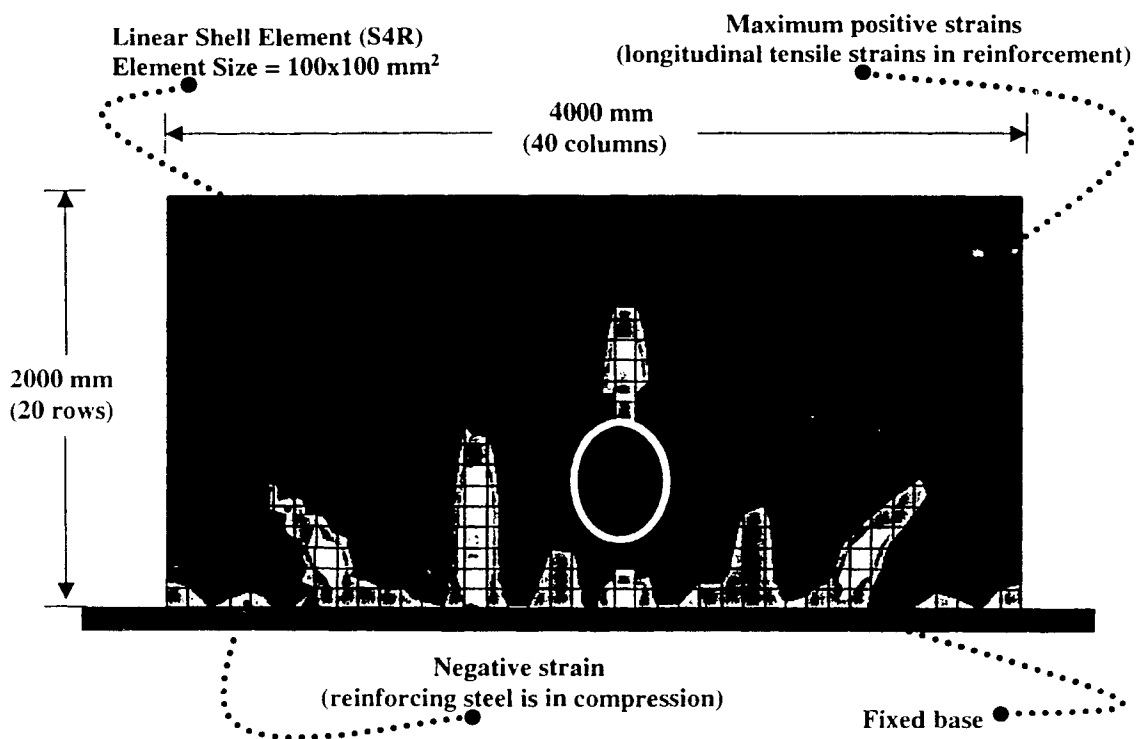


Figure 6.8: Mesh density of the simulated wall, and contour plot of longitudinal steel strains, (standard spectrum)

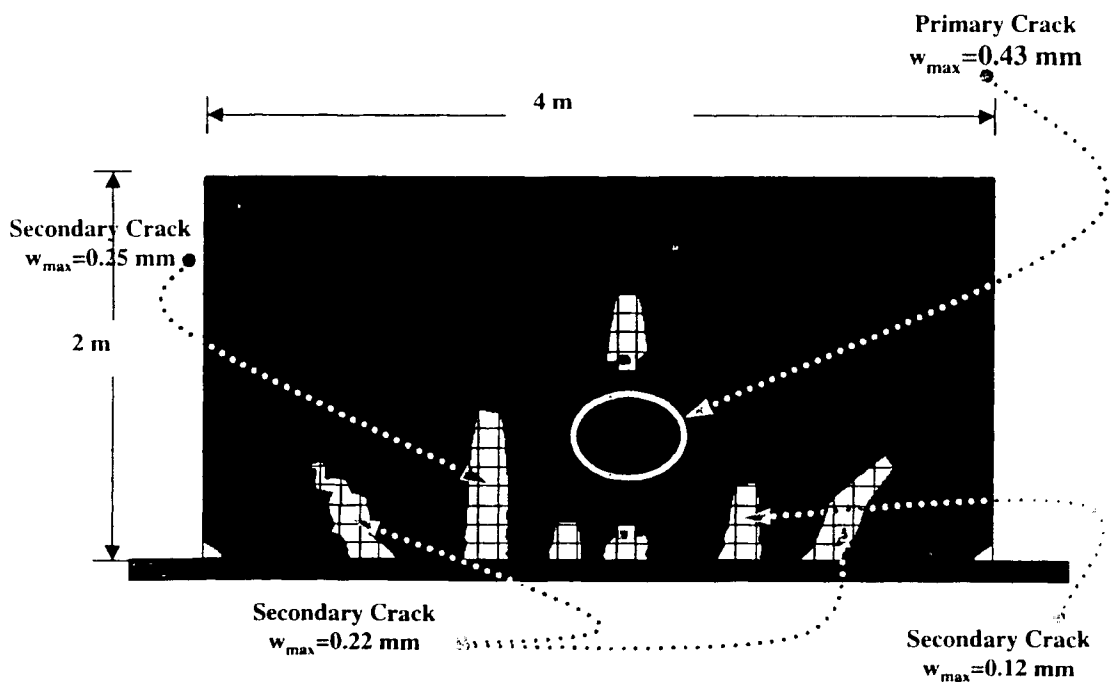


Figure 6.9: Contour plot of longitudinal steel strains, (reduced spectrum)



Most design codes provide limited guidelines on amount of reinforcement that can limit the crack width. Information about relation between crack width and reinforcement ratio is limited because of practical difficulties and associated costs in full-scale experiments. But, with the case study discussed above, it is shown that numerical tool could be used to produce data for this purpose, which may be used in design. The maximum allowable crack width for each structure type is specified in design codes. Using code's specification for allowable crack width and ABAQUS/CMC, the required amount of reinforcement can be determined. In the following sections, a particular design code (ACI 350) will be considered. Based on specified allowable crack width, adequate reinforcement ratio for various wall dimensions will be investigated.

#### **6.6 Minimum Reinforcement for Liquid Retaining Structures**

Crack control is achieved primarily by use of reinforcing steel. Design codes such ACI 318 and ACI 350 recommends minimum amount of reinforcement to control cracks as was shown in Tables 6.1 and 6.2. Both Tables provide very small amount of information for designers. In practice, even the simplest structures may not fit into design guides similar to Tables 6.1 and 6.2. As a result, in most cases, engineers have to use their own judgment to select sufficient amount of reinforcement to control cracks. This may cause increase in cost or insufficient reinforcement, which may have adverse effects. Experimental study to determine the required reinforcement to control the crack width on full-scale structures that is beyond the dimensions given in Tables 6.1 and 6.2 is difficult. However, as discussed in section 6.3, numerical analysis may be used to predict crack width with reasonable accuracy. Using numerical analysis tool, design guidelines may be expanded that would provide more information for designers. Sufficient amount of data for designers would produce efficient and durable structures. In this section, design guides provided in Tables 6.1 and 6.2 will be expanded using a parametric study. The required amount of reinforcement to control shrinkage and thermal cracks is sought in various walls with different dimensions. A wall with fixed base is considered as in the case study discussed earlier. For comparison and calibration purposes the ACI 350 code is selected. This is a special design Code that is developed for the design of environmental structures, which includes liquid retaining structures. Since the subject

structures of ACI 350 are more sensitive to cracks, the requirements for crack width are more strict. ACI 350 specifies that maximum crack width in flexural members should not exceed 0.25 mm in normal environmental exposure and 0.23 mm in severe exposure (ACI 350/R10.6.4). It is reasonable to ask whether this specification on flexural crack width would apply to tensile cracks as well. Allowable tensile crack width for liquid retaining structures is given by ACI 224R and it was shown in Table 6.3. In water retaining structures, even the smallest crack would cause leakage, but a natural process called autogenous healing would stop leakage over the time.

To examine the requirements for crack control in the ACI 350 Code, walls with reinforcement ratios and dimensions that are similar to those shown in Table 6.2 are selected for investigation. Based on the provided design guide in Table 6.2, Table 6.4 is prepared for initial analysis.

Table 6.4: Design walls that are in the range of Code guide (Table 6.2), and ACI 350-01 recommendation for temperature and shrinkage reinforcement ratios

Wall Height = 4 m, Wall Thickness = 300 mm, Steel Grade = 420									
Length (m)	4	5	6	7	8	9	10	11	12
Reinforcement Ratio	0.003	0.003	0.003	0.003	0.003	0.003	0.004	0.004	0.005

Parameters considered in this investigation are length, height, and thickness of the wall with different reinforcement ratios. Table 6.5 presents the selected wall length, height, and thickness.

Table 6.5: Variables for parametric study (Dimensions for selected walls)

Length, m	4, 5, 6, 7, 8, 9, 10, 11, 12, 18, 24, 30, and 60
Height, m	4, 6, and 8
Thickness, mm	300, 450, and 600
Reinforcement Ratio	0.003, 0.004, 0.005, 0.006, 0.007, and 0.008
Temperature and shrinkage strains	400, 600 and 800 microstrain

### 6.6.1 Total Thermal and Shrinkage Strain

According to Klein et al. (1981), ACI 350 design guide for minimum temperature and shrinkage reinforcement ratio (Table 6.2) is developed based on an experimental study. However, the details of the experimental study are not provided, and they are not discussed in Klein et al. Some important parameters such as total temperature and shrinkage strains, and recorded crack width using certain reinforcement ratio is not known. It is stated that recommended reinforcement ratios for temperature and shrinkage would be sufficient in terms of serviceability.

Total temperature and shrinkage strains are an important parameter that will affect the maximum crack width. Higher thermal and shrinkage strains would cause wider cracks particularly when the wall length is relatively short. To determine the amount of total volume change to be considered, possible thermal and shrinkage strains for walls need to be examined.

To estimate the total thermal strain, the maximum and minimum temperature of concrete need to be determined. Calculated temperature change can be multiplied by expansion coefficient to convert thermal change to strain. ACI 207.2R suggests using temperature change from peak hydration temperature to minimum weekly ambient temperature to estimate thermal strains. This approach is conservative in some way, but it underestimates thermal strains in another way. It is conservative because it does not account for compressive strains developed when concrete reaches peak hydration temperature during the expansion phase. On the other hand, weekly ambient temperature may not be sufficient to calculate total thermal deformation. Concrete temperature may

drop well below minimum weekly temperature when seasonal thermal changes considered. ACI 207.2R states this fact, but it suggests that lower temperature due to seasonal variations is temporary. This means that crack that may widen during minimum annual temperature, would narrow down in next season when average ambient temperature increases. ACI suggests that since widening of cracks due to seasonal temperature variation is temporary, it may be neglected and only minimum weekly temperature may be considered. When temporarily widening of cracks are not a concern, ACI approach is realistic. However, in liquid retaining structures even temporarily widen cracks may cause important serviceability problems.

In Chapter 4, it was discussed that even though strength gain is in development stage, compressive stresses would develop while hydration temperature increases (Figure 4.14). Even though elastic modulus is low, compressive stresses develops during hydration. Therefore, rather than peak hydration temperature, placing temperature of concrete may be considered for maximum temperature of concrete. Maximum placing temperature is mostly during the summer months and minimum temperature would be the coldest time of the year. To find this total temperature change from maximum to minimum, climatological information of a particular location as shown in Table 6.6 may be considered.

Table 6.6: Average monthly temperature of Toronto (Environment Canada)

Climatological Information of Toronto		
Month	Mean Temperature	
	Daily Minimum	Daily Maximum
Jan	-6.3	-1.1
Feb	-6.3	-0.2
Mar	-2	4.6
Apr	3.8	11.3
May	9.9	18.5
Jun	14.8	23.5
Jul	17.9	25.3
Aug	17.3	20.7
Sep	13.2	13.8
Oct	7.3	7.4
Nov	2.2	1.8
Dec	-3.7	

\*RH stands for relative humidity and detailed explanation for notional size is given in Chapter 3

Notional sizes of the walls considered for parametric study are 293, 433 and 571 mm for wall thickness of 300, 450 and 600 mm respectively. Considering that water-retaining structures are naturally exposed to water during their lifetime, relative humidity is higher than 80%. Based on CEB recommendation given in Table 6.7, maximum shrinkage strain that may occur for studied walls is 260 micro strains for 600 mm wall. However, compared to CEB recommendations, ACI values for ultimate shrinkage strain is quite different. ACI 209 Committee report indicate that the ultimate shrinkage strains for concrete is in the range of 415 to 1070 micro strain, and suggested ultimate shrinkage strain is 730 to 800 micro strain. ACI 209 recommendation is well beyond the values in the Table 6.7. In fact, the shrinkage strain of this magnitude alone is sufficient to cause unacceptable crack width in liquid retaining structures. For these high values of shrinkage strain, ACI 350 recommendation for minimum reinforcement may not be sufficient to limit the crack width within the specifications. This conflict can be explained by the fact that liquid retaining structures are not exposed to dry conditions that may cause moisture loss, which is the primary reason for shrinkage.

An optimum value for shrinkage strain is needed for simulation of selected walls. The subject structures for this parametric study are liquid retaining structures that have high relative humidity and low moisture loss. One may suggest that CEB recommendations underestimate ultimate shrinkage for ordinary structures. But, it is also clear that ACI values for ultimate shrinkage strain is too conservative for water retaining structures. Since the subject walls have special service conditions during their lifetime, it is assumed that CEB estimation for shrinkage is appropriate to use in simulation process. Based on Table 6.7, an approximate value of 300 micro strains can be chosen for drying shrinkage, which would be on conservative side.

For thermal strains of about 200 to 300 micro strains, and shrinkage strains of about 300 micro strains, total volume change due to thermal and shrinkage strains may be assumed as  $600 \times 10^{-6}$ . Interestingly, total of  $600 \times 10^{-6}$  strains of volume change is consistent with ACI 224R-01 and Gilbert's case study (Gilbert, 1992). ACI 224 report on crack control

discusses shrinkage cracks. This report specifies a typical value for final shrinkage strains of concrete is about  $600 \times 10^{-6}$ . This recommended value is for ordinary structures, and not for liquid retaining structures. Gilbert also considers a case study to predict crack width and the selected total strain for the study is  $600 \times 10^{-6}$ . In following parametric study, total volumetric deformation of 400, 600 and 800 micro strains were considered. Based on the results of analysis, the effects of change in total volumetric deformation will be discussed.

### 6.6.2 Calculated Crack Widths

Using the computer program ABAQUS/6.4, for walls given in Table 6.4 and 6.5 analyses were performed. Concrete tensile strength was assumed to be  $f_t = 3$  MPa. Linear shell elements (200x200) was used in the models. With this element size, there were 400 elements in smallest wall ( $L=4$  m,  $H=4$  m), and 12000 elements in largest wall ( $L=60$  m,  $H=8$  m). Rebar layer that represents the reinforcement, can be distributed through the thickness of shell elements. In order to simulate the concrete cover, each rebar layer was placed 50 mm away from the surface of the shell elements. The same concrete cover was used in the calculation of crack width. For reinforced concrete analysis, Hibbitt et al. (2004) recommend to use uniformly distributed reinforcement in each element. To eliminate errors that may cause by reinforcement distribution, one rebar in each element was placed. Since the dimensions of the elements were 200 mm in each direction, one rebar in each element result in 200 mm of bar spacing. During analysis, longitudinal strains of reinforcing bars were requested from ABAQUS/6.4 as an output. Using the maximum longitudinal strains of reinforcement and Eq.6.9, crack width was calculated. To calculate crack width using Eq.6.9 (Frosch, 1999), first, the control-cover-distance,  $d^*$ , need to be determined. Based on the considered concrete cover and bar spacing, the control cover distance can be calculated as shown in Figure 6.4. The following illustrates the calculation of control-cover-distance:

$$d^* = \sqrt{d_c^2 + \left(\frac{s}{2}\right)^2}, \text{ (Frosch, 1999)}$$

$$d_c = 50 \text{ mm (concrete cover)}$$

$$s = 200 \text{ mm (bar spacing)}$$

$$d^* = 112 \text{ mm}$$

Using calculated control-cover-distance, crack spacing,  $S_c$ , can be calculated as follows:

$$S_c = \Psi_s d^* = 112 \Psi_s \text{ mm}$$

where,

$\Psi_s$  is the crack spacing factor and that has following values (Frosch, 1999):

$\Psi_s = 1.0$  for minimum crack spacing

$\Psi_s = 1.5$  for average crack spacing

$\Psi_s = 2.0$  for maximum crack spacing

In order to determine a proper value of the crack spacing factor, analysis of walls given in Table 6.4 was performed. After determination of crack spacing factor, using Eq.6.9 crack width can be calculated as follows:

$$w_c = S_c \varepsilon_s = 112 \Psi_s \varepsilon_s \text{ mm}$$

where,

$w_c$  = crack width

$\varepsilon_s$  = reinforcing steel strain

Although the above equation can be used to calculate crack width in any cracked element, maximum longitudinal strain of reinforcement will be used in order to find the maximum crack width.

After the analysis of walls given in Table 6.4, using the crack width equation above, crack widths were calculated for three different crack spacing factor that is shown in Figure 6.10. In this figure, it can be seen that  $\Psi_s = 2$  results maximum of 0.5 mm crack width, while  $\Psi_s = 1$  produces maximum of 0.25 mm crack width. It is important to keep

in mind that analyzed walls dimension and reinforcement ratios shown in Figure 6.10 are developed based on ACI 350 recommendations (Tables 6.2 and 6.4). According to ACI 350-01 the allowable maximum crack width is about 0.25 mm. Assuming that the ACI recommendations for reinforcement ratios should result average of 0.25 mm crack width, the value of crack spacing factor can be selected as  $\Psi_s = 1$ .

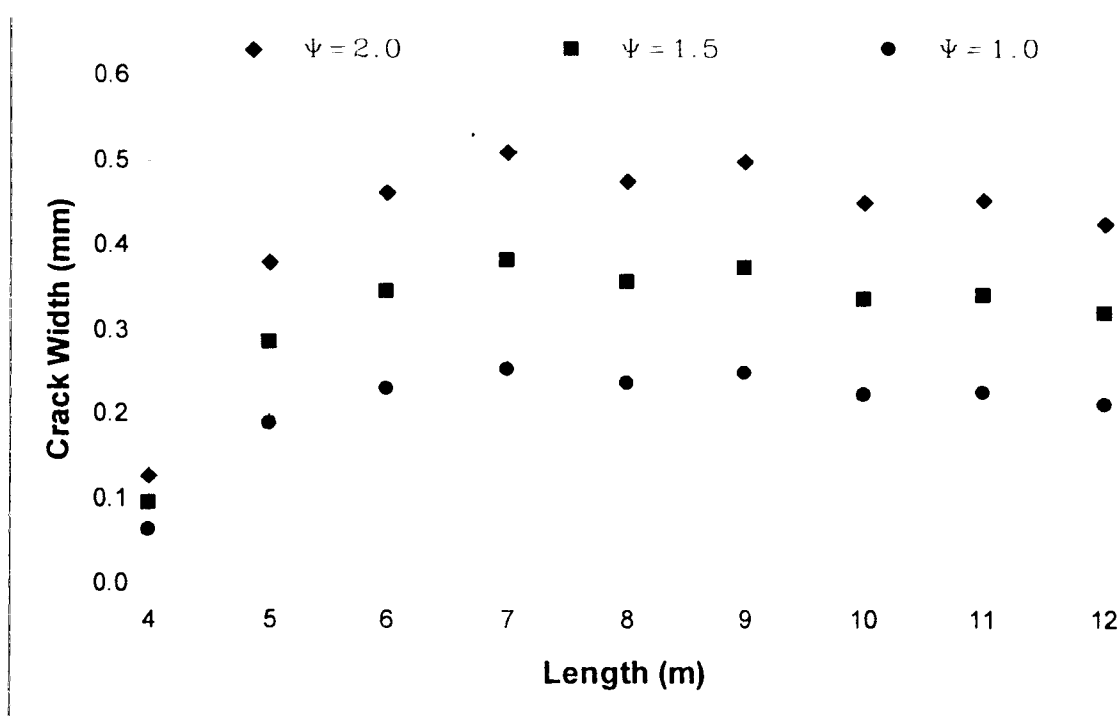


Figure 6.10: Calculated maximum crack widths for different crack spacing factors that are based on ACI 350 minimum reinforcement ratio, ( $H=4$  m,  $t=300$  mm,  $\epsilon_{tmp+slrm} = 600 \times 10^{-6}$ )

Since a proper value of crack spacing factor is determined, crack width equation can be rewritten as follows:

$$w_c = S_c \epsilon_s = 112 \Psi_s \epsilon_s = 112 \epsilon_s \text{ mm}$$

In order to observe the effect of reinforcement ratios on crack width, Figure 6.10 is plotted again as different series, which is shown in Figure 6.11. This figure shows the



calculated crack widths for walls with reinforcement ratios of ACI 350 recommendations. It can be observed that by increasing the length of the wall for the same amount of reinforcement ratio, crack width increases with the exception of  $L = 8$  m. When the wall length is less than 8 m, there is a single major crack. But, when the length is increased to 8 m, two major cracks are observed (see Figures A.1.1 and A.1.2). Increasing the number of cracks is expected to reduce the crack width in structures.

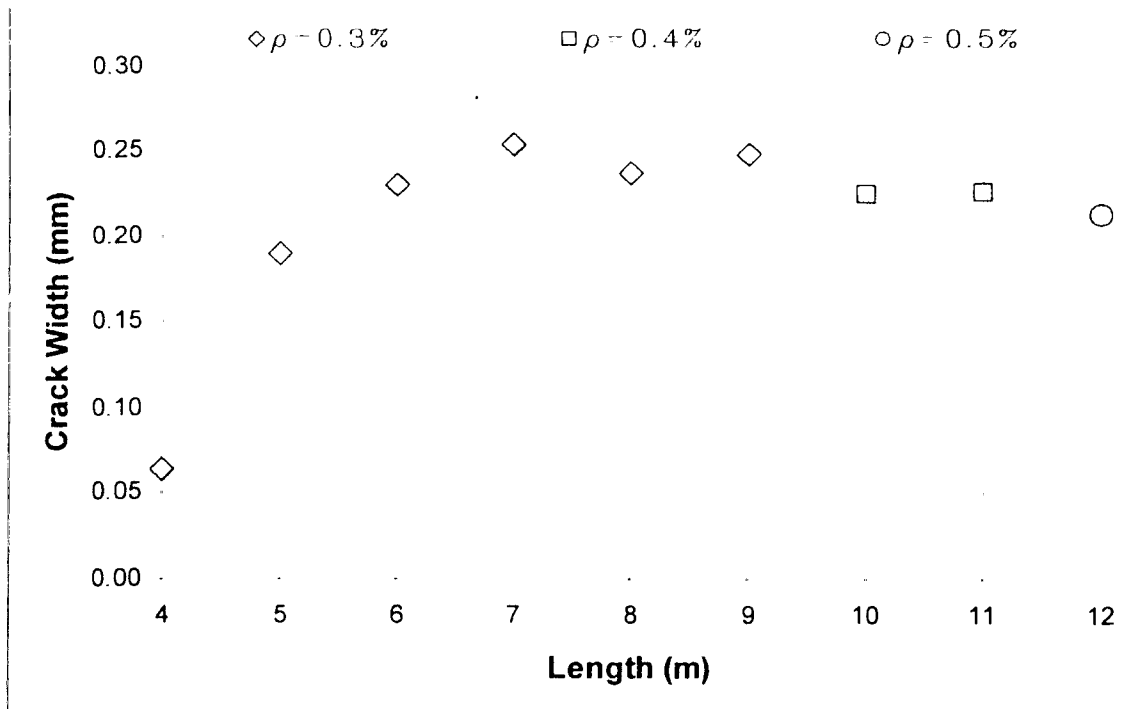


Figure 6.11: Calculated maximum crack widths for walls that are designed based on ACI 350 minimum reinforcement ratio ( $H=4$  m,  $t=300$  mm,  $\epsilon_{imp+shrn} = 600 \times 10^{-6}$ )

Figure 6.11, also shows that by increasing the reinforcement ratio, the crack width is reduced. Wall dimensions shown in Figure 6.11 are relatively small. In this study, the effect of wall length, height, thickness and reinforcement ratios are investigated. Figures 6.12 to 6.26 represent the results of parametric study.

Figures 6.12 and 6.13 present calculated maximum crack widths for 21 different walls. Three different heights (4, 6 and 8 m.) with length varying from 6 to 60 m were used. Reinforcement ratio and wall thickness were kept constant ( $t=300$  mm, and  $\rho=0.5\%$ ). In

Figure 6.12, reinforcing steel is assumed to behave elastic, while in Figure 6.13 steel is modeled as elasto-plastic. It is important to keep in mind that maximum crack width is estimated from the most strained elements in each wall, and the location of that element may change for each different wall geometry. For these reason, one may expect randomness in comparison of estimated crack widths.

Observation of Figure 6.12 indicates that the rate of increase in maximum crack width decreases with the increase in length. Also, it can be seen that the effect of wall height on maximum crack width is insignificant for the same length of wall. The crack widths do not increase significantly beyond the length grater than 24 m. This can be explained due to the fact that when  $L/H$  ratio is high, wall behaves similar to a continuous wall. In this case, the increase in length does not increase the crack width, but it increases the number of cracks. The increase in the number of cracks distributes the overall elongation of reinforcement and that limits the crack width.

Considering the non-linear behaviour of the reinforcing steel, crack widths are calculated in the same walls and it is shown in Figure 6.13. In this figure, it is clear that when the steel yields wide cracks would develop, which are unacceptable for liquid retaining structures.

It was mentioned that wall height does not affect the crack width significantly when the length of wall is the same. However, provided that  $L/H$  ratios are the same, the higher walls results wider cracks as compared to shorter walls. Kheder (1997) suggested that the increasing  $L/H$  ratio increases the degree of restraint, which would generate wider cracks. This phenomenon can be observed in Figure 6.14, in which increasing  $L/H$  ratio results in wider cracks. The higher walls generate wider cracks as compared to shorter walls with same  $L/H$  ratios. This means that although the length is shorter, higher walls would develop wider cracks as compared to shorter walls with the same  $L/H$  ratio. Similar to Figure 6.13, effect of the yielding in steel can be observed in Figure 6.15.

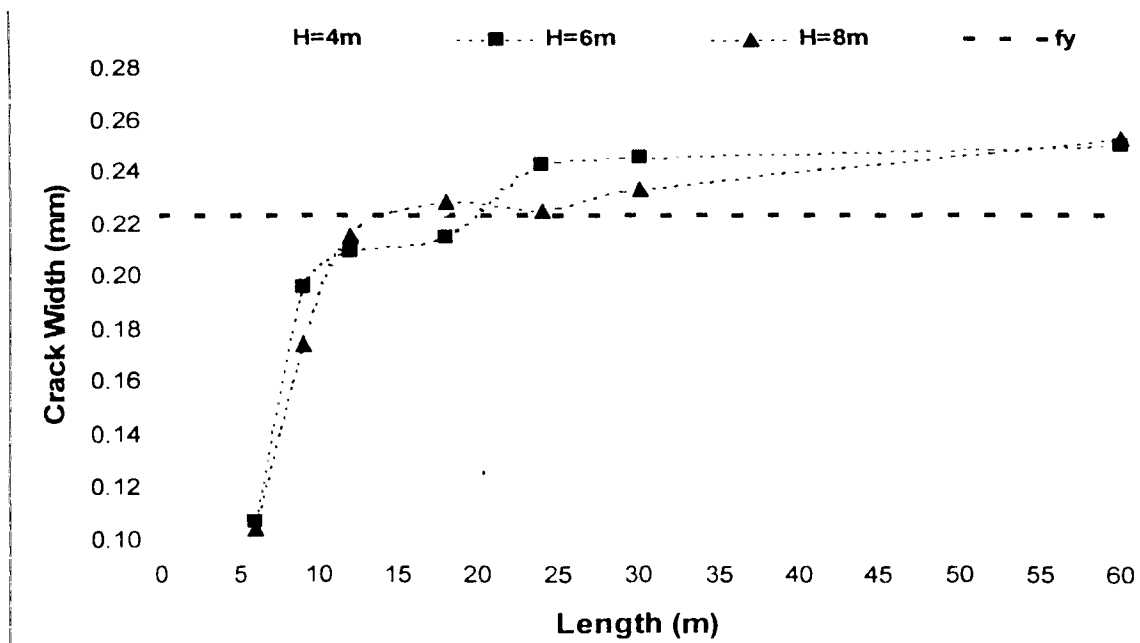


Figure 6.12: Calculated maximum crack widths in walls with different heights, assuming that steel behaviour is linearly elastic ( $t=300$  mm,  $\rho=0.5\%$ ,  $\epsilon_{imp+shrn} = 600 \times 10^{-6}$ )

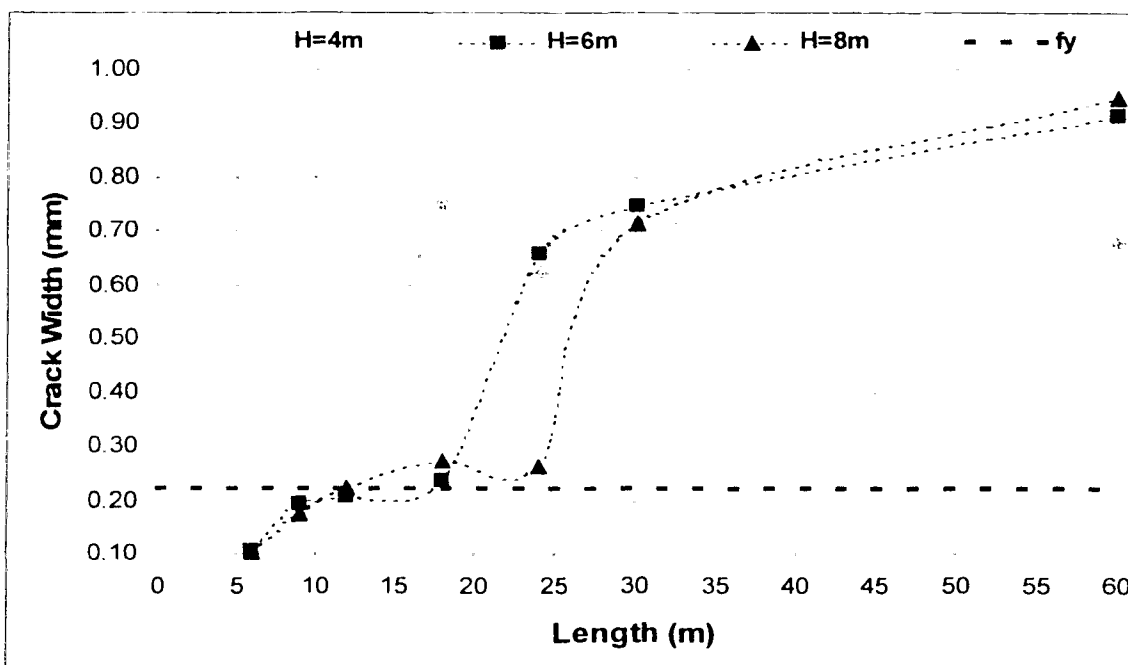


Figure 6.13: Calculated maximum crack widths in walls with different heights, non-linearity of the steel is included ( $t=300$  mm,  $\rho=0.5\%$ ,  $\epsilon_{imp+shrn} = 600 \times 10^{-6}$ )

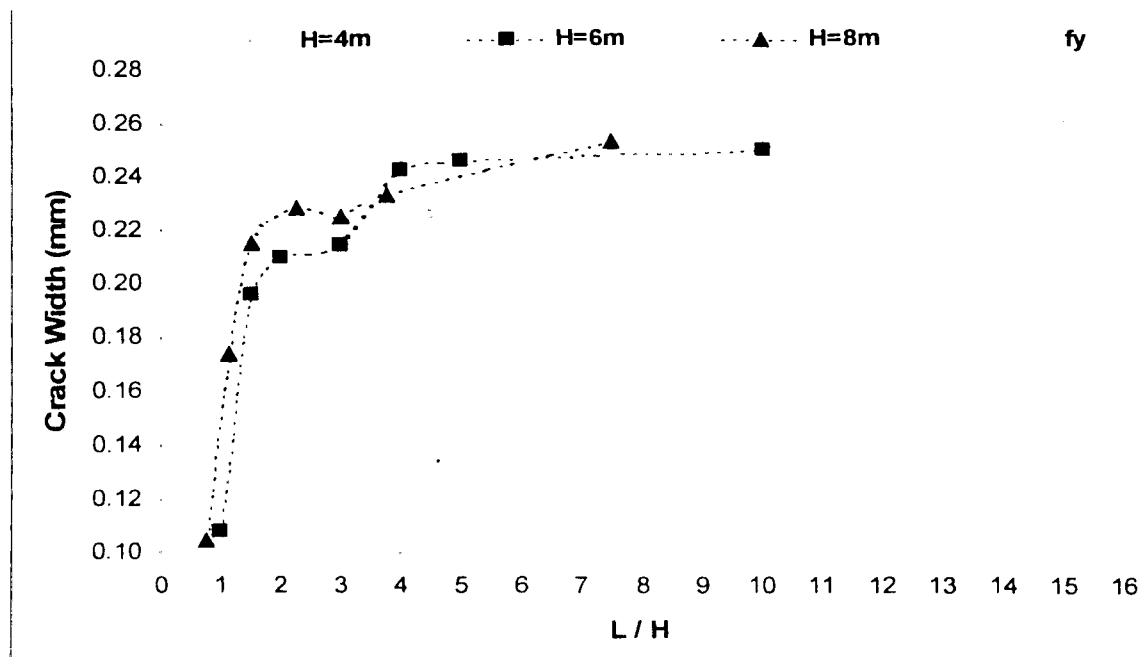


Figure 6.14: Effect of wall length to height ratio on crack width, assuming that steel behaviour is linearly elastic ( $t=300$  mm,  $\rho=0.5\%$ ,  $\varepsilon_{imp+shrn} = 600 \times 10^{-6}$ )

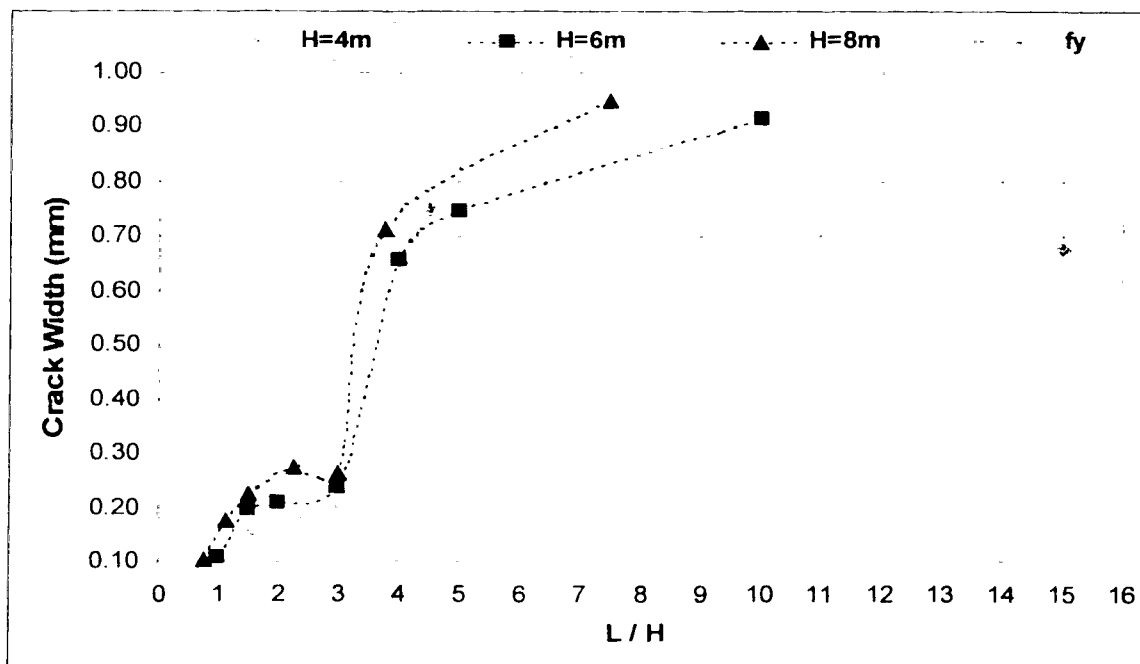


Figure 6.15: Effect of wall length to height ratio on crack width, non-linearity of the steel is included ( $t=300$  mm,  $\rho=0.5\%$ ,  $\varepsilon_{imp+shrn} = 600 \times 10^{-6}$ )

The effect of wall thickness on maximum crack width is shown in Figure 6.16. In this case, the wall height and reinforcement ratios were kept constant ( $H=4$  m and  $\rho=0.5\%$ ). In order to be able to observe the effect of wall thickness, the steel is assumed to behave linearly. Results as shown in Figure 6.16 indicate that varying wall thickness does not affect the maximum crack width unless the length is relatively small. The effect of variation of wall thickness on crack width when the non-linear behaviour of the reinforcement is considered is shown in Figure 6.17.

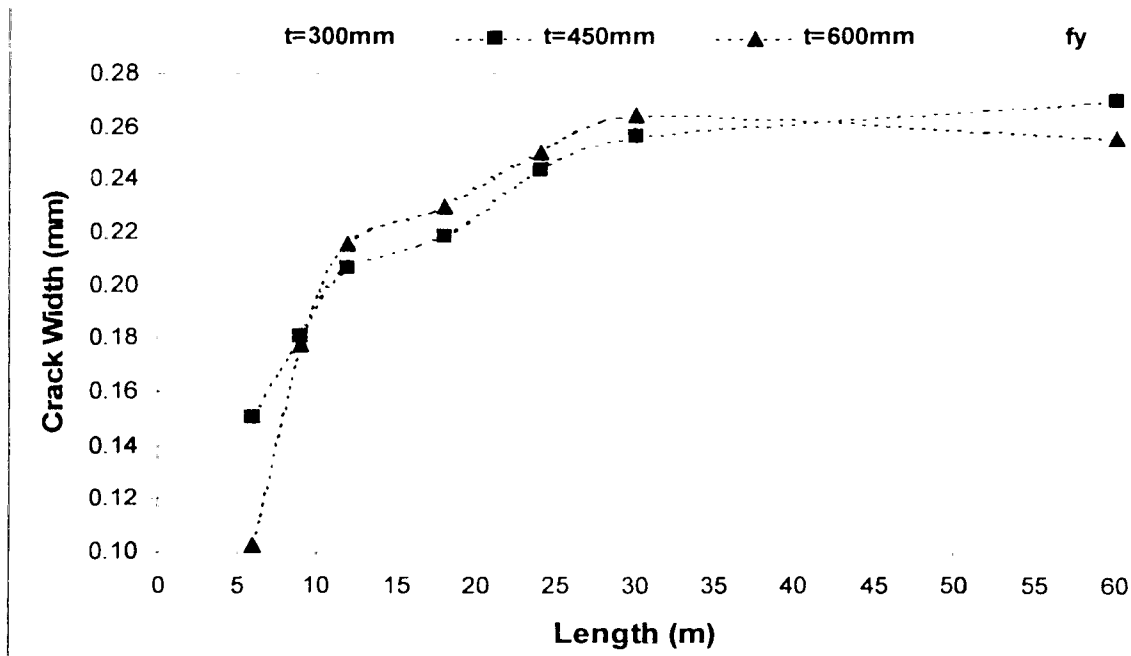


Figure 6.16: Effect of variation of wall thickness on crack width, assuming that steel behaviour is linearly elastic ( $H=4$  m.,  $\rho=0.5\%$ ,  $\epsilon_{imp+shrn} = 600 \times 10^{-6}$ )

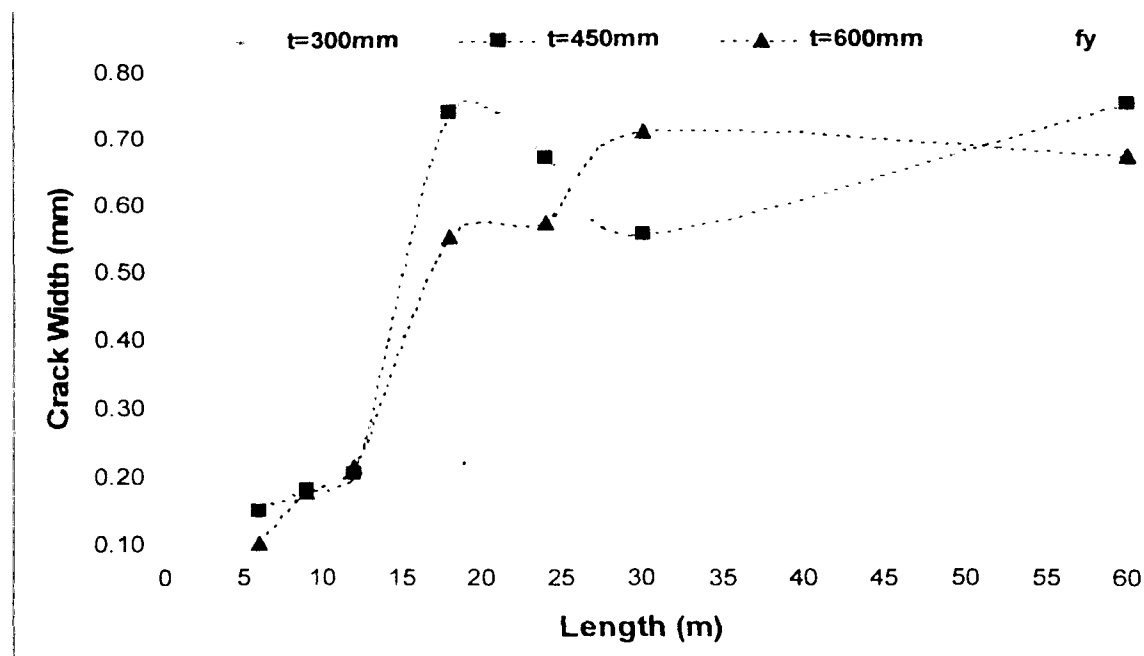


Figure 6.17: Effect of variation of wall thickness on crack width, non-linearity of the steel is included ( $H=4$  m.,  $\rho=0.5\%$ ,  $\epsilon_{imp+shrn} = 600 \times 10^{-6}$ )

In Figures 6.12 to 6.17, reinforcement ratios and volumetric deformations were kept constant in order to observe the effects of wall thickness and height on the maximum crack width. Normally, reinforcement ratio would be designed based on the restrained strains, which is a parameter of the wall length and the amount of volumetric deformation. In order to determine the amount of reinforcement, different reinforcement ratios were used for different wall lengths. The magnitude of volumetric deformation was also considered. The effect of variation of crack width with different reinforcement ratios are shown in Figures 6.18, 6.19, and 6.20 for volumetric deformation of 400, 600, and 800 micro strains respectively.

In these three figures, the effect of yielding of steel can be observed. In long walls that have small amount of reinforcement, reinforcement yields and wide cracks develop. Maximum crack width reaches up to 1.2 mm for 400 micro strains, while 1.5 mm crack width is observed for 800 micro strains. For liquid retaining structures, such large cracks are unacceptable. In order to determine the design reinforcement ratio for liquid retaining structures a maximum width of 0.1 mm crack will be considered acceptable and the

corresponding reinforcement ratio will be selected. However, the variation of crack width with varying temperature and shrinkage strains need to be investigated first.

Figures 6.21 to 6.26 present comparison of different total volumetric deformations on maximum crack width. Figures 6.21 to 6.25 show that for wall length less than about 16 m, increasing the volumetric deformation from 400 to 800 micro strain, increases the maximum crack width by about 0.1 to 0.15 mm. However, when the length of wall reaches 16 m, the effect of magnitude of volumetric deformation on crack width diminishes. This phenomenon is particularly clear in Figure 6.25, which represents 0.7% of reinforcement ratio. The series shown in Figure 6.26 has a different trend, which can be explained with the aid of Figure A.1.19. It is important to keep in mind that walls shown in Figure 6.26 have 0.8% reinforcement ratio. In these walls, due to high reinforcement ratio, very fine cracks were observed in most part of the wall. As can be seen in Figure A.1.9, when the reinforcement ratio is 0.8%, maximum cracks were recorded at the locations that are closer to the free ends of the wall. The generated tensile stresses at both free ends of the wall increases with increasing volumetric deformation. Since the maximum crack width were measured closer to the free ends of the wall, increase in crack width with increasing volumetric deformation is expected.

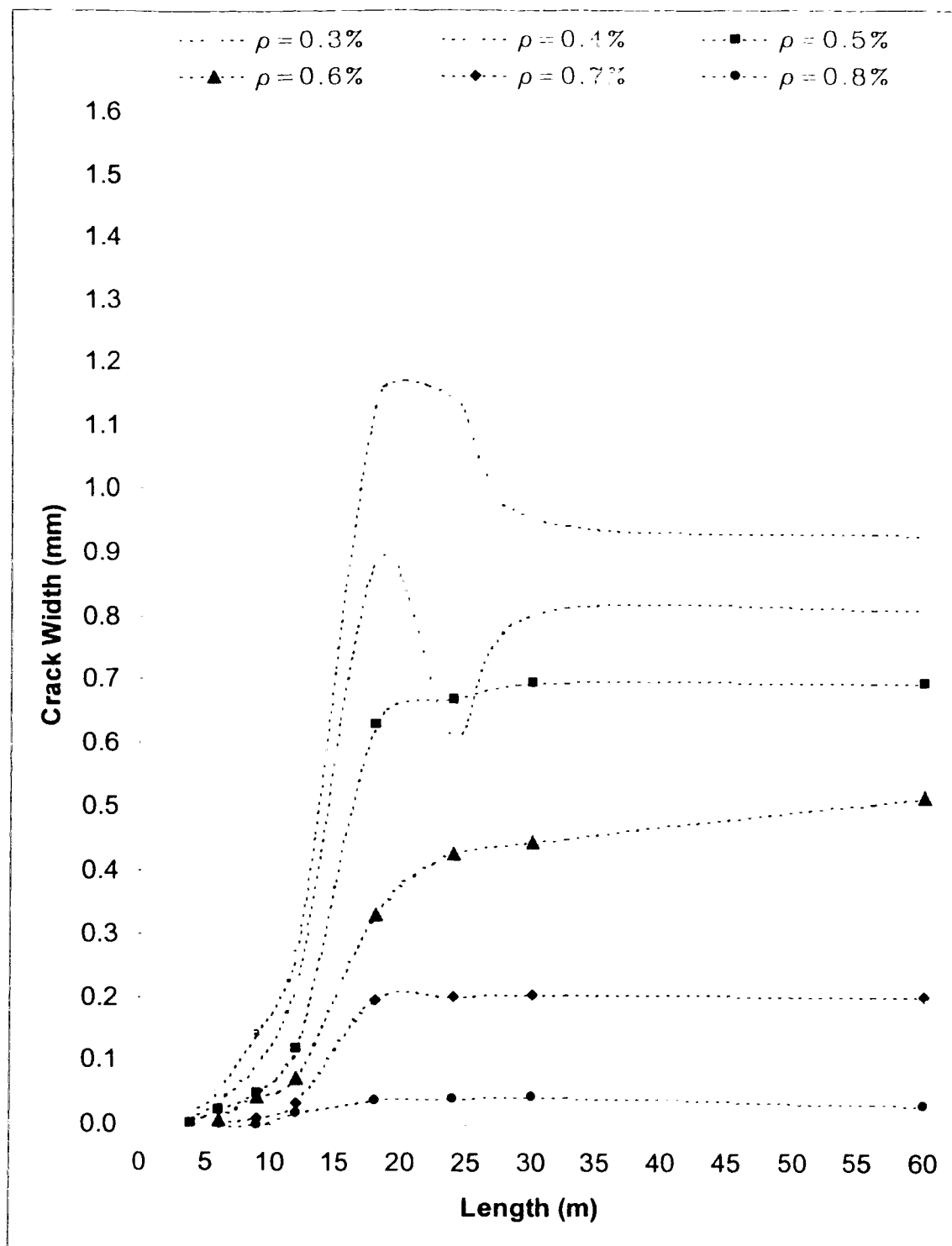


Figure 6.18: Variation of crack width with different reinforcement ratios, ( $\epsilon_{temp.+shrinkg.} = 400 \times 10^{-6}$ ,  $H=4$  m,  $t=300$  mm)



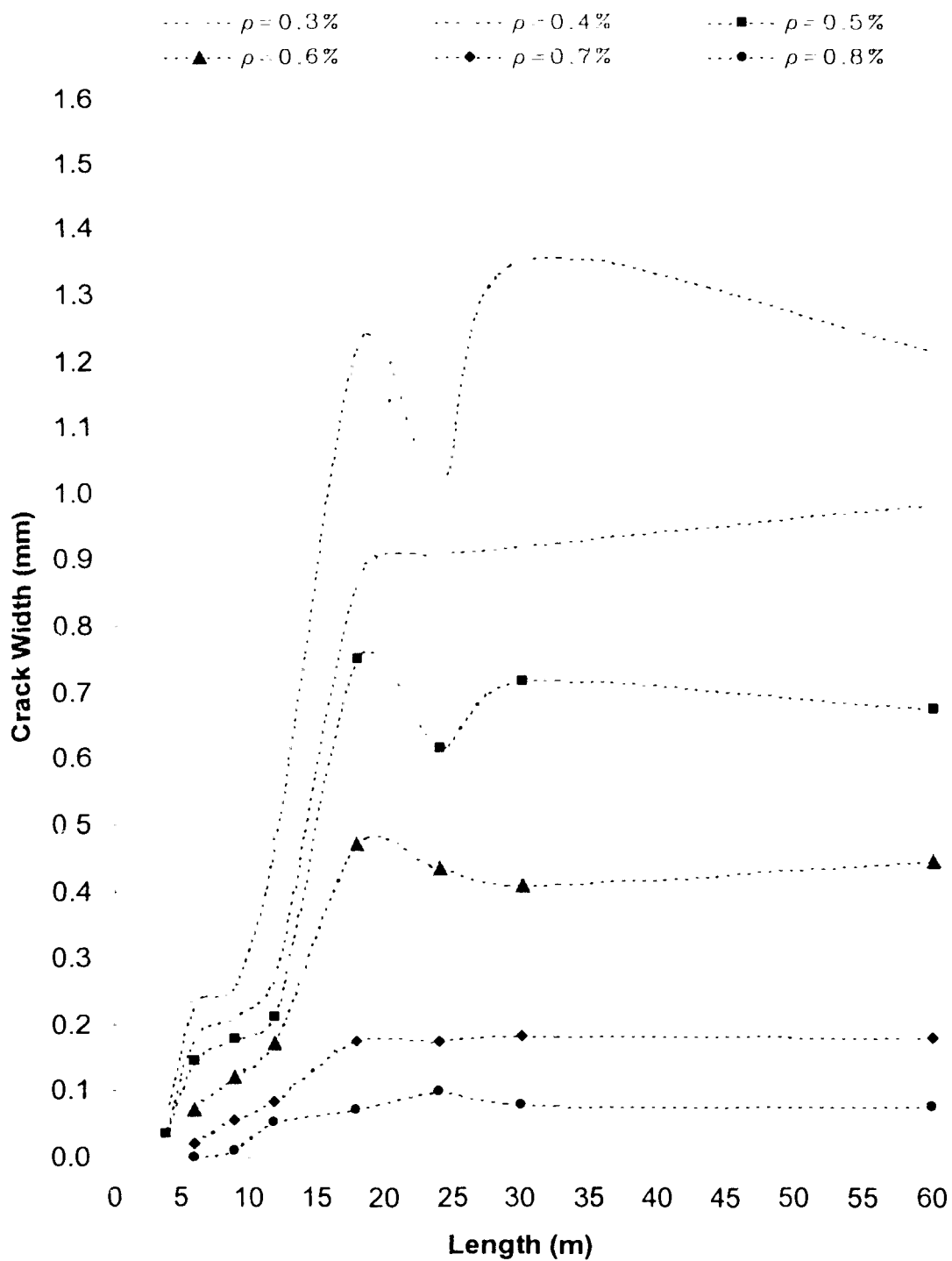


Figure 6.19 Variation of crack width with different reinforcement ratios,  
 ( $\epsilon_{temp.+shrinkg.} = 600 \times 10^{-6}$ ,  $H=4$  m,  $t=300$  mm)

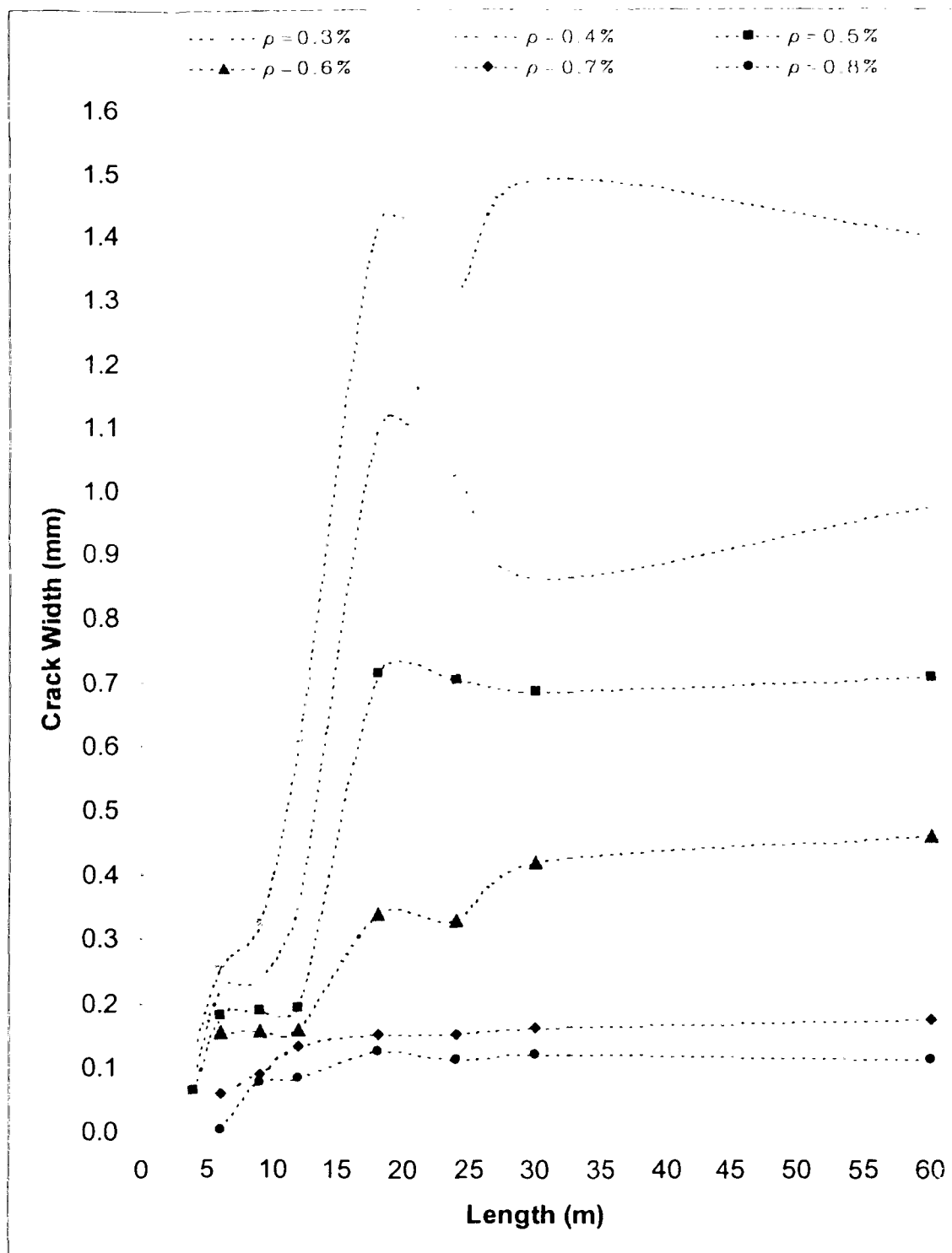


Figure 6.20 Variation of crack width with different reinforcement ratios,  
 ( $\epsilon_{temp+shrinkg.} = 800 \times 10^{-6}$ ,  $H=4$  m,  $t=300$  mm)

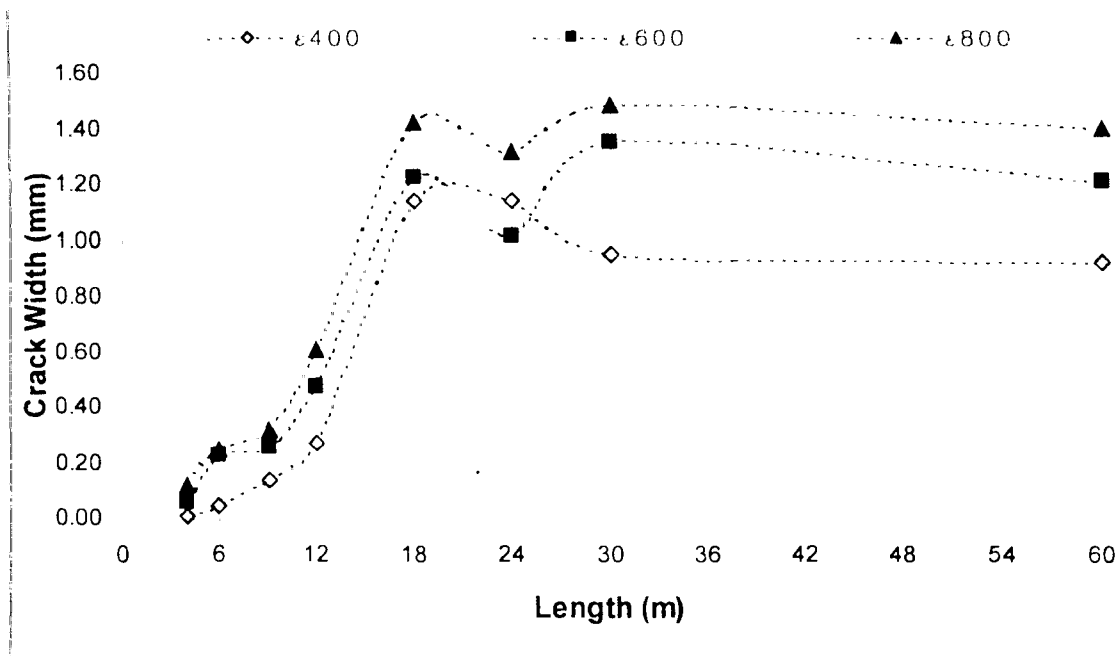


Figure 6.21: Effect of increasing temperature and shrinkage strains on maximum crack width, (reinforcement ratio = 0.3%, H=4 m, t=300 mm)

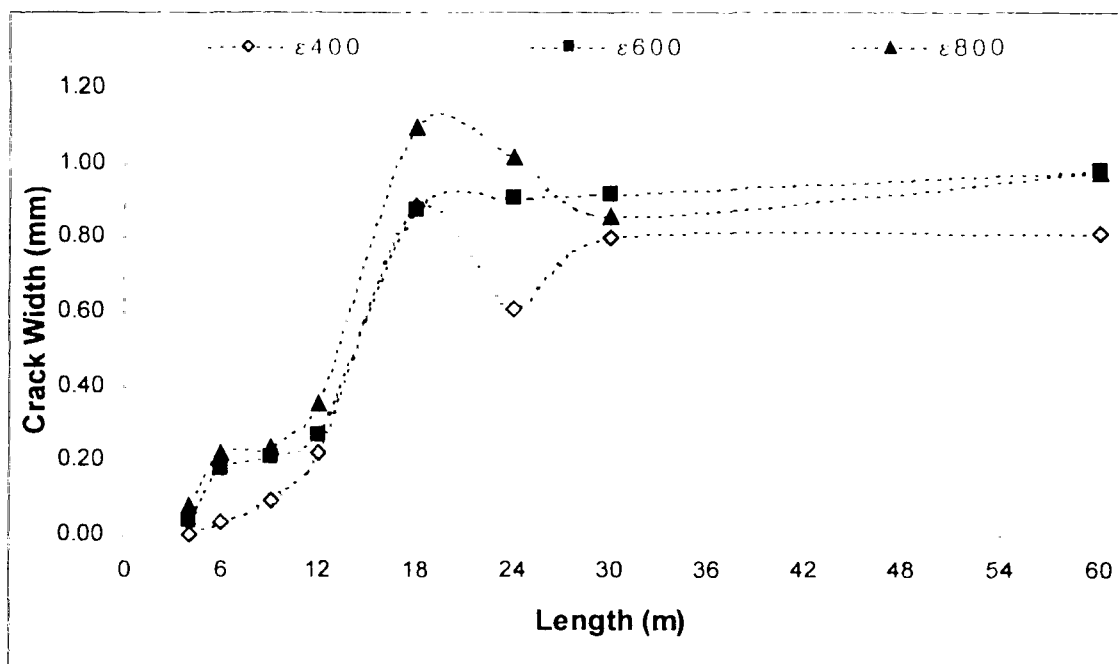


Figure 6.22: Effect of increasing temperature and shrinkage strains on maximum crack width, (reinforcement ratio = 0.4%, H=4, t=300 mm)

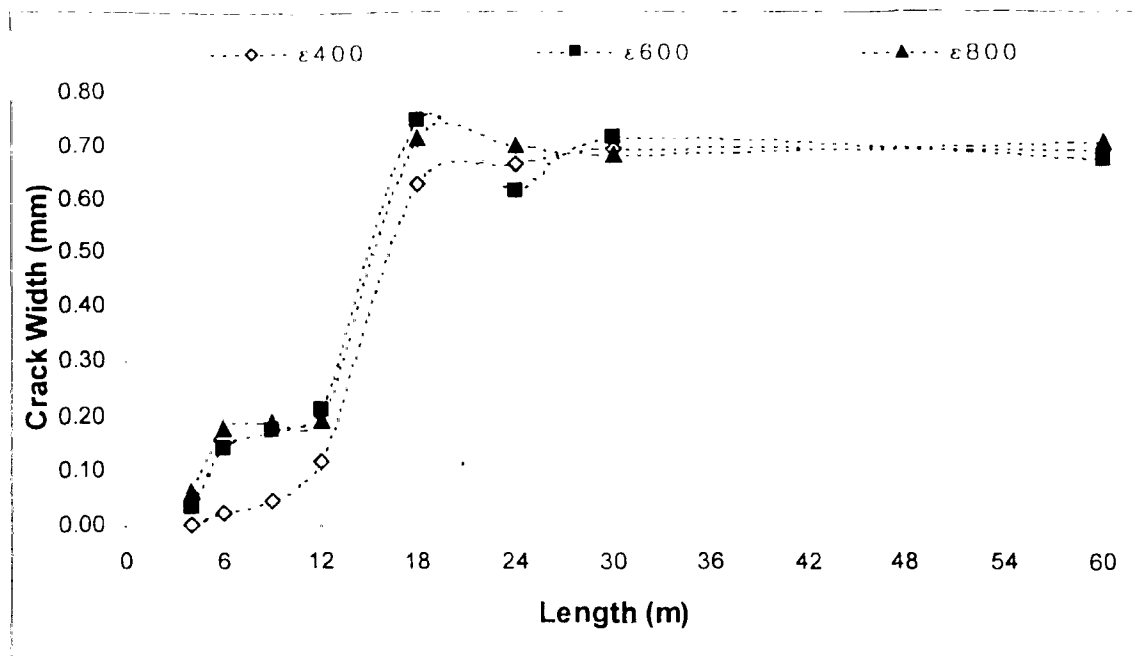


Figure 6.23: Effect of increasing temperature and shrinkage strains on maximum crack width, (reinforcement ratio = 0.5%, H=4, t=300 mm)

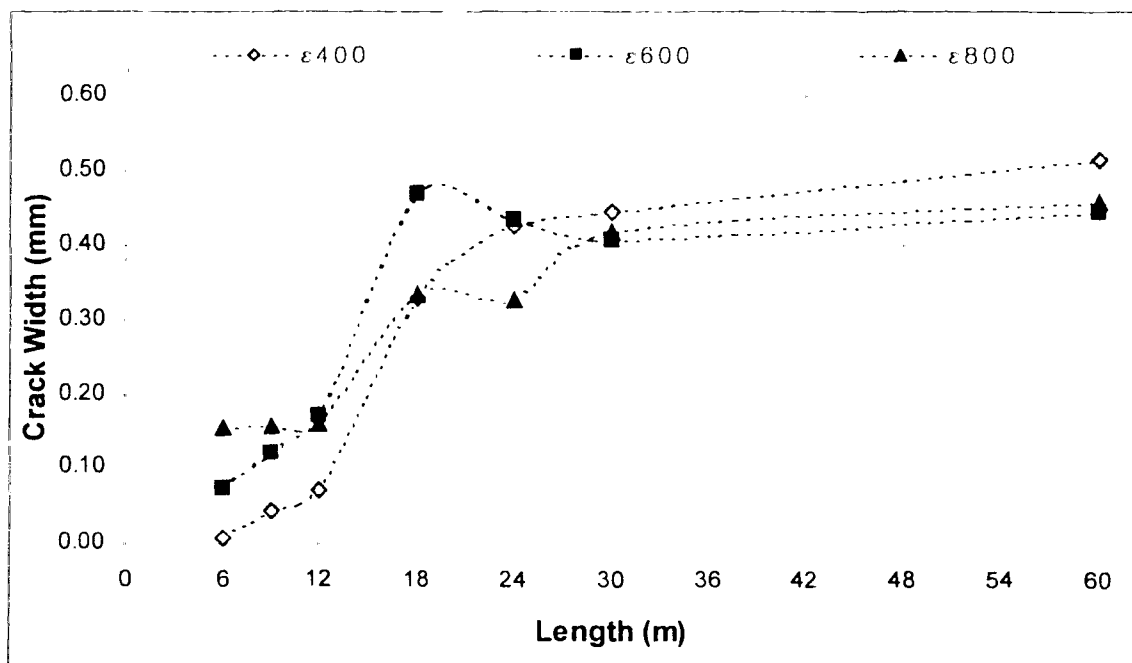


Figure 6.24: Effect of increasing temperature and shrinkage strains on maximum crack width, (reinforcement ratio = 0.6%, H=4 m, t=300 mm)

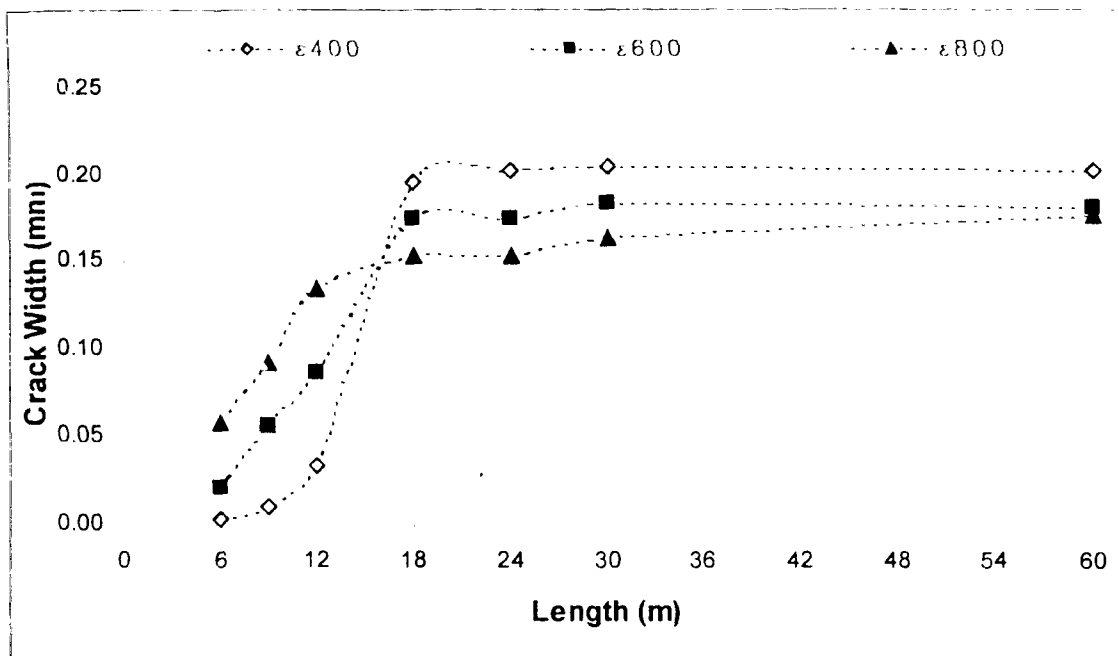


Figure 6.25: Effect of increasing temperature and shrinkage strains on maximum crack width, (reinforcement ratio = 0.7%, H=4 m. t=300 mm)

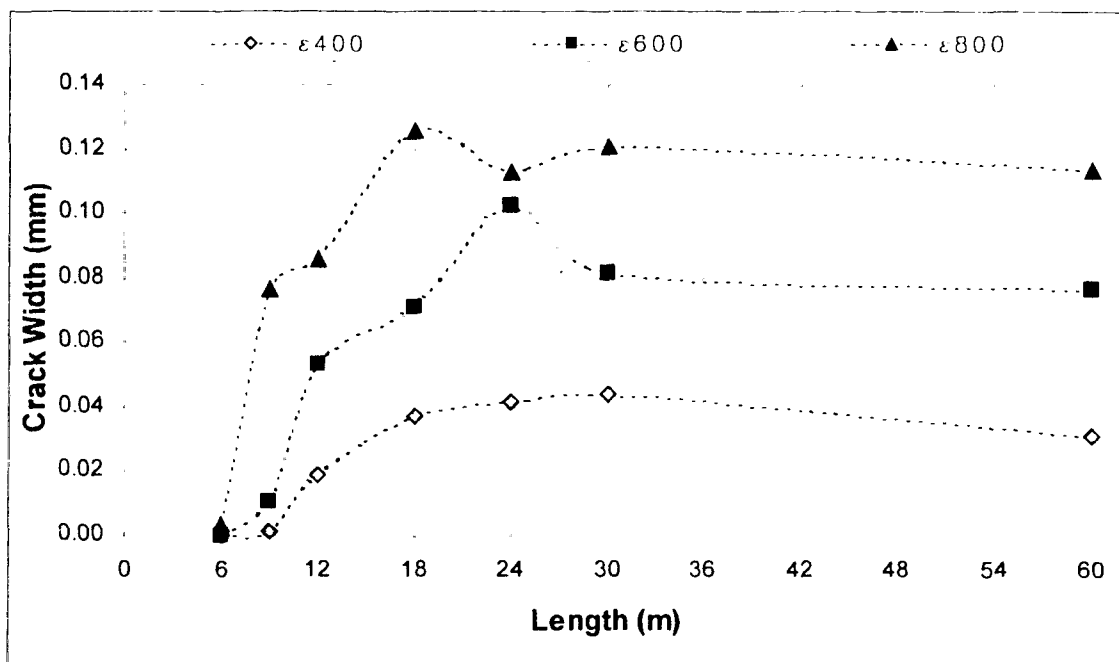


Figure 6.26: Effect of increasing temperature and shrinkage strains on maximum crack width, (reinforcement ratio = 0.8%, H=4, t=300 mm)

The overall behaviour of the maximum crack width that is observed in Figures 6.12 to 6.26 provides the following conclusions, which will be considered in determination of the amount of reinforcement for liquid retaining structures.

- For wall lengths greater than 20 m, the maximum crack width is almost constant
- Wall thickness does not affect maximum crack width significantly
- For the same wall length, the variation in wall height does not affect maximum crack width significantly
- The effect of magnitude of the volumetric deformation diminishes after about 16m away from the free ends of wall

Considering the conclusions listed above and Figures 6.18, 6.19 and 6.20 an idealized design chart can be developed. Figure 6.27 shows the idealized design chart for temperature and shrinkage reinforcement ratio. Based on the allowable maximum crack width, using Figure 6.27, the required amount of reinforcement can be determined. According to Table 6.3, the allowable maximum crack width should be 0.1 mm for liquid retaining structures. In Figure 6.27, the intersection points of 0.1 mm crack width and the series of reinforcement ratio would provide the amount of design reinforcement.

## **6.7 Summary**

In this Chapter, it was shown that using the FEM in combination with a crack width equation, it was possible to estimate the crack width in reinforced concrete structures. Normally, expansive and difficult experimental studies are required in order to reach the conclusions that are provided in this Chapter. One of the main objectives of this research is to determine the sufficient amount of reinforcement ratio for walls that are used in liquid retaining structures. In this Chapter, particular concern was environmental structures that are designed based on ACI 350-01. ACI 350, clause 7.12.2.1 provides minimum reinforcement ratios, which are summarized in Table 6.2. ACI 350-01 recommends the same reinforcement ratio for a wide range of wall length. Results of the parametric study provided more details for the required reinforcement ratio that can be used in design. ACI 350-01 specifies the maximum crack width for liquid-retaining

structures as 0.25 mm. However, the limit of 0.25 mm for maximum crack width is based on the flexural type of cracks. On the other hand, temperature and shrinkage induced stresses generates tensile type of cracks. Since the tensile types of cracks are generally full-depth cracks, they cause more leakage as compared to flexural type cracks. For this reason, in order to prevent leakage, more strict rules should apply on allowable crack width. Based on Table 6.3, 0.1 mm of allowable crack width can be selected for temperature and shrinkage reinforcement in liquid retaining structures. Using Figures 6.18, 6.19 and 6.20 the required reinforcement ratio can be selected that corresponds to 0.1 mm of crack width for any wall dimension. In addition to that, the idealized design chart shown in Figure 6.27 provides a summary of the analysis, which also can be used for design purposes. With this approach, Table 6.8 is prepared, in which the minimum amount of reinforcement based on the results of the FE analysis is recommended.

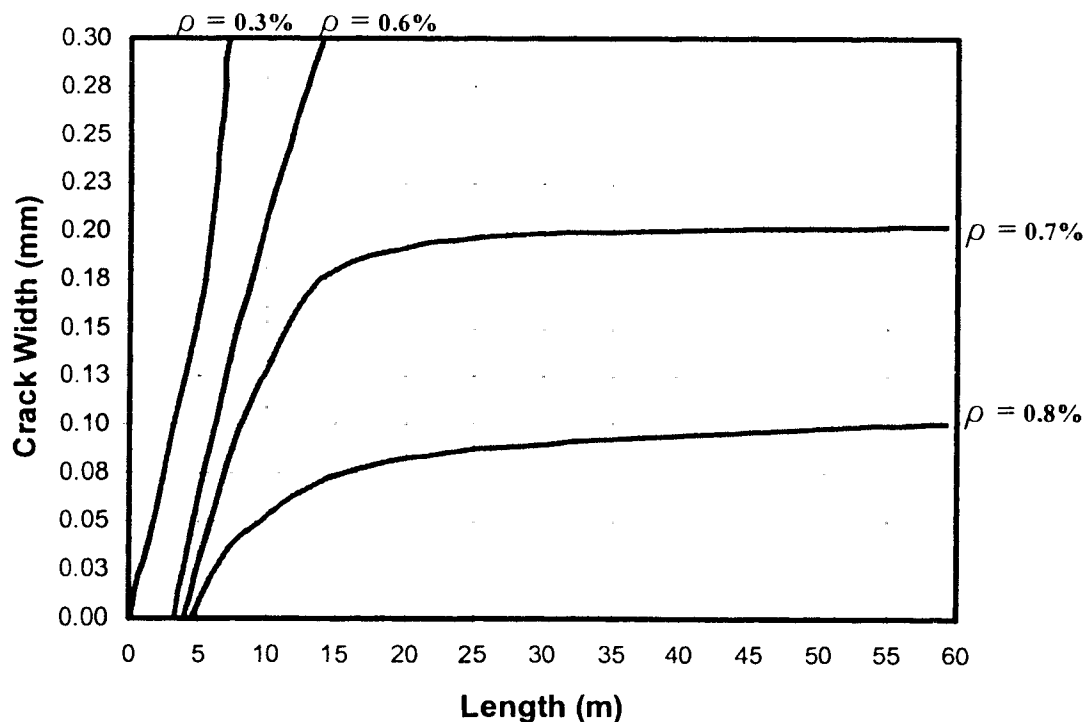


Figure 6.27: Idealized design chart for temperature and shrinkage reinforcement

Table 6.8: Recommended shrinkage and temperature reinforcement ratio

Length Between Joints, (m)	Minimum Shrinkage and Temperature Reinforcement Ratio, (%)		
	ACI 350-01	ABAQUS/6.4	
		Maximum crack width=0.1 mm	Maximum crack width=0.25 mm
Less than 4	0.30	0.25	0.10
4	0.30	0.30	0.10
5	0.30	0.35	0.15
6	0.30	0.40	0.20
7	0.30	0.45	0.25
8	0.30	0.50	0.30
9	0.30	0.55	0.35
10	0.40	0.65	0.40
11	0.40	0.70	0.45
12	0.50	0.71	0.50
13	0.50	0.72	0.52
14	0.50	0.73	0.54
15	0.50	0.74	0.56
16	0.50	0.75	0.58
17	0.50	0.76	0.60
18	0.50	0.77	0.62
19	0.50	0.78	0.64
20 and greater	0.50	0.80	0.68

Table 6.8 includes ACI 350 recommendations and calculated reinforcement ratios determined from analysis. For maximum allowable crack width of 0.1 mm and 0.25 mm, the required reinforcement ratios are shown separately. It can be observed that ACI 350 provides only three different reinforcement ratios for a wide range of wall dimensions. In some situations this will lead to an overestimation of the required reinforcement ratio. On the other hand, results of parametric study can be used to select an optimum reinforcement ratio. This will lead to an optimum design that is efficient in terms of serviceability as well as economy.



## CHAPTER 7

### CONCLUSION

#### 7.1 Summary

A study on reinforced concrete that is subjected to temperature and shrinkage induced stresses, was carried out. The main objective was to estimate the required temperature and shrinkage reinforcement ratio for design. In order to reach this aim, the FEM was used. To understand the temperature and shrinkage associated problems in concrete, different aspects of the issue was studied in depth. This study is documented in seven chapters and presented in this thesis.

Chapter 1 presented the introduction, literature review, objectives and organization of the thesis. Temperature and shrinkage problems of concrete and the reasons for these problems were explained. Review of the literature was given in background section.

One of the major components of volumetric deformation is thermal strain, and that starts at early ages of concrete. Thermal strains are related to the temperature history of concrete. Chapter 2 presented determination of the temperature history of concrete. Using the FEM, hydration process of concrete was simulated.

Concrete gains strength with time. Strength development of concrete is a function of time and its temperature history, which is the basis of equivalent age concept. In Chapter 3, based on the calculated temperature history, time dependent properties of concrete were estimated. In Chapter 4, considering the time dependent mechanical properties, and volumetric deformations, stress history of hardening concrete was estimated. It was shown that incremental numerical analysis technique using the computer program ABAQUS/6.4 can be used for realistic simulation of hardening concrete.

The restrained volumetric deformations generate stresses in concrete. Degree of restraint for fixed base walls was studied and it was discussed in Chapter 5. Using the FEM, degree of restraint was calculated. It was shown that degree of restraint depends on the geometric properties of the structure. For fixed base walls, relation between length/height and degree of restraint was shown.

Chapter 6 deals with estimating the required amount of reinforcement ratio for the walls that are used in liquid retaining structures. A parametric study was carried out. Using the

FEM, and a crack prediction equation that is developed by Frosch (1999), crack width in walls was estimated. Based on the serviceability requirements of ACI 350, required amount of reinforcement ratio was established. From the results of the parametric study, a design chart was developed that can be used in determination of temperature and shrinkage reinforcement ratio.

## **7.2 Conclusions**

The main objective of this thesis is to determine the required amount of reinforcement to control shrinkage and temperature cracks. During this research, a particular type of structure that is base restraint walls was considered. The effect of temperature and shrinkage induced stresses in these walls was studied. Volumetric deformations of concrete that induce stresses start shortly after the placing. In order to assess the risk of cracks at early ages, simulation of hardening concrete was performed. Due to complexity of the problem, using the computer program ABAQUS/6.4, a special methodology that is based on incremental analysis, was used. Incremental numerical analysis provided a realistic simulation that included time dependent properties of concrete. This simulation technique can be used to estimate the crack risk at early ages of concrete.

Cracking of concrete due to temperature and shrinkage may cause important serviceability problems in liquid retaining structures. Crack formation should be controlled in order to secure structural integrity, prevent deterioration, and meet serviceability requirements. The major technique to control cracking in concrete is to use sufficient amount of reinforcement. Design codes such as ACI 350 provide limited guide for designers to deal with temperature and shrinkage cracks. One way to determine adequate reinforcement ratio that can be used in design, is the experimental studies. However, experimental studies may not be possible in large size structures. In this thesis, it was shown that the FEM can be used to determine adequate amount of temperature and shrinkage reinforcement that would keep the crack width within specifications.

As shown in this thesis, the FEM can be used to conduct a parametric study. Considering different variables, structural problems can be solved to determine the effect of each variable. As shown in this thesis, the results of parametric study may provide practical design solutions as well as a wider view of structural design problems. The results of

parametric study discussed in Chapter 6 showed the characteristics of crack formations in base restrained walls. It was seen that wall thickness and height do not affect crack width significantly. This observation allowed recommending the same reinforcement ratio for different wall thickness and height. Also, the crack width was almost constant for wall lengths greater than 20 m. Based on this observation, it was recommended that reinforcement ratio need not to be increased for walls lengths greater than 20 m. Throughout the thesis, detailed discussion was made about the magnitude of total volumetric deformation. In order to find the required reinforcement ratio, the magnitude of thermal and shrinkage strains needed to be determined. The results of the parametric study showed that the magnitude of total volumetric deformation affect the crack width for certain wall dimensions. In wall lengths that are greater than 16 m, the effect of volumetric deformation was observed to be more severe closer to the ends of the wall. It can be concluded that in continuous walls, the maximum crack width would not change significantly with variation of volumetric deformation. However, it was observed that in walls that are shorter than 16 m, increase of the volumetric deformation would increase the crack width.

The required amount of reinforcement for serviceability is based on allowable crack width. Based on the recommendation given by design guidelines (Table 6.3), it was assumed that 0.1 mm of maximum crack width would meet the serviceability requirements of liquid retaining structures. From the results of the parametric study, a design chart was developed. Considering the allowable crack width, adequate reinforcement ratio can be determined from the proposed design chart. Unlike ACI recommendations (Table 6.2), proposed design chart can be used for any wall dimensions. Parametric study provided more details on adequate amount of temperature and shrinkage reinforcement ratio for fixed base walls. Recommended reinforcement ratios that are presented in Table 6.8 can be used for optimum reinforcement design.

### **7.3 Suggestions for Further Research**

Throughout this research, the computer program ABAQUS/6.4 was used for FE analysis. ABAQUS/6.4 is powerful tool for analysis of reinforced concrete. Incremental numerical analysis provides realistic simulation that can be used to predict stress/strain history of

hardening concrete. ABAQUS/6.4 also provides explicit solution technique that can be used for highly non-linear problems such as reinforced concrete under tension. In this thesis, fixed base walls were studied but this may be extended to different types of structures.

Simulation of hardening concrete to estimate stress/strain history is a broad research area and ABAQUS/6.4 may be used for this purpose. In addition to that, "Cracking Model for Concrete" that is offered by ABAQUS/6.4 may be used to simulate cracks in reinforced concrete that may eventually solve many design problems. However, it is important to keep in mind that ABAQUS/6.4 provides a computer simulation. As shown in this thesis, verification of simulated models by experimental studies is essential. After all, behavior of reinforced concrete materials is difficult to predict. In structural problems of reinforced concrete, numerical analysis alone may not be sufficient to provide solid conclusions. However, when simple experimental data is provided for calibration of numerical analysis, most structural problems may be solved. In this perspective, particular suggestions would be as follows:

- In this thesis, a simple structure was considered for simulation of hardening concrete that required preparation of input data for both heat transfer and stress-displacement analysis. Considering this additional work, a parametric study would require substantial amount of time. However, a subroutine can be developed for ABAQUS/6.4, which could save a significant amount of time. Providing this practical solution, incremental numerical analysis technique may be used for a parametric study that may help to improve understanding of early age concrete.
- "Cracking Model for Concrete" was used for fixed base walls. This model may be used to estimate the adequate reinforcement ratio for other structural elements such as slabs and beams.

## REFERENCES

ACI Committee 207, 1995, "Effect of Restraint, Volume Change, and Reinforcement on Cracking of Mass Concrete", (ACI 207.2R-95), American Concrete Institute, Detroit.

ACI committee 207, 1996, "Mass Concrete", (ACI 207.1R-96), American Concrete Institute, Detroit.

ACI Committee 209, 1997, "Prediction of Creep, Shrinkage and Temperature Effects in Concrete Structures", (ACI 209R-92), American Concrete Institute, Detroit.

ACI Committee 224, 1992, "Cracking of Concrete Members in Direct Tension", (ACI 224.2R-92), American Concrete Institute, Detroit.

ACI Committee 224, 2001, "Control of Cracking in Concrete Structures", (ACI 224R-01), American Concrete Institute, Detroit.

ACI Committee 306, 1997, "Cold Weather Concreting", (ACI 306R), American Concrete Institute, Detroit.

ACI committee 318, 2002, "Building Code Requirements for Structural Concrete (ACI 318-02) and Commentary (ACI 318R-02)", American Concrete Institute, Detroit.

ACI Committee 350, 2001, "Code Requirements for Environmental Engineering Concrete Structure, (ACI 350M-01) and Commentary (ACI 350RM-01)", American Concrete Institute, Detroit.

Aloia, L.D., 2002, "Early Age Kinetics, Activation Energy, Maturity and Equivalent Age", Laboratoire Central des Ponts et Chaussees, Section Formulation et Mise en oeuvre des Betons, Paris, France./ RILEM TC 181-EAS: Final Repoart-July 2002.

Andersen, M.E., 1998, "Design and Construction of Concrete Structures Using Temperature and Stress Calculations to Evaluate Early-age Thermal Effects", G.M. Idorn Consult, Ramboll, Denmark. Material Science of Concrete V, 1998, Published by The American Ceramic Society, 735 Ceramic Place Westerville, Ohio 43081.

Ayotte, E., Massicotte, B., Houde, J., and Gocevski, V., 1997, " Modeling the Thermal Stresses at Early Ages in a Concrete Monolith", ACI Materials Journal, V.94, No.6, November-December 1997, Title no. 94-M65, pp.577-587.

Baetens, B., Schlangen, E., Beek, T.V., Roelfstra, P., and Bijan, J., 2002, "Computer Simulation for Concrete Temperature Control", Concrete International, December 2002.

Borst, R., and Boogaard, A.H., 1994, " Finite-Element Modeling of Deformation and Cracking in Early-Age Concrete", Journal of Engineering Mechanics, Vol. 120, No. 12. December 1994, pp.2519-2535.

Bosnjak, D., Kanstad, T., 2001, "Structural Behavior Numerical Simulation of the Maridal Culvert", Published by Department of Civil &Mining Engineering, NTNU, Norway, IPACS Report BE96-3843/2001:33-8.

Branco, F.A., Mendes, P.A., and Mirambell, E., 1992, "Heat of Hydration Effects in Concrete Structures", V.89, No.2, March-April 1992, pp.139-145.

Carlson, R.W., and Reading, T.J., 1988, "Model Study of Shrinkage Cracking in Concrete Building Walls", ACI Structural Journal, July-August 1988, pp.395-404.

CEB-FIP Model Code 1990, Model Code for Concrete Structures, Comité Euro-International du Béton/Fédération Internationale de la Précontrainte, Paris 1990.

Chantelois, A., Leger, P., Tinawi, R., and Veilleux, M., 1999, "Experimental and Numerical Predictions of Critical Cooling Temperature for Crack Propagation in Concrete Structures". ACI Structural Journal, V.96, No.2, March-April 1999, Title no. 96-S22, pp.203-211.

Cusson, D., and Repette, W.L., 2000, "Early-Age Cracking in Reconstructed Concrete Bridge Barrier Walls", (Institute for Research in Construction National Research Council Canada), ACI Material Journal, 97(4), July-August 2000, pp. 438-446.

Elbadry, M., and Ghali, A., 1995, "Control of Thermal Cracking of Concrete Structures", ACI Structural Journal, V.92, No.4, July-August 1995, Title no. 92-S42, pp.435-450.

Emborg M., and Bernander, S., 1994, "Assessment of Risk of Thermal Cracking in Hardening Concrete", Journal of Structural Engineering, Vol. 120, No. 10, October 1994, pp.2893-2912.

Frosch, R.J., 1999, "Another Look at Cracking and Crack Control in Reinforced Concrete", ACI Structural Journal, V.96, No.3, May-June 1999, pp.437-442.

Gilbert, R.I., 1992, "Shrinkage Cracking in Fully Restrained Concrete Members", ACI Structural Journal, V.89, No.2, March-April 1992, pp.141-149.

Harrison, T.A., 1981, "Early-age Thermal Crack Control In Concrete", CIRIA Report No.91, Construction, Industry, Research and Information association, London, 1981, 48 p.

Hibbitt, H. D., Karlson, B. I., and Sorenson, E. P., 2004. "ABAQUS version 6.4. finite element program". Hibbitt, Karlson & Sorenson, Inc, Providence, R. I.

Huang, C.X., 1999, "The Three Dimensional Modeling of Thermal Cracks in Concrete Structures". *Materials and Structure/Materiaux et Constructions*, Vol.32, November 1999, pp 673-678.

Huo, X.S., Omaishi, N.A., and Tadros, M.K., 2001, "Creep, Shrinkage, and Modulus of Elasticity of High Performance Concrete", *ACI Material Journal*, V.98, No.6, November-December 2001, pp.440-449.

Kheder, G.F., Rawi, R.S.A., and Dhahi, J.K.A., 1994, " Study of the Behavior of Volume Change Cracking in Base-Restraint Concrete Walls". *ACI Materials Journal*, V.91, No.2, March-April 1994, Title no. 91-M13, pp.150-157.

Kheder, G.H., 1997, " A New Look at the Control of Volume Change Cracking of Base Restrained Concrete Walls". *ACI Structural Journal*, V.94, No.3, May-June 1997, Title no. 94-S24, pp.262-271.

Klein, F., Hoffman, E.S., and Rice, P.F., 1981, "Application of Strength Design Methods to Sanitary Structures", *Concrete International*, April, 1981, pp.35-40.

Kosmatka, S.H., Kerkhoff, B., Panarese, W.C., MacLeod, N.F., and McGrath, R.J., 2002, "Design and Control of Concrete Mixtures", Seventh Canadian Edition, Cement Association of Canada, 1500-60 Queen Street, Ottawa, ON.

Lange, D.A., and Altoubat, S.A., 2002, "Early Thermal Changes", Department of civil Engineering, University of Illinois, RILEM TC 181-EAS: Final Report-July 2002.



Liou, D.D., 1999, "Thermal Effects in Large-Sized Diaphragm Wall", *Journal of Performance of Constructed Facilities*, V.13, No.1, February 1999, pp.17-21.

Lu, H.R., Swaddiwudhipong, S., and Wee, T.H., 2000, "Evaluation of Internal Restrained Strain in Concrete Members at Early Age", *ACI Materials Journal*, V.97, No.5, September-October 2000, Title no. 97-M70, pp.612-618.

MacGregor, J.G., Bartlett, F.M., 2000, "Reinforced Concrete Mechanics and Design", First Canadian Edition, Prentice Hall Canada Inc., Scarborough, Ontario.

Mitchell, D., Khan, A.A., and Cook, W.D., 1998, "Early age properties for thermal and stress analysis during hydration", Department of Civil Engineering and Applied Mechanics, McGill University, Montreal. *Material Science of Concrete V*, 1998, Published by The American Ceramic Society, 735 Ceramic Place Westerville, Ohio 43081.

Neville, A. M. 1995, "Properties of Concrete", fourth edition, Pearson Education Limited, Prentice Hall.

Oh B.H., and Cha, S.W., 2003, "Nonlinear Analysis of Temperature and Moisture Distributions in Early-Age Concrete Structures Based on Degree of Hydration", *ACI Material Journal*, V.100, No.5, September-October 2003, pp.361-370.

Pettersson, D., and Thelandersson, S., 2001, "Crack Development in Concrete Structures Due to Imposed Strains- Part 1: Modeling", *Materials and Structures/Materiaux et Constructions*, Vol.34, January-February 2001, pp.7-13.

Pettersson, D., and Thelandersson, S., 2001, "Crack Development in Concrete Structures Due to Imposed Strains- Part 2: Parametric Study of a Wall Fully Restrained at the Base", *Materials and Structures/Materiaux et Constructions*, Vol.34, January-February 2001, pp.14-20.

Reddy, J.N., 1984, "An Introduction to the Finite Element Method", Second Edition, McGraw-Hill, Inc., Boston, Massachusetts.

Saetta, A., Scotta, R., and Vitaliani, R., 1995, "Stress Analysis of Concrete Structures Subjected to Variable Thermal Loads". *Journal of Structural Engineering*, Vol. 121, No. 3, March 1995, pp.446-457.

Schindler, A.K., 2004, "Effect of Temperature on Hydration of Cementitious Materials", *ACI Material Journal*, V. 01, No.1, January-February 2004, pp.72-81.

Truman, K.Z., Petruska, D., Ferhi, A., and Fehl, B., 1991, "Nonlinear, Incremental Analysis of Mass-Concrete Lock Monolith", *Journal of Structural Engineering*, V.117, No.6, June, 1991, pp.1834-1851, Paper No.25923.

Vitharana, N.D., Priestley, M.J.N., and Dean, J.A., 1998, "Behavior of Reinforced Concrete Reservoir Wall Elements under Applied and Thermally-Induced Loadings", *ACI Structural Journal*, V.95, No.3, May-June 1998, pp.238-248.

Vitharana, N.D., and Priestley, M.J.N., 1999, "Significance of Temperature-Induced Loadings on Concrete Cylindrical Reservoir Walls", *ACI Structural Journal*, V.96, No.5, September-October 1999, pp.737-747.

Wang, C., and Dilger, W.H., 1994, "Prediction of Temperature Distribution in Hardening Concrete", Department of Civil Engineering, The University of Calgary, (Thermal Cracking of Concrete at Early Ages, International RILEM Symposium), Munich October 1994. Published by E&FN Spon, 2-6 Boundary Row, London SE1 8HN, U.K.

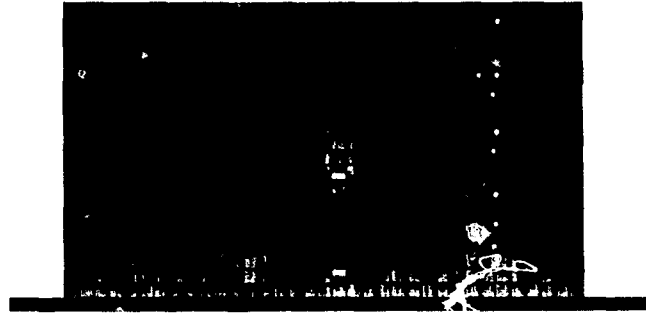


Figure A.1.1: Contour plot of longitudinal steel strains ( $L = 7m$ ,  $H = 4m$ ,  $t = 300mm$ ,  $\rho = 0.3\%$ ,  $\varepsilon = 600 \times 10^{-6}$ )

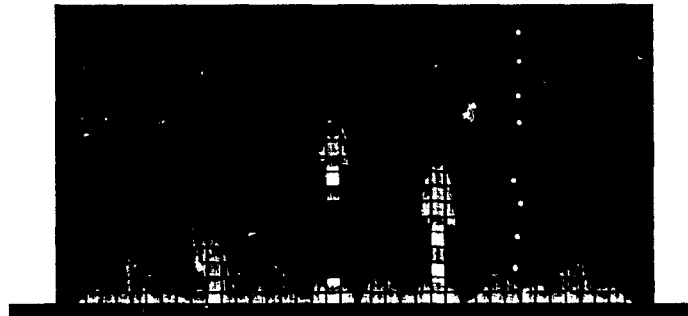


Figure A.1.2: Contour plot of longitudinal steel strains ( $L = 8m$ ,  $H = 4m$ ,  $t = 300mm$ ,  $\rho = 0.3\%$ ,  $\varepsilon = 600 \times 10^{-6}$ )

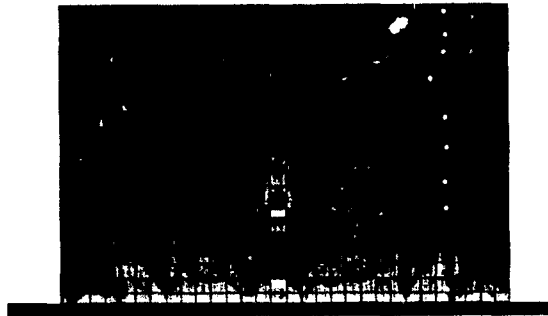


Figure A.1.3: Contour plot of longitudinal steel strains ( $L = 6m$ ,  $H = 4m$ ,  $t = 300mm$ ,  $\rho = 0.5\%$ ,  $\varepsilon = 600 \times 10^{-6}$ ), formation of cracks with increasing wall length



Figure A.1.4: Contour plot of longitudinal steel strains ( $L = 9m$ ,  $H = 4m$ ,  $t = 300mm$ ,  $\rho = 0.5\%$ ,  $\varepsilon = 600 \times 10^{-6}$ ), formation of cracks with increasing wall length



Figure A.1.5: Contour plot of longitudinal steel strains ( $L = 12m$ ,  $H = 4m$ ,  $t = 300mm$ ,  $\rho = 0.5\%$ ,  $\varepsilon = 600 \times 10^{-6}$ ) formation of cracks with increasing wall length

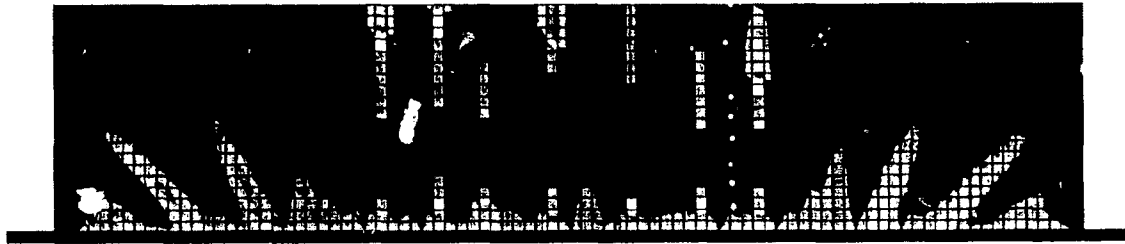


Figure A.1.6: Contour plot of longitudinal steel strains ( $L = 18m$ ,  $H = 4m$ ,  $t = 300mm$ ,  $\rho = 0.5\%$ ,  $\varepsilon = 600 \times 10^{-6}$ ) formation of cracks with increasing wall length



Figure A.1.7: Contour plot of longitudinal steel strains ( $L = 24m$ ,  $H = 4m$ ,  $t = 300mm$ ,  $\rho = 0.5\%$ ,  $\varepsilon = 600 \times 10^{-6}$ ) formation of cracks with increasing wall length



Figure A.1.8: Contour plot of longitudinal steel strains ( $L = 30m$ ,  $H = 4m$ ,  $t = 300mm$ ,  $\rho = 0.5\%$ ,  $\varepsilon = 600 \times 10^{-6}$ ) formation of cracks with increasing wall length



Figure A.1.9: Contour plot of longitudinal steel strains ( $L = 60m$ ,  $H = 4m$ ,  $t = 300mm$ ,  $\rho = 0.5\%$ ,  $\varepsilon = 600 \times 10^{-6}$ ), formation of cracks with increasing wall length

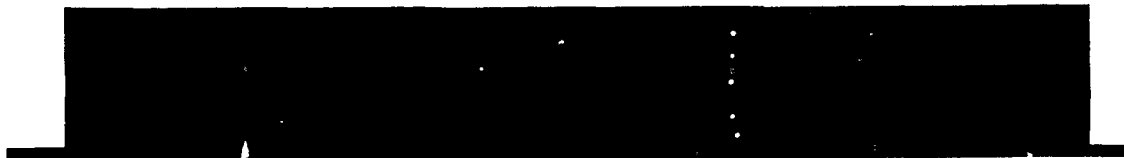


Figure A.1.10: Contour plot of longitudinal steel strains ( $L = 30m$ ,  $H = 4m$ ,  $t = 300mm$ ,  $\rho = 0.5\%$ ,  $\varepsilon = 0.00$ ), development of cracks with increasing volumetric deformation



Figure A.1.11: Contour plot of longitudinal steel strains ( $L = 30m$ ,  $H = 4m$ ,  $t = 300mm$ ,  $\rho = 0.5\%$ ,  $\varepsilon = 75 \times 10^{-6}$ ), development of cracks with increasing volumetric deformation



Figure A.1.12: Contour plot of longitudinal steel strains ( $L = 30m$ ,  $H = 4m$ ,  $t = 300mm$ ,  $\rho = 0.5\%$ ,  $\varepsilon = 150 \times 10^{-6}$ ), development of cracks with increasing volumetric deformation

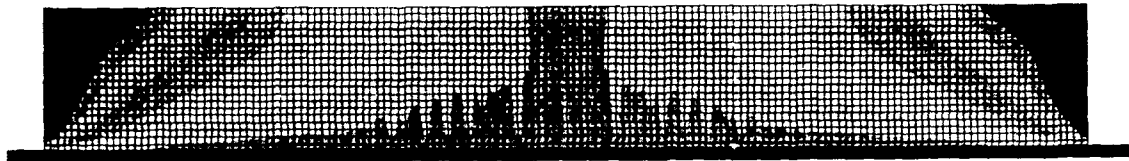


Figure A.1.13: Contour plot of longitudinal steel strains ( $L = 30m$ ,  $H = 4m$ ,  $t = 300mm$ ,  $\rho = 0.5\%$ ,  $\varepsilon = 225 \times 10^{-6}$ ), development of cracks with increasing volumetric deformation



Figure A.1.14: Contour plot of longitudinal steel strains ( $L = 30m$ ,  $H = 4m$ ,  $t = 300mm$ ,  $\rho = 0.5\%$ ,  $\varepsilon = 300 \times 10^{-6}$ ), development of cracks with increasing volumetric deformation



Figure A.1.15: Contour plot of longitudinal steel strains ( $L = 30m$ ,  $H = 4m$ ,  $t = 300mm$ ,  $\rho = 0.5\%$ ,  $\varepsilon = 375 \times 10^{-6}$ ), development of cracks with increasing volumetric deformation





Figure A.1.16: Contour plot of longitudinal steel strains ( $L = 30m$ ,  $H = 4m$ ,  $t = 300mm$ ,  $\rho = 0.5\%$ ,  $\varepsilon = 450 \times 10^{-6}$ ), development of cracks with increasing volumetric deformation



Figure A.1.17: Contour plot of longitudinal steel strains ( $L = 30m$ ,  $H = 4m$ ,  $t = 300mm$ ,  $\rho = 0.5\%$ ,  $\varepsilon = 525 \times 10^{-6}$ ), development of cracks with increasing volumetric deformation



Figure A.1.18: Contour plot of longitudinal steel strains ( $L = 30m$ ,  $H = 4m$ ,  $t = 300mm$ ,  $\rho = 0.5\%$ ,  $\varepsilon = 600 \times 10^{-6}$ ), development of cracks with increasing volumetric deformation

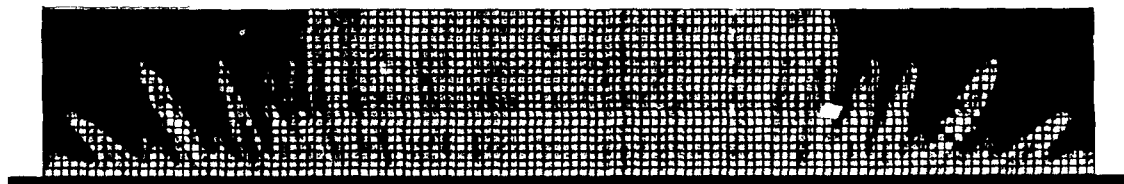


Figure A.1.19: Contour plot of longitudinal steel strains ( $L = 24m$ ,  $H = 4m$ ,  $t = 300mm$ ,  $\rho = 0.8\%$ ,  $\varepsilon = 600 \times 10^{-6}$ ), affect of high reinforcement ratio on crack formation

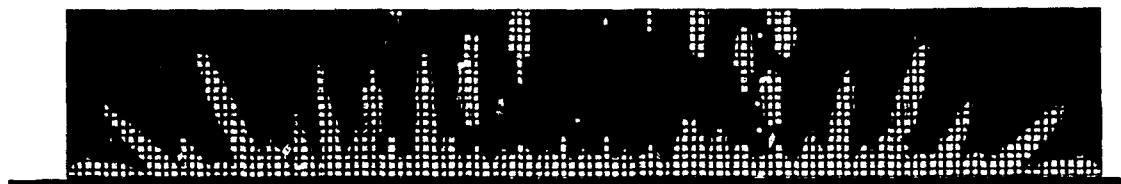


Figure A.1.20: Contour plot of longitudinal steel strains ( $L = 24m$ ,  $H = 4m$ ,  $t = 300mm$ ,  $\rho = 0.7\%$ ,  $\varepsilon = 600 \times 10^{-6}$ ), affect of high rei.forcement ratio on crack formation

## A.1 Example Input File for Crack Width Estimation

```
*Heading
** Job name: L9H4 Model name: L9H4
*Preprint, echo=NO, model=NO, history=NO, contact=NO
**
** PARTS
**
*Part, name=L9H4
*End Part
**
** ASSEMBLY
**
*Assembly, name=Assembly
**
*Instance, name=L9H4-1, part=L9H4
*Node
-----
*Element, type=S4R
-----
** Region: (wall:Picked)
*Elset, elset=_PickedSet2, internal, generate
  1, 900, 1
** Section: wall
*Shell Section, elset=_PickedSet2, temperature=1, material=concrete
0.3, 9
*Rebar Layer
R1A, 0.00015, 0.2, 0.1, steel, 0., 1
R1B, 0.00015, 0.2, 0.1, steel, 90., 1
R2A, 0.00015, 0.2, -0.1, steel, 0., 1
R2B, 0.00015, 0.2, -0.1, steel, 90., 1
*End Instance
*Nset, nset=_PickedSet13, internal, instance=L9H4-1, generate
  1, 46, 1
*Elset, elset=_PickedSet13, internal, instance=L9H4-1, generate
  1, 45, 1
*Nset, nset=_PickedSet14, internal, instance=L9H4-1, generate
  1, 966, 1
*Elset, elset=_PickedSet14, internal, instance=L9H4-1, generate
  1, 900, 1
*End Assembly
**
** MATERIALS
**
*Material, name=concrete
*Density
```

```

2400.,
*Elastic
2.3e+10, 0.18
*brittle cracking
3e+6, 0
0, 0.002
*brittle shear
1, 0
0, 0.002
*Expansion
1e-05,
*Material, name=steel
*Density
7800.,
*Elastic
2.1e+11, 0.
**
** BOUNDARY CONDITIONS
**
** Name: BC-1 Type: Symmetry/Antisymmetry/Encaastre
*Boundary
_PickedSet13, ENCASTRE
**
** FIELDS
**
** Name: Field-1 Type: Temperature
*Initial Conditions, type=TEMPERATURE
_PickedSet14, 60.
** -----
**
** STEP: Step-1
**
*Step, name=Step-1
*Dynamic, Explicit
, 1.
*Bulk Viscosity
0.06, 1.2
**
** FIELDS
**
** Name: Field-1 Type: Temperature
*Temperature
_PickedSet14, 0.
**
** OUTPUT REQUESTS
**

```

\*Restart, write, number interval=1, time marks=NO  
\*\*  
\*\* FIELD OUTPUT: F-Output:-1  
\*\*  
\*Output, field  
\*Element Output, rebar  
LE, S  
\*Output, history, frequency=0  
\*End Step

## A.2 Example Input File for Hardening Concrete Stress Displacement Analysis

```
*Heading
** Job name: SD Model name: clv
*Preprint, echo=NO, model=NO, history=NO, contact=NO
**
** PARTS
**
*Part, name=FOUNDATION-1
*End Part
*Part, name=R1-1
*End Part
*Part, name=R2-1
*End Part
*Part, name=WALL-1
*End Part
**
** ASSEMBLY
**
*Assembly, name=Assembly
**
*Instance, name=WALL-1, part=WALL-1
*Node
Geometry)
*Element, type=C3D8R
Geometry)
*Elset, elset=_PICKEDSET2, internal, generate
1, 1064, 1
** Region: (wallsection:Picked)
*Elset, elset=_PickedSet3, internal, generate
1, 1064, 1
** Section: wallsection
*Solid Section, elset=_PickedSet3, material=FreshConcrete
,
*End Instance
**
*Instance, name=FOUNDATION-1, part=FOUNDATION-1
*Node
Geometry)
*Element, type=C3D8R
Geometry)
*Elset, elset=_PICKEDSET2, internal, generate
1, 1064, 1
** Region: (foundationsection:Picked)
*Elset, elset=_PickedSet3, internal, generate
1, 1064, 1
```

```

** Section: foundationsection
*Solid Section, elset=_PickedSet3, material=MatureConcrete
1.,
*End Instance
**
*Instance, name=R1-1, part=R1-1
*Node
(Geometry)
*Element, type=SFM3D4R
(Geometry)
*Elset, elset=_PICKEDSET2, internal, generate
1, 360, 1
** Region: (reinforcement1:Picked)
*Elset, elset=_PickedSet3, internal, generate
1, 360, 1
** Section: reinforcement1
*Surface Section, elset=_PickedSet3
*Rebar Layer
R1, 0.0003, 0.15, , Steel, 0., 1
R2, 0.0003, 0.15, , Steel, 90., 1
*End Instance
**
*Instance, name=R2-1, part=R2-1
*Node
(Geometry)
*Element, type=SFM3D4R
(Geometry)
*Elset, elset=_PICKEDSET2, internal, generate
1, 360, 1
** Region: (reinforcement2:Picked)
*Elset, elset=_PickedSet3, internal, generate
1, 360, 1
** Section: reinforcement2
*Surface Section, elset=_PickedSet3
*Rebar Layer
R1, 0.0003, 0.15, , Steel, 0., 1
R2, 0.0003, 0.15, , Steel, 90., 1
*End Instance
*Nset, nset=_PICKEDSET26, internal, instance=WALL-1, generate
1, 1755, 1
*Elset, elset=_PICKEDSET26, internal, instance=WALL-1, generate
1, 1064, 1
*Nset, nset=_PICKEDSET27, internal, instance=FOUNDATION-1, generate
1, 1560, 1
*Elset, elset=_PICKEDSET27, internal, instance=FOUNDATION-1, generate
1, 1064, 1

```

```

*Nset, nset=_PICKEDSET28, internal, instance=WALL-1, generate
  1, 1755, 1
*Elset, elset=_PICKEDSET28, internal, instance=WALL-1, generate
  1, 1064, 1
*Elset, elset=__PICKEDSURF21_S4, internal, instance=WALL-1, generate
  14, 1064, 14
*Elset, elset=__PICKEDSURF22_S5, internal, instance=FOUNDATION-1, generate
  799, 874, 1
*Elset, elset=__PICKEDSURF23_S5, internal, instance=FOUNDATION-1
*Elset, elset=__PICKEDSURF24_S6, internal, instance=FOUNDATION-1
*Elset, elset=__PICKEDSURF24_S4, internal, instance=FOUNDATION-1
*Elset, elset=__PICKEDSURF25_S5, internal, instance=FOUNDATION-1
*Elset, elset=_PickedSet29, internal, instance=R1-1, generate
  1, 360, 1
*Elset, elset=_PickedSet29, internal, instance=R2-1, generate
  1, 360, 1
*Elset, elset=_PickedSet30, internal, instance=WALL-1, generate
  1, 1064, 1
*Elset, elset=P1, instance=WALL-1
  517,
*Elset, elset=P2, instance=WALL-1
  516,
*Elset, elset=P3, instance=WALL-1
  513,
*Elset, elset=P4, instance=WALL-1
  506,
*Nset, nset=nall, instance=WALL-1, generate
  1, 1755, 1
*Nset, nset=_PickedSet42, internal, instance=WALL-1, generate
  1, 1755, 1
*Elset, elset=__PICKEDSURF21_S4, internal, instance=WALL-1, generate
  14, 1064, 14
*Surface, type=ELEMENT, name=_PICKEDSURF21, internal
__PICKEDSURF21_S4, S4
*Elset, elset=__PICKEDSURF22_S5, internal, instance=FOUNDATION-1, generate
  799, 874, 1
*Surface, type=ELEMENT, name=_PICKEDSURF22, internal
__PICKEDSURF22_S5, S5
*Elset, elset=__PICKEDSURF23_S5, internal, instance=FOUNDATION-1

*Surface, type=ELEMENT, name=_PICKEDSURF23, internal
__PICKEDSURF23_S5, S5
*Elset, elset=__PICKEDSURF24_S6, internal, instance=FOUNDATION-1
*Elset, elset=__PICKEDSURF24_S4, internal, instance=FOUNDATION-1
*Surface, type=ELEMENT, name=_PICKEDSURF24, internal
__PICKEDSURF24_S6, S6

```



```

__PICKEDSURF24_S4, S4
*Elset, elset=__PICKEDSURF25_S5, internal, instance=FOUNDATION-1
*Surface, type=ELEMENT, name=__PICKEDSURF25, internal
__PICKEDSURF25_S5, S5
*Elset, elset=__PickedSurf27_S4, internal, instance=WALL-1, generate
14, 1064, 14
*Surface, type=ELEMENT, name=__PickedSurf27, internal
__PickedSurf27_S4, S4
*Elset, elset=__PickedSurf28_S5, internal, instance=FOUNDATION-1, generate
799, 874, 1
*Surface, type=ELEMENT, name=__PickedSurf28, internal
__PickedSurf28_S5, S5
*Elset, elset=__PickedSurf32_S5, internal, instance=FOUNDATION-1

*Surface, type=ELEMENT, name=__PickedSurf32, internal
__PickedSurf32_S5, S5
*Elset, elset=__PickedSurf33_S6, internal, instance=FOUNDATION-1, generate
875, 986, 3
*Surface, type=ELEMENT, name=__PickedSurf33, internal
__PickedSurf33_S6, S6
*Elset, elset=__PickedSurf34_S1, internal, instance=FOUNDATION-1
75, 76, 265, 266
*Elset, elset=__PickedSurf34_S2, internal, instance=FOUNDATION-1, generate
875, 877, 1
*Surface, type=ELEMENT, name=__PickedSurf34, internal
__PickedSurf34_S1, S1
__PickedSurf34_S2, S2
*Elset, elset=__PickedSurf35_S6, internal, instance=FOUNDATION-1, generate
1, 75, 2
*Surface, type=ELEMENT, name=__PickedSurf35, internal
__PickedSurf35_S6, S6
*Elset, elset=__PickedSurf36_S1, internal, instance=FOUNDATION-1, generate
986, 988, 1
*Elset, elset=__PickedSurf36_S2, internal, instance=FOUNDATION-1
1, 2, 191, 192
*Surface, type=ELEMENT, name=__PickedSurf36, internal
__PickedSurf36_S1, S1
__PickedSurf36_S2, S2
** Constraint: Constraint-1
*Tie, name=Constraint-1, adjust=yes
__PickedSurf28, __PickedSurf27
** Constraint: Constraint-2
*Embedded Element, host elset=__PickedSet30
__PickedSet29
*End Assembly
**

```

**\*\* MATERIALS**

**\*\***

\*Material, name=FreshConcrete

\*Elastic, dependencies=1

1.27e+10, 0.15, , 0.  
1.27e+10, 0.15, , 1.  
1.95e+10, 0.15, , 2.  
2.42e+10, 0.15, , 3.  
2.76e+10, 0.15, , 4.  
2.98e+10, 0.15, , 5.  
3.12e+10, 0.15, , 6.  
3.28e+10, 0.15, , 7.  
3.42e+10, 0.15, , 8.  
3.53e+10, 0.15, , 9.  
3.58e+10, 0.15, , 10.

\*Expansion

8.5e-06,

\*Concrete Damaged Plasticity

34., 0.1, 1.16, 0.666, 0.

\*Concrete Compression Hardening, dependencies=1

491000., 0., , , 0.  
950000., 4e-05, , , 0.  
1.38e+06, 8e-05, , , 0.  
1.78e+06, 0.00012, , , 0.  
6.35e+06, 0.00096, , , 0.  
7.63e+06, 0.00196, , , 0.  
7.65e+06, 0.00216, , , 0.  
7.6e+06, 0.00246, , , 0.  
491000., 0., , , 1.  
950000., 4e-05, , , 1.  
1.38e+06, 8e-05, , , 1.  
1.78e+06, 0.00012, , , 1.  
6.35e+06, 0.00096, , , 1.  
7.63e+06, 0.00196, , , 1.  
7.65e+06, 0.00216, , , 1.  
7.6e+06, 0.00246, , , 1.  
769000., 0., , , 2.  
1.52e+06, 4e-05, , , 2.  
2.24e+06, 8e-05, , , 2.  
2.94e+06, 0.00012, , , 2.  
1.35e+07, 0.00096, , , 2.  
1.79e+07, 0.00196, , , 2.  
1.8e+07, 0.00216, , , 2.  
1.78e+07, 0.00246, , , 2.  
960000., 0., , , 3.  
1.91e+06, 4e-05, , , 3.

2.83e+06, 8e-05,, , 3.  
 3.75e+06, 0.00012,, , 3.  
 1.92e+07, 0.00096,, , 3.  
 2.75e+07, 0.00196,, , 3.  
 2.77e+07, 0.00216,, , 3.  
 2.72e+07, 0.00246,, , 3.  
 1.1e+06, 0.,,, , 4.  
 2.19e+06, 4e-05,, , 4.  
 3.26e+06, 8e-05,, , 4.  
 4.33e+06, 0.00012,, , 4.  
 2.36e+07, 0.00096,, , 4.  
 3.57e+07, 0.00196,, , 4.  
 3.62e+07, 0.00216,, , 4.  
 3.51e+07, 0.00246,, , 4.  
 1.19e+06, 0.,,, , 5.  
 2.37e+06, 4e-05,, , 5.  
 3.54e+06, 8e-05,, , 5.  
 4.7e+06, 0.00012,, , 5.  
 2.64e+07, 0.00096,, , 5.  
 4.15e+07, 0.00196,, , 5.  
 4.21e+07, 0.00216,, , 5.  
 4.05e+07, 0.00246,, , 5.  
 1.25e+06, 0.,,, , 6.  
 2.48e+06, 4e-05,, , 6.  
 3.71e+06, 8e-05,, , 6.  
 4.94e+06, 0.00012,, , 6.  
 2.83e+07, 0.00096,, , 6.  
 4.55e+07, 0.00196,, , 6.  
 4.62e+07, 0.00216,, , 6.  
 4.41e+07, 0.00246,, , 6.  
 1.31e+06, 0.,,, , 7.  
 2.61e+06, 4e-05,, , 7.  
 3.91e+06, 8e-05,, , 7.  
 5.2e+06, 0.00012,, , 7.  
 3.03e+07, 0.00096,, , 7.  
 5.01e+07, 0.00196,, , 7.  
 5.1e+07, 0.00216,, , 7.  
 4.82e+07, 0.00246,, , 7.  
 1.37e+06, 0.,,, , 8.  
 2.73e+06, 4e-05,, , 8.  
 4.09e+06, 8e-05,, , 8.  
 5.44e+06, 0.00012,, , 8.  
 3.22e+07, 0.00096,, , 8.  
 5.44e+07, 0.00196,, , 8.  
 5.55e+07, 0.00216,, , 8.  
 5.17e+07, 0.00246,, , 8.

1.41e+06, 0.,,, 9.  
 2.82e+06, 4e-05,,, 9.  
 4.22e+06, 8e-05,,, 9.  
 5.62e+06, 0.00012,,, 9.  
 3.36e+07, 0.00096,,, 9.  
 5.78e+07, 0.00196,,, 9.  
 5.91e+07, 0.00216,,, 9.  
 5.41e+07, 0.00246,,, 9.  
 1.43e+06, 0.,,, 10.  
 2.86e+06, 4e-05,,, 10.  
 4.28e+06, 8e-05,,, 10.  
 5.7e+06, 0.00012,,, 10.  
 3.42e+07, 0.00096,,, 10.  
 5.94e+07, 0.00196,,, 10.  
 5.08e+07, 0.00216,,, 10.  
 5.51e+07, 0.00246,,, 10.

Concrete Tension Stiffening, dependencies=1

474000., 0.,,, 0.  
 863000., 5.7e-05,,, 0.  
 1.14e+06, 0.000103,,, 0.  
 1.24e+06, 0.000145,,, 0.  
 932000., 0.000388,,, 0.  
 621000., 0.000632,,, 0.  
 311000., 0.000876,,, 0.  
 100000., 0.001122,,, 0.  
 474000., 0.,,, 1.  
 863000., 5.7e-05,,, 1.  
 1.14e+06, 0.000103,,, 1.  
 1.24e+06, 0.000145,,, 1.  
 932000., 0.000388,,, 1.  
 621000., 0.000632,,, 1.  
 311000., 0.000876,,, 1.  
 100000., 0.001122,,, 1.  
 752000., 0.,,, 2.  
 .42e+06, 6.2e-05,,, 2.  
 .96e+06, 0.00011,,, 2.  
 2.2e+06, 0.000154,,, 2.  
 .65e+06, 0.000395,,, 2.  
 1.1e+06, 0.000637,,, 2.  
 550000., 0.000878,,, 2.  
 100000., 0.001122,,, 2.  
 945000., 0.,,, 3.  
 .82e+06, 6.3e-05,,, 3.  
 1.56e+06, 0.000112,,, 3.  
 1.93e+06, 0.000157,,, 3.  
 2.2e+06, 0.000398,,, 3.

1.47e+06, 0.000638, , , 3.  
 733000., 0.000879, , , 3.  
 100000., 0.001121, , , 3.  
 1.09e+06, 0., , , 4.  
 2.11e+06, 6.3e-05, , , 4.  
 3.01e+06, 0.000113, , , 4.  
 3.5e+06, 0.000158, , , 4.  
 2.62e+06, 0.000399, , , 4.  
 1.75e+06, 0.000639, , , 4.  
 875000., 0.00088, , , 4.  
 100000., 0.001121, , , 4.  
 1.18e+06, 0., , , 5.  
 2.3e+06, 6.4e-05, , , 5.  
 3.3e+06, 0.000114, , , 5.  
 3.87e+06, 0.00016, , , 5.  
 2.9e+06, 0.0004, , , 5.  
 1.94e+06, 0.00064, , , 5.  
 968000., 0.00088, , , 5.  
 100000., 0.001121, , , 5.  
 1.23e+06, 0., , , 6.  
 2.42e+06, 6.4e-05, , , 6.  
 3.49e+06, 0.000114, , , 6.  
 4.12e+06, 0.000161, , , 6.  
 3.09e+06, 0.000401, , , 6.  
 2.06e+06, 0.00064, , , 6.  
 1.03e+06, 0.00088, , , 6.  
 100000., 0.001121, , , 6.  
 1.3e+06, 0., , , 7.  
 2.56e+06, 6.5e-05, , , 7.  
 3.7e+06, 0.000116, , , 7.  
 4.4e+06, 0.000163, , , 7.  
 3.3e+06, 0.000402, , , 7.  
 2.2e+06, 0.000641, , , 7.  
 1.1e+06, 0.000881, , , 7.  
 100000., 0.001121, , , 7.  
 1.36e+06, 0., , , 8.  
 2.68e+06, 6.7e-05, , , 8.  
 3.89e+06, 0.000119, , , 8.  
 4.65e+06, 0.000166, , , 8.  
 3.49e+06, 0.000405, , , 8.  
 2.33e+06, 0.000643, , , 8.  
 1.16e+06, 0.000882, , , 8.  
 100000., 0.001121, , , 8.  
 1.4e+06, 0., , , 9.  
 2.77e+06, 7e-05, , , 9.  
 4.04e+06, 0.000124, , , 9.

```

1.86e+06, 0.000172, , , 9.
3.64e+06, 0.000409, , , 9.
2.43e+06, 0.000646, , , 9.
1.21e+06, 0.000883, , , 9.
100000., 0.001121, , , 9.
1.42e+06, 0., , , 10.
2.81e+06, 7.2e-05, , , 10.
4.11e+06, 0.000127, , , 10.
4.95e+06, 0.000177, , , 10.
3.71e+06, 0.000413, , , 10.
2.47e+06, 0.000648, , , 10.
1.24e+06, 0.000884, , , 10.
100000., 0.001121, , , 10.
Material, name=MatureConcrete
Elastic
2e+10, 0.15
Expansion
1e-05,
Material, name=Steel
Elastic
2.1e+11, 0.
initial conditions, type=field, variable=1
all, 0.
*
* INTERACTION PROPERTIES
*
Surface Interaction, name=INTPROP-1
,,
Gap Conductance
).5, 0.
0., 1.
*
* PHYSICAL CONSTANTS
*
Physical Constants, absolute zero=-273., stefan boltzmann=5.68e-08
*
* FIELDS
*
* Name: Field-1 Type: Temperature
Initial Conditions, type=TEMPERATURE
PickedSet42, 20.
*
* INTERACTIONS
*
* Interaction: Int-1
Foundation

```

```

__PickedSurf34_S1, F1, 6e+07
__PickedSurf34_S2, F2, 6e+07
** Interaction: Int-2
*Foundation
__PickedSurf32_S5, F5, 6e+07
** Interaction: Int-3
*Foundation
__PickedSurf33_S6, F6, 6e+07
** Interaction: Int-4
*Foundation
__PickedSurf35_S6, F6, 6e+07
** Interaction: Int-5
*Foundation
__PickedSurf36_S1, F1, 6e+07
__PickedSurf36_S2, F2, 6e+07
** -----
**
** STEP: Step-1
**
*Step, name=Step-1, nlgeom=YES, inc=1000
*Static
2160., 21600., 0.216, 21600.
*field, variable=1
nall, 1.
**
** FIELDS
**
** Name: Field-1  Type: Temperature
*Temperature
__PickedSet42, 21.8
**
** OUTPUT REQUESTS
**
*Restart, write, frequency=1
**
** FIELD OUTPUT: F-Output-1
**
*Output, field
*Element Output
COORD, LE, PE, PEEQ, PEMAG, S
**
** HISTORY OUTPUT: H-Output-1
**
*Output, history
*Element Output, elset=P1
LE11, MISES, S11

```

```

**
** HISTORY OUTPUT: H-Output-2
**
*Element Output, elset=P2
LE11, MISES, S11
**
** HISTORY OUTPUT: H-Output-3
**
*Element Output, elset=P3
LE11, MISES, S11
**
** HISTORY OUTPUT: H-Output-4
**
*Element Output, elset=P4
LE11, MISES, S11
*El Print, freq=999999
*Node Print, freq=999999
*End Step
** -----
**
** STEP: Step-2
**
*Step, name=Step-2, nlgeom=YES, inc=1000
*Static
2160., 21600., 0.216, 21600.
*field, variable=1
nall, 2.
**
** FIELDS
**
** Name: Field-1  Type: Temperature
*Temperature
_PickedSet42, 27.1
**
** OUTPUT REQUESTS
**
*Restart, write, frequency=1
**
** FIELD OUTPUT: F-Output-1
**
*Output, field
*Element Output
COORD, LE, PE, PLEQ, PEMAG, S
**
** HISTORY OUTPUT: H-Output-1
**

```



```

*Output, history
*Element Output, elset=P1
LE11, MISES, S11
**
** HISTORY OUTPUT: H-Output-2
**
*Element Output, elset=P2
LE11, MISES, S11
**
** HISTORY OUTPUT: H-Output-3
**
*Element Output, elset=P3
LE11, MISES, S11
**
** HISTORY OUTPUT: H-Output-4
**
*Element Output, elset=P4
LE11, MISES, S11
*End Step
** -----
**
** STEP: Step-3
**
*Step, name=Step-3, nlgeom=YES, inc=1000
*Static
2160., 21600., 0.216, 21600.
*field, variable=1
nall, 3.
**
** FIELDS
**
** Name: Field-1   Type: Temperature
*Temperature
_PickedSet42, 35.5
**
** OUTPUT REQUESTS
**
*Restart, write, frequency=1
**
** FIELD OUTPUT: F-Output-1
**
*Output, field
*Element Output
COORD, LE, PE, PEEQ, PEMAG, S
**
** HISTORY OUTPUT: H-Output-1

```

```

**
*Output, history
*Element Output, elset=P1
LE11, MISES, S11
**
** HISTORY OUTPUT: H-Output-2
**
*Element Output, elset=P2
LE11, MISES, S11
**
** HISTORY OUTPUT: H-Output-3
**
*Element Output, elset=P3
LE11, MISES, S11
**
** HISTORY OUTPUT: H-Output-4
**
*Element Output, elset=P4
LE11, MISES, S11
*End Step
** -----
**
** STEP: Step-4
**
*Step, name=Step-4, nlgeom=YES, inc=1000
*Static
2160., 21600., 0.216, 21600.
*field, variable=1
nall, 4.
**
** FIELDS
**
** Name: Field-1  Type: Temperature
*Temperature
_PickedSet42, 43.
**
** OUTPUT REQUESTS
**
*Restart, write, frequency=1
**
** FIELD OUTPUT: F-Output-1
**
*Output, field
*Element Output
COORD, LE, PE, PEEQ, PEMAG, S
**

```

```

** HISTORY OUTPUT: H-Output-1
**
*Output, history
*Element Output, elset=P1
LE11, MISES, S11
**
** HISTORY OUTPUT: H-Output-2
**
*Element Output, elset=P2
LE11, MISES, S11
**
** HISTORY OUTPUT: H-Output-3
**
*Element Output, elset=P3
LE11, MISES, S11
**
** HISTORY OUTPUT: H-Output-4
**
*Element Output, elset=P4
LE11, MISES, S11
*End Step
** -----
**
** STEP: Step-5
**
*Step, name=Step-5, nlgeom=YES, inc=1000
*Static
2160., 21600., 0.216, 21600.
*field, variable=1
nall, 5.
**
** FIELDS
**
** Name: Field-1   Type: Temperature
*Temperature
_PickedSet42, 44.1
**
** OUTPUT REQUESTS
**
*Restart, write, frequency=1
**
** FIELD OUTPUT: F-Output-1
**
*Output, field
*Element Output
COORD, LE, PE, PEEQ, PEMAG, S

```

```

**
** HISTORY OUTPUT: H-Output-1
**
*Output, history
*Element Output, elset=P1
LE11, MISES, S11
**
** HISTORY OUTPUT: H-Output-2
**
*Element Output, elset=P2
LE11, MISES, S11
**
** HISTORY OUTPUT: H-Output-3
**
*Element Output, elset=P3
LE11, MISES, S11
**
** HISTORY OUTPUT: H-Output-4
**
*Element Output, elset=P4
LE11, MISES, S11
*End Step
** -----
**
** STEP: Step-6
**
*Step, name=Step-6, nlgeom=YES, inc=1000
*Static
2160., 21600., 0.216, 21600.
*field, variable=1
nall, 6.
**
** FIELDS
**
** Name: Field-1  Type: Temperature
*Temperature
_PickedSet42, 42.5
**
** OUTPUT REQUESTS
**
*Restart, write, frequency=1
**
** FIELD OUTPUT: F-Output-1
**
*Output, field
*Element Output

```

```

COORD, LE, PE, PEEQ, PEMAG, S
**
** HISTORY OUTPUT: H-Output-1
**
*Output, history
*Element Output, elset=P1
LE11, MISES, S11
**
** HISTORY OUTPUT: H-Output-2
**
*Element Output, elset=P2
LE11, MISES, S11
**
** HISTORY OUTPUT: H-Output-3
**
*Element Output, elset=P3
LE11, MISES, S11
**
** HISTORY OUTPUT: H-Output-4
**
*Element Output, elset=P4
LE11, MISES, S11
*End Step
** -----
**
** STEP: Step-7
**
*Step, name=Step-7, nlgeom=YES, inc=1000
*Static
4320., 43200., 0.432, 43200.
*field, variable=1
nall, 7.
**
** FIELDS
**
** Name: Field-1  Type: Temperature
*Temperature
_PickedSet42, 34.1
**
** OUTPUT REQUESTS
**
*Restart, write, frequency=1
**
** FIELD OUTPUT: F-Output-1
**
*Output, field

```

```

*Element Output
COORD, LE, PE, PEEQ, PEMAG, S
**
** HISTORY OUTPUT: H-Output-1
**
*Output, history
*Element Output, elset=P1
LE11, MISES, S11
**
** HISTORY OUTPUT: H-Output-2
**
*Element Output, elset=P2
LE11, MISES, S11
**
** HISTORY OUTPUT: H-Output-3
**
*Element Output, elset=P3
LE11, MISES, S11
**
** HISTORY OUTPUT: H-Output-4
**
*Element Output, elset=P4
LE11, MISES, S11
*End Step
** -----
**
** STEP: Step-8
**
*Step, name=Step-8, nlgeom=YES, inc=1000
*Static
8640., 86400., 0.864, 86400.
*field, variable=1
nall, 8.
**
** FIELDS
**
** Name: Field-1   Type: Temperature
*Temperature
_PickedSet42, 21.7
**
** OUTPUT REQUESTS
**
*Restart, write, frequency=1
**
** FIELD OUTPUT: F-Output-1
**

```

```

*Output, field
*Element Output
COORD, LE, PE, PEEQ, PEMAG, S
**
** HISTORY OUTPUT: H-Output-1
**
*Output, history
*Element Output, elset=P1
LE11, MISES, S11
**
** HISTORY OUTPUT: H-Output-2
**
*Element Output, elset=P2
LE11, MISES, S11
**
** HISTORY OUTPUT: H-Output-3
**
*Element Output, elset=P3
LE11, MISES, S11
**
** HISTORY OUTPUT: H-Output-4
**
*Element Output, elset=P4
LE11, MISES, S11
*End Step
** -----
**
** STEP: Step-9
**
*Step, name=Step-9, nlgeom=YES, inc=1000
*Static
17280., 172800., 1.728, 172800.
*field, variable=1
nall, 9.
**
** FIELDS
**
** Name: Field-1  Type: Temperature
*Temperature
_PickedSet42, 7.
**
** OUTPUT REQUESTS
**
*Restart, write, frequency=1
**
** FIELD OUTPUT: F-Output-1

```

```

**
*Output, field
*Element Output
COORD, LE, PE, PEEQ, PEMAG, S
**
** HISTORY OUTPUT: H-Output-1
**
*Output, history
*Element Output, elset=P1
LE11, MISES, S11
**
** HISTORY OUTPUT: H-Output-2
**
*Element Output, elset=P2
LE11, MISES, S11
**
** HISTORY OUTPUT: H-Output-3
**
*Element Output, elset=P3
LE11, MISES, S11
**
** HISTORY OUTPUT: H-Output-4
**
*Element Output, elset=P4
LE11, MISES, S11
*End Step
** -----
**
** STEP: Step-10
**
*Step, name=Step-10, nlgeom=YES, inc=1000
*Static
17280., 172800., 1.728, 172800.
*field, variable=1
nall, 10.
**
** FIELDS
**
** Name: Field-1  Type: Temperature
*Temperature
_PickedSet42, -3.5
**
** OUTPUT REQUESTS
**
*Restart, write, frequency=1
**

```



```
** FIELD OUTPUT: F-Output-1
**
*Output, field
*Element Output
COORD, LE, PE, PEEQ, PEMAG, S
**
** HISTORY OUTPUT: H-Output-1
**
*Output, history
*Element Output, elset=P1
LE11, MISES, S11
**
** HISTORY OUTPUT: H-Output-2
**
*Element Output, elset=P2
LE11, MISES, S11
**
** HISTORY OUTPUT: H-Output-3
**
*Element Output, elset=P3
LE11, MISES, S11
**
** HISTORY OUTPUT: H-Output-4
**
*Element Output, elset=P4
LE11, MISES, S11
*End Step
```

### A.3 Example Input File for Heat transfer Analysis

```
*Heading
** Job name: HT Model name: HT
*Preprint, echo=NO, model=NO, history=NO, contact=NO
**
** PARTS
**
*Part, name=FOUNDATION-1
*End Part
*Part, name=WALL-1
*End Part
**
** ASSEMBLY
**
*Assembly, name=Assembly
**
*Instance, name=WALL-1, part=WALL-1
*Node
(Geometry)
*Element, type=DC3D20
(Geometry)
*Elset, elset=_PICKEDSET2, internal, generate
  1, 180, 1
** Region: (Section-1-_PICKEDSET2:_PICKEDSET2)
** Section: Section-1-_PICKEDSET2
*Solid Section, elset=_PICKEDSET2, material=CONCRETE
1.,
*End Instance
**
*Instance, name=FOUNDATION-1, part=FOUNDATION-1
*Node
(Geometry)
*Element, type=DC3D20
(Geometry)
*Elset, elset=_PICKEDSET2, internal, generate
  1, 45, 1
** Region: (Section-2-_PICKEDSET2:_PICKEDSET2)
** Section: Section-2-_PICKEDSET2
*Solid Section, elset=_PICKEDSET2, material=CONCRETE
1.,
*End Instance
*Nset, nset=_PICKEDSET6, internal, instance=WALL-1, generate
  1, 1163, 1
*Elset, elset=_PICKEDSET6, internal, instance=WALL-1, generate
  1, 180, 1
```

```

*Elset, elset=__PICKEDSURF14_S4, internal, instance=WALL-1, generate
6, 180, 6
*Elset, elset=__PICKEDSURF15_S4, internal, instance=FOUNDATION-1, generate
2, 44, 3
*Elset, elset=__PICKEDSURF16_S1, internal, instance=WALL-1, generate
169, 180, 1
*Elset, elset=__PICKEDSURF16_S6, internal, instance=WALL-1, generate
1, 175, 6
*Elset, elset=__PICKEDSURF16_S2, internal, instance=WALL-1, generate
1, 12, 1
*Elset, elset=__PICKEDSURF16_S3, internal, instance=WALL-1
*Elset, elset=__PICKEDSURF16_S5, internal, instance=WALL-1
*Nset, nset=_PickedSet19, internal, instance=WALL-1, generate
1, 1163, 1
*Nset, nset=Point3, instance=WALL-1
757,
*Nset, nset=Point2, instance=WALL-1
767,
*Nset, nset=Point1, instance=WALL-1
768,
*Nset, nset=Point4, instance=WALL-1
746,
*Elset, elset=Set-1, instance=FOUNDATION-1
40,
*Nset, nset=nall, instance=WALL-1, generate
1, 1163, 1
*Nset, nset=nall, instance=FOUNDATION-1, generate
1, 408, 1
*Elset, elset=__PICKEDSURF14_S4, internal, instance=WALL-1, generate
6, 180, 6
*Surface, type=ELEMENT, name=_PICKEDSURF14, internal
__PICKEDSURF14_S4, S4
*Elset, elset=__PICKEDSURF15_S4, internal, instance=FOUNDATION-1, generate
2, 44, 3
*Surface, type=ELEMENT, name=_PICKEDSURF15, internal
__PICKEDSURF15_S4, S4
*Elset, elset=__PICKEDSURF16_S1, internal, instance=WALL-1, generate
169, 180, 1
*Elset, elset=__PICKEDSURF16_S6, internal, instance=WALL-1, generate
1, 175, 6
*Elset, elset=__PICKEDSURF16_S2, internal, instance=WALL-1, generate
1, 12, 1
*Elset, elset=__PICKEDSURF16_S3, internal, instance=WALL-1
*Elset, elset=__PICKEDSURF16_S5, internal, instance=WALL-1
*Surface, type=ELEMENT, name=_PICKEDSURF16, internal
__PICKEDSURF16_S1, S1

```

```

__PICKEDSURF16_S6, S6
__PICKEDSURF16_S2, S2
__PICKEDSURF16_S3, S3
__PICKEDSURF16_S5, S5
*Elset, elset=__PickedSurf31_S6, internal, instance=FOUNDATION-1, generate
1, 45, 1
*Surface, type=ELEMENT, name=_PickedSurf31, internal
__PickedSurf31_S6, S6
*Elset, elset=__PickedSurf37_S4, internal, instance=FOUNDATION-1
*Surface, type=ELEMENT, name=_PickedSurf37, internal
__PickedSurf37_S4, S4
*Elset, elset=__PickedSurf38_S3, internal, instance=FOUNDATION-1, generate
1, 43, 3
*Elset, elset=__PickedSurf38_S5, internal, instance=FOUNDATION-1, generate
3, 45, 3
*Surface, type=ELEMENT, name=_PickedSurf38, internal
__PickedSurf38_S3, S3
__PickedSurf38_S5, S5
*Elset, elset=__PickedSurf41_S3, internal, instance=WALL-1
*Surface, type=ELEMENT, name=_PickedSurf41, internal
__PickedSurf41_S3, S3
*Elset, elset=__PickedSurf42_S5, internal, instance=WALL-1
*Surface, type=ELEMENT, name=_PickedSurf42, internal
__PickedSurf42_S5, S5
*Elset, elset=__PickedSurf43_S3, internal, instance=WALL-1, generate
1, 169, 12
*Elset, elset=__PickedSurf43_S5, internal, instance=WALL-1, generate
7, 175, 12
*Elset, elset=__PickedSurf43_S6, internal, instance=WALL-1, generate
1, 175, 6
*Surface, type=ELEMENT, name=_PickedSurf43, internal
__PickedSurf43_S3, S3
__PickedSurf43_S5, S5
__PickedSurf43_S6, S6
*End Assembly
**
** MATERIALS
**
*Material, name=CONCRETE
*Conductivity
2.2,
*Density
2500.,
*Specific Heat
1100.,
**

```

```

** INTERACTION PROPERTIES
**
*Surface Interaction, name=INTPROP-1
1.,
*Gap Conductance
0.5,0.
0.,1.
**
** PHYSICAL CONSTANTS
**
*Physical Constants, absolute zero=-273., stefan boltzmann=5.68e-08
**
** FIELDS
**
** Name: Field-1  Type: Temperature
*Initial Conditions, type=TEMPERATURE
_PickedSet19, 20.
**
** INTERACTIONS
**
** Interaction: INTPROP-1-1
*Contact Pair, interaction=INTPROP-1
_PICKEDSURF15, _PICKEDSURF14
** -----
**
** STEP: Step-1
**
*Step, name=Step-1, amplitude=RAMP
*Heat Transfer, end=PERIOD, deltmx=100.
216., 21600., 0.216, 21600.,
**
** LOADS
**
** Name: BODYFLUX-1  Type: Body heat flux
*Dflux
_PICKEDSET6, BF, 490.7
**
** INTERACTIONS
**
** Interaction: FndBtm
*Sradiate
_PickedSurf31, R, 0., 1.
** Interaction: FndSide
*Sradiate
_PickedSurf38, R, 0., 1.
** Interaction: FndTop

```

```

*Sradiate
_PickedSurf37, R, 0., 1.
** Interaction: NorthFace
*Sradiate
_PickedSurf41, R, -12., 0.4
** Interaction: SouthFace
*Sradiate
_PickedSurf42, R, -12., 0.4
** Interaction: TopFace
*Sradiate
_PickedSurf43, R, -12., 0.4
**
** OUTPUT REQUESTS
**
*Restart, write, frequency=1
**
** FIELD OUTPUT: F-Output-1
**
*Output, field
*Node Output
√T,
*Element Output
TEMP,
**
* HISTORY OUTPUT: H-Output-1
**
*Output, history
*Node Output, nset=Point1
√T,
**
* HISTORY OUTPUT: H-Output-2
**
*Node Output, nset=Point2
√T,
**
* HISTORY OUTPUT: H-Output-3
*
Node Output, nset=Point3
√T,
*
* HISTORY OUTPUT: H-Output-4
*
Node Output, nset=Point4
√T,
*
* HISTORY OUTPUT: H-Output-5

```

```

**
*Node file, nset=nall
NT,
*El Print, freq=999999
*Node Print, freq=999999
*End Step
** -----
**
** STEP: Step-2
**
*Step, name=Step-2, amplitude=RAMP
*Heat Transfer, end=PERIOD, deltmx=100.
216., 21600., 0.216, 21600.,
**
** LOADS
**
** Name: BODYFLUX-1  Type: Body heat flux
*Dflux
_PICKEDSET6, BF, 736.
**
** INTERACTIONS
**
** Interaction: NorthFace
*Sradiate
_PickedSurf41, R, -12., 0.4
** Interaction: SouthFace
*Sradiate
_PickedSurf42, R, -12., 0.4
** Interaction: TopFace
*Sradiate
_PickedSurf43, R, -12., 1.
**
** OUTPUT REQUESTS
**
*Restart, write, frequency=1
**
** FIELD OUTPUT: F-Output-1
**
*Output, field
*Node Output
NT,
*Element Output
TEMP,
**
** HISTORY OUTPUT: H-Output-1
**

```

```

*Output, history
*Node Output, nset=Point1
NT,
**
** HISTORY OUTPUT: H-Output-2
**
*Node Output, nset=Point2
NT,
**
** HISTORY OUTPUT: H-Output-3
**
*Node Output, nset=Point3
NT,
**
** HISTORY OUTPUT: H-Output-4
**
*Node Output, nset=Point4
NT,
**
** HISTORY OUTPUT: H-Output-5
**
*Node file, nset=nall
NT,
*End Step
** -----
**
** STEP: Step-3
**
*Step, name=Step-3, amplitude=RAMP
*Heat Transfer, end=PERIOD, deltmx=100.
216., 21600., 0.216, 21600.,
**
** LOADS
**
** Name: BODYFLUX-1  Type: Body heat flux
*Dflux
_PICKEDSET6, BF, 1717.3
**
** OUTPUT REQUESTS
**
*Restart, write, frequency=1
**
** FIELD OUTPUT: F-Output-1
**
*Output, field
*Node Output

```



```

NT,
*Element Output
TEMP,
**
** HISTORY OUTPUT: H-Output-1
**
*Output, history
*Node Output, nset=Point1
NT,
**
** HISTORY OUTPUT: H-Output-2
**
*Node Output, nset=Point2
NT,
**
** HISTORY OUTPUT: H-Output-3
**
*Node Output, nset=Point3
NT,
**
** HISTORY OUTPUT: H-Output-4
**
*Node Output, nset=Point4
NT,
**
** HISTORY OUTPUT: H-Output-5
**
*Node file, nset=nali
NT,
*End Step
** -----
**
** STEP: Step-4
**
*Step, name=Step-4, amplitude=RAMP
*Heat Transfer, end=PERIOD, deltmx=100.
216., 21600., 0.216, 21600.,
**
** LOADS
**
** Name: BODYFLUX-1  Type: Body heat flux
*Dflux
_PICKEDSET6, BF, 1349.3
**
** OUTPUT REQUESTS
**

```

```

*Restart, write, frequency=1
**
** FIELD OUTPUT: F-Output-1
**
*Output, field
*Node Output
NT,
*Element Output
TEMP,
**
** HISTORY OUTPUT: H-Output-1
**
*Output, history
*Node Output, nset=Point1
NT,
**
** HISTORY OUTPUT: H-Output-2
**
*Node Output, nset=Point2
NT,
**
** HISTORY OUTPUT: H-Output-3
**
*Node Output, nset=Point3
NT,
**
** HISTORY OUTPUT: H-Output-4
**
*Node Output, nset=Point4
NT,
**
** HISTORY OUTPUT: H-Output-5
**
*Node file, nset=nall
NT,
*End Step
** -----
**
** STEP: Step-5
**
*Step, name=Step-5, amplitude=RAMP
*Heat Transfer, end=PERIOD, deltmx=100.
216., 21600., 0.216, 21600.,
**
** LOADS
**

```

\*\* Name: BODYFLUX-1 Type: Body heat flux

\*Dflux

\_PICKEDSET6, BF, 368.

\*\*

\*\* OUTPUT REQUESTS

\*\*

\*Restart, write, frequency=1

\*\*

\*\* FIELD OUTPUT: F-Output-1

\*\*

\*Output, field

\*Node Output

NT,

\*Element Output

TEMP,

\*\*

\*\* HISTORY OUTPUT: H-Output-1

\*\*

\*Output, history

\*Node Output, nset=Point1

NT,

\*\*

\*\* HISTORY OUTPUT: H-Output-2

\*\*

\*Node Output, nset=Point2

NT,

\*\*

\*\* HISTORY OUTPUT: H-Output-3

\*\*

\*Node Output, nset=Point3

NT,

\*\*

\*\* HISTORY OUTPUT: H-Output-4

\*\*

\*Node Output, nset=Point4

NT,

\*\*

\*\* HISTORY OUTPUT: H-Output-5

\*\*

\*Node file, nset=all

NT,

\*End Step

\*\* -----

\*\*

\*\* STEP: Step-6

\*\*

```

*Step, name=Step-6, amplitude=RAMP
*Heat Transfer, end=PERIOD, deltmx=100.
216., 21600., 0.216, 21600.,
**
** LOADS
**
** Name: BODYFLUX-1  Type: Body heat flux
*Dflux
_PICKEDSET6, BF, 122.7
**
** OUTPUT REQUESTS
**
*Restart, write, frequency=1
**
** FIELD OUTPUT: F-Output-1
**
*Output, field
*Node Output
NT,
*Element Output
TEMP,
**
** HISTORY OUTPUT: H-Output-1
**
*Output, history
*Node Output, nset=Point1
NT,
**
** HISTORY OUTPUT: H-Output-2
**
*Node Output, nset=Point2
NT,
**
** HISTORY OUTPUT: H-Output-3
**
*Node Output, nset=Point3
NT,
**
** HISTORY OUTPUT: H-Output-4
**
*Node Output, nset=Point4
NT,
**
** HISTORY OUTPUT: H-Output-5
**
*Node file, nset=nall

```

```

NT,
*End Step
** -----
**
** STEP: Step-7
**
*Step, name=Step-7, amplitude=RAMP
*Heat Transfer, end=PERIOD, deltmx=100.
432., 43200., 0.432, 43200.,
**
** LOADS
**
** Name: BODYFLUX-1  Type: Body heat flux
*Dflux
_PICKEDSET6, BF, 30.7
**
** INTERACTIONS
**
** Interaction: NorthFace
*Sradiate
_PickedSurf41, R, -12., 1.
** Interaction: SouthFace
*Sradiate
_PickedSurf42, R, -12., 1.
**
** OUTPUT REQUESTS
**
*Restart, write, frequency=1
**
** FIELD OUTPUT: F-Output-1
**
*Output, field
*Node Output
NT,
*Element Output
TEMP,
**
** HISTORY OUTPUT: H-Output-1
**
*Output, history
*Node Output, nset=Point1
NT,
**
** HISTORY OUTPUT: H-Output-2
**
*Node Output, nset=Point2

```

```

NT,
**
** HISTORY OUTPUT: H-Output-3
**
*Node Output, nset=Point3
NT,
**
** HISTORY OUTPUT: H-Output-4
**
*Node Output, nset=Point4
NT,
**
** HISTORY OUTPUT: H-Output-5
**
*Node file, nset=nall
NT,
*End Step
** -----
**
** STEP: Step-8
**
*Step, name=Step-8, amplitude=RAMP
*Heat Transfer, end=PERIOD, deltmx=100.
864., 86400., 0.864, 86400.,
**
** LOADS
**
** Name: BODYFLUX-1  Type: Body heat flux
*Dflux
_PICKEDSET6, BF, 15.3
**
** OUTPUT REQUESTS
**
*Restart, write, frequency=1
**
** FIELD OUTPUT: F-Output-1
**
*Output, field
*Node Output
NT,
*Element Output
TEMP,
**
** HISTORY OUTPUT: H-Output-1
**
*Output, history

```

```

*Node Output, nset=Point1
NT,
**
** HISTORY OUTPUT: H-Output-2
**
*Node Output, nset=Point2
NT,
**
** HISTORY OUTPUT: H-Output-3
**
*Node Output, nset=Point3
NT,
**
** HISTORY OUTPUT: H-Output-4'
**
*Node Output, nset=Point4
NT,
**
** HISTORY OUTPUT: H-Output-5
**
*Node file, nset=all
NT,
*End Step
** -----
**
** STEP: Step-9
**
*Step, name=Step-9, amplitude=RAMP
*Heat Transfer, end=PERIOD, deltmx=100.
1728., 172800., 1.728, 172800.,
**
** LOADS
**
** Name: BODYFLUX-1  Type: Body heat flux
*Dflux
_PICKEDSET6, BF, 7.7
**
** OUTPUT REQUESTS
**
*Restart, write, frequency=1
**
** FIELD OUTPUT: F-Output-1
**
*Output, field
*Node Output
NT,

```

```

*Element Output
TEMP,
**
** HISTORY OUTPUT: H-Output-1
**
*Output, history
*Node Output, nset=Point1
NT,
**
** HISTORY OUTPUT: H-Output-2
**
*Node Output, nset=Point2
NT,
**
** HISTORY OUTPUT: H-Output-3
**
*Node Output, nset=Point3
NT,
**
** HISTORY OUTPUT: H-Output-4
**
*Node Output, nset=Point4
NT,
**
** HISTORY OUTPUT: H-Output-5
**
*Node file, nset=nall
NT,
*End Step
** -----
**
** STEP: Step-10
**
*Step, name=Step-10, amplitude=RAMP
*Heat Transfer, end=PERIOD, deltmx=100.
1728., 172800., 1.728, 172800.,
**
** OUTPUT REQUESTS
**
*Restart, write, frequency=1
**
** FIELD OUTPUT: F-Output-1
**
*Output, field
*Node Output
NT,

```



```
*Element Output
TEMP,
**
** HISTORY OUTPUT: H-Output-1
**
*Output, history
*Node Output, nset=Point1
NT,
**
** HISTORY OUTPUT: H-Output-2
**
*Node Output, nset=Point2
NT,
**
** HISTORY OUTPUT: H-Output-3
**
*Node Output, nset=Point3
NT,
**
** HISTORY OUTPUT: H-Output-4
**
*Node Output, nset=Point4
NT,
**
** HISTORY OUTPUT: H-Output-5
**
*Node file, nset=nall
NT,
*End Step
```